STUDY THE PERMEABILITY OF MULTI-LAYER WOVEN FABRICS

A thesis submitted in partial fulfillment

of the requirements

for the Degree of Doctor of Philosophy

by

Liu Yi

Institute of Textiles and Clothing

The Hong Kong Polytechnic University

April, 2005

CERTIFICATE OF ORIGINALITY

I hereby declare that this thesis is my own work and that, to the best of my knowledge and belief, it reproduces no material previously published or written, nor material that has been accepted for the award of any other degree or diploma, except where due acknowledgement has been made in the text.

_____ (Signed)

_____Liu Yi_____(Name of student)

ABSTRACT

The aim of this study is to explore the permeability of 3D multi-layer woven fabrics and the mechanism of void formation due to the permeability difference within it. The results provide theoretical support for designing and producing high-performance composite materials.

Realizing the limitations of most existing models, which do not offer a realistic representation of the woven fabric architecture, the present developments introduce the notion of a micro/macro unit cell from a different perspective and are based on a more realistic representation of the three-dimensional fabric architecture which includes stitch, spacing and other fabric parameters. New models to study the effect of fabric microstructure and other properties of 3D multi-layer woven fabrics on permeability have been discussed. A permeability model based on fractal theory was established to predict the permeability of the preform fabricated with porous yarns. At the same time, another permeability model based on a unit cell of quadratic fibre packing was also proposed to predict the permeability of the 3D multi-layer woven fabrics fabricated with mono-filaments. It has been demonstrated that stitch structure plays an important role in the permeability of 3D multi-layer woven fabrics. The relationship between the fabric microstructure parameters and permeability has been established. The experimental validation of these two models was conducted over a series of stitch structures and the tendency predicted by the model agreed with the experimental data.

The mechanism of void formation in the multi-layer woven fabrics was also studied. The objective of current study is to carry out a theoretical analysis of in-plane impregnation in multi-layer woven fabrics (MWFs) to understand the

mechanism of void formation. Unlike the previous work, where the void was formed in the plane of one layer of woven fabric, in this thesis void formation in a cross-section of MWFs was studied. In this thesis, two simplified unit cells for in-plane impregnation in multi-layer woven fabrics were suggested. A mathematical model was developed to describe the mechanism of void formation during the resin transfer moulding (RTM) processes. The flow fronts and void formation in these two cells were also numerically simulated using the control-volume method. The simulated results agree well with the results predicted by the mathematical models and verified by the experimental studies. The results show that, for a given fibre preform, the ratio of the weft axial permeability to the warp transverse permeability is responsible for the formation of void and the void size.

A numerical simulation based on the control volume method was used to simulate the effect of stitch structure on equivalent permeability of the interbundle channels. The results show that the stitches would severely affect the permeability of the channels, even if the size of the stitches was very small. So this effect has to be considered when establishing the effective permeability model of multi-layer fabrics with stitches. The numerical simulation also demonstrates that the permeability varied greatly with the stitch changing in terms of the stitch size, off-centre position, slope, array, distribution density in the flow direction, and average Darcy velocity in the fibre bundles.

Several 3D multi-layer woven fabrics were designed and six kinds of fabrics with different stitch structures were produced. These specimens were tested using in-plane permeability measurement based on the radial flow method. The predictions from the permeability models and the data obtained from the numerical simulation were well supported by the experimental results.

Key words: 3D multi-layer woven fabrics, stitch structure, permeability, interbundle channel, Resin Transfer Moulding (RTM), void formation, numerical simulation

Acknowledgements

I would like to express sincere gratitude to my supervisor, Dr. Hu Jinlian, for giving me the opportunity to work on this project and guiding me throughout my research studies. I am deeply obliged to her for her constant support and availability, as well as for her helpful and numerous suggestions.

The author would also like to acknowledge the following for their contribution and support in this work:

Dr. Shao Xueming (Department of Mechanics, Zhejiang University) who helped me a lot in establishing the numerical simulation model and providing me with much beneficial information at the beginning of this project.

Mr. Szeto Yu-cheung who helped me with the fabrication of 3D multi-layer woven fabrics.

Mr. Ji Fenglong who provided his friendship to help me do some permeability testing and gave me many useful suggestions.

A special thanks is due to my parents and my wife, Xiaoke, for their support and endless love all of these years. This work is dedicated to all of them with all my love.

Publications Arising from the Thesis

1. J. L. Hu, Y. Liu, X. M. Shao, Study on void formation in multi-layer woven fabrics, Composites Part A: Applied Science and Manufacturing, 35(5), 595-603, 2004

2. J. L. Hu, X. M. Shao, Y. Liu, The effect of stitch on the permeability of interbundle channels in stitched fabrics, Textile Research Journal, 73(8), 691-699, 2003

3. Yi Liu, J. L. Hu, Effects of fabric stitch model on preform permeability, Accept by Composites: part A, Dec. 2004

4. Yi Liu, J. L. Hu, Effect of stitch structure on permeability of mono-filament multi-layer woven fabrics, submitted to Textile Research Journal, June 2005

5. Yi Liu, J. L. Hu, X. M. Shao, Study on void formation in multi-layer woven fabrics, The Fourth International Conference on Composite Science and Technology (ICCST/4), 2003, South Africa

6. Yi Liu, J. L. Hu, X. M. Shao, The effect of stitch on the permeability of 3D woven fabrics, The Fourth International Conference on Composite Science and Technology (ICCST/4), 2003, South Africa

7. Yi Liu, J. L. Hu, Study the effects of fabric stitch structure on preform permeability, Eleventh International Conference on Composites or Nano Engineering, August 8-14, 2004 in Hilton Head Island, South Carolina, USA

List of Symbols and Abbreviations

( ) ----- ----- Row vector

[ ] ----- ----- Matrix

2D----- ----- Two-dimensional

3D ----- ----- Three-dimensional

a=W/2 ----- The half width of the representative cell

A ---- ----- -The cross-sectional area of channel

b=H/2-------The half height of the representative cell

BC ---- ----- Boundary condition

C_f ----- -----A coefficient to define the maximum fiber volume fraction

D_f ----- -----The pore area fractal dimension

D_T ----- -----The tortuosity fractal dimension

F_i (i=x, y, z)-The external body forces

h(x) ---- ---- The half height of the channel

h_z ----- ---- The thickness of preform

H------- ----- -The height of the representative cell

$H_{channel}$ ---- The height of rectangularly shaped interbundle channel

K ---- ---- ----The permeability of the channel with stitches

K_0 ---- ---- ---The permeability of the channel without stitches

K_b^a ---- ---- -The axial permeability of fibre tow

K_b ---- ---- --- Permeability of intra-fibre bundle

$K_{channel}$ ----- - Permeability of interfibre channel

K_e ---- ---- ----Equivalent permeability

l_{ao} ---- ---- ---Length between points a and o

l_{bo} ---- ---- ---Length between points b and o

L ---- ---- ----- Length of the representative cell

L_t (λ) ---- --- Tortuous length along the flow direction

MWF--- ---- ---Multi-Layer Woven Fabric

p ---- ---- -----Static pressure

P_0 ---- ---- -----Pressures at inlet

P_f ---- --- -------Pressures at flow front

$\triangle$P ---- ---- ----- Difference between the pressure at the flow front P_f and the inlet pressure Po

$\triangle$P / L---- -------Pressure gradient along the computational cell

Q ---- ---- -------Flow rate

r_0 ---- ---- -------Inlet port radius

r_f ------ ---- -----Flow front radius

R ---- ---- -------Radius of stitch

t ------ ---- ------Time from the start of the injection to when a specified point in the cavity is reached

T_1 ---- ---- ----Time for flow front in path 1 to reach position B

T_2 ---- ---- -----Time for flow front in path 2 to reach position B

u= (μ , ν , ω)-- Velocity vector

u_f ---- ---- ------Superficial velocity at the flow front

V_f---- ---- -------Fibre volume fraction within the bundle

$V_{f,max}$---- ---- ----Maximum fibre volume fraction

W---- ---- --------Width of the representative cell

W_b ---- ---- ------Width of a bias yarn

$W_{channel}$ ---- ---- -Width of rectangularly shaped interbundle channel

W_L---- ---- -------Width of an axial yarn

x_f ---- ---- -------The $x-$coordinate of flow front along path 1 when transverse flow reaches point C

ρ ---- ---- --------Density of fluid

ε ---- ---- --------Porosity

μ ---- ---- --------Viscosity of fluid

λ ---- ---- --------Size of a pore channel in a fibre preform

θ---- ---- ---------Angle between stitch orientation and y-axis

List of Figures

Figure 1.1: Schematic diagram of Resin Transfer Moulding (RTM)

Figure 1.2: Schematic diagrams of 2D and 3D architectures

Figure 2.1: Micrograph of fibres and resin

Figure 2.2: Process of a textile composite structure

Figure 2.3: Schematic for pressure bag moulding

Figure 2.4: Bag moulding during stage one

Figure 2.5: Commonly used 2D weave patterns

Figure 2.6: Angles of the diagonal patterns formed by exchange locations

Figure 2.7: Triaxial weave

Figure 2.8: Some common 2D braid patterns

Figure 2.9: (a) Simple warp and weft knits; (b) Multi-axial warp knit insertion

Figure 2.10: Figure 2.10 Types of stitching used for through-thickness reinforcement: Weft Knit; Warp Knit

Figure 2.11: Three-dimensional weave patterns

Figure 2.12: Schematic illustration of generalised 3D woven fabric projected to the x-z (fabric length-thickness) plane

Figure 2.13: Unit cell geometry of plain weave

Figure 2.14 3D model for woven fabrics

Figure 2.15 3D model for braided fabrics

Figure 2.16: Examples of net shape structures 3D braiding

Figure 2.17: Multi-axial warp knit with four layers (0°, 90° and $\pm\theta$) of inserted yarns and (a) chain stitch or (b) tricot stitch

Figure 2.18: Multi-axial warp knit system

Figure 2.19: Orthogonal woven fabrics

Figure 2.20: 3D orthogonal fabrics

Figure 2.21: Unit cell for orthogonal non-woven fabrics

Figure 3.1: Illustration of dual scale flow

Figure 3.2: The difference between open weave and closed weave

Figure3.3: The directional characteristics of Kxx, Kyy, Kzz

Figure 3.4: Experimental schematic of in-plane permeability measurement

Figure 3.5: Schematic diagram of multi-layer woven Fabric Ⅰ

Figure 3.6: Schematic diagram of multi-layer woven Fabric Ⅱ

Figure 3.7: Schematic diagram of multi-layer woven Fabric Ⅲ

Figure 3.8: Schematic diagram of multi-layer woven fabrics with stitch density 1

Figure 3.9: Schematic diagram of multi-layer woven fabrics with stitch density 2

Figure 3.10: Schematic diagram of multi-layer woven fabrics with stitch density 3

Figure 3.11a, b, c and d: Set-up of the warping machine

Figure 3.12: a) Simple Weaving Machine; b) Shedding; c) Let-off; d) Reading equipment; e) Take-up

Figure 3.13: a) Front & back face of the Picanol Shuttle loom; b) Shedding; c) Reading Mechanism; d) Let-off; e) Take-up

Figure 3.14a and b: The tension device of the Simple Weaving Machine and Picanol Shuttle loom

Figure 3.15a and b: The electronic card-punching machine and the punched card

Figure 3.16 Comparisons of the permeabilities between fabrics with different types of stitch density

Figure 3.17 Comparisons of the permeabilities between fabrics with different weave type

Figure 4.1: Schematic for three different stitch models of multi-layer woven fabrics

Figure 4.2: Cross-sectional view of three types of multi-layer woven fabrics with different stitch density

Figure 4.3: Definition sketch of the idealised mono-filament reinforcement arrangement and the representative unit cell of quadratic fibre packing

Figure 4.4: Definition sketch in the analysis of the flow between the fibres

Figure 4.5: Definition sketch of quadratic and hexagonal array

Figure 4.6: The permeability of three different structures of the unit cells

radial experimental data for 3D woven fabric preforms

Figure 4.7: (a) architecture of the structure 2, (b) an idealised structure, (c) an idealised unit cell structures of 3D woven fabric preform

Figure 4.8: Schematic of multi-layer laminar flow

Figure 4.9: Comparisons in terms of the permeabilities between the model prediction and the experimental data

Figure 4.10: Comparison of the permeabilities among the 3D woven fabric preforms with three different stitch density structures

Figure 4.11: Micrograph of fibres and resin

Figure 4.12: Structures of 3 different stitch structure fabrics

Figure 4.13: Experimental cross-sectional views of 3 different stitch structure fabrics

Figure 4.14: Schematic of the resin channels and fabric sub-domains

Figure 4.15: Comparisons of the experimental permeabilities

Figure 5.1: Architecture of the plain woven fabric

Figure 5.2: Two typical multiple modes of MWFs

Figure 5.3: Typical cells of cross-section for MWFs

Figure 5.4: Unit cells for mode I and mode Π

Figure 5.5: Sub-domains of MWFs

Figure 5.6: Control volume

Figure 5.7: Illustration of the flow front advancing technique

Figure 5.8: Flow chart of the numerical simulation using control-volume method

Figure 5.9: Boundary injections from one side of a rectangular mould

Figure 5.10: Comparison of analytical and numerical results of flow fronts

Figure 5.11: Flow fronts at different injection time of point injection in a square preform

Figure 5.12: Simplified unit cells for mode I

Figure 5.13: Flow fronts at different stages of mould filling

Figure 5.14: The size of void for different K_b^a / K_b^t

Figure 5.15: Experimental cross-sections of MWFs

Figure 6.1: Computational cells for different situations

Figure 6.2: Steps of segregated solution method

Figure 6.3: Convergence of numerical simulation

Figure 6.4: Change of K/ K0 with V_b/V_a on different boundaries conditions

Figure 6.5: Change of K/ K0 with Vb/Va o for boundary conditions BC2 and BC3

Figure 6.6: Change of K/ K0 with L/W on different boundary conditions

Figure 6.7: Results of 2D simulation: change of K/ K0 with R/a

(L/W=2.0, Vb/Va =0.4)

Figure 6.8: Unit cell of channel flow with different stitch size

Figure 6.9: The simulation impregnation process of resin flow through the unit cell of channel with different stitch size

Figure 6.10: The effect of stitch size on permeability

Figure 6.11: Change of $K / K0$ with d / a

Figure 6.12: Unit cell of channel flow with stitch off-centre position

Figure 6.13: The simulation impregnation process of resin flow through the unit cell of channel with stitch off-centre position

Figure 6.14: The effect of stitch off-centre position on permeability

Figure 6.15: Change of $K / K0$ with stitch slope θ

Figure 6.16: Change of $K / K0$ with L / W in case of array-1 and array-2

Figure 6.17: Unit cell of channel flow with stitch off-centre position (2 stitches)

Figure 6.18: The simulation impregnation process of resin flow through the unit cell of channel with stitch off-centre position

Figure 6.19: the effect of stitch off-centre position (2 stitches) on permeability

Figure A1: Geometric details of one-dimensional test problem: (a) injection at horizontal position and (b) injection at vertical position

Figure B1: Rotation of coordinate system for permeability measurement in an arbitrary direction

Figure B2: Transformation to quasi-isotropic system

CONTENTS

ABSTRACT ..... **III**

ACKNOWLEDGEMENTS ..... **VI**

PUBLICATIONS ARISING FROM THE THESIS ..... **VII**

LIST OF SYMBOLS AND ABBREVIATIONS ..... **VIII**

LIST OF FIGURES ..... **XII**

CHAPTER 1 INTRODUCTION **1**

1.1 3D WOVEN COMPOSITES **1**

1.1.1 INTRODUCTION 1
1.1.2 MANUFACTURING PROCESSES FOR COMPOSITES 2

1.2 MATERIAL SELECTION FOR COMPOSITES **5**

1.3 PERMEABILITY ISSUE OF FABRIC PREFORM **6**

1.4 RESEARCH OBJECTIVES OF THE PRESENT STUDY **7**

1.5 SIGNIFICANCE & VALUES OF THE PRESENT STUDY **8**

1.6 TECHNIQUES USED IN THIS STUDY **9**

1.6.1 COMPUTER SIMULATION 9
1.6.2 MATHEMATICAL MODELING 10
1.6.3 EXPERIMENTAL STUDY 11

1.7 ORGANIZATION OF THE THESIS **12**

CHAPTER 2 OVERVIEW OF TEXTILE COMPOSITES **14**

2.1 INTRODUCTION **14**

2.2 CLASSIFICATION OF TEXTILE PREFORMS **20**

2.3 PROCESSING OF TEXTILE COMPOSITES **23**

2.4 GEOMETRY OF TEXTILE REINFORCEMENT **29**

2.4.1 IDEAL GEOMETRY 29
2.4.2 2D FABRICS 30
2.4.2.1 2D WEAVES 30
2.4.2.2 2D BRAIDS 34
2.4.2.3 2D KNITS 37
2.4.3 3D FABRICS 40
2.4.3.1 3D WEAVES 41
2.4.3.2 3D BRAIDS 52
2.4.3.3 3D KNITTED FABRICS 55
2.4.3.4 ORTHOGONAL NONWOVEN FABRICS 57

2.5 CONCLUSION **60**

CHAPTER 3 PERMEABILITY TEST **63**

3.1 INTRODUCTION 63

3.2 RESIN FLOW IN FABRICS 65

3.2.1 DARCY FLOW 65
3.2.2 SATURATED VS. UNSATURATED FLOW 67
3.2.3 FABRIC COMPRESSIBILITY 71

3.3 PERMEABILITY 73

3.3.1 PERMEABILITY AS A FUNCTION OF WEAVES TYPE 74
3.3.2 DIRECTION OF PERMEABILITY MEASUREMENT 75
3.3.3 ISOTROPIC AND ANISOTROPIC PERMEABILITY 76

3.4 MEASUREMENT OF PERMEABILITY 77

3.4.1 PERMEABILITY TEST 78
3.4.2 PERMEABILITY TESTING EQUATION 78

3.5 PERMEABILITY TESTING DEVICES 81

3.6 SAMPLE PREPARATION 82

3.6.1 MATERIAL USED 83
3.6.2 WEAVE DESIGN 83
3.6.3 EQUIPMENT USED FOR FABRIC FORMATION 89
3.6.3.1 WARPING MACHINE 89
3.6.3.2 WEAVING MACHINE 90
3.6.3.3 TENSIONING DEVICE 94
3.6.3.4 STAUBLI SYSTEM 95
3.6.4 PREPARATION FOR WEAVING 96
3.6.4.1 WARPING 96
3.6.4.2 DRAWING-IN 96
3.6.5 PRODUCTION OF THREE DIMENSIONAL MULTI-LAYER WOVEN FABRIC SAMPLES 97

3.7 PERMEABILITY TEST RESULTS 98

3.8 CONCLUSION 100

CHAPTER 4 PERMEABILITY MODEL 103

4.1 INTRODUCTION 103

4.2 MONO-FILAMENT PERMEABILITY MODEL 111

4.2.1 CHARACTERIZATION OF PORE MICROSTRUCTURES 111
4.2.2 PERMEABILITY MODEL OF UNIT CELL 1 114
4.2.3 EVALUATION OF $V_{F,MAX}$ 117
4.2.4 PREDICTED PERMEABILITY OF THE UNIT CELL 1 118
4.2.5 PERMEABILITY MODEL OF UNIT CELL 2 119
4.2.6 PERMEABILITY OF WHOLE STRUCTURE 121
4.2.7 EXPERIMENTAL RESULTS AND DISCUSSION 122
4.2.8 CONCLUSION REMARKS 126

4.3 FRACTAL PERMEABILITY MODEL 126

4.3.1 FRACTAL CHARACTERIZATION OF PORE MICROSTRUCTURES IN FIBER PREFORMS 126
4.3.2 FRACTAL MODEL FOR PERMEABILITY 128
4.3.3 EXPERIMENTAL STUDIES 130
4.3.4 CONCLUDING REMARKS 132

4.4 CONCLUSION 132

CHAPTER 5 VOID FORMATION 135

5.1 INTRODUCTION 135

5.2 NUMERICAL MODEL OF VOID FORMATION 138

5.2.1 UNIT CELL OF THE PLAIN WOVEN FABRIC 138
5.2.2 VOID FORMATION PREDICTION BASED ON NEWLY DEVELOPED MODEL 141

5.3 NUMERICAL SIMULATION OF VOID FORMATION 145

5.3.1 GOVERNING EQUATIONS 145
5.3.2 CONTROL VOLUME METHOD 147

5.4 RESULTS AND DISCUSSION 151

5.4.1 BASIC TESTING OF NUMERICAL SIMULATION 151
5.4.2 VOID FORMATION IN MWFS 154
5.4.3 EXPERIMENTAL RESULTS 159

5.5 CONCLUSION 160

CHAPTER 6 NUMERICAL SIMULATION OF EFFECT OF STITCH 162

6.1 INTRODUCTION 162

6.2 NUMERICAL SIMULATION 166

6.2.1 BASIC ASSUMPTIONS 166
6.2.2 GOVERNING EQUATIONS 168
6.2.3 COMPUTATION OF GOVERNING EQUATIONS 171

6.3 RESULTS AND DISCUSSION 172

6.3.1 THE EFFECT OF STITCH SIZE, DISTRIBUTION DENSITY 172
6.3.2 THE EFFECT OF STITCH OFF-CENTER POSITION IN CHANNEL 181
6.3.4 THE EFFECT OF STITCH ARRAY 185

6.4 CONCLUSION 190

CHAPTER 7 CONCLUSION AND FUTURE WORK 192

7.1 SUMMARY AND CONCLUSION 192

7.1.1 PERMEABILITY TEST 192
7.1.2 PERMEABILITY MODEL 193
7.1.4 VOID FORMATION 197

7.2 FUTURE RESEARCH 198

7.2.1 EXPERIMENTAL VERIFICATION 198
7.2.2 NUMERICAL SIMULATION 198
7.2.3 VOID FORMATION 199

APPENDIX A ANALYTICAL SOLUTION FOR 1-D ISOTHERMAL FLOW 200

APPENDIX B THE GOVERNING EQUATION FOR TWO DIMENSIONAL FLOW 204

APPENDIX C COMPUTER PROGRAM FOR SIMULATION 209

REFERENCES 240

Chapter 1

Introduction

1.1 3D woven composites

1.1.1 Introduction

Composites represent the new materials consisting of two or more distinct constituent materials. The requirements of various engineering applications can be met by the combination of the appropriate selection of the distinct constituent materials and the properly choosing of the composite microstructures as well as the optimisation of the mechanics of the materials.

The development of composite materials has a long history and can be dated back many centuries, starting with straw-reinforced clay bricks, then steel-reinforced concrete, and now fibre-reinforced polymers and metals.

Composite materials have wide applications. Composite products are readily found in the daily life serving as office chairs, dinner tables and entertainment centres and so on. The commercial and industrial applications of composites are so diverse that it is impossible to list them all. The major structural application areas include aircrafts, military facilities, space, automotives, sporting goods, and marine vessels. (Mallick, 1993)

The most advanced composites used in the most critical applications are continuous fibre composites (Daniel, 1993). As one sort of continuous fibre composites, the textile structural composite has a very important position in the composite family. In particular, 3D textile composites offer the improved damage

tolerance and the benefit of near net-shape manufacturing. In general, 3D textile composites can be classified by four basic manufacturing techniques: woven, orthogonal non-woven, braided and knitted. In the present thesis, the 3D multi-layer woven fabrics are the focus of attention.

1.1.2 Manufacturing Processes for Composites

Today, in many weight-critical industries, like the automotive and aerospace industries, composite materials are becoming more and more popular because they are lighter than metal and are able to be customised to fit the need for strength that provides great flexibility in design.

Although there are many ways to fabricate advanced composite parts, all processes have several basic steps in common. For example, all advanced composite parts require the fabrication of an intricate fibre network structure specific for the particular part geometry and microstructure. These fibre structures must be wetted out and infiltrated by the matrix resin. The resin, in turn, must be solidified while the part is being supported, in some way, by rigid tooling.

Generally speaking, there are two groups of the major manufacturing processes for composites: (a) those that once had been used in production and (b) those that are currently in production or under development. The first category includes (1) hand lay-up or machine-assisted hand lay-up followed by autoclave cure, (2) filament winding, and (3) pultrusion and (b), (4) textile preform and resin transfer moulding, (5) deformation forming, and (6) automated tow placement.

There are many manufacturing processes currently used in production, however, the fabricating of composite materials possess many drawbacks. It is difficult to

manufacture a large, complex, three-dimensional structure using traditional processes. The RTM process is then introduced to meet the requirements for making complicated structures.

As shown in Figure 1.1, in the RTM process, dry (i.e., unimpregnated) reinforcement is pre-shaped and oriented into a skeleton of the actual part known as the preform, which is inserted into a matched die mould. The mould is then closed, and a low-viscosity reactive fluid is injected into the tool. The air is displaced and escapes from vent ports placed at the high points. During this time, known as the injection or infiltration stage, the resin "wets out" the fibres. Heat applied to the mould activates polymerisation mechanisms that solidify the resin in the step known as cure. The resin cure begins during filling and continues after the filling process. Once the part develops sufficient green strength, it is moved or demoulded. Green strength refers to the strength of a part before it has completely cured. When a part comes out of the mould it is still warm, and therefore still reacting. The green strength is an indication of how well it holds its shape until it is completely cross-linked.

On first inspection, the RTM appears to be a simple three-step process: preforming followed by injection and cure, as shown in Figure 1.1. In reality, however, as shown by this schematic, it is much more complicated because processing is integrally coupled to performance. (Schwartz, 1997)

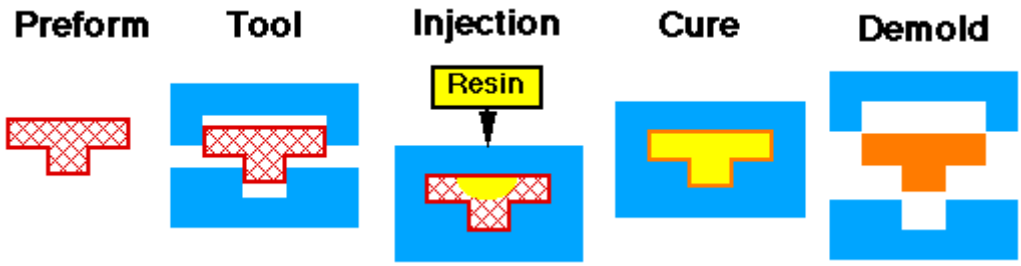

Figure 1.1 Schematic diagram of Resin Transfer Moulding (RTM)

Each step of the process affects the subsequent steps. Furthermore, every decision affects both the processing and the performance of the final part. For example, the microstructure of the preform must be designed based on not only the thermo-mechanical loading the part is expected to undergo but also the influence of the proposed microstructure on the permeability and therefore the time to fill the mould (thus also affecting resin selection, viscosity, and processing temperature, which in turn affects selection of tooling material and demould time). Similarly, injection must reflect the delicate balance among the desire for a short cycle time, the integrity of the microstructure (avoiding processing-induced movement of the reinforcement), the wet-out of fibre bundles, and the removal of entrapped air. So resin selection, moulding temperature, pressure, and viscosity must be controlled to preserve the preform integrity. Also, tooling must be designed not only for the shape and features of the part but also for the specifics of injection, permeability, cure, and demoulding. These are but a few examples of the challenges associated with RTM, making it essential that processing and performance issues be considered simultaneously to ensure that the final product is of high quality and yet economical.

It should be noted that for all of these manufacturing processes, to ensure final product quality and decrease the cycle time, permeability is the key parameters in processing fibre-reinforced composite. The greater the values, the easier the fluid

passes through the fibre preform.

1.2 Material Selection for composites

The basic materials used in composite manufacturing include reinforcement and resin. Selection of the reinforcing fibre is based on the mechanical requirements of the moulded component, its environmental requirements and cost. Many types of fibres can be used for composite, including carbon, several types of glass and Kevlar®. These are available in strands known as rovings or twisted into yarns. The fibres for use in the RTM may be stitched or woven into various 2D or 3D architectures as shown in Figure 1.2.

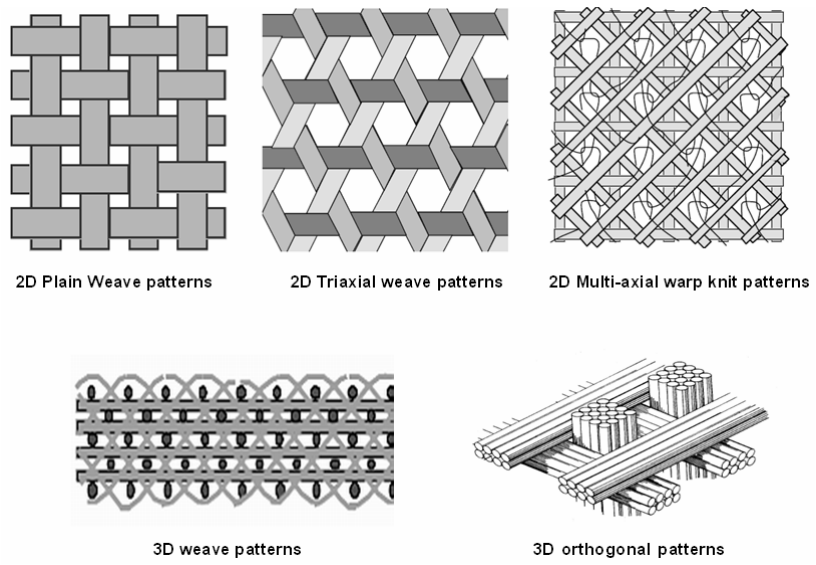

Figure 1.2 Schematic diagrams of 2D and 3D architectures

Fiber architecture selection depends on performance issues such as modulus, strength, durability, compressibility during preforming to attain adequate volume fractions and drapability to ensure proper placement of the reinforcement during preforming operations. Moreover, the selection of fiber preform architecture also depends on processing issues such as permeability, compressibility and drapability.

These issues are summarized in the table below:

Table 1.1: Summary of Processing Issues

Processing Issues	Performance Issues
Permeability (X,Y and Z directions) Compressibility Drapability	Module, strengths, etc. Durability Compressibility Drapability

Among all of these preform properties, we focus on the permeability, especially the permeability of multi-layer woven fabrics.

1.3 Permeability issue of fabric preform

From the introduction of the manufacturing processes of the composites and related material selection, permeability of a textile preform (transport of resin) is a key aspect of fiber reinforced plastic composite fabrication processes such as RTM. As one of the elemental performances of fiber materials, the importance of the permeability lies in the following points. First, it can determine the filling and packing time in injection, and determine the mold design, the location of injection port and exhaust port, thus it is the critical parameter for numerical simulation. Second, it determines the attribute of fluid flow, determine the degree of impregnation, thus it is the key factor to produce the high-performance products.

The problems related to permeability include the formation of dry spots or voids within the preform. These dry spots and voids will deteriorate the performance of products, so it is significant to eliminate them. But these are not easy to solve,

particularly when the preform is composed of multi-layers of reinforcement. Only when we find the relationship between fabric permeability and fabric construction can we eliminate dry spots and voids and improve product performance.

At present, composites reinforced by textile preforms represent a class of advanced materials for many applications because of their unique combination of light weight, flexibility, strength and toughness. Composite materials are finding increasing applications in demanding areas such as the aerospace and automotive industries. They are gaining wider acceptance because of their specific strength and specific stiffness and their ability to replace metals in many structural applications. For widespread composite utilization, improving the cost effectiveness and achieving the optimum material properties in the manufacturing process are major challenges facing the composite industry. And the use of resin transfer moulding (RTM) as an economic means of producing high-performance fiber-reinforced composites is critically limited by the permeability of the fabrics employed. So solving this problem is our motivation to establish the relationship between the fabric permeability and the fabric construction.

1.4 Research objectives of the present study

Permeability refers to the ability of a textile preform to let the resin transport through it in composite fabrication. Related problems include the formation of dry spots or voids within composites. The permeability of a fabric is determined mainly by fabric microstructures. There have been very few studies on the relationship between the permeability and the microstructure of the three dimensional multi-layer woven fabrics (3D MWFs). This is an obstacle for a rational design of a 3D MWF preform. Thus the objectives of this study are:

- To study the permeability of 3D MWFs during the composites fabrication process experimentally
- To investigate theoretically the relationship between the fabric permeability and the fabric construction, particularly the effect of the stitching parameters of 3D MWFs
- To propose an analytical model to describe the formation of dry spots or voids within the preform
- To establish a numerical simulation model to simulate the effects of fabric construction on permeability

Because the key feature of 3D MWFs is their through-the-thickness stitching, the key issues therefore addressed are: how does inter-layer stitch affect the effective (average) permeability and the void formation within the fabrics and how can we achieve a complete and uniform resin penetration by a suitable fabric design without sacrificing other properties?

1.5 Significance & Values of the present study

The textile composites can be defined as the combination of a resin system with a textile fiber, yarn or fabric system. Starting with linear assemblies of fibers in continuous and/or discrete form, these micro-fibers can be organized into two-dimensional (2D) and three-dimensional (3D) structures by means of textile processes such as interlacing, intertwining, or interlooping. Properly selecting the geometry and the method of placement or geometric arrangement of the fibers can influence the resulting structural performance of the composite. These fiber placement methods create textile preforms that possess a wide spectrum of pore

geometries and pore distribution; a broad range of structural integrity and fiber volume fraction; and fiber orientation distribution. Only when we find the internal relationship between the structure of a textile preform and the relevant properties, can we design the most optimum composite product with perfect performance.

So the significance and values of the present study are:

◆ Providing a clear picture of the formation of dry spots or voids, thus to improve the performance of the composite products.

◆ Establishing a simulation system, thus to predict the flow behavior (flow front, pressure distribution, etc.) and to reduce production cost and save time.

◆ Setting up an analytical model, thus to help improve the impregnation process and improve overall permeability of preform.

This can lead to the introduction of high-value-added products for the textile industry and will improve the competitiveness of the resin manufacturing as well as composites fabrication industry. Theoretical results will contribute to the performance in textiles, such as apparel comfort, and composite areas such as mold filling and void formation.

1.6 Techniques used in this study

In order to achieve the objectives stated in section 1.5, three research techniques- computer simulation, mathematical modeling and experimental study- were employed in this study.

1.6.1 Computer simulation

Simulation is the process by which understanding of the behavior of an already

existing (or to be constructed) physical system is obtained by observing the behavior of a model representing the system (Kheir, 1996). Simulation can help avoid costly design errors, save time used in prototype building and testing and ensure safe, high-quality and cost-effective products.

Simulation has been widely applied to the automobile industry, aerospace, manufacturing, computer-aided design, economics, health/medicine, power/energy and education (Kheir, 1996). The general procedure of a simulation consists of the following steps (murthy et al., 1990).

1) Building the simulation model. This is done by breaking the system into sections and identifying entities, attributes, activities and events;

2) Writing the computer program. This converts the simulation model into a simulation program;

3) Running the program. This performs the simulation on computer.

In this study, computer simulation mainly based on the control volume finite element method and was used to simulate the effect of a fabric structure on permeability and void formation in the resin impregnate process.

1.6.2 Mathematical modeling

The use of mathematics in solving real-world problems has become widespread in recent times (Murthy et al., 1990).

Mathematical models are patiently constructed using a well-tried process and can be based either on data, assumptions or a combination of both. In general, a mathematical model takes the form of a set of equations describing a number of

variables (Fowler, 1997). Mathematical modeling is the activity of translating a real problem into mathematics for subsequent analysis (Edwards and Hamson, 1996).

In this study, the permeability model for multi-layer woven fabrics was established based on the data collected from experiments and the simulation data using the control volume finite element method.

1.6.3 Experimental study

1.6.3.1 Experimental material preparation

The mono-filaments were used for making various fabrics. This can eliminate the effects of other factors such as fiber bundle on the permeability and allow us to concentrate on the effect of fabric microstructure. The fabrics fabricated with multi-filament yarn were used also for comparison and validation purposes. In addition, the 3D multi-layer woven fabrics with different stitching designs, say, the self-stitching with different stitching structures, were made.

1.6.3.2 Experimental test

The Darcy law (Darcy, 1856) was used to model the flow through the reinforcement fibers where the permeability was a measure for the resistance of the fibers to the flow. For the successful process modeling it is essential to ensure the reliability of the permeability measured. Generally speaking there are two different configurations for the flow in the fabrics: one-dimensional channel and the two-dimensional radial, and therefore the permeability measurements should be correspondingly accomplished through the one-dimensional channel flow experiment and the two-dimensional radial flow experiment. The main attraction of the radial flow experiment is that both the principal permeability values and their

orientation can be determined in a single experiment. And there is no race tracking during the experimental process. So we choose radial flow experiment as the basic testing method.

The fabric microstructures such as void dimension and distribution were measured by an image analyzer after cutting the resin-embedded fabrics for the analysis of the pore volume distribution (Mahale et al, 1992).

1.7 Organization of the Thesis

In Chapter 1, a review of the researches regarding 3D multi-layer woven fabrics is given and the reasons for exploring the permeability of 3D woven fabrics are outlined. Three research techniques, which have been used in this study, are introduced.

In Chapter 2, an overview of textile composites is presented. The classifications of the textile preforms, the structural geometry of 3D textiles and the geometry of textile reinforcement are discussed.

In Chapter 3, a permeability test apparatus based on the Darcy' law and radial flow method is established. The permeability data of 3D multi-layer woven fabrics are tested by this testing system.

In Chapter 4, a permeability model is established using mathematical modeling based on the data obtained from experimental study. The permeability model is verified by experimental and simulation data.

In Chapter 5, the void formation in multi-layer woven fabrics is presented. The model to predict the void formation in 3D multi-layer woven fabrics is established and verified by the simulation results and the experimental analysis.

In Chapter 6, a numerical simulation of the effect of stitch on the permeability of interbundle channels in stitched fabrics is established. The effects of the stitch structures and array, such as stitch size, off-centre position, slope, array, distribution density, on permeability are simulated and discussed.

In the last chapter, a conclusion is drawn and some new ideas and suggestions for future research are described.

Chapter 2

Overview of textile composites

2.1 Introduction

Composite materials have been known to man for thousands of years, and occur naturally in many living things. The earliest composite materials were straw reinforced brick, which was similar to modern steel reinforced concrete (Parnas, 2000). Some composites that exist naturally are wood and bone. A composite is generally any material that is made up of different constituent materials. Typically, the composite material has properties exceeding those of the constituent elements alone. Composites are now being used in almost every industry as the demands on materials continue to increase and become more specific. They are used for applications in aerospace, sporting goods, boats, wind turbines, and automobiles.

Because the composite is made up of two or more materials, there is almost an infinite amount of possible combinations. Because of this, composites can be engineered to have properties that are very specific to a particular application. Composites can be engineered or requirements in stiffness, strength, damage tolerance, corrosion resistance, conductivity, and many others. One property that has been of particular importance is the stiffness to weight ratio, where carbon fiber has excelled. Carbon fiber can have a five times higher stiffness to weight ratio than aluminum (Parnas, 2000). This has encouraged its use in the aerospace industry where weight is critical. Composites have also been chosen for reasons that are not related to mechanical performance. They have been used to create materials with almost zero thermal expansion for use in space applications, and have also been used

in applications where corrosion resistance is critical such as storage tanks and piping.

Composites are often combined in pairs where one material is in the form of a fiber, and the other creates a matrix to support the fiber. Typically the material with the highest stiffness and tensile strength is used as the fiber to give the material its strength (Agarwal and Broutman, 1980). The matrix can serve several purposes. Mainly, it keeps the fibers aligned and provides compressive and shear strength. Since the fiber would easily buckle in compression, the matrix is intended to stabilize the fiber. The matrix also adds toughness to the material by creating a large damage zone. The matrix transmits the load to the fibers and distributes it throughout the part. In addition to supporting the fiber, the matrix also protects it. The matrix protects the fibers from abrasion between fibers, as well as from environmental degradation (Mallick, 1988). Figure 2.1 is a micrograph of a typical composite material. The picture is looking along the direction of the fibers of a D155 fabric at 60X magnification.

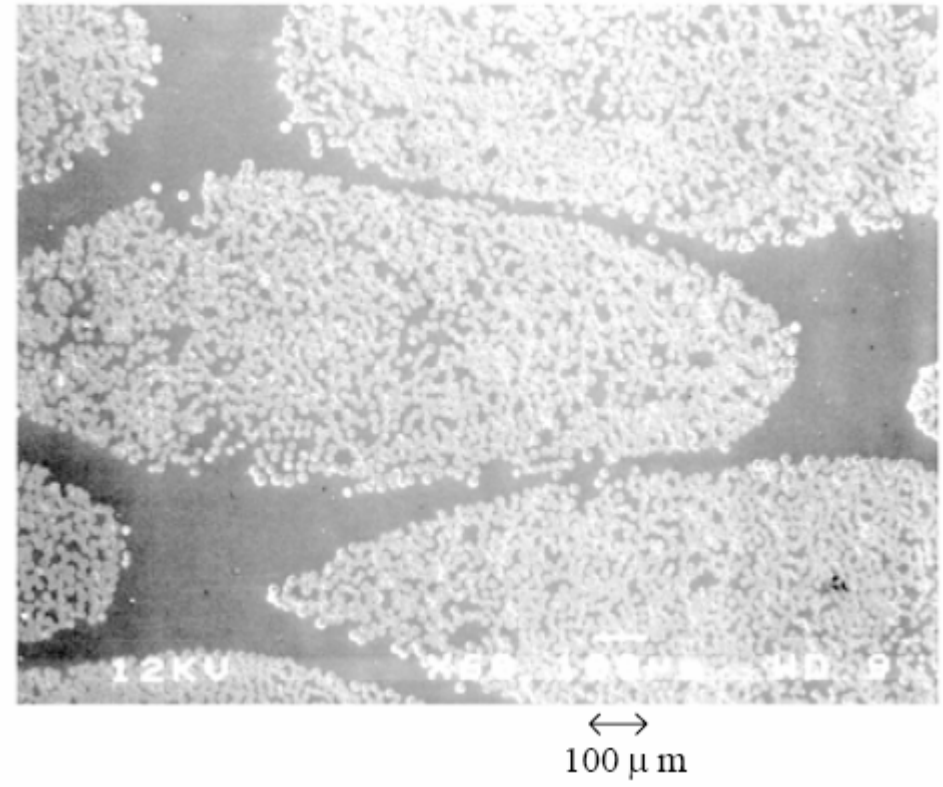

Figure 2.1 Micrograph of fibers and resin

Matrix Materials

Composites utilize many different materials to form the matrix. There are metal matrix composites, ceramic matrix composites, and polymer matrix composites. The first two can be very difficult to process, and have been used sparsely for very specific applications. The most common structural composite materials are fiber reinforced plastics, or FRPs (Schey, 2000). These materials typically use one of two types of plastic for the matrix. The first types are thermosetting plastics such as epoxy, otherwise known as thermosets. Thermosets are polymer chains infused into the reinforcement in the liquid form where they then become strongly cross-linked over a short period of time. Due to the cross-linking, these matrix materials tend to be quite stiff, and are resistant to creep. Unfortunately, they can also be very brittle (Askeland, 1994). The second type of polymer used is the thermoplastic such as

nylon. Thermoplastics are also combined with the reinforcement in the liquid form. However, they contain much longer polymeric chains which give them a very high viscosity. As a result, thermoplastics cannot be used in many of the manufacturing processes that thermosets can. The bonding structure is also different in thermoplastics. They form much weaker secondary bonds to hold the polymer chains together. For this reason, thermoplastics can be reshaped and reused to some extent. At the same time, they are also less stiff and prone to creep. One advantage of the weaker intermolecular bonds is an increase in damage tolerance.

Reinforcement Materials

The most common reinforcement materials are glass fibers. E-glass is the most widely used glass fiber and is very similar to window glass. The principal ingredient is silica (SiO_2), with additions of other oxides to improve workability and corrosion resistance. Glass reinforced plastics have a moderately high strength at a relatively low cost. Typically, bulk glass is considered to be a very “weak” material. However, this is primarily due to the presence of flaws in the glass and its low fracture toughness. Pure glass has a very high strength, but it is very brittle due to the bonding structure. Any flaws present quickly turn to cracks which can propagate with very little stress. The use of very small fibers in a plastic matrix alleviates this effect in a couple of ways. First, by using very small fibers the average flaw size in the glass is dramatically reduced. Secondly, fiber failure is isolated by the matrix. If a single fiber breaks, the crack will not propagate though the matrix, and the remaining fibers carry the load. The combination of fibers and matrix also spreads damage over a large area, which can dissipate a large amount of energy. These effects, among others, make fiberglass very strong and damage tolerant. Among

composite materials, fiberglass also has one of the lowest costs. The limitations of fiberglass are primarily due to its high density and low tensile modulus.

Carbon fibers are the second most common reinforcement, and boast one of the highest strength and stiffness to weight ratios of any material. Its primary use has been in the aerospace industry, although it is becoming more widely used in all fields. It has seen increased usage in sporting goods especially, for items such as bicycle frames and tennis rackets. Carbon fiber also has very good fatigue resistance which is important in many designs, especially wind turbines (Mandell, etc., 2002). The primary drawback of carbon fiber is the cost. Bulk glass fibers are produced for around $2/kg, while the lowest cost carbon fibers are currently about $19.80/kg (Griffen and Ashwill, 2003). This has limited the use of carbon fiber in many industries, and will continue to do so in the future. Another weakness of carbon fiber is due to its high degree of anisotropy. Because the fibers are typically oriented in a single direction or plane, the part is very stiff in that direction, but not in the other planes. For this reason, any waviness or misalignment of the fibers can cause high stress concentrations. This is particularly true in compression where any defect can greatly reduce the compressive strength (Mandell, etc., 2003).

Reinforcement Textile Preforms

Textile preforms are fibrous assemblies with prearranged fiber orientation preshaped and often preimpregnated with matrix for composite formation. The microstructural organization of fibers within a preform, or fiber architecture, determines the pore geometry, pore distribution and tortuosity of the fiber paths within a composite. Textile preforms not only play a key role in translating fiber properties to composite performance but also influence the ease or difficulty in

matrix infiltration and consolidation. Textile preforms are the structural backbone for the toughening and net shape manufacturing of composites.

When combined with high-performance fibers, matrices and properly tailored fiber/matrix interfaces, the creative use of fiber architecture promises to expand the design options for strong and tough structural composites.

Among the large family of textile structures, 3D fabrics have attracted the most serious interest in the aerospace industry and served as a catalyst in stimulating the revival of interest in textile composites. 3D fabrics for structural composites are fully integrated continuous fiber assemblies having multiaxial in-plane and out of plane fiber orientation. More specifically, a 3D fabric is one that is fabricated by a textile process，resulting in three or more yarn diameters in the thickness direction with fibers oriented in three orthogonal planes. The engineering application of 3D composite has its origin in aerospace carbon-carbon composites.

The expansion of global interest in recent years in 3D fabrics for resin, metal and ceramic matrix composites is a direct result of current trend in the expansion of the use of composites from secondary to primary load-bearing applications in automobiles, building infrastructures, surgical implants, aircraft and space structures. This requires a substantial improvement in the through-the-thickness strength, damage tolerance and reliability of composites. In addition, it is also desirable to reduce the cost and broaden the usage of composites from aerospace to automotive applications. This calls for the development of capability for quantity production and the direct formation of structural shapes. In order to improve the damage tolerance of composites, a high level of through-thickness and interlaminar strength is required. The reliability of a composite depends on the uniform distribution of the materials

and consistency of interfacial properties. The structural integrity and handleability of the reinforcing materials for the composite is critical for large-scale, automated production. A method for direct formation of the structural shapes would therefore greatly simplify the laborious hand lay-up composite formation process. With the experience gained in the 3D carbon-carbon composites and the recent progress in fiber technology, the class of 3D fabric structures is increasingly being recognized as serious candidates for structural composites.

The importance of 3D fabric reinforced composites in the family of textile structural composites is reflected in many books. This chapter is intended to provide an introduction to 3D textile reinforcements for composites. The discussion focuses on the performing process and structural geometry of the four basic classes of integrated fiber architecture: woven, Knit and braid, and orthogonal non-woven 3D structure.

2.2 Classification of Textile Preforms

There is a large family of textile performing methods suitable for composite manufacturing (Ko, 1989). The key criteria for the selection of textile preforms for structural composites are (a) the capability for in-plane multiaxial reinforcement, (b) through-thickness reinforcement and (c) the capability for formed shape and/or net shape manufacturing. Depending on the processing and end use requirements some or all of these features are required.

On the basis of structural integrity and fiber linearity and continuity, fiber architecture can be classified into four categories: discrete, continuous, planar interlaced (2D) and fully integrated (3D) structures. In Table 2.1 the nature of the

various levels of fiber architecture is summarized (Scardino, 1989).

Table 2.1 Fiber architecture for composites

Level	Reinforcement system	Textile construction	Fiber length	Fiber orientation	Fiber entanglement
Ⅰ	Discrete	Chopped fiber	Discontinuous	Uncontrolled	None
Ⅱ	Linear	Filament yarn	Continuous	Linear	None
Ⅲ	Laminar	Simple fabric	Continuous	Planar	Planar
Ⅳ	Integrated	Advanced fabric	Continuous	3D	3D

A discrete fiber system such as a whisker or fiber mat has no material continuity; the orientation of the fibers is difficult to control precisely, although some aligned discrete fiber systems have recently been introduced. The structural integrity of the fibrous preform is derived mainly from interfiber friction. The strength translation efficiency, or the fraction of fiber strength translated to the non-aligned fibrous assembly of the reinforcement system, is quite low.

The second category of fiber architecture is the continuous filament, or unidirectional (0^{o}) system. This architecture has the highest level of fiber continuity and linearity, and consequently has the highest level of property translation efficiency and is very suitable for filament wound and angle ply tape lay-up structures. The drawback of this fiber architecture is its intra- and inerlaminar

weakness owing to the lack of in-plane and out-of-plane yarn interlacings.

A third category of fiber reinforcement is the planar interlaced and interloped system. Although the intralaminar failure problem associated with the continuous filament system is addressed with this fiber architecture, the interlaminar strength is limited by the matrix strength owing to the lack of through-thickness fiber reinforcement.

The fully integrated system forms the fourth category of fiber architecture wherein the fibers are oriented in various in-plane and out-of-plane directions. With the continuous filament yarn, a 3D network of yarn bundles is formed in an integral manner. The most attractive feature of the integrated structure is the additional reinforcement in the through-thickness direction which makes the composite virtually delamination-free. Another interesting aspect of many of the fully integrated structures such as 3D woven, knits, braids and non-wovens is their ability to assume complex structural shapes.

From the point of view of preform fabrication and the macrostructural geometry of the textile preforms, textile structural reinforcements can be classified according to the axis of fiber or yarn introduction and geometric dimension (Fukuta, etc., 1984). As shown in table 2.2, the axis, or the direction of yarn introduction, is divided into 0 (or “nonaxial”), monoaxial, biaxial, triaxial and multiaxial systems for reinforcements wherein yarns are introduced from four or more directions.

Table2.2 Types of reinforcement

Dimension \ Axis		0 NON-AXIAL	1 MONO-AXIAL	2 BIAXIAL	3 TRIAXIAL	4~ MULTI-AXIAL
1D			 ROVING-YARN			
2D		 CHOPPED STRAND MAT	 PRE-IMPREG-NATION SHEET	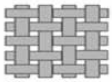 PLANE WEAVE	 TRIAXIAL WEAVE	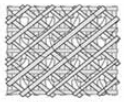 MULTI_AXIAL WEAVE, KNIT
3D	Linear Element	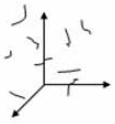	 3-D Braiding	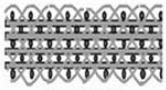 MULTI-PLY WEAVE	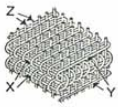 TRIAXIAL 3-D WEAVE	 MULTI-AXIAL 3-D WEAVE
	Plane Element	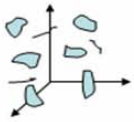	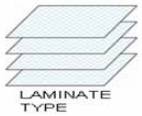 LAMINATE TYPE	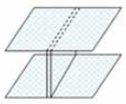 H or I BEAM	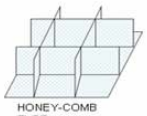 HONEY-COMB TYPE	

2.3 Processing of Textile Composites

Figure 2.2 illustrates scales in one textile process. The part shown is an integrally formed skin/stiffener assembly. The first processing step is the formation of yarns from fibers. In the second step, the yarns are woven into plain woven cloth. The cloths are then laid up in the shape of the skin and stiffener and stitched together to create an integral perform. Finally, the composite part is consolidated by the infiltration of resin and curing in a mold.

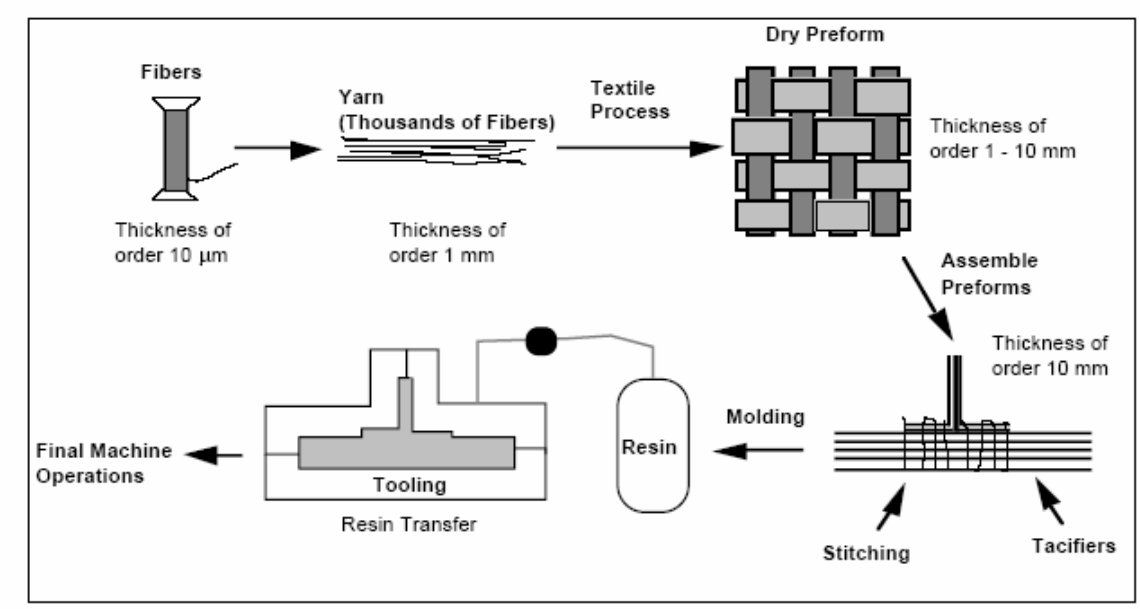

Figure 2.2 Production process of a textile composite structure.

There are many techniques available today for manufacturing thermoset composite parts. Some are still very low tech and labor intensive, while some involve very sophisticated tooling and computer controls. However, all of these processes share some of the same challenges and requirements. They all consist of a tool to hold the fabric in the correct position while the resin is curing, and require some means of forcing the resin into the fabric. The major differences in the processes are the resulting part quality, limitations in size and geometry, cost of tooling, and process time.

The most basic and labor intensive process is known as hand lay-up. In hand layup fabric is placed onto a tool where resin is applied by hand using rollers and squeegees. Each ply must be saturated as it is applied to the tool to ensure that no bubbles are left between plies. This makes hand lay-up very time consuming, but it does have its advantages. Carefully applying resin to each ply can ensure a part without dry spots. Unfortunately, the process is not performed under vacuum so

micro-porosity is possible. Hand lay-up is very attractive due to the low cost of the tooling required. Since there is no pressure applied to the tool it does not have to be very robust, and can be made out of a variety of materials. In many cases, the tool will only have one side to produce a nice finish on the outside of the part. Hand lay-up can also be used to produce very large parts. As long as there are enough people to apply the resin to the fabric before it cures, there are really no limitations on the size of the part. Hand lay-up is currently the most utilized method of manufacture for large wind turbine blades. Unfortunately, there are also many disadvantages to hand lay-up. The most obvious is the labor cost. In addition, the application of the resin in an open environment allows very volatile emissions to escape from the resin that can be harmful to humans and to the environment (Skramstad, 1999). It is anticipated that the use of hand lay-up for wind turbines will eventually be restricted due to the high volume of emissions. Other disadvantages are lower dimensional tolerances, poor fatigue performance, and less aerodynamic surfaces. Even with these considered, hand lay-up is still the fastest and cheapest way to produce a small number of composite parts with few defects, but the process is limited.

Beginning in the 1950’s, more industrialized processes began to evolve for use on aircraft. These processes are generally referred to as resin transfer molding processes, or RTM. In RTM the fabric is laid into a tool where the resin is forced into the fabric under pressure. These processes have several advantages over the hand lay-up process. The process has the potential to be more repeatable and consistent since the human involvement is reduced. This reduction in human involvement also reduces labor costs. In addition, the amount of volatile emissions is reduced. Much higher fiber contents can also be achieved since the tool can clamp down on the fiber

preform. Dimensional tolerances can also be increased if the tool is two sided Gebart, 1992). The disadvantages are the cost of the mold and the difficulty in forcing the resin through the fabric.

Modifications of the RTM process have been developed recently that reduce these disadvantages. Although there are many variants being used today, they all deal with these problems in a similar manner. Lower tool costs are achieved with the use of onesided molds. In these processes a vacuum is drawn on the fabric, while a flexible bagging is forced against the preform by atmospheric pressure. To deal with the problem of getting the resin to flow large distances through the fabric, a distribution network is used. This distribution network allows the resin to flow through high permeability channels or layers to disperse it throughout the mold. The resin must then flow a much shorter distance in the plane or though the thickness of the part. Several variants of these processes are described in detail by Larson (Larson, 2004), and will be discussed briefly here.

One process that has been successfully used on large structures is the Seemanns Composite Resin Infusion Molding Process (SCRIMP™). This process has been used since the 1980’s and its use continues to increase. There are several variations of SCRIMP™. One uses a series of channels above the fabric for resin distribution, and the resin is then forced to flow in the plane of the fabric between the channels. In other variants, a high permeability layer may be placed over the fabric for resin distribution. The resin is then forced to flow though the thickness of the fabric. This layer is then peeled off after the process is complete. SCRIMP™ is capable of producing large parts very quickly, cheaply, and with high fiber volume fractions (Han, etc.,2000).

A very similar process known as the Fast Remotely Actuated Channeling process (FASTRAC) is a more recent variation of this general principle. The main difference in the FASTRAC process compared to SCRIMP™ is a more refined distribution strategy. The distribution network is created by a “FASTRAC layer” which is a flexible membrane with tightly spaced channels formed into it. The major difference is that these channels can be collapsed to force the extra resin though the fabric or out of the mold, rather than leaving them attached to the part as in SCRIMP™. The FASTRAC layer also allows a positive pressure to be applied to the fabric to achieve even higher fiber volume fractions.

A process very similar to FASTRAC was developed by Larson which will be referred to as pressure bag molding. In pressure bag molding the distribution system is a channel that covers the whole surface of the fabric. Once the resin fills the channel, pressure is applied to a flexible film to force the resin into the fabric as in FASTRAC. In order to apply a positive pressure to the bagging, a second tool half is required. Although this adds an additional cost in the tooling, the second mold half would not require the surface finish and dimensional tolerance that the first half would. The mold for this process is illustrated in Figures 2.3 and 2.4. In these figures the flow channel is just empty space; however, it could also represent a highly permeable layer as in SCRIMP™ or FASTRAC.

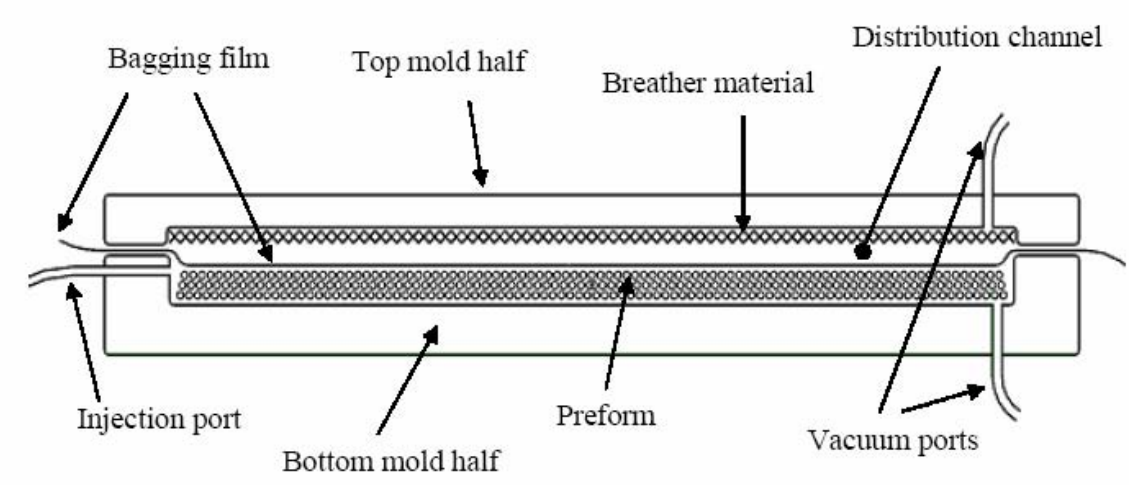

Figure 2.3 Schematic for pressure bag molding

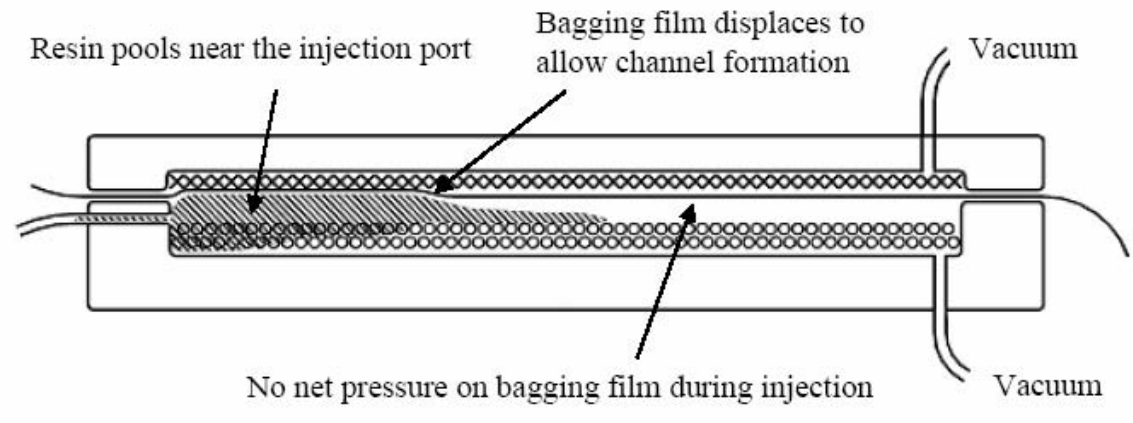

Figure 2.4: Pressure bag molding during stage one

Of the processes examined, the FASTRAC and pressure bag molding process have been identified as having the largest injected volume per port. This is due to the fact that the distribution system covers the whole part. For this reason, these processes are the most viable for large wind turbine blades, and will be the focus of this study. For future modeling this process will be described in two stages. Stage one consists of injecting the resin into the mold, and stage two is when pressure is applied to the bagging to force the resin through the thickness.

A summary of several of the processes described is presented in Table 1 which is

taken from Larson. Due to their similarity, the FASTRAC and pressure bag molding processes are presented together.

Table 2.3 Summary of manufacturing process details.

Process	Basic Principles	Advantages	Disadvantages
Hand Lay-up	Open mold Manual infusion One sided mold	Low cost Fastest implementation	Volatile emissions Health risks Inconsistent results Less efficient material usage
RTM	Closed mold In-plane resin flow Two-sided mold	Higher dimensional consistency Less volatile emissions Both sides finished	Higher mold cost Resin flow pattern critical Costly equipment required Lowest volume per port
VARTM	Closed mold In-plane resin flow Two-sided mold Evacuated mold	Higher dimensional consistency Less volatile emissions Both sides finished Higher quality products than RTM	Higher mold cost Resin flow behavior critical Costly equipment required Complexity of vacuum porting
SCRIMP™	Closed mold In-plane resin flow One-sided mold Evacuated mold	Higher dimensional consistency Less volatile emissions Higher quality products than RTM	Proprietary process One side finished
FASTRAC + Pressure Bag	Closed mold Channel flow One side critical Evacuated mold	High quality High dimensional consistency Less volatile emissions Largest injection volume per port	Added cost of FASTRAC layer or top mold half Highest complexity Possible artifacts from bag Costly equipment required

2.4 Geometry of Textile Reinforcement

2.4.1 Ideal Geometry

The geometry of a periodic textile is conveniently described in terms of unit cells, following the example of crystallography (Kittel, 1967). The unit cell is defined by the requirement that the entire textile can be constructed from spatially translated copies of it, without the use of rotations or reflections. The unit cell is not unique. Nevertheless, as in crystallography, symmetry in the textile usually suggests a preference.

2.4.2 2D fabrics

2.4.2.1 2D Weaves

Woven fabrics are probably by far the most commonly used form of textile composites in structural applications (Laroche, D., etc., 1994).They are produced principally by the multiple warp weaving method, and generally consist of two sets of interlaced yarn components, known as warp and weft (or fill) yarns according to the yarn orientation(Naik, N. K., etc., 1991). Warp yams run vertically or lengthwise in woven fabrics, while weft yarns run horizontally or crosswise(Miller, E.,1973).Each yarn is a bundle of filaments (or fibres) and its size is measured by the number of filaments in the yarn(Naik, R. A.,1995). Three-dimensional (3D) woven fabrics have additional yarns placed in through-the-thickness direction (Kuo, W. S., 1995), and can be generally classified into three types, namely, 3-d, 3-x and interlockns(Brandt, J., etc., 1990). They have higher delaminate resistance and damage tolerance than 2D woven laminates(Cox, B. N., etc., 1996). 3D woven fabrics can be produced by using either conventional looms with multilayer constructions or entirely new equipment(Du, G. W. and Chou, T. W., 1991). The interlacing pattern of the warp and weft yarns is known as weave(Naik, N. K. and Ganesh, V. K., 1992).

Currently, most of the pure and hybrid woven fabrics used in textile composites are simple 2D fundamental weaves, i.e., plain, twill and satin weaves, which are identified by the repeating patterns of the interlaced regions in warp and weft directions(Iihikawa, T. and Chou, T. W., 1982).

Woven fabrics generally exhibit good dimensional stability in the warp and weft

directions, offer highest cover or yam packing density, and provide higher out-of plane strength which can carry the secondary loads due to load path eccentricity, local bucking, etc. In addition, woven fabrics generally have a very low shear rigidity which gives a very good formability (Chou, T. W. and Ko, F. K., 1989). However, they offer anisotropy, and relatively less extensibility for deep draw moulding compared to knitted and braided fibres, and they are poor in resisting in-plane shear.

Weaves may be classified by the patterns of interlacing. The simplest pattern is the plain weave shown in Figure 2.5 (a). A disadvantage of the plain weave is the frequent exchanges of position from top to bottom made by each yarn. This waviness or yarn crimp reduces the strength and stiffness of the composite. Other weave patterns reduce the number of exchanges and increase the lengths of straight segments of yarn (known as the “float”). Of particular interest are the satin weaves shown in Figure 2.5 (b), (c), and (d). The satin weave pattern is defined by the number of yarn width between exchanges. For example, the five-harness satin weave shown in Figure 2.5 (c) has a 4-over, 1-under pattern. In addition, the exchanges are arranged so as not to connect; or in the case of the crow foot pattern (Figure 2.5 (b)), so as not to lie on continuous diagonals.

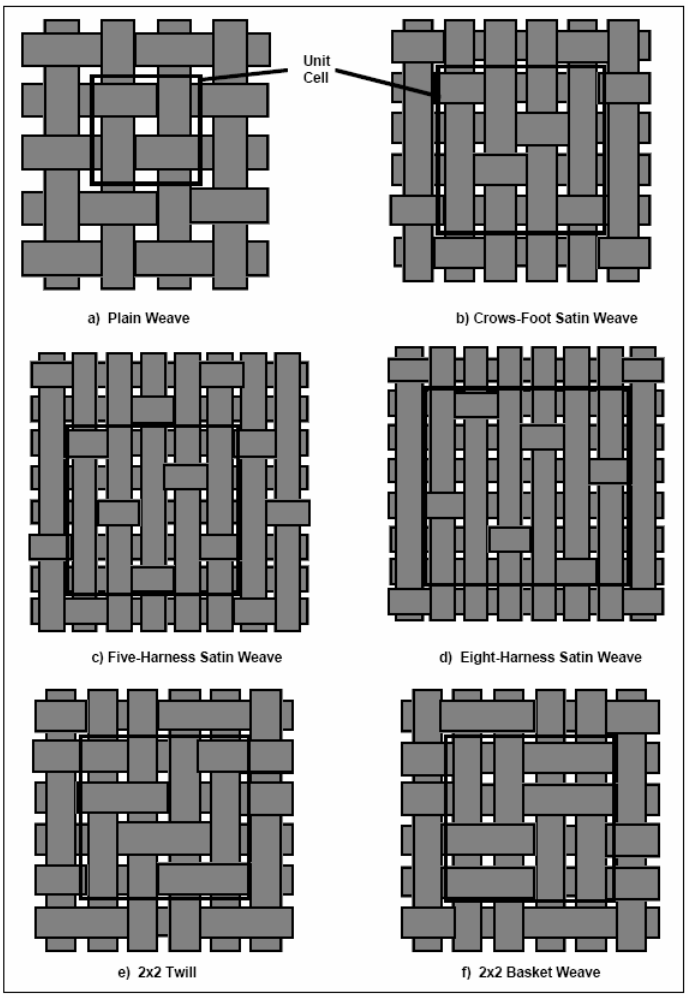

Figure 2.5 Commonly used 2D weave patterns

Individual layers of satin weave fabrics are asymmetric. One side of the fabric is predominantly warp yarns; the other is fills. Exchange sites also break symmetry because they bend yarns in an asymmetric way. Bending and stretching in a satin weave ply are consequently coupled. There is also coupling between stretching and in-plane shear, because exchange locations are not symmetric about either in-plane axis (Figure 2.6). Coupling between bending and stretching will tend to cause warping during cure because of thermal strains. Warping can be minimized in a multilayer laminate by considering which side of each ply should face the tool.

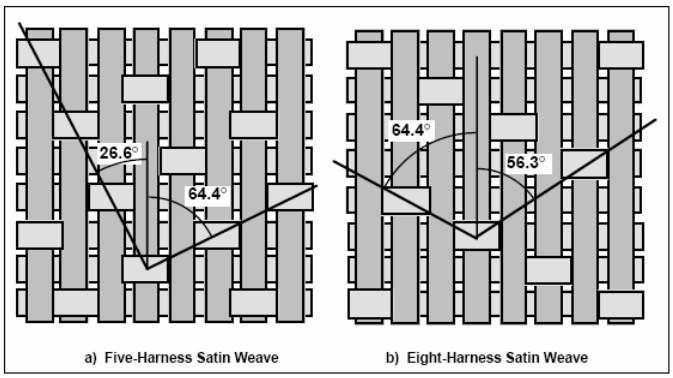

Figure 2.6 Angles of the diagonal patterns formed by exchange locations

The selection of a weave involves manufacturing considerations as well as final mechanical properties. The type of weave affects dimensional stability and the conformability (or drape) of the fabric over complex surfaces. Satin weaves, for example, exhibit good conformability. Unfortunately, good conformability and resistance to shear are mutually exclusive. Thus, while woven fabrics are frequently the material of choice for complex geometries, the designer must be aware that specified material directions may be impossible to maintain on a doubly curved surface; and initially orthogonal yarns may not remain orthogonal in the fabricated product.

Most 2D weaves involve two orthogonal directions of yarn, implying weak in-plane shear resistance within a single ply. However, triaxial weaves, in which the yarns form 60°angles to each other, have also been fabricated (Figure 2.7). A single ply of triaxial material would have approximately isotropic in-plane elasticity (Hasselbrack, etc., 1992).

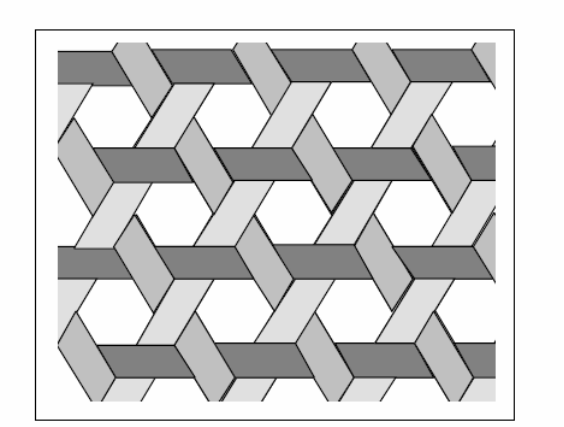

Figure 2.7 Triaxial weave

2.4.2.2 2D Braids

Braided fabrics are one of the textile composites under consideration for aircraft applications that can be used at a lower cost and provide higher impact resistant/tolerant materials. These fabrics are constructed by intertwining or orthogonally interlacing two (or more) sets of yarns to form an integral structure. One set of yarns is called axial yarns while the other is named as braided yarn(Du, G. W. and Ko, F. K., 1993; Byun, J. H. and Chou, T. W., 1996). Hence, the structures of braided fabrics consist of parallel axial yarns, interconnected with braided yarns that are placed along complex spatial orientations. Generally, braider yarns follow the + 8 and - 0 directions and usually interlace in either 1 × 1 or 2 × 2 patterns(Naik, R. A., 1994; Naik, R. A., etc., 1994). The common fabrication methods for creating braided fabrics are traditional horn-gear method, solid braiding method, two step braiding method, four-step braiding method and trackand-column braiding method. These methods differ only in the way that the yam carriers are moved (Du, G. W. and Ko, F. K., 1993).

The major parameters affecting the mechanical properties of braided fabrics

include: (1) braid parameters such as braid architecture, yam sizes, yarn spacing length, fibre volume fraction, fibre orientation angle; and (2) material parameters such as mechanical properties of the fibre and matrix (Naik, R. A., 1995). The major process parameters adjustable to control the microstructure of braids are speed ratio between braiding and taking up, linear density ratio of braider and axial yam(Naik, R. A., etc., 1994).

The integral structures of braided fabrics enable them to endure twisting, shearing and impact better. Due to their higher impact resistance/tolerance and stability or conformability under tension in the braided yarn system, the braided fabrics can be designed for multi-directional conformity. However, braided fabrics exhibit poor stability under an axial compression in the yam system direction.

Figure 2.8 (a) shows the interlacing pattern for a $\pm\theta$. bias braid. Structurally, a 1x1 braid with yarns oriented at $\pm 45^{\circ}$. is indistinguishable from a plain weave rotated by 45°. (In a 2D braid, the designation "nxn" refers to the number of bias yarns between crossover points.)

Longitudinal or axial yarns can be introduced into the braiding process to create a triaxial braid. The axial yarns are trapped within the crossovers of the bias yarns. In principle, the axial yarns can remain straight, and therefore retain much of their unidirectional properties. By controlling the relative size of the axial yarns and the angle of the bias yarns, a wide range of final properties can be obtained. As with woven fabrics, the pattern of crossovers can be controlled. Figures 2.8 (b), (c), and (d) show three possible patterns for triaxial brads. These figures show the braid patterns with gaps between the yarns for clarity; the actual braid would normally have

complete coverage.

Applications for braids can be limited by the size of the braiding machines available. A large braider has 144 yarn carriers and a bed diameter of 2.25m. Often, full coverage of the mandrel by the bias yarns alone is required on each pass to minimize gaps and resin pockets in the structure. Full coverage is obtained when (Yang and Chou, 1989)

$$w_b/\cos\theta = P/2N \quad (2.1)$$

where wb is the width of a bias yarn as it lies on the mandrel, P is the perimeter of the mandrel, N is the number of bias yarn carriers in operation, and θ is the angle between the bias yarns and the longitudinal axis of the structure. A less severe constraint is for full coverage on a pass including the area covered by the axial yarns.

In that case, full coverage is obtained when $w_L + w_b / \cos\theta = P / 2N$ (2.2)

Where wL is the width of an axial yarn. The maximum width of the yarns is controlled by several parameters, including the linear density of the yarn, the degree of twist (twisting a yarn tends to prevent flattening), and the size of the carrier guides. The last factor imposes an upper limit to the width of approximately 5 mm.

The minimum and maximum braid angles are limited by the phenomenon of jamming, which is related to the maximum shear distortion that can be put on a fabric. Jamming also limits the ratio of the minimum and maximum radii of the mandrel.

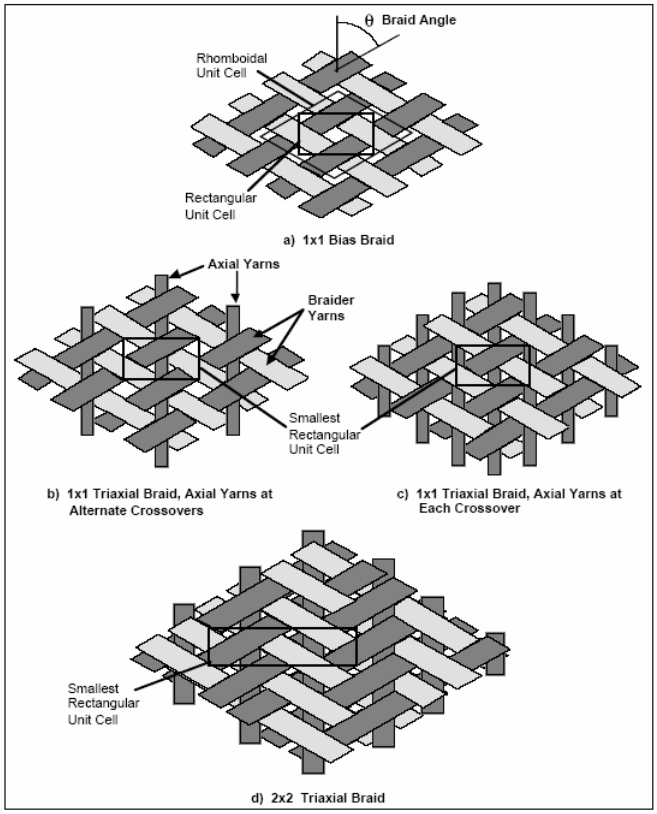

Figure 2.8 Some common 2D braid patterns.

The total thickness of a braided part may be controlled by overbraiding, in which multiple passes of the mandrel are made through the braiding machine. This lays down a series of nearly identical layers, similar to a lamination. For 2D braiding, there is no mechanical connection between the layers.

2.4.2.3 2D Knits

Knitted fabrics are characterized by their interlocking loops of yarns (Curiskis, J. I., 1996). Generally knitted fabrics can be divided into 2 types, i.e., the weft-knitted and warp-knitted fabric composites. In the weft-knitted fabric, yarns widthwise, and loops are formed by a single weft yarn (Fujita., Yokoyama, A. and Hamada, H., 1995). A row of loops in the longitudinal direction is called ‘wale’ or ‘warp’, and that in the width direction is named as ‘course’ or ‘weft’. In the warp-knitted fabric,

overlaps in alternative wale at alternate courses are produced with one thread crossing between adjacent wales in which loops incline in the course direction.

The major parameters affecting the mechanical properties of knitted fabrics are knit architecture, mechanical properties of yarns in both wale and course directions, matrix (or resin) properties. fibre volume fraction and yam orientation angle(Ruan, X. P. and Chou, T. W., 1996).

Compared to other conventional textile fabrics, knitted fabrics possess high productivity and low cost. In addition, knitted fabrics have high extensibility which means good formability to fit in complicated shapes(Chou, S. and Wu. C. J., 1992). Hence, they are quite suitable for deep draw moulded composites. Compared to woven fabric composites, knitted fabric composite exhibited a better resistance to impact4'. Knitted fabrics are not often used as reinforcement in composites unlike the woven and braided fabrics. This is because knitted fabric composites have lower in-plane mechanical properties than the conventional composites due to the low fibre volume fraction and the loop configuration of fibres(Wu, W. L., etc., 1993).

Knits fabrics are usually made by interlooping one or more yarns and offer a much wider range of forms and behaviors than wovens. Simple fill (or weft) and warp knit constructions (Figure. 2.9 a) provide considerable extensity in all directions and therefore are quite suitable for deep-draw molded composites. They can also be added to a woven or braided preform for specific directional extensibility and good stability. In this case, the knitting threads are passed around the primary yarns and one another in interpenetrating loops as shown in Figure. 2.9 b.

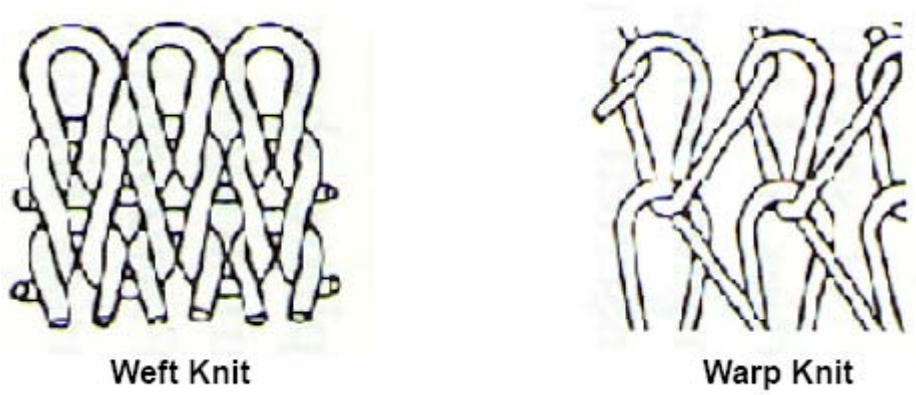

(a)

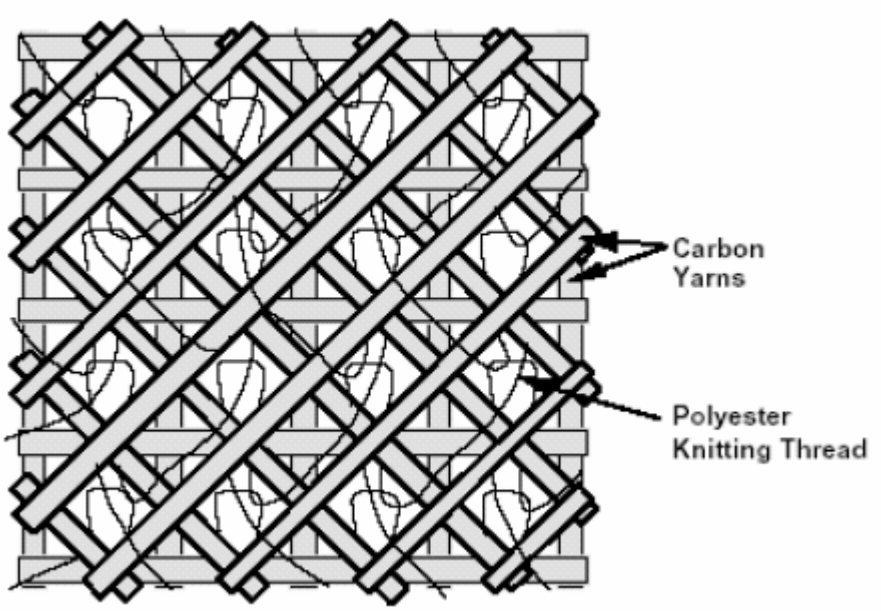

(b)

Figgure 2.9 (a) Simple warp and weft knits; (b) Multi-axial warp knit insertion

Knit fabrics offer higher yarn-to-fabric tensile strength translation efficiencies, greater in-plane shear resistance and better handling than comparable wovens. The process of knitting can also be used to provide through-thickness reinforcement in composite structures. The process, called stitching, significantly enhances damage tolerance and often represents a helpful step in the fabrication of textile structural

composites. Figure 2.10 shows the two forms of stitching that are of interest for structural applications: the modified lock stitch and the chain stitch.

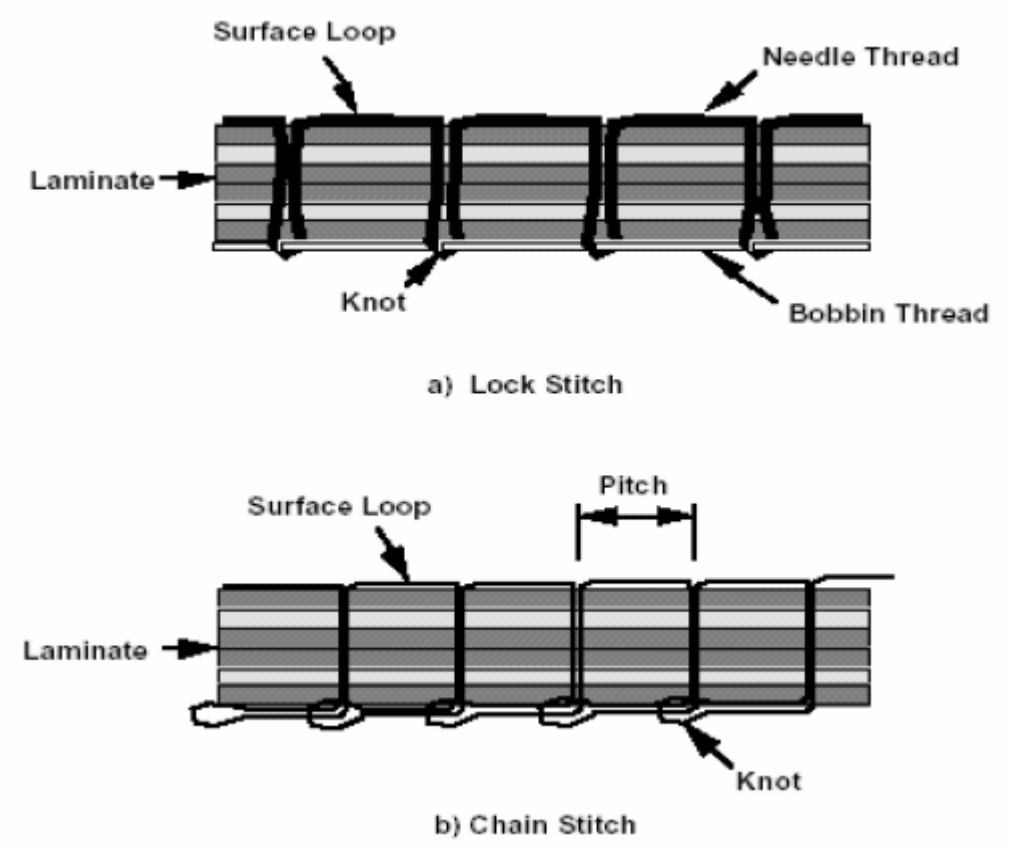

Figure 2.10 Types of stitching used for through-thickness reinforcement: Weft Knit; Warp Knit

2.4.3 3D Fabrics

The structural geometry of 3D textiles can be characterized at both the macroscopic and the microscopic levels. At the macroscopic level, the external shape and the internal cellular structures are the result of particular textile process and fabric construction employed in the creation of the structure. Similar shape and cellular geometry may be created by different textile processes. For example, a net shape I-beam can be produced by a weaving, braiding or knitting process. However,

the microstructure or the fiber architecture produced by these three processes is quite different. This will lead to different levels of translation efficiency of the inherent fiber properties to the composites as well as different levels of damage-resistant characteristics. The efficient translation of fiber properties to the composite depends on the judicious selection of fiber architecture which is governed by the directional concentration of fibers. This directional fiber concentration can be quantified by fiber volume fraction V_f and fiber orientation, θ. Depending upon the textile manufacturing process used and the type of fabric construction, families of V_f-θ functions can be generated. These V_f-θ functions can be developed by geometrical modeling as detailed by Ko and Du(Ko, F.K. and Du, G.W., 1989). Accordingly, the structure-property relationship of 3D textile composites is a result of dynamic interaction of microstractural and macrostructural geometries. In this section, the structural shapes, cellular structures and fiber architectures expressed in terms of V_f-θ functions are presented for the four basic classes of 3D textile reinforcements.

2.4.3.1 3D Weaves

Three-dimensional woven structures have a number of distinct advantages over their 2D counterparts and these are outlined below:

- 3D weaving can produce near net shaped preforms;
- 3D woven composites with complex geometry can be less expensive to produce;
- 3D weaving allows the tailoring of properties for specific applications;
- 3D woven composites show better delamination resistance and damage

tolerance.

3D weaving takes a number of different forms, orthogonal, layer interlock and multi-axis woven textiles. Weaving of these technical textiles can be achieved quite easily with minor modifications to standard weaving machinery used to manufacture cloth for textile applications. The 3D weaving process involves the integration of z-axis or through-the-thickness yarns or tows within the structure of a multi-layer dry reinforcement. The binding of the 3D structure is normally achieved through the use of warp yarns. The nature of the design process for these structures allows the designer/engineer to weave properties into different areas of the reinforcement, hence facilitating the tailoring of the mechanical properties of the composite.

A 3D woven reinforcement, a form of technical textile, is comprised of warp and weft stuffers that are bound together by a series of warp binder tows. Various arrangements of tow placement are used to produce a wide range of multi-layer 3D reinforcements for composite applications. These are broadly categorised under two distinct headings:

- integrated structures, in which binder tows link one layer to any other layer within the textile structure;
- interlinked structures, in which the binder tows link the outer two layers, top to bottom.

In 3D weaving, a number of the warp (or 0° direction) tows provide through-the-thickness reinforcement to consolidate the preform. The through-the-thickness tows are arranged in different areas and levels of the reinforcement according to the net shape and mechanical properties required. These

through-the-thickness tows have been shown to provide increases in interlaminar shear strength of composite components. [Quinn J.P, 2001]

3D woven fabrics are produced principally by the multiple-warp weaving method which has long been used for the manufacturing of double and triple cloths for bags, weddings and carpets. A 3D weave contains multiple planes of nominally straight warp and weft yarns that are connected together by warp weavers to form an integral structure. The most common classes are shown in Figure 2.11. Within each class, there are several parameters that can be varied.

The angle interlock type of structure is a variation of 2D weaving wherein more than two yarns are in the thickness direction. The angle interlock structure allows the preform to be up to 10 cm in thickness. In this fabric, warp yarns are used to bind several layers of weft yarns together. Weft yarns could be used for binding as well. In place of warp or weft yarns, an additional third yarn may also be used as binder. Stuffer yarns, which are straight, can be used to increase fiber volume fraction and in-plane strength. Angle interlock weaves can be categorized by the number of layers that the warp weavers penetrate. Figure 2.11 (a) shows a through-the-thickness interlock fabric, in which the warp weavers pass though the entire thickness. Figures 2.11 (b) and (c) show layer-to-layer interlock patterns, where a given weaver connects only two planes of weft yarns, but the weavers collectively bind the entire thickness. Various intermediate combinations can be fabricated, with the weavers penetrating a specified number of layers.

In orthogonal interlock weaves, the warp weavers pass through the thickness orthogonal to both in-plane directions, as shown in Figure 2.11 (d).

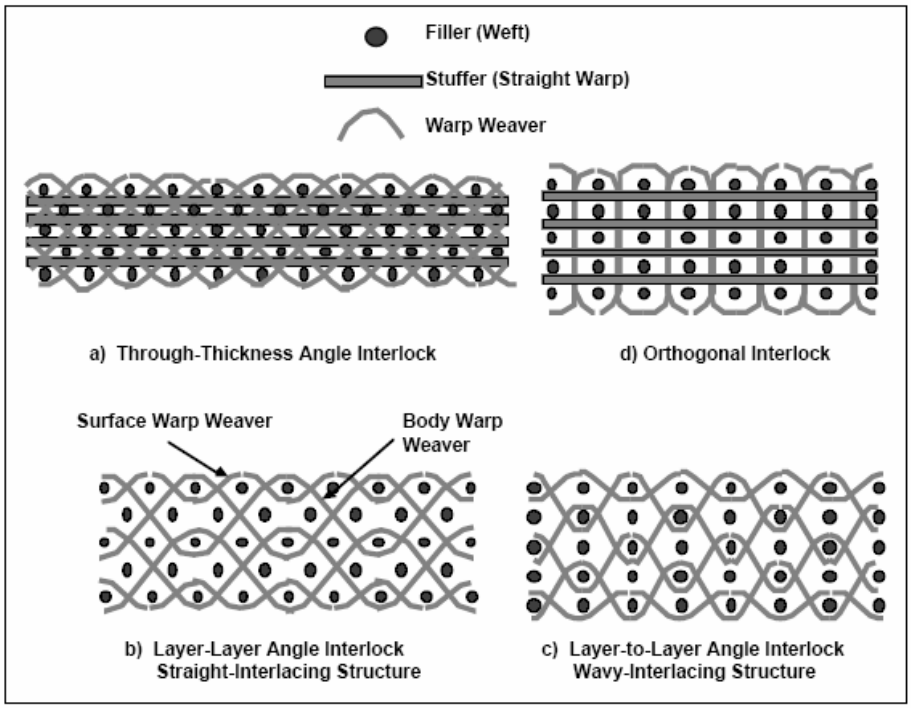

Figure 2.11. Three-dimensional weave patterns.

Interlock weaves are sometimes manufactured without straight warp yarns (stuffers) to produce a composite reinforced predominantly in one direction. They may also be fabricated with weft rather than warp yarns used for interlock.

A major limitation of 3D weaves is the difficulty of introducing bias direction yarns to achieve in-plane isotropy. One solution is to stitch additional 2D fabric plies oriented at 45° onto the woven preform.

As illustrated in Figure 2.12 (Pastore and Cai, 1990a), there are four basic components to a generalized three-dimensional woven fabric geometry: warp, web, fill and surface weave yarns. Warp yarns are the system of yarns which run in the machine direction and have no crimp. These are also called ’stuffer’ yarns or ’longitudinals’. Because of their very low crimp, these yarns provide the primary strength and stiffness in the longitudinal (x) direction of the material. Web yarns run

in the machine direction and provide the interlacing necessary for fabric integrity. These yarns contain crimp in the through thickness direction, providing the z-directional properties of the system. These yarns are sometimes called ‘weavers’. The ‘weave angle’ of the web yarns refers to the angle of orientation of the web yarn with respect to the warp direction. Fill yarns are perpendicular to machine direction and interlace with the web yarns. These yarns are sometimes called ’picks’. These yarns also possess crimp in the through thickness direction, but this crimp is negligible compared to that of the warp yams for these fabric systems. These yarns provide the transverse (y) directional properties of the composite system. Surface weave yarns run in the machine direction and form what is essentially a two-dimensional weave on the surface of the fabric. Surface weave yarns are incorporated into the structure when the web yarns are insufficient to provide a smooth surface on the face and back of the cloth. These yarns experience crimp in the through-thickness direction. When surface weave yarns are employed in the fabric, there are two yarns for every warp plane of the fabric. This system of yarns contributes the least to the mechanical properties of the composite.

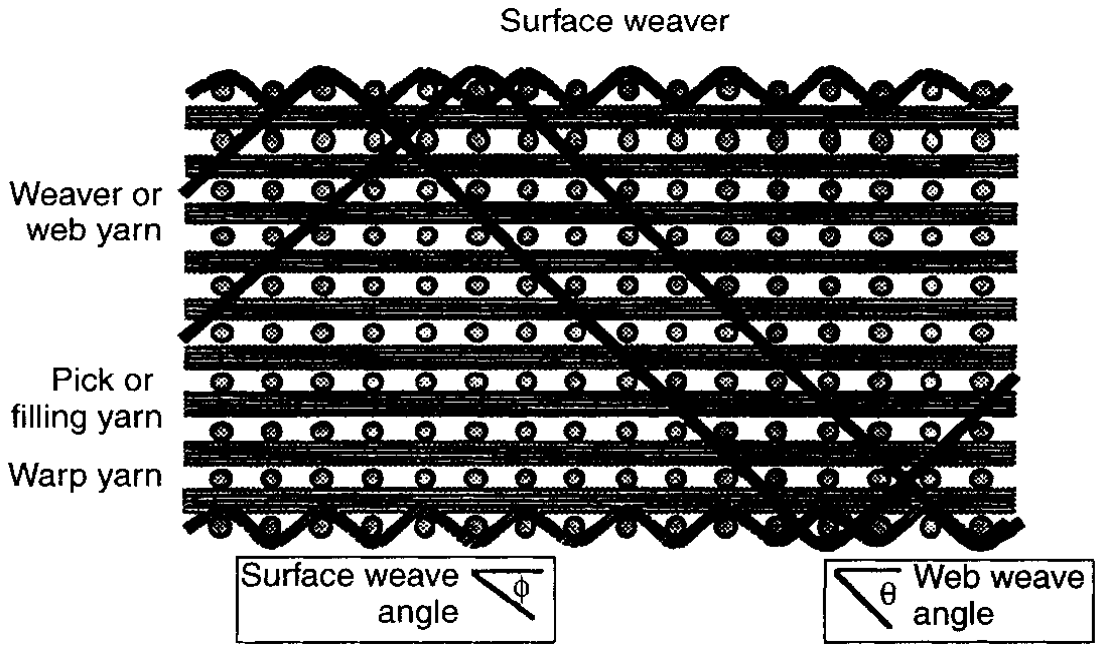

Figure 2.12 Schematic illustration of generalized 3D woven fabric projected to the x-z (fabric length-thickness) plane.

Figure 2.13 gives the unit cell geometry for plain biaxial weave, as proposed by Dow and Ramnath (1987). In their analysis, Dow and Ramnath assumed circular yarn cross-section, the same yam diameter and pitch length for both fill and warp yarns. The expression of the fiber volume fraction was derived:

$$V_f = (\frac{\pi}{4})k \frac{\frac{2L}{d} + 4\theta}{(\frac{L}{d})^2 (\frac{T}{d})} \qquad (2\text{-}3)$$

where K is the fiber packing fraction, d is the yarn diameter, L is the pitch length, T is the fabric thickness, I is the dimension shown in Figure 2.13. The yarn inclination angle to the fabric plane, θ, is given by:

$$\theta = \tan^{-1}\frac{2}{\sqrt{(\frac{L}{d})^2 - 3}} - \tan^{-1}(\frac{d}{L}) \quad (2\text{-}4)$$

The fabric thickness is very close to two yarn diameter, i.e

$$T=2d \quad (2\text{-}5)$$

and approximately:

$$\frac{l}{d} = \frac{1}{\tan\theta} \quad (2\text{-}6)$$

Equation (2-3) is then simplified to

$$V_f = (\frac{\pi}{4})k\frac{\frac{1}{\tan\theta} + 2\theta}{(\frac{L}{d})^2} \quad (2\text{-}7)$$

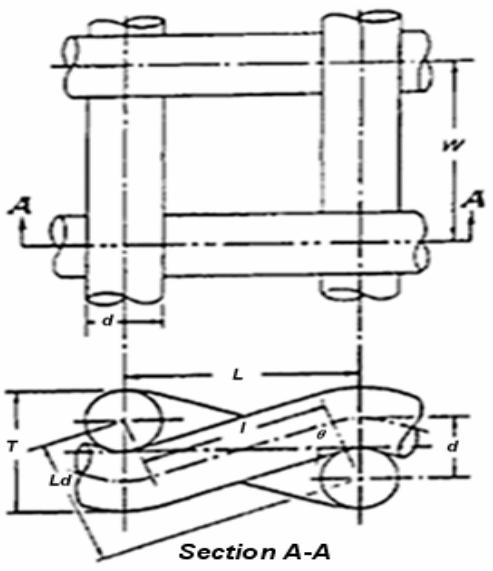

Figure 2.13 Unit cell geometry of plain weave.

The above analysis is given only for the simplest of woven structures. Different weave patterns, non-circular yarn cross-sectional shape, different yarn dimensions

and pitch lengths for fill and warp yarns can be analyzed.

Based on the structural geometry shown in Figure 2.13, the orientations and volumetric distributions of all yarns in the 3D weave can be calculated also using the unit cell method. Detailed analysis is given by Ko and Du (1992).

Sabit also presented a three-dimensional models of fabric reinforcements for composite components by using computer aided geometric design (CAGD) techniques. In his study, a novel approach to structural representation of fabric preforms is described in both parametric and graphic forms. The philosophy behind the development of the computer generated model of composite fabric reinforcement is discussed. The model can produce a 3D representation of any 2D and 3D fabrics.[Sabit Adanur and Tianyi Liao, 1998]

In woven fabrics, the three main types of single layer weave geometry are plain, twill and satin weave and in each case the warp and the weft yarns are oriented at 0° and 90°, respectively. The 3D CAGD models of typical weaves can be illustrated in graphic forms in Figures 2.14.

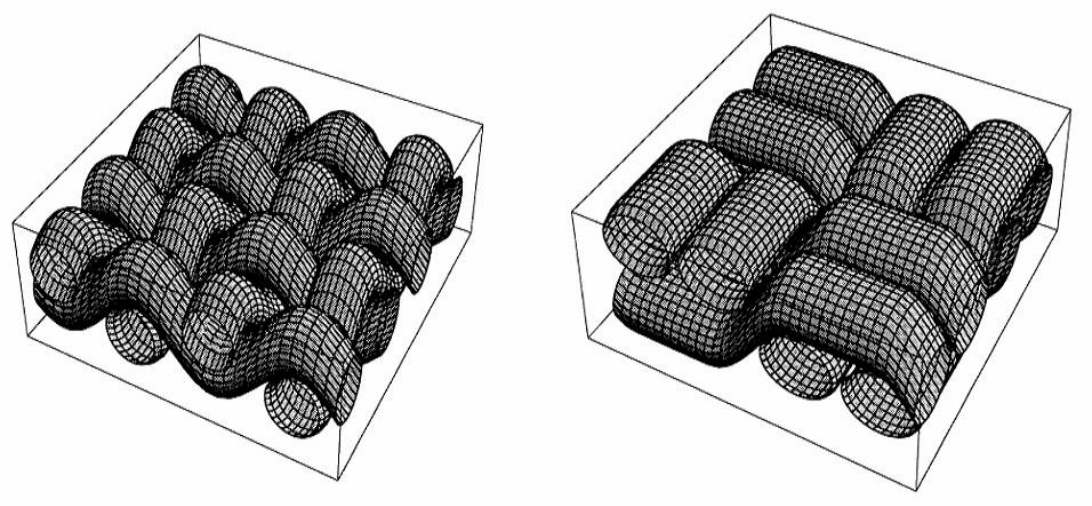

(a) plain woven fabric (b) 2/2 basket woven fabric

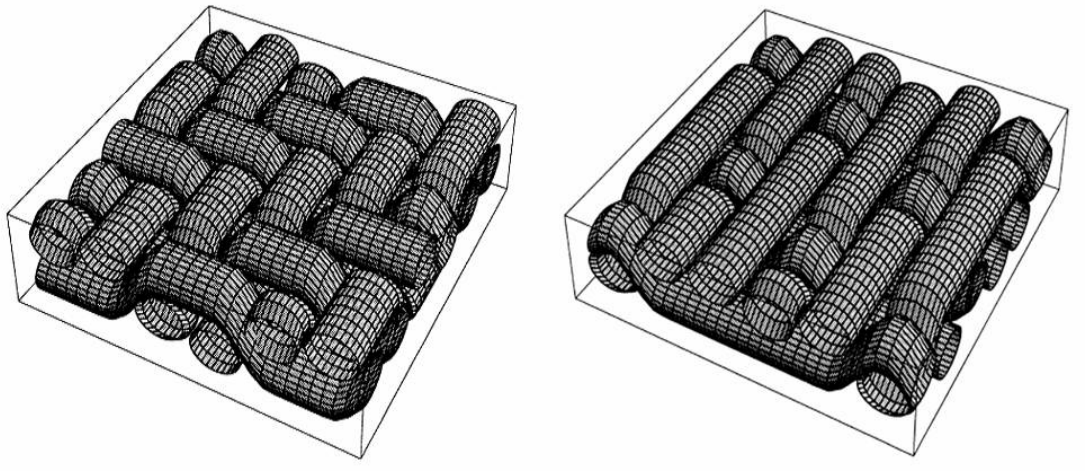

(c) balanced 2/2 twill fabric (d) five end satin with a counter of three

Figure 2.14 3D model for woven fabrics

For plain weave, one warp alternately crosses over and under consecutive weft yarns, while the next warp yarn crosses under and over the wefts. The pattern is classified as 1/1 and is illustrated in Figure 2.14(a). Plain weave gives the highest frequency of yarn interlacing, hence the highest level of structural integrity and a greater extendibility to the fabric, due to the high degree of bending or crimp of the fibers and yarns. One permutation of the simple plain weave is basket weave, where two warp yarns interlace with two weft yarns as shown in Figure 2.14(b).

Twill weave is characterized by two or more warp yarns crossed by a weft yarn, with a progression of interlacing of one weft yarn to the right or left to form a distinctive diagonal line. Twill weave can be even-sided, i.e. the same amount of warp and weft faced, or with a predominance of warp or weft yarns on the upper surface. Due to the weave geometry, this type of fabric may exhibit anisotropic elastic properties. An even weave, with each warp crossing two wefts and vice versa, is classified as a 2/2 twill and is shown in Figure 2.14(c).

Figure 2.14(d) is a five end satin with a counter three, in which the weft has longer

float and the warp is embedded below the surface. For a satin weave fabric, each weft yarn crosses at least four warp yarns and interlaces with the fifth warp yarn, with a progression of interlacing to the left or right. Satin weave fabrics, due to the low level of interlacing, have the lowest structural integrity of the woven fabrics and the highest level of fiber volume fraction, and hence have the highest level of fiber to composite translation strength.

Textile composites, i.e., composites fabricated using reinforcements made with textile preforming processes, combined with cost effective composite fabrication such as resin infusion, are being researched and developed at an ever increasing pace. The form and architecture of the fibrous reinforcement is perhaps the single most important component determining both the performance and cost in a textile composite material. The increasing interest and use of textile composites, particularly 3D textile composites, is attributed to two factors: 1) improved performance due to controlled fiber distribution; and 2) lower cost through the use of automated textile processing equipment. One of the most promising recently developed textile processes is a new form of 3D weaving [Brandt, J., 1992; Dickinson, L.C., 1999] being commercialized under the trademark 3WEAVE™ by 3TEX, Inc. With completely controlled and tailorable fiber orientations in the X, Y and Z directions, the ability to weave aramid, carbon, glass, polyethylene, steel fibers, etc. and any hybrid combination, thickness up to one inch (2.54 cm), width up to 72 inches (183 cm) and the ability to make net shapes, an almost infinite number of 3WEAVE materials are possible with a tremendously wide range of performance [Mohamed, M. H., 2001]. Although these materials are typically more expensive than 2D fabrics and mats, reduction of labor, higher performance and improved

process efficiency result in overall cost savings in a variety of applications. When compared on a cost per square foot of finished composite structure, 3WEAVE reinforcements consistently outperform traditional 2D materials.

Traditional 2D weaving has been around for thousands of years. 2D weaving is a relatively high-speed economical process. However, woven fabrics have an inherent crimp or waviness in the interlaced yarns, and this is undesirable for maximum composite properties. Most of the marine and wind blade industry currently use glass non-crimp stitch-bonded or knitted fabrics, more properly known as multi-axial-warp-knits. These materials are cost-competitive. However, they do not conform well to complex forms and often have significant fiber distortion in the final composite. A fully automated 3D weaving process with simultaneous multiple filling insertions, has been developed at the NC State University College of Textiles [Dickinson, L.C. and M. H. Mohamed, 2000]. This process is inherently 3D from the onset, and does not involve the building up of layers one layer at a time. Rather, a single unit of thick fabric is formed during each weaving cycle. The essence of the innovation/patent centers around this simultaneous multiple insertion from one or both sides of the fabric.

Preforms made by the 3WEAVE™ process provide several important advantages in composites fabrication. The most obvious advantage of this material shows in manufacturing thick composites, owed to a dramatically reduced labor time, when multiple layers of 2D fabric plies are replaced by one or few number of 3WEAVE plies to obtain the required thickness in a composite structure. In many cases, a single 3WEAVE layer can replace multiple 2D layers [Singletary, J.N. and A.E. Bogdanovich, 2001].

It is natural to expect that the processing advantages of thick 3WEAVE preforms come at the expense of reduced conformability. In fact, it has been demonstrated that these preforms conform as well or better than the most conformable 2D fabrics. The absence of interlacing between warp and filling yarns allow the fabric to bend and internally shear rather easily, without buckling within the in-plane reinforcement [Mohamed, M. H., 2003].

2.4.3.2 3D Braids

The 3D braiding technology is an extension of the well-established 2D braiding technology wherein the intertwining or orthogonal interlacing of two or more yarn systems to form an integral structure constructs the fabric. The 3D braiding is one of the textile processes in which a wide variety of solid complex structural shapes can be produced integrally resulting in a highly damage-resistant structural preform.

Braided fabrics are formed by the intertwining of yarn systems and can be obtained in a variety of forms with laidin yarn systems. At any time one half of the yarns are travelling in one direction at some angle to the axis down the fabric, while the other half are travelling in the opposite direction, passing over and under the strands of the first group. Figure 2.15(a) shows a braid fabric plaited by five strands. Braided fabrics have yarns interlacing at angles other than 0° and 90°. For a yarn orientation of $\pm 45^\circ$ interlacing is half that for the plain weave. This results in better adoption of fiber properties by the composite fabric due to reduced crimp. Therefore, braiding is one of the major manufacturing processes for textile composite preforms although braiding is not a major manufacturing process for traditional textiles relative to weaving and knitting.

In comparison to woven structures, due to the lack of beat-up during braid formation, braided fabric structure usually has low shear resistance and therefore highly deferrable in axial and radial directions. This characteristic of braided structures makes it particularly suitable to conform to surfaces of varying cross-sectional shapes such as cones and nozzles, and allows the production of near-net shape structures. Hence, interest in braiding has grown for composite manufacturing in recent years.

Figure 2.15(b) shows the local yarn structure in a circular braid consisting of three yarn systems. Two groups of yarns, one having an angle of ¹v and other having an angle of þv to the mandrel axis, interlock to form a biaxial fabric. As an option, a third group of yarns mounted on the back side of the track ring of a braiding machine can be inserted through the center of each horn gear. These yarns are deposited onto the mandrel in the axial direction. Clearly, the angle made by this group of yarns is 0 ° to the mandrel axis. All three groups, namely ± θ and 0°, form a biaxially interlocked braid as shown in Figure 2.15(b).

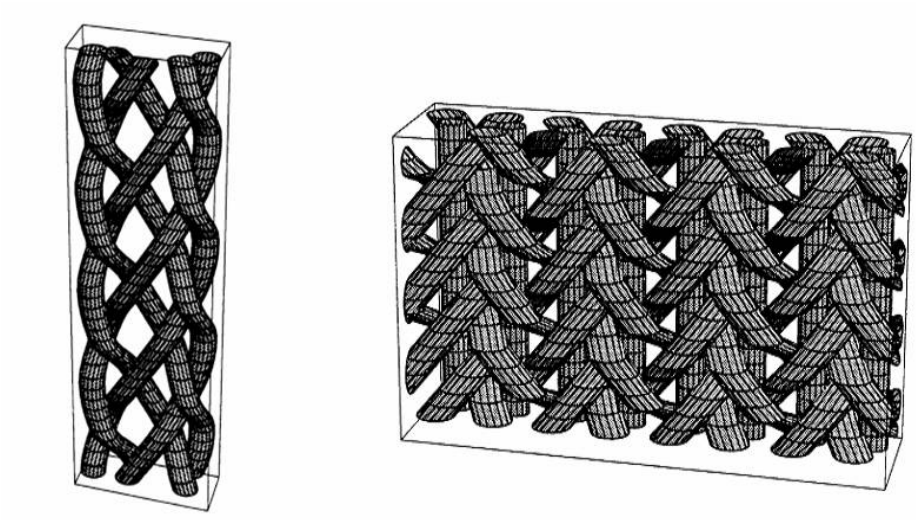

(a) flat braided fabric (b) circular braid fabric

Figure 2.15 3D model for braided fabrics

The 3D braids are produced by a number of processes including the Track and Column (3D circular loom) method (Brown, etc., 1989), the two-step braiding method (Popper and McConnell 1987), and a variety of displacement braiding techniques. The basic braiding motion includes the alternate X and Y displacement of yarn carriers followed by a compacting motion. The proper positioning of the carriers and the joining of various rectangular groups through selected carrier movements accomplish shape formation. Examples of the structural shapes successfully demonstrated as shown in figure 2.16.

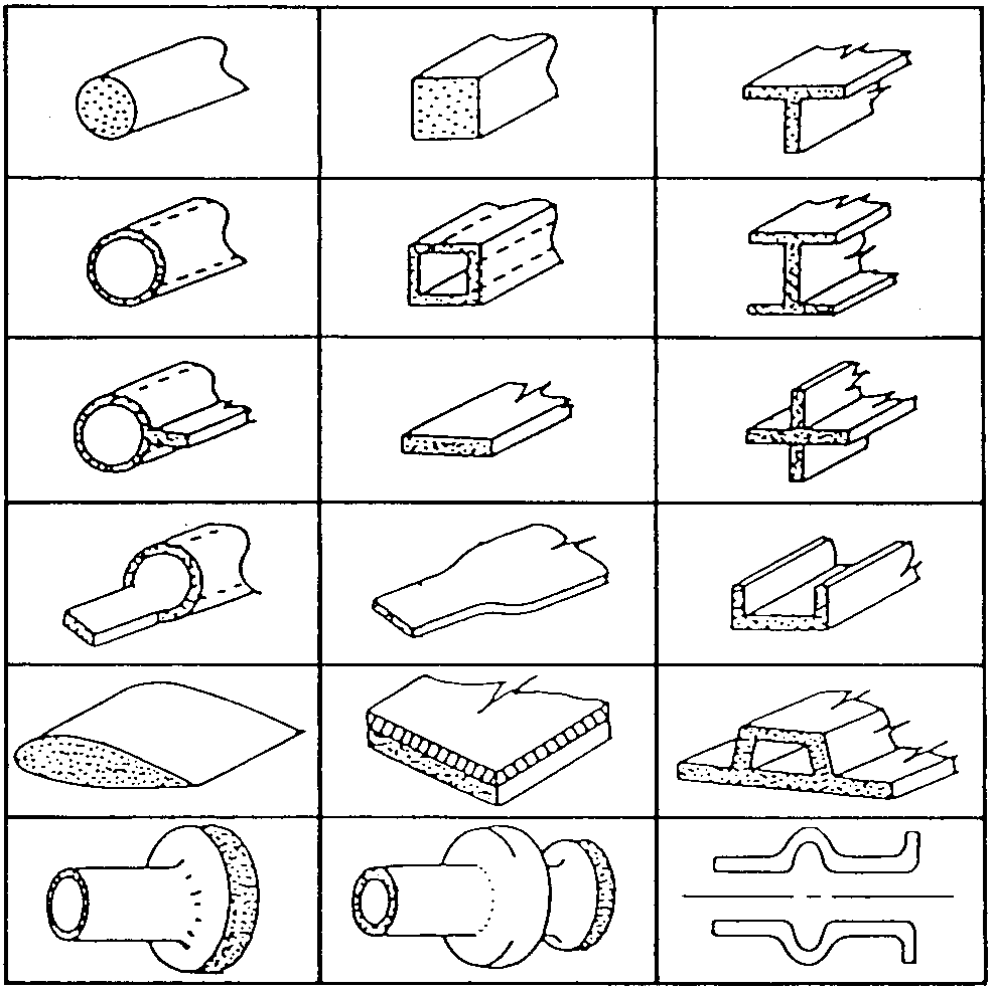

Figure 2.16 Examples of net shape structures 3D braiding

2.4.3.3 3D Knitted Fabrics

Knitting is the interlocking of one or more yarns through a series of loops (also called stitches). The lengthwise columns of stitches corresponding to the warp in woven fabrics are called wales, the crosswise rows of stitches corresponding to the filling are known as courses. Knitted structures can be classified by basic loop formation mechanism into weft knits and warp knits. In weft knitting, yarn feeding and loop formation occur at each needle in succession along the wale direction and all the courses of loops are composed of single strands of yarn. In warp knitting, there is a simultaneous yarn-feeding and loop-forming action occurring at every needle and all the wales of loops are composed of single strands of yarn.

Stitch (loop) formation is similar in both weft and warp knitting. In a knitting operation, each of the needles is controlled by a cam to rise and fall in synchronization with the other needles. Detailed description of the knitting technology can be found in Spencer (1983) and Raz (1987).

Knitted 3D fabrics are produced either by weft or warp knitting. An example of a weft knit is the near net shape structure knitted under computer control by the Pressure Foot®process (Williams, 1978). In a collapsed form this preform has been used for carbon-carbon aircraft brakes. While weft knitted structures have applications in limited areas, multiaxial warp knit (MWK) 3D structures are more promising and have undergone a great deal more development in recent years. Schematic of a MWK LIBA system is given in Figure 2.17, in which up to six layers of insertion yarns plus one layer of non-woven can be stitched together.

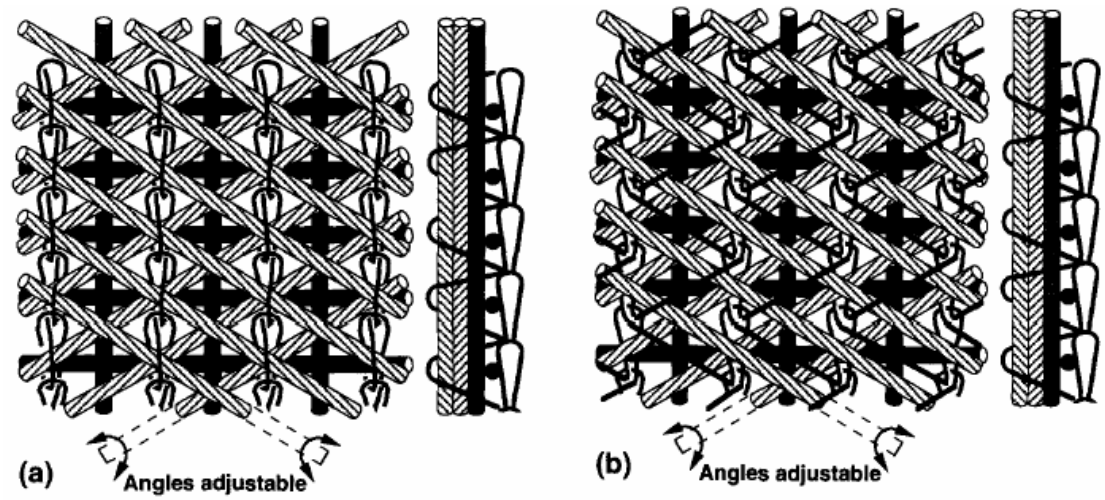

Figure 2.17 Multiaxial warp knit with four layers (0°, 90° and $\pm\theta$) of inserted yarns and (a) chain stitch or (b) tricot stitch.

In the search for methods to reduce composite manufacturing costs, textile preforms including knitted structures are receiving increasing interest in the composite industry. While conformability and productivity are obvious attributes for knitted preforms, the availability of a broad range of micro- and macrostructural geometries has only recently been recognized. The non-linearity of knitting loops, severe bending of yarns during the knitting process and limited fiber packing density resulting in the formation of resin pockets within a knitting loop prevent knits from being considered for structural applications.

The MWK fabric system consists of warp (0°), weft (90°) and bias ($\pm\theta$) yarns held together by a chain or tricot stitch through the thickness of the fabric, as illustrated in Figure 2.18 Theoretically, the MWK can be made to as many layers of multiaxial yarns as needed, but current commercially available machines only allow four layers (the Mayer system) of 0°, 90°, $\pm\theta$ and 4 insertion yarns, or six layers (the LIBA system) of 2(90°), 0°, 2($+\theta$) and 2($-\theta$) insertion yarns to be stitched

together. All layers of insertion yarns are placed in perfect order each on top of the other in the knitting process. Each layer shows the uniformity of the uncrimped parallel yarns. The insertion yarns usually possess a much higher linear density than the stitch yarns and are therefore the major load bearing component of the fabric.

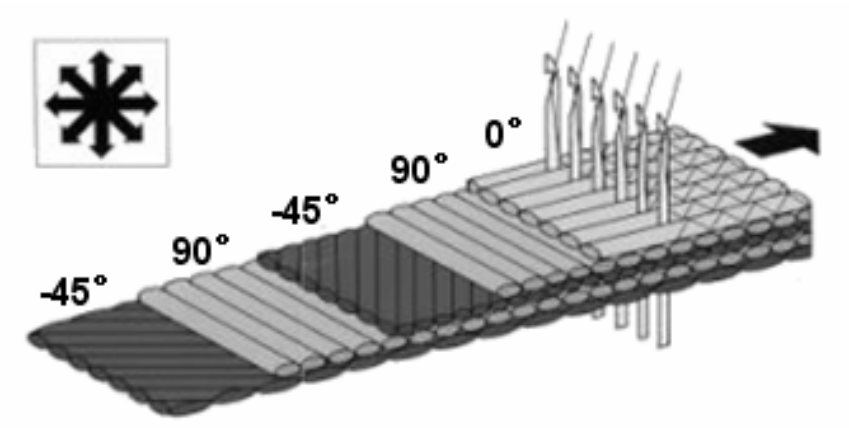

Figure 2.18 Multiaxial warp knit system

2.4.3.4 Orthogonal Nonwoven Fabrics

There is a long history of 3D, non-woven reinforcements, primarily in carbon-carbon composites. Orthogonal 3D materials are fabricated by fixing a series of yarns in one direction (or rods which will later be withdrawn and replaced by yarns), and then inserting planar yarns in the two orthogonal directions around the fixed yarns.

Pioneered by aerospace companies such as General Electric, the non-woven 3D fabric technology was developed further by fibre Materials Incorporated. Recent progress in automation of the non-woven 3D fabric manufacturing process was made in France by Aerospatiale (Pastenbaugh, 1988), SEP (Geoghegan 1988) and Bruno

(Bruno, et al,1986) and in Japan by Fukuta and co-workers (Fukuua, et al 1982 & 1986).

The structural geometries resulting from the various processing techniques are shown in figure. 2.19. Figure 2.19(a) and (b) show the single bundle XYZ fabrics in a rectangular and cylindrical shape. In figure 2.19 (b), the multidirectional reinforcement in the plane of the 3D structure is shown. Although most of the orthogonal non-woven 3D structures consist of linear yarns in a non-linear manner, as shown in Figure 2.19 (c) ,(d) and (e) can result in an open lattice or a flexible and conformable structure.

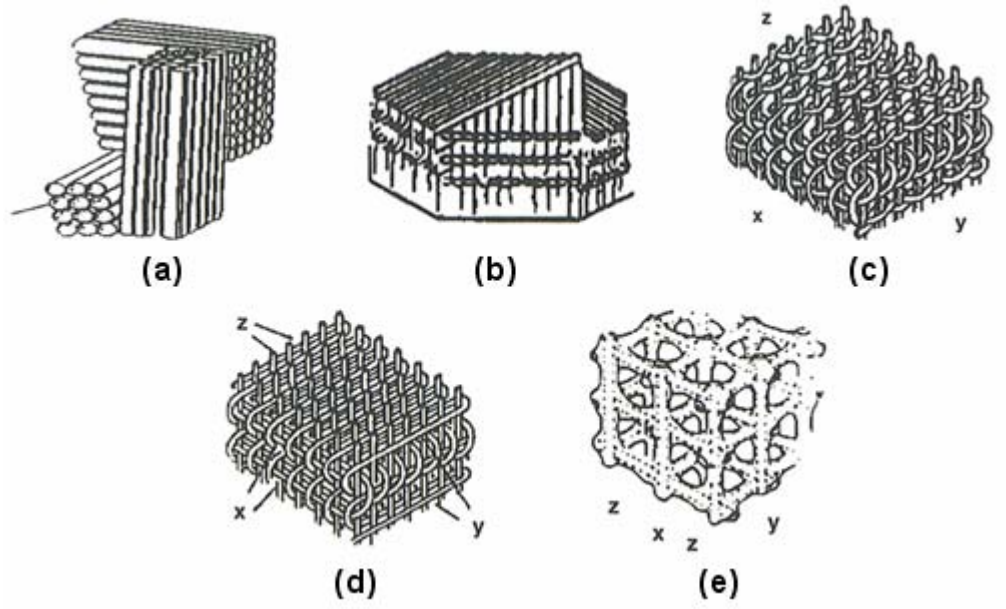

Figure 2.19 Orthogonal woven fabrics

As shown in figure 2.20 is a typical arrangement of fiber bundles that might be obtained in this process. Unlike other textile forms, the reinforcement remains relatively straight throughout the preform in all directions. This pattern of reinforcement requires volumes of pure matrix material to fill the substantial interstitial areas created by the fiber bundles. The problem of shaping and arranging

straight elements in several directions while maximizing the volume they occupy is an interesting one (Maistre, 1980).

The concept of multiple direction linear reinforcement can be extended to a larger number of non-orthogonal fiber bundle orientations. These are termed nD materials (in a somewhat loose use of the term dimension) For example; a 4D material could be created with fiber directions that connect the diagonal corners of a cube. There can be significant strength advantages to using a 4D or 5D material when shear and multidirectional loading are considered (Naik, 1994)

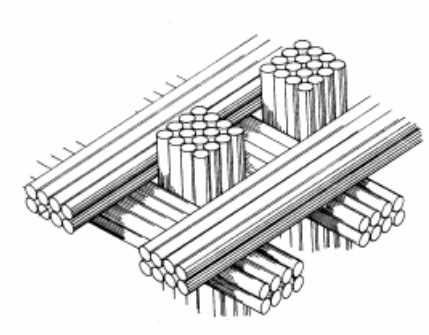

Figure2.20 3D orthogonal fabrics.

The unit cell geometry of orthogonal non-woven fabrics is shown in Figure 2.21.

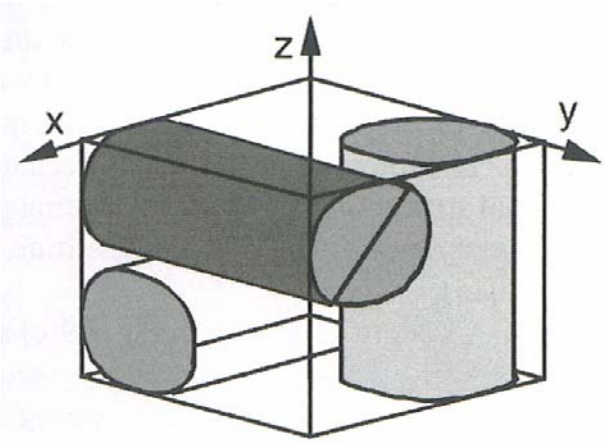

Figure 2.21 Unit cell for orthogonal non-woven fabrics

2.5 Conclusion

Txtile structural composites offer a wide range of shapes, architectures and manufacturing processes. In the choice between textile composites and conventional tape laminates, we have to weigh the advantages and disadvantages of each option in terms of weight, performances and the ease and cost of fabrication.

Textile structural composites often possess a good tailorability and good drapability. Moreover, most of the textile composite preform can be manufactured on highly automated machines (e.g loom for woven fabrics, mandrels for 2D braids) already used in the textile industry. This allows a production at low cost and a high productivity.

In terms of mechanical properties, textile composites have interesting advantages over unidirectional laminates. Indeed, laminates made from unidirectional layers have no fibres in the thickness direction. The layers are usually preimpregnated tape. On the other hand, textile composites are characterised by their 3D architecture. The interlacing yarns of most textiles either pass completely or go through the textile and give true through-the-thickness reinforcement. Compared to laminates, some textiles might have lower in-plane properties but manage to give a good balance between in-plane and out-of-plane properties.

The fabrication process of textile composites also illustrates fairly high utilization of the axial stiffness and strength of the fibers. The fibers in the skin are arranged approximately in-plane and straight and with reasonably high volume fraction. High in-plane composite stiffness and strength can therefore be expected.

In addition, textile preforms have much to offer in the toughening and manufacture

of next generation high-performance structural composites. With a large family of high performance fibers, linear fiber assemblies, and 2D and 3D fiber architectures, a wide range of composite structural performances may be tailored to meet specific requirements.

An examination of the literature indicated that only a limited number of systematic studies have been carried out on 3D multilayer woven fabrics (3D MWF composites). A well-established data base is needed to stimulate the usage of fabric-reinforced products for structural applications.

The literature suggests a trend toward using 3D fiber architecture for structural toughening composites which poses important technical challenges. One of challenges is the question of converting high-modulus yarns to textile structures. The processing difficulty with brittle fibrous structures calls for an innovative combination of materials systems such as the concept of material and geometric hybridization.

The infiltration or placement of matrix material in a dense, 3D fiber network also creates new challenges and demands an understanding of the dynamics of the process-structure interaction. Questions that must be answered relate to the optimum preform geometry for matrix infiltration, the pore distribution, and the pore size.

To take advantage of the attractive features that textile structural composites offer, a sound data base and design methodologies need to be developed. The fabric geometry models developed so far established a necessary, but not entirely complete, first step in the modeling of 3D fiber network. Future work in the modeling of fabric-reinforced composites requires a better understanding of the dynamic

interactions among fibers, matrix processing condition, and fiber architecture.

Chapter 3

Permeability test

3.1 Introduction

Three-dimensional multi-layer woven fabrics are becoming increasingly important owing to its excellent performance: permeability, compressibility, drapeability, ease of handling, ability to conform to complex shapes. Three-dimensional multi-layer woven fabrics are textile structures having fibers oriented along the three directions of a unit cell. A three-dimensional fabric should have three or more yarns in the thickness direction in order to distinguish itself from a planar fiber assembly.

On the other hands, resin transfer moulding (RTM) is becoming the most popular manufacturing process for composite materials because of its ability to manufacture complex-shaped parts at low-pressure operating conditions. However, the use of resin transfer moulding as an economic and efficient means of producing high-performance fibre-reinforced composites is critically limited by the properties of the fabrics employed.

As discussed in the descriptions of the material parts, tradeoffs between the desired final properties and the processability of a part must be made in material selection. The practical aspects of the choice of a preform include a number of issues.

The first is permeability, which is a measure of the ability of the resin to flow through the preform. Permeability can be highly directional (anisotropic), a serious concern for mold design in terms of the placement of inlets and vents. Permeability is directly affected by the amount of compaction of the preform in the mold as well

as the preform architecture.

Another issue is compressibility. Some compressibility of the preform is desirable and necessary for the reinforcing fibers to be properly distributed through the mold. However, a high degree of compression improves the mechanical properties of the part at the expense of permeability.

Next, handling, or more specifically, ease of handling -- in terms of cutting, stacking and insertion of preform plies -- is a serious concern in moderate to high-volume production modes.

Drapeability, or the ability for the reinforcement layers to conform to curvature in the mold is a factor of the choice of reinforcement forms -- that is, random mat, woven, etc. Drapeability must be considered for molds with significant curvature.

Finally, strength, stiffness and fiber volume fraction must be considered. From the view of the ultimate properties, particularly for strength and stiffness, a very high fiber volume fraction might be desirable. The limiting factor is the effective permeability of such tightly packed preforms which seriously impacts the processability in the RTM.

In this study, we have focused on the permeability, especially the permeability of Multi-layer Woven Fabrics. A framework for flow permeability measurement in resin transfer molding will be concerned. Darcy law is used to model the flow through the reinforcement fibers where the permeability is a measure for the resistance of the fibers to the flow. For a successful process modeling it is essential to test permeability reliably.

3.2 Resin Flow in Fabrics

3.2.1 Darcy Flow

The flow of resin through the fabric is governed by Darcy's law, which is very similar to the resulting equation for channel flow. Darcy's law expresses the flow of the fluid through the fabric by relating the velocity to the pressure drop, and the fabric permeability, which is a conductance, to the flow. The permeability is actually a second order tensor, meaning its value depends on the direction of the flow.

For a porous medium having a permeability of 1 Darcy, a fluid with a viscosity of 1 cps will flow at 1 cm^3/sec per 1 cm^2 cross section with a pressure drop of 1 atm per cm length.

The equation of Darcy law:

$$v = \frac{q}{A} = -\frac{k}{\mu}\frac{\Delta p}{\Delta L} \quad (3\text{-}1)$$

v = velocity cm/s

q= flow rate cm^3/sec

A = cross section cm^2

μ = viscosity cps

k = permeability cm^3 flow/sec(cps)(cm length)/(cm^2(area))(atm pressure drop)

p = atmospheric pressure

L = length cm

Chapter 3 Permeability test

Darcy unit = $cm^2 \cdot cps/sec \cdot atm$ = 1 Darcy

The permeability characterizes the porous material in terms of resistance to the fluid flow for a given injection pressure. The greater the value of permeability, the faster the resin permeates through the fibrous reinforcement. In the case of an isotropic fabric, the permeability tensor reduces to a single scalar. The most general situation of orthotropic reinforcement requires three values k1, k2 and k3 for the permeability in the principal directions of the material. However, most RTM moulded parts are thin shells and the preform does not consist of a multi-layer reinforcement. So it is not always necessary to determine the through-thickness permeability k3. The purpose of this study is essentially to measure the first two principal permeabilities k1 and k2, the so-called in-plane permeabilities (Pierre Ferland, et al, 1996).

For flow through the fabric, it is extremely difficult to calculate the permeability constant (K) by knowing only the geometric information. Micro-models exist for estimating the permeability of a fabric given fiber diameters, fiber spacing, and other relevant information(Cairns, etc., 1999; Delerue, etc., 2003; Simacek and Advani, 1996). However, these models are very complex and have varying accuracy. In addition, there must still be tests performed in order to determine some of the parameters needed as input to the models. The most accurate and direct way to determine the permeability is through testing. By knowing the velocity, pressure drop, and viscosity of a fluid moving through a fabric the permeability can be calculated. Because most RTM modeling has been done for closed mold processes, the permeability in the plane of the fabric was typically of the greatest concern (Rossell,2000; Ferland. etc., 1996; Lai, etc., 1997; Adams and Rebenfeld, 1991). For

this reason, the majority of available permeability data is for flow in the plane. For the two-stage processes such as pressure bag molding and FASTRAC, the most important value is the permeability through the thickness. This is because the distribution channel covers the surface of the fabric so all the in-plane flow occurs in the channel and the flow in the fabric is primarily though the thickness. For a process such as SCRIMP™ where there may be a large spacing between the flow channels the in-plane permeability would be more important. The in-plane permeability can be either higher or lower than the through thickness value depending on the fabric type and compaction pressure. Parnas et al. have found in general the in-plane permeability in the direction of the fibers is 6-8 times larger than it is for through the thickness (Parnas, etc., 1997). However, if the flow in the plane is transverse to the fibers the permeability could be expected to be close to the through thickness value or possibly even less.

3.2.2 Saturated vs. Unsaturated Flow

Darcy's law was originally intended for modeling saturated flow of water through soil (Darcy, 1856). Because of this, it has some deficiencies when modeling unsaturated flow though a fabric. In order to use it to model this type of flow it must be modified slightly. In calculating the permeability, the velocity is determined by dividing the flow rate by the cross sectional area. The area used is the total flow area of the fabric. This means that the velocity in Darcy's law is the superficial velocity, or the velocity averaged over the whole area. Due to the presence of the fabric, the actual flow area is less than the total area. This means that the actual velocity of the fluid through the preform is higher than the superficial velocity because the flow area is reduced. This reduction in flow area can be determined by knowing the fiber

volume fraction of the fabric. Actually, the term commonly used is called the porosity (e) of the fabric which is one minus the fiber volume fraction. The modified equation becomes:

$$v_{actual} = -\frac{k}{\mu_e}\frac{dp}{dz}$$

Another additional term required to model unsaturated flow is the capillary pressure. This is a consequence of the wicking behavior of the fabric caused by surface tension. This tends to pull the resin along, which results in a higher apparent pressure than the applied pressure. The -dP term will be replaced by ΔP, recognizing the pressure drop is linear, and that the flow occurs from high to low pressure. Darcy's law is modified accordingly.

$$v_{actual} = -\frac{k}{\mu_e}\frac{(\Delta P_{app} + P_{cap})}{dz}$$

Where:

ΔP_{app} is the drop in fluid pressure

P_{cap} is the capillary pressure

The capillary pressure is dependant on properties of the fabric and the resin. One equation for determining the surface tension as presented by (Ahn, etc., 1991) is

$$P_{cap} = \frac{F}{D_f}\frac{1-e}{e}\sigma\cos\theta$$

Where:

F is the form factor

σ is the surface tension

D_f is the diameter of a fiber

cosθ is the wetting angle

The fiber diameter, porosity, and form factor are all properties of the fabric, while the surface tension is a property of the resin. The wetting angle is a property of the resin and fabric. Its value can vary depending on the measurement method. For the most accurate results in an infusion process, the dynamic contact angle is the most appropriate (Skartsis et al, 1992). It is measured as the fluid is moving in relation to the solid interface. Both an advancing and receding angle can be determined. However, the static contact angle gives a very good approximation for the resin systems used in RTM, and is easier to measure. Fortunately, the wetting angle is only dependent on the fabric material and not on the fabric architecture. Therefore, once the fabric properties are known for a given fabric, the capillary pressure can be calculated for any resin with that fabric if its surface tension and wetting angle are known. The form factor depends on the fabric architecture and whether the flow is along the fibers or transverse. Transverse flow typically has a form factor with a value from one to two. The porosity is included because as the porosity decreases, the surface area to volume ratio increases, which increases the capillary pressure. Capillary pressure is not very temperature dependent since both the contact angle and surface tension are very weak functions of temperature .

Although the capillary pressure is typically much smaller than the injection pressure, it can change the results of a test by a noticeable amount. Some researchers have

claimed that the capillary effect was negligible in their permeability tests while others have claimed capillary pressures had a significant effect (Parnas, *et al*, 1995). The extent of this effect is going to vary depending on the fabric, the resin, and the injection pressures. Luo et al. conducted a study on the capillary pressures of a silicone oil and corn syrup with a couple of fabrics. The largest capillary pressure they found was approximately 5 kPa for the silicone oil and was less for the corn syrup although they did not give a specific value. This is consistent with the result found by Rossell for the capillary pressure of a polyester resin transverse to the fibers of 3 kPa (Luo, *et al*, 2001).

Another phenomenon of unsaturated flow arises from the fact that there is flow occurring between the fiber tows as well as within them. During a saturated permeability test, the flow in both these regions is factored into the total permeability. Because of the presence of macroscopic channels between tows and microscopic channels within them, a fabric is commonly referred to as a dual scale porous media. The consequence of this dual nature in unsaturated flow is that the flow in the macroscopic channels will advance much faster than the inside of the tows can be saturated. Cairns et al. found that the equivalent permeability of the channels between tows could be an order of magnitude larger than the permeability within the tow. This effect is shown in Figure 3.1.

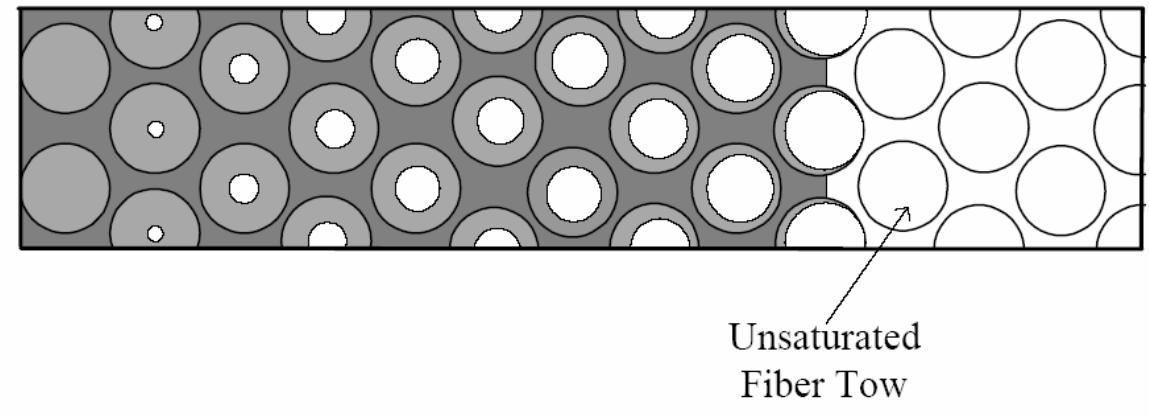

Figure 3.1: Illustration of dual scale flow.

This can be a problem in modeling as well as for part quality. Acheson et al. found that the effect on flow modeling was minor (Acheson, *et al*, 2004). This is mostly due to the fact that this only occurs at the flow front, and not in the saturated regions. It was determined, however, that this could have a large impact on part quality. This is why the use of a vacuum pump has become so critical in reducing porosity in RTM processes. The use of a vacuum reduces the amount of air that is trapped as the resin encircles a fiber tow.

3.2.3 Fabric Compressibility

Fabric compressibility is very important in all RTM processes, and affects both the material and processing properties of the part. As the fabric is compressed by fluid pressure or the mold surface the fibers get compacted and the fiber volume fraction increases. This decreases the thickness of the part, decreases the permeability, and decreases the porosity. Compressibility is possibly more important to understand in one-sided molding processes than in closed-mold processes. In a closed mold process the permeability and fabric thickness are fixed at a certain value which is determined by the mold gap. Throughout the process the permeability is a constant and independent of the injection pressure. In one-sided molding processes the

compaction of the fabric can lead to several important phenomena. In processes where the flow is in the plane of the fabric such as VARTM and SCRIMP™, a part with non-uniform thickness can be created since the net compaction pressure varies throughout the mold.

In processes where the resin is forced though the thickness, the pressure applied to the fluid is also the pressure compacting the fabric. Therefore, the permeability and fabric thickness can change throughout a process and depend on the pressure at which the process is taking place. This can create an interesting competing mechanism in these types of processes. According to Darcy's law, an increase in pressure will increase the velocity of the fluid though the fabric. However, increasing the pressure of the fluid will increase the compaction pressure and lower the permeability. It could be possible in certain cases for an increase in pressure to increase injection time, although this is not common. For most fabrics the decrease in thickness tends to compensate for the decreased permeability in through thickness flow. The effect of compaction on permeability is very dependant on the fabric architecture, which means some fabrics are more affected than others.

Fabric compaction also affects the porosity of the fabric, which will affect the saturation time for unsaturated flow. This fact adds yet another complication to the problem. Although permeability decreases with compaction, the decrease in porosity can increase the velocity of the fluid through a preform. Decreasing the porosity also increases the capillary pressure. However, in most cases these effects are minor.

As a fabric is compressed there are three distinct regimes that have been identified. The first is where the spacing in the fabric caused by the stitching and weaving is compressed. This occurs at very low pressures, and results in fiber on fiber contact.

This region is also very linear in nature. In the second regime, both the solid and the voids are compressed. This is the most complex region, and is the most studied. Very complex models have been generated to predict the behavior of the fabric in this region. Although the fibers are touching, they are still moving due to fiber bending, slippage, and nesting (Bickerton, *et al*, 2003). The third region is where the fabric has been fully compressed. Most fabrics are fully compressed with 1-2 MPa pressure. In the third regime, all the fibers have been manipulated into a stable position and cannot be moved any further. The only compression occurring in this regime is due to the solid material compressing. Many fabrics have compressed to half their original thickness by this point.

3.3 Permeability

Permeability is a key aspect in the fabrication of the fiber reinforced composites. Therefore, the strength of the composites and mold filling during the injection step would be influenced. And the relevant problems, such as the formation of dry spots or voids within composites in the fabrication, are truly tough to overcome, particularly in the case of multi-layer woven fabrics. In order to solve these problems, it is essential to investigate the relationship between permeability and the microstructure of three-dimensional multi-layer woven fabrics.

The RTM process consists of placing fiber-reinforcing preforms composed of many layers into a mold cavity, closing the mold, and then injecting the resin into the mold cavity. After the resin cures, the mold is opened and the net-shaped part is removed. (Chui, *et al*, 1997 & Cairns, *et al*, 1999)

Proper mold filling requires proper positioning of the inlets and outlets, close

monitoring of mold temperature and filling pressure, and selection of optimum resin flow rate. If inlet pressure or resin flow rate is set too high, fiber wash-out could occur (Um and Lee, 1991).

Furthermore, the permeability of preforms could be affected by the porosity. Porosity is that the fraction of volume that is open in preforms. And then, a high viscosity fluid will take more force to push through the pores than a low viscosity fluid.

3.3.1 Permeability as a function of weaves type

There are hundreds of possible woven fabric combinations, which can be divided into biaxial and triaxial woven structures according to in-plane fiber orientation.

The plane weave has the highest frequency of yarn interlacing, whereas the satin weave has the least number of yarn interlacing, with the twill weave somewhere in between. Accordingly, woven fabrics have a higher level of structural integrity and greater ductility due to the crimp geometry produced by yarn interlacings. On the other hand, the satin weave has the highest level of fiber to fabric strength and modulus translation efficiency, due to the low level of yarn interlacing and yarn linearity. The low level of yarn integration in satin weave also allows freedom of yarn mobility, which contributes to higher fiber packing density and consequently higher level of fiber volume fraction (Frank and Guang, 1997).

Open weave results in higher porosity and higher permeability. However, closed weave mats are difficult to penetrate, but offer relatively higher strength and module.

For the three-dimensional multi-layer woven fabric, the more porous or open preform structures have higher values of permeability and can be easier filled. The

difference between open weave and closed weave is shown as Figure 3.2.

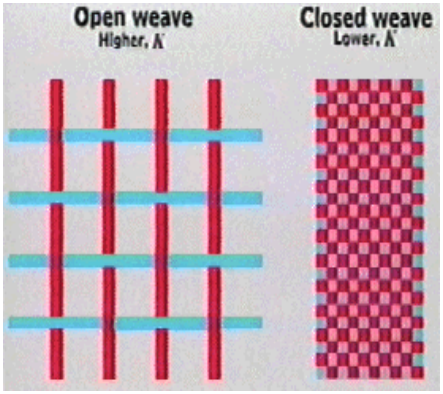

Figure 3.2 The difference between open weave and closed weave

3.3.2 Direction of Permeability Measurement

The permeability tensor is represented by its components K*xx*, K*yy*, as the in-plane permeabilities, and K*t*, as the transverse permeability (Advani, 1995).

Bear showed at 1972 that effective (or directional) permeability in three dimensions follows the shape of an ellipsoid. Six independent measurements are required to determine the permeability tensor.

The first channel flow experiment to measure principal permeability is conducted in an arbitrary coordinate system x, y, z along the x-axis (Weitzenbock and Wilson, 1998).

For the permeability, there is some directional character in such anisotropic preforms, three values for the permeability may be required – K*xx*, K*yy*, K*zz*. And then, in isotropic preforms, one value is sufficient. – K = K*xx* = K*yy* = K*zz*. The directional characteristics of K*xx*, K*yy*, K*zz* are shown as the Figure 3.3.

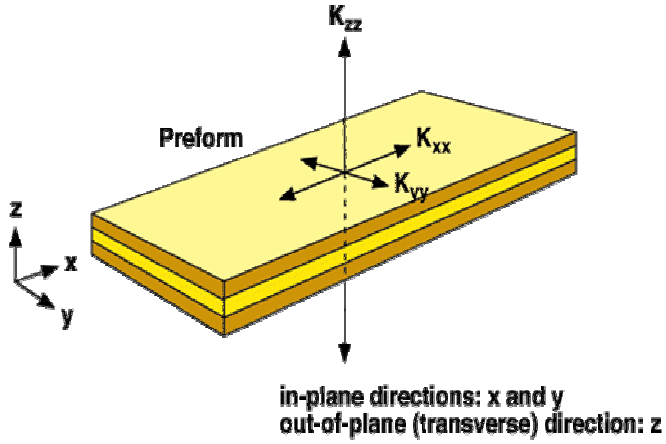

Figure3.3 The directional characteristics of Kxx, Kyy, Kzz

3.3.3 Isotropic and Anisotropic Permeability

For isotropic materials a circular flow front can be observed in the radial flow experiment while for anisotropic materials the flow front becomes elliptic.

Isotropic permeability

To calculate isotropic permeability the pressure gradient within the mould has to be determined as a function of the flow front position. This is achieved by solving the Laplace equation in polar coordinates (Weitzenböck, etc., 1999a and 1999b).

If a preform is isotropic in the in-plane directions such that K*xx* = K*yy*, then the flow fronts progress as circles. Some fabrics such as random fiber mats, 4-harness woven fiberglass mat and symmetric bi-directional fabrics produce isotropic preforms.

Anisotropic permeability

So far only flow in isotropic porous materials has been considered. However for many fabrics commonly used in RTM an elliptical flow front is observed. As a

consequence the second order partial differential equation of the pressure distribution is no longer Laplace equation, where K*xx* and K*yy* are two principal permeabilities (Weitzenböck, etc., 1999a and 1999b).

If the preform is anisotropic in the plane with K*xx* different from K*yy*, the flow fronts become elliptic and remain elliptic through out filling. Furthermore, this situation can be encountered with unidirectional stitched mats.

3.4 Measurement of Permeability

Generally speaking there are two different configurations for permeability measurement. These are the one-dimensional channel flow experiment and the two-dimensional radial flow experiment. For isotropic materials a circular flow front can be observed in the radial flow experiment while for anisotropic materials the flow front becomes elliptic. The main attraction of the radial flow experiment is that both the principal permeability values and their orientation can be determined in a single experiment. In addition, no racetracking occurs during the experimental process. So it is widely used by researchers (Adams, etc., 1986, Chan, etc., 1991, Hirt, etc., 1987, Parnas, etc., 1993). For constant inlet pressure three algorithms to calculate permeability data from flow front measurement have been developed (Adams, etc., 1988, Carter, etc., 1995, Rudd, etc., 1995). In all these approaches the orientation of the flow front ellipse needs to be determined visually since the algorithms apply only to flow front measurements along the principal axes. For all methods permeability is assumed to be a symmetric tensor. As a consequence there is a set of two mutually orthogonal axes where all the off-diagonal tensor components become zero.

3.4.1 Permeability Test

To simplify the theoretical analysis, our work concentrated on the Newtonian fluid. Corn oil was used for the test fluid in all experiments due to its handing and cleanup. The viscosity of the corn oil is tested at room temperature with the value of 102cp.

The flow front and pressure data were collected during the experiments and these results were analyzed to produce permeability values. The flow front position at different times was recorded with the help of CCD camera and an image snapping system. So the solution is a permeability equation which is to characterize the permeability in terms of flow front radius, time and pressure.

3.4.2 Permeability Testing Equation

Below is a list of assumptions on which the new approach is based:

- All experiments considered are constant inlet pressure experiments where the flow front position is measured during the experiment. As a consequence of the constant inlet pressure, flow is unsteady as the pressure gradient and the velocity of the flow front change with time. The pressure at the flow front is ambient pressure.

- Microscopic flow is ignored. During an experiment flow occurs not only in the pores of a fabric or mat but also on a microscopic level within the individual fibre bundles. However, there is currently no measurement technique which allows the simultaneous measurement of microscopic and macroscopic flow.

- Gravitational and surface tension effects are ignored.

- The porous material is homogenous with interconnected pore space. Moreover, it is undeformable which means it does not move or deform during injection.

- The viscosity remains constant throughout the experiment because:
  - The fluid used for the experiment is Newtonian and incompressible.
  - The experiment is carried out under isothermal conditions.
  - No cure takes place during the injection.
- In the radial flow experiment the flow front is moving throughout the duration of the experiment. The initially dry fabric is wetted by the advancing flow front hereby displacing the air. The wetted domain is assumed to be fully saturated with test fluid (no air bubbles).

Based on the assumptions above, we can deduct the final equation to calculate the permeability from experimental images as following:

Darcy law for the two-dimensional flow is $\{u\} = -\frac{1}{\mu}[k]\nabla p$ (3-2)

Where {u} is the superficial velocity vector, [K] is the in-plane permeability tensor. ▽P is the pressure gradient vector.

[K] is given by: $[K] = \begin{pmatrix} k_{xx} & k_{xy} \\ k_{yx} & k_{yy} \end{pmatrix}$ (3-3)

For an anisotropic medium, [K] is symmetrical, (i.e., $k_{xy}=k_{yx}$)

Applying the incompressible flow criterion to Eq.(3-2), leads to an equation for the pressure field: $\nabla \cdot ([K] \cdot \nabla P) = 0$ (3-4)

For an isotropic preform, [K] takes on the form: $[K] = k\begin{pmatrix} 1 & 0 \\ 0 & 1 \end{pmatrix}$ (3-5)

Eq(3-4) for an isotropic preform can be rewritten in polar coordinates as

$$\frac{dp}{dr^2} + \frac{1}{r}\frac{dp}{dr} = 0 \qquad (3\text{-}6)$$

For constant pressure mold filling, the boundary conditions for Eq.(3-6) are

$P=p_0$ at $r=r_0$ and $P=0$ at $r=r_f$

Where P_0 is the constant inlet pressure, r_0 is the inlet port radius; r_f is the flow front radius.

The solutions for the pressure gradient and pressure fields are:

$$\left(\frac{dp}{dr}\right)_r = \frac{-p_0}{r \cdot \ln\left(\frac{r_f}{r_0}\right)} \qquad \frac{P}{p_0} = 1 - \frac{\ln\left(\frac{r}{r_0}\right)}{\ln\left(\frac{r_f}{r_0}\right)} \qquad (3\text{-}7)$$

The definition for actual fluid velocity in the pore spacers is

$$\frac{dr_f}{dt} = \frac{u_f}{\varepsilon} = \frac{kP_0}{\varepsilon\mu r_f \ln\left(\frac{r_f}{r_0}\right)} \qquad (3\text{-}8)$$

where u_f is the superficial velocity at the flow front.

Eq.(3-8) can be intergraded to yield a relationship between flow front position r_f and time t:

$$r_f^2\left[2\ln\left(\frac{r_f}{r_0}\right) + \left(\frac{r_0}{r_f}\right)^2 - 1\right] = \frac{4kp_0}{\varepsilon\mu} \cdot t \qquad (3\text{-}9)$$

So we can get the average permeability equation under constant inlet pressure:

$$K_e = r_f^2[2\ln(\frac{r_f}{r_0}) + (\frac{r_0}{r_f})^2 - 1] \cdot \frac{\varepsilon\mu}{4\Delta pt} \quad (3\text{-}10)$$

where ε is the porosity, μ is the dynamic viscosity of the fluid, t is the time from the start of the injection to when a specified point in the cavity is reached and r_f and r_o are the radius of the flow front and inlet. △P is the difference between the pressure at the flow front P_f and the inlet pressure P_0. The inlet pressure is usually measured as the pressure above the ambient pressure. Hence △P is equal to the pressure applied at the inlet P_0 (Chan, et al, 1993).

For the isotropic permeability, $r_f = r_x = r_y$

For the anisotropic permeability, $r_f = \sqrt{r_x \cdot r_y}$

The governing equation for the general anisotropic case for two dimensional flow in porous media is derived in Appendix C.

3.5 Permeability Testing Devices

The schematic of the in-plane permeability measurement device based on the radial flow method (Lekakou, etc., 1996a, Weitzenböck, etc., 1998) is shown in Figure3.4. All of the testes were performed in a rectangular RTM mould. The dimensions of the mould cavity were 200 by 300 mm. The thickness of the mold could be adjusted by using different spacers with different height. The porosity was changed by altering the height of the spacers. A 20mm thick toughened glass upper plate permits recording the progress of the flow front. And the thickness of the toughened glass can assure the deformation of the mould is at the permit level.

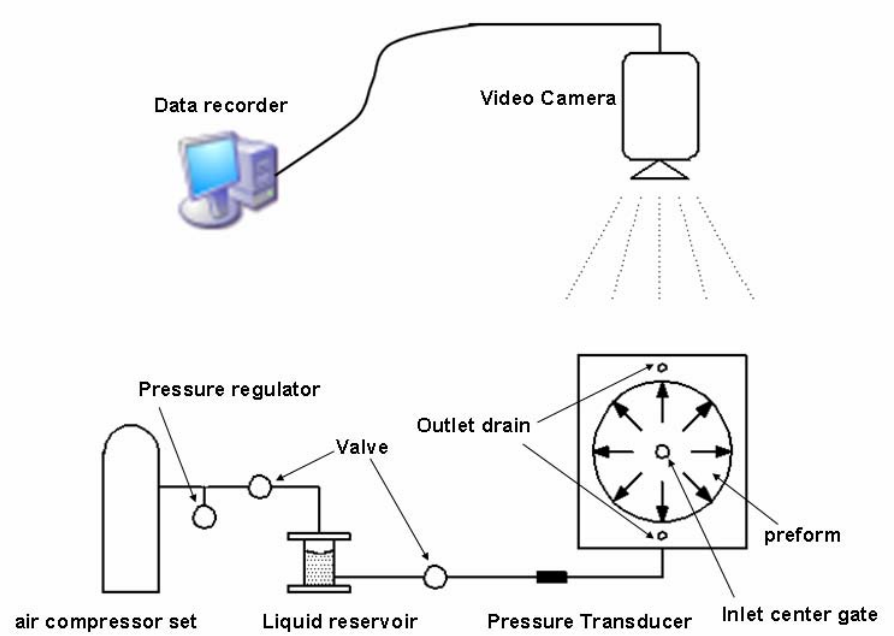

Figure 3.4 Experimental schematic of in-plane permeability measurement

A radial in-plane flow is achieved by injecting the oil through a central 1.0 cm diameter. The constant pressure inflow was provided by air compressor set. During the injecting process, the pressure of the corn oil was measured by the pressure transducer.

3.6 Sample Preparation

Three-dimensional multi-layer woven fabrics were produced with different weave constructions and yarns. And then, the number of fabric layers, the end density and filling density were kept constant. The variable parameter was the weave geometry and material used. The preparation of fabric samples such as fabrics made of polypropylene and nylon mono-filament was carried out in the weaving laboratory of the Institute of Textile and Clothing (ITC) of the Hong Kong Polytechnic University.

3.6.1 Material Used

The fiber chosen for producing the three dimensional multi-layer woven fabrics had to meet the properly requirements necessary for high performance composites. These properties included high tensile strength and good impact resistance. In this study, polypropylene (PP) and nylon monofilament were chosen, as it would meet our requirements and more convenience to get. A 900 denier, 90 filament yarn was used in warp and weft yarns for polypropylene (PP) fabrics. Furthermore, a different diameter of yarn between warp (0.5mm) and weft (1.2mm) will be used to produce the nylon monofilament fabric.

3.6.2 Weave Design

A number of different weave constructions are possible in order to design three-dimensional multi-layer woven fabrics. In this study, three weave constructions were designed which used polypropylene (PP) as the material. Each fabric has a total of five layers, a layer being defined as containing both a warp and weft yarn. All weaves are designed as plain weave and weft yarns are used as stitches to interconnect adjacent layers. The interlacing method of three-dimensional multi-layer woven fabrics is distinguished with each other by stitches. Weave Ⅰ consisted of a layer-to-layer interlacement with stitches penetrating two layers. In weave Ⅱ, stitches penetrated to a depth of three layers and in weave Ⅲ stitches penetrated to a depth of four layers. The weave plans and schematic diagrams of fabrics 1, 2 and 3 are shown in Figures 3.5, 3.6, 3.7 and Tables 3.1, 3.2 and 3.3.

Table 3.1 Weave Plan for Fabric Ⅰ

Weft										
8	**X**	**X**	**X**	**X**	**X**	**X**	**X**	**X**		
7	**X**	**X**	**X**	**X**		**X**	**X**			
6	**X**	**X**	**X**			**X**	**X**	**X**	**X**	**X**
5	**X**	**X**	**X**			**X**				
4	**X**	**X**				**X**	**X**	**X**	**X**	
3	**X**	**X**								
2	**X**					**X**	**X**	**X**		
1						**X**	**X**			
	1	**2**	**3**	**4**	**5**	**6**	**7**	**8**	**9**	**10**
	Warp									

X—Warp up

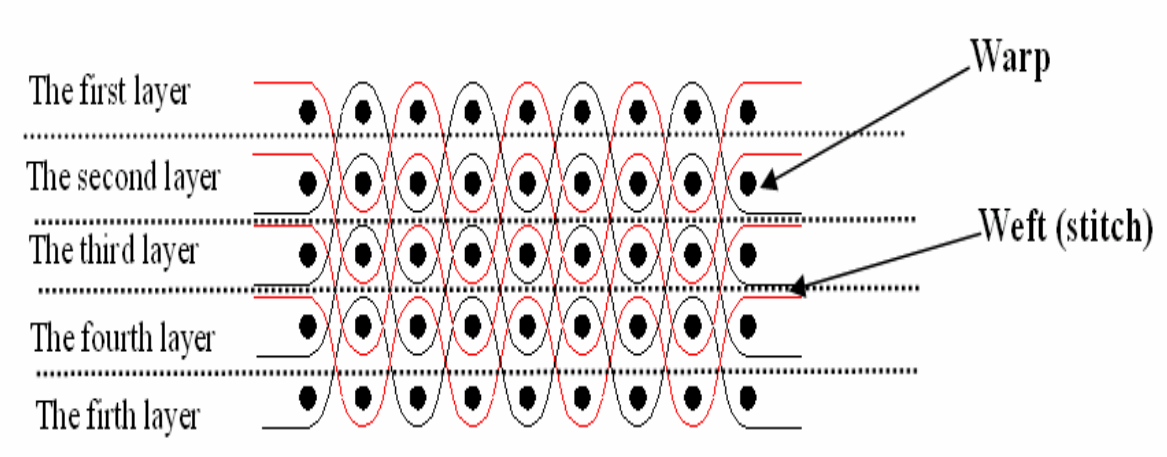

Figure 3.5 Schematic diagram of multi-layer woven Fabric Ⅰ

Table 3.2 Weave Plan for Fabric Ⅱ

Weft										
8	**X**	**X**	**X**	**X**	**X**	**X**	**X**			
7	**X**	**X**	**X**	**X**		**X**	**X**	**X**	**X**	X
6	**X**	**X**	**X**	X		**X**	**X**	**X**	**X**	**X**
5	**X**	**X**	**X**							
4	**X**	**X**				**X**	**X**	**X**	**X**	X
3	**X**					**X**	**X**	**X**	**X**	
2	**X**									
1						**X**	**X**	**X**		
	1	**2**	**3**	**4**	**5**	**6**	**7**	**8**	**9**	**10**
	Warp									

X—Warp up

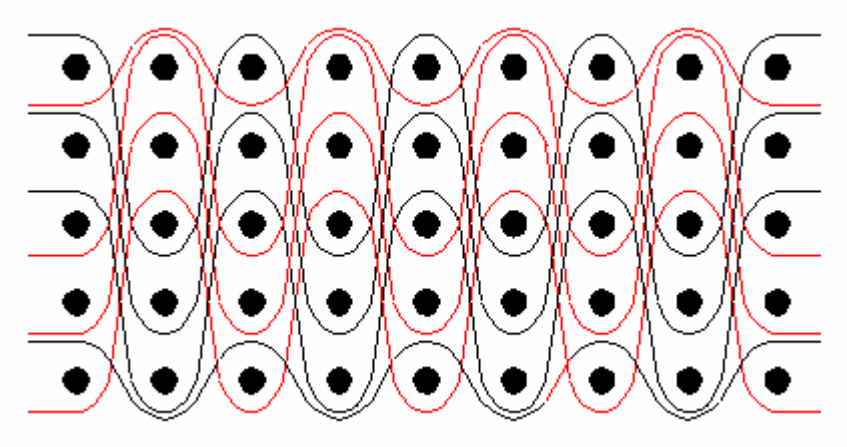

Figure 3.6 Schematic diagram of multi-layer woven Fabric Ⅱ

Table 3.3 Weave Plan for Fabric Ⅲ

Weft										
8	**X**	**X**	**X**	**X**	**X**	**X**				
7	**X**	**X**	**X**	**X**		**X**	**X**	**X**	**X**	**X**
6	**X**	**X**	**X**	**X**						
5	**X**	**X**	**X**			**X**	**X**			
4	**X**	**X**				**X**	**X**	**X**		
3	**X**					**X**	**X**	**X**	**X**	**X**
2	**X**									
1						**X**	**X**	**X**	**X**	
	1	**2**	**3**	**4**	**5**	**6**	**7**	**8**	**9**	**10**
	Warp									

X—Warp up

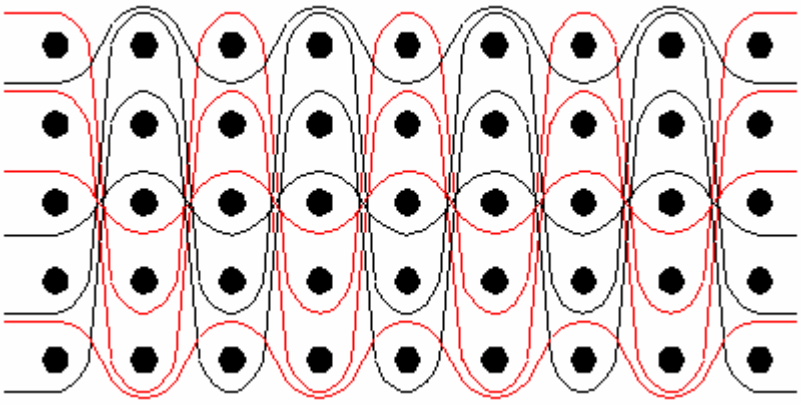

Figure 3.7 Schematic diagram of multi-layer woven Fabric Ⅲ

Other than the number of different weave constructions for the polypropylene (PP) three-dimensional multi-layer woven fabrics, nylon mono-filament also used as material for producing three-dimensional multi-layer woven fabrics. Furthermore, each fabric has a total of four layers, a layer being defined as containing both a warp and weft yarn. All weaves are designed as plain weave the warp ends were used as stitching yarn. Three

types of testing samples with different stitch density were produced. The weave plans and schematic diagrams of these fabrics are shown in Figure 3.8, 3.9, 3.10 and Table 3.4, 3.5 and 3.6.

Table 3.4 Weave Plan for Fabric with stitch density 1

Weft								
10					**X**	**X**	**X**	**X**
9	**X**	**X**	**X**	**X**				
8				**X**				
7			**X**	**X**				**X**
6		**X**	**X**	**X**			**X**	**X**
5	**X**	**X**	**X**	**X**		**X**	**X**	**X**
4								**X**
3				**X**			**X**	**X**
2			**X**	**X**		**X**	**X**	**X**
1		**X**	**X**	**X**	**X**	**X**	**X**	**X**
	1	**2**	**3**	**4**	**5**	**6**	**7**	**8**
	Warp							

X—Warp up

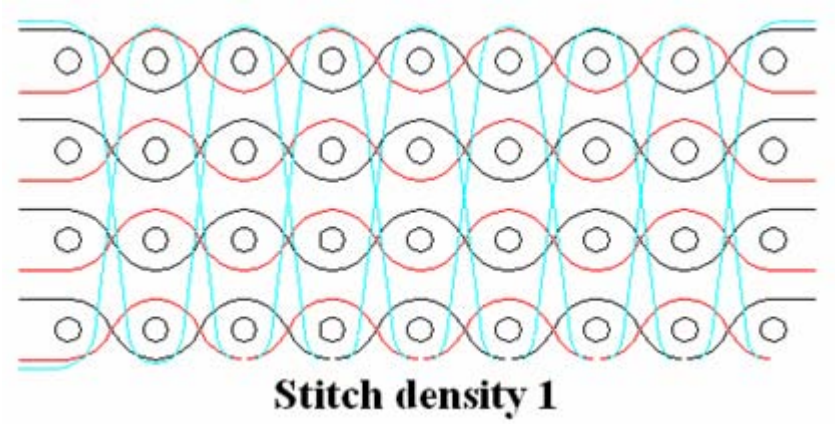

Figure 3.8 Schematic diagram of multi-layer woven fabrics with stitch density 1

Table 3.5 Weave plan for fabric with stitch density 2

weft																
10					X											X
9				X	X					X					X	X
8			X	X	X				X	X				X	X	X
7		X	X	X	X			X	X	X			X	X	X	X
6	X	X	X	X	X		X	X	X	X		X	X	X	X	X
5					X								X			
4				X	X					X		X	X			
3			X	X	X				X	X	X	X	X			
2		X	X	X	X			X	X	X	X	X	X			X
1	X	X	X	X	X		X	X	X	X	X	X	X		X	X
	1	2	3	4	5	6	7	8	9	10	11	12	13	14	15	16
	warp															

X—Warp up

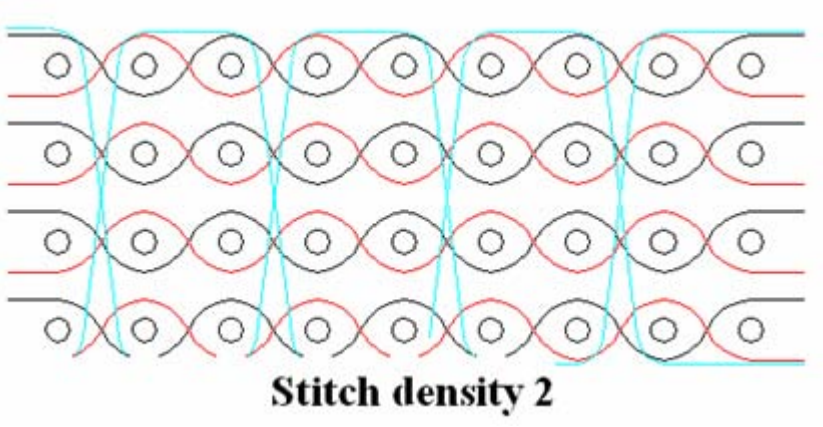

Figure 3.9 Schematic diagram of multi-layer woven fabrics with stitch density 2

Table 3.6 Weave plan for fabric with stitch density 3

weft																								
10	X	X	X	X	X	X	X	X	X	X	X	X												
9	X	X	X	X	X	X	X		X	X	X	X	X	X	X		X	X	X	X	X	X	X	
8	X	X	X		X	X	X	X	X	X	X		X	X	X	X	X	X	X		X	X	X	X
7	X	X	X		X	X			X	X	X		X	X			X	X	X		X	X		
6	X	X			X	X	X		X	X			X	X	X		X	X			X	X	X	
5	X	X			X				X	X			X				X	X			X			
4	X				X	X			X				X	X			X				X	X		
3	X								X								X							
2					X								X								X			
1													X	X	X	X	X	X	X	X	X	X	X	X
	1	2	3	4	5	6	7	8	9	10	11	12	13	14	15	16	17	18	19	20	21	22	23	24
	warp																							

X—Warp up

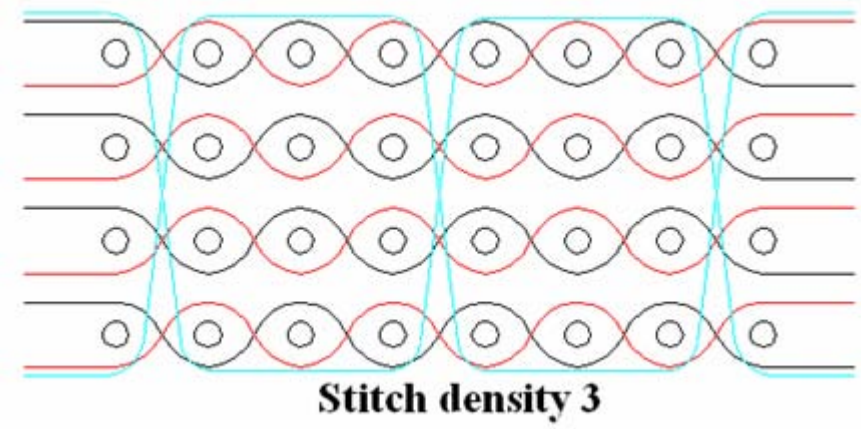

Figure 3.10 Schematic diagram of multi-layer woven fabrics with stitch density 3

3.6.3 Equipment Used for Fabric Formation

3.6.3.1 Warping Machine

The purpose of warping is to arrange threads in a long line parallel to one another preparatory to further processing. The primary operation of warp making, in which ends withdrawn from a warping creel, evenly spaced in sheet form, are wound threads onto a beam to substantial length.

For the fabric formation, the yarn preparation process is very important for controlling the even tension of the warp. Furthermore, the evenness and quality will also be affected. So, a sectional wrapper was used for warping. The set-up of the warping machine is shown in Figure 3.11a, b, c and d.

Figure 3.11a, b, c and d The setup of warping machine

3.6.3.2 Weaving Machine

The purpose of weaving is to interlace two or more yarns at right angles to each other to produce woven fabric. The yarns which run lengthwise are called warp (end), while the cross yarns running at right angles to the warp are called filling or weft (pick).

The machine used for weaving is called a loom. The basic operations of a loom include shedding, picking, beating-up, warp let-off and cloth take-up motions. The

functions of these operations are:

Shedding - raising and lowering of the warp yarns by the harnesses to make an opening for the weft yarn to pass through.

Picking - the passage of the shuttle or other device across the loom to put a weft yarn in the shed.

Beating-up - the pushing of each loose weft yarn into the cloth by the reed, after the shuttle has been moved through the reed.

Warp let-off - this motion delivers warp to the weaving area at the required rate and at a suitable constant tension by unwinding it from a warp beam

Cloth take-up- this motion withdraws fabric from the weaving area at the constant rate that will give the required pick-spacing and then winds it onto a roller.

In order to produce three dimensional multi-layer woven fabrics which is made of different material such as polypropylene (PP) and nylon monofilament. Due to the thickness of the three dimensional fabrics, the warp densities are much greater than conventional two-dimensional fabrics. Therefore, the interaction among warp ends in going from one shed to the next would be very severe. It is important that different weaving machine will be used because the strength and stiffness of the nylon monofilament are very high. Therefore, it is necessary that the beating up force of the weaving machine should be high enough to process the beat up motion successfully. To have good beat up motion, the Picanol Shuttle loom is advised to use which also suitable to weave plain weave fabric.

In addition, the strength of polypropylene (PP) is relatively lower and the softness is high. So, other weaving machine is recommended to use such as Simple Weaving

Machine. It is because this machine is suitable for weaving softer yarn and easier to exercise complete control over the weaving process. The weaving machine had a working width of 15 inches and the harness motion was controlled by electronic dobby. The reed spacing of Simple Weaving Machine was setting to 12 dents per inch and Picanol Shuttle loom was setting to 10 dents per inch. The different parts of different weaving loom were shown in Figure 3.12a, b, c, d, e and 3.13a, b, c, d, e.

Figure 3.12a Simple Weaving Machine

Figure 3.12b Shedding

Figure 3.12c Let-off

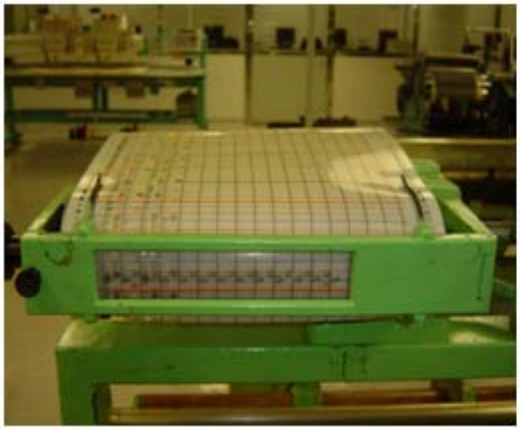

Figure 3.12d Reading equipment

Figure 3.12e Take-up

Figure 3.13a: Front & back face of the Picanol shuttle loom

Figure 3.13b Shedding

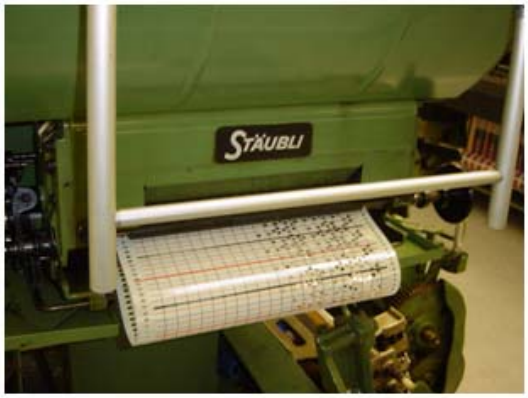

Figure 3.13c Reading Mechanism

Figure 3.13d Let-off

Figure 3.13e Take-up

3.6.3.3 Tensioning Device

In the weaving process of three-dimensional multi-layer woven fabric, it is essential that to maintain proper tension of the warp yarns. In order to obtain a stable fabric and to form a proper shed, a high degree of tension had to be applied to the warp ends. When weaving the polypropylene (PP) and nylon mono-filament, it is very important that high tension must be particularly applied. Slack ends in the warp transform into slack ends in the fabric, which cause entanglements in the warp and prevent the formation of a clear shed.

There are some tensioning devices used in both the Simple Weaving Machine and the

Picanol Shuttle loom, shown in Figure 3.14a and b. In the Simple Weaving Machine, consisted of one pair of rollers mounted onto a frame and the two ends of the beam is collected to some weight by belt. It is necessary that the degree of warp tension for optimum weavability is adjusted by the weight applied and negative let-off.

Moreover, in the Picanol Shuttle loom, there is mechanism for controlling tension of the warp yarns. The mechanism consists of some gears and a dobby.

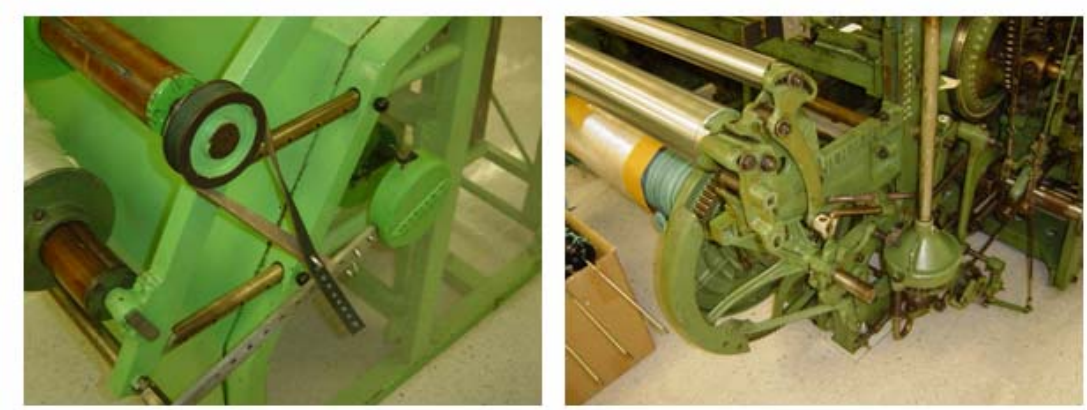

Figure 3.14a and b The tension device of Simple Weaving Machine and Picanol Shuttle loom

3.6.3.4 Staubli System

The motion of the heald shafts is controlled by the Staubli System. Therefore, the electronic card-punching machine should be used to punch the number of holes on the card. The holes of the card are used to control the up or down motion of the heald shaft during weaving. The electronic card punching machine and the punched card as shown as Figure 3.15a and b.

Figure 3.15a and b The electronic card punching machine and the punched card

3.6.4 Preparation for Weaving

3.6.4.1 Warping

In preparing the yarn for weaving, both polypropylene (PP) and nylon mono-filament warp yarn were wound onto the warp beam. For the polypropylene (PP) yarn, a total of 100 cones were prepared and placed on the creel of the warping machine.

And then, for the nylon monofilament yarn, a total of 200 packages of length 100 meters were prepared and placed on the creel of the warping machine.

3.6.4.2 Drawing-in

After the warping process was finished, the warp beam could be transferred from warping machine to weaving loom. The yarns were drawn-in through each appropriate heald wire on the heald shaft individually. For the polypropylene (PP) yarn, the warp ends were drawn-in using a straight-draw method' or 'the warp ends used a straight-draw method with a density of 5 ends per dent.

On the other hand, for the nylon mono-filament, the warp ends were drawn-in

using a straight-draw method' or 'the warp ends used a straight-draw method with a density of 4 ends per dent.

3.6.5 Production of Three dimensional Multi-layer Woven Fabric Samples

Because man-made fibres are used to produce three-dimensional multi-layer woven fabric such as nylon mono-filament and polypropylene (PP) yarn, which have very good water resistance, it is not necessary to have sizing process. Therefore, the surface of the yarn would be would be easier to damage during weaving' or 'would be more easily damaged during weaving. In order to minimise the degree of yarn damage and prevent yarn breaking down due to the shuttle was clipped in the shed or the shuttle flight through the shed, this needs to be clarified the process of weft insertion (pick by pick) should be done by hand.

The 400 warp ends, reeded 5 ends/dent, with a reed density of 12 dents/inch were woven into fabric approximately 12 inches in width. It is necessary to provide adequate material for testing, and a total of forty-eight inches of each structure was produced.

It is regarded that three-dimensional multi-layer woven fabric preforms offer many advantages over both two-dimensional fabrics and other categories of three-dimensional preforms. Compared to two-dimensional fabrics, multi-layer fabrics offer better processability and eliminate delamination of fabrics. Other categories of three-dimensional preforms require extensive modifications to present equipment or new equipment, whereas multi-layer woven fabrics can be produced using existing textile manufacturing techniques on conventional equipment with few modifications.

This study also shows that conventional weaving equipment can be used to produce three-dimensional multi-layer fabrics without extensive modification of present equipment, which provides the greatest immediate benefit in applications.

3.7 Permeability Test Results

Table 3.7 and 3.8 reports the tested radial experimental results. As shown in figure 3.16 and 3.17 are the comparisons of the permeabilities between fabrics with different types of stitch density and different stitch structure.

Table3.7(a). The permeability of the 3D woven fabrics for the stitch density 1

Fiber volume farction	0.43	0.491	0.543	0.602
Radial flow experiment	2.23E-09	1.20E-09	4.97E-10	2.33E-10

Table 3.7(b). The permeability of the 3D woven fabrics for the stitch density 2

Fiber volume farction	0.44	0.503	0.551	0.609
Radial flow experiment	2.35E-09	1.19E-09	6.70E-10	3.33E-10

Table 3.7(c). The permeability of the 3D woven fabrics for the stitch density 3

Fiber volume farction	0.447	0.512	0.559	0.618
Radial flow experiment	2.98E-09	1.54E-09	8.40E-10	4.27E-10

Table 3.8(a). The permeability of the 3D woven fabrics for weave Ⅰ

Fiber volume farction	0.504	0.566	0.596	0.658
Radial flow experiment	3.79E-11	2.21E-11	1.64E-11	8.71E-12

Table 3.8(b). The permeability of the 3D woven fabrics for weave Ⅱ

Fiber volume farction	0.534	0.575	0.629	0.719
Radial flow experiment	4.24E-11	2.14E-11	1.35E-11	5.73E-12

Table 3.8(c). The permeability of the 3D woven fabrics for weave Ⅲ

Fiber volume farction	0.564	0.627	0.692
Radial flow experiment	3.11E-11	1.73E-11	7.84E-12

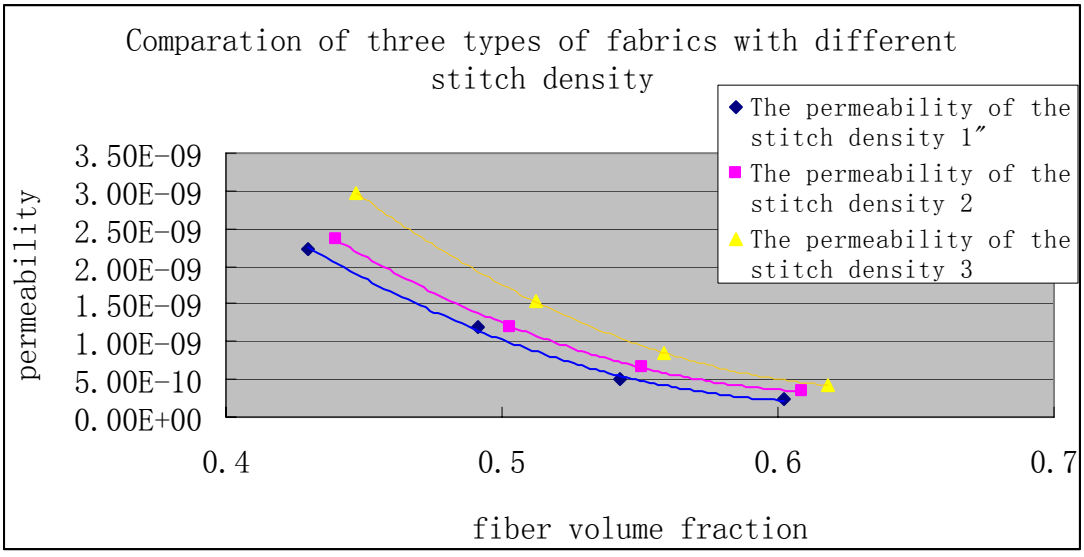

Figure 3.16 Comparisons of the permeabilities between fabrics with different types of stitch density

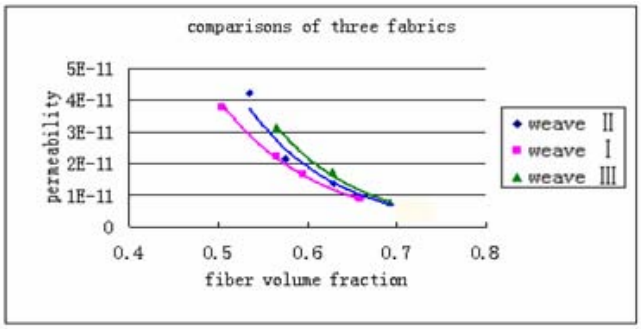

Figure 3.17 Comparisons of the permeabilities between fabrics with different weave type

The most interesting phenomenon could be found from this comparison is that the effect of stitching model on permeability. The comparison shows that at the same fiber volume fraction, different stitching model fabrics have different permeability. When the fiber volume fraction (V_f) approaches the maximum possible fiber volume fraction (V_m), the permeability decrease accordingly and the effect of stitching model on permeability is weaken. These results clearly indicate that the type of stitch model plays a quite important role in the permeability of the reinforcements.

3.8 Conclusion

It is regarded that three-dimensional multilayer woven fabric preforms offer many advantages over both two-dimensional fabrics and other categories of three-dimensional performs. Compared to two-dimensional fabrics, multi-layer fabrics offer better processability and eliminate delamination of fabrics. Other categories of three-dimensional preforms which require extensive modifications of present equipment or new equipment whereas multi-layer woven fabrics can be produced using existing textile manufacturing techniques on conventional equipment with few modifications. This study also has shown that conventional weaving

equipment can be used to produce three-dimensional multi-layer fabrics without extensive modifications of present equipment which provides the greatest immediate benefit in applications.

For fabric Preform, there are many basic properties such as Permeability, Compressibility, Ease of handling, Drapeability, Strength, stiffness and Fiber volume fraction, etc. In all of these properties, the permeability is a key aspect in fiber reinforced composite fabrication. It will determine key processing parameters, such as filling time and injection pressure. Therefore, the strength of the composites and mould filling during the injection step would be influenced. So in this study, we will focus on the permeability, especially the permeability of Multi-layer Woven Fabrics

The permeability is a property that is dependent on the size of the fibers and the fiber architecture. It can be treated as a tensor and it generally has different values in different directions. Knowledge of the permeability values is also essential for the development of highly permeable fiber reinforcements. Hence, in this study, testing methods to measure the permeability were developed. This work focuses on the in-plane permeability, which is the interest for liquid composites moulding techniques such as the Resin Transfer Moulding (RTM) process.

The in-plane permeability of the fiber reinforcement was determined through two principal methods, the parallel flow technique and the radial flow technique. By considering the advantages of radial flow method, we designed a set of experimental apparatuses based on the two-dimensional radial flow method. In this study, the final equation to calculate the permeability of the preform was deduced. The relationship between the permeability and the experimental parameters, such as injection pressure, fluid viscosity and flow velocity was therefore investigated.

Chapter 3 Permeability test

In order to study the permeability of 3D multi-layer woven fabrics, the multi-layer woven fabrics with different stitch parameters were designed and investigated. The influences of the stitch parameters on permeability were evaluated and compared with each other. The comparison shows that at the same fiber volume fraction, different stitching model fabrics have different permeability. It was found that both weave designs and stitching methods would affect the permeability of 3D multi-layer woven fabrics.

Chapter 4

Permeability model

4.1 Introduction

From the foregoing discussion, it is apparent that the permeability of a textile preform (transport of resin) is a key aspect of fibre reinforced plastic composite fabrication processes such as RTM. As one of the elemental performances of fibre materials, the importance of the permeability lies in the following points: firstly, it can determine the filling and packing time in injection, and determine the mold design, the location of injection port and exhaust port, thus it is the critical parameter for numerical simulation; secondly, it determines the attribute of fluid flow, the degree of impregnation, thus it is the key factor to manufacture high-performance products.

The problems related to the permeability include the formation of dry spots or voids within the preforms. These dry spots and voids will deteriorate the performance of products, so it is significant to eliminate them. But these are not easy to solve, particularly when the preform is composed of multi layers of reinforcement. Only when we find the relationship between fabric permeability and fabric construction can we eliminate dry spots and voids and improve the performance of the products.

The studies of the permeability of textile preforms have been reviewed by (Lee, 1997) and discussed in a related monograph titled Liquid Molding Technologies (Rudd, *et al*, 1997). The preform permeability can be obtained by experiments,

empirical and analytical equations, and numerical simulations (Lee,1994; Wang, *et al*, 1994; Berdichevsky and Cai, 1993; Skartsisl, *et al*, 1992).

For resin flow through the interstices and between layers of fiber beds, the Newtonian flows in macroscopically homogeneous domains was described originally by Darcy (Darcy, H. 1856), who developed the constitutive description by observing water flow through beds of sand. Application of Darcy's model to composite processes, from laminates to molded materials, is widespread. The percolation flow is generally applied to thermosetting resins in autoclave (laminate) or liquid molding processes. The familiar Darcy model may be written $\bar{v} = \frac{-K}{\mu}\nabla p$

where v is the average fluid velocity, μ is the fluid viscosity, K is the permeability of the porous medium, and ▽P is the pressure gradient and can be written in tensorial form for anisotropic preforms, where up to 3 scalar permeabilities are required in the plane case. Such implementations thus require determination of the permeability or components of a permeability tensor, via experimental or theoretical means. In application to actual processing, various factors are commonly used to account for flow "tortuosity," or circuitousness of the path that must be traversed to penetrate the material, the shape of the particles, material anisotropy, and the average volume fraction. Several modifications to Darcy's lwa have thus been proposed in the polymer processing arena and in other areas of fluid-structure interaction; for example, Kozeny (Kozeny, J. 1927) treated a permeated porous medium as a bundle of capillary tubes and obtained a relationship to adapt Darcy's law to include capillarity effects with an empirical relation; Blake (Blake, F.C. 1922) derived a similar expression. Carman (Carman, P.C. 1937) modified Kozeny's work by

defining S, the specific surface with respect to a unit volume of solid, instead of a unit volume of porous medium. The “Kozeny-Carman relationship” arose through these sequential contributions. Carman experimentally determined a range of “Kozeny constants” for a variety of packing schemes and geometries of reinforcements.

Such relations have commonly been used to model polymeric flow in composite materials in the last 20 years (Coulter, J.P. and S.I. Guceri. 1988). Williams et al. (Williams, J.G., etc., 1974) considered the flow of several fluids through aligned reinforcements, both dry and pre-saturated with liquid. They obtained higher permeabilities for saturated than for unsaturated reinforcement, as did Martin and Son (Martin, G.Q. and J.S. Son. 1986). Many authors since the late 1980s have specifically studied the permeability of fibrous preforms for liquid molding. More recent work has focused on complex geometries. In 1996, Rudd (Rudd, C.D., 1996) established a “permeability map” for complex geometries. Smith (Smith, P., etc., 1997) related permeabilities of sheared fabrics to ply angle. Lai and Young (Lai, C.-L. and W.-B. Young. 1997) related similar experimental data to a geometry-based flow model.

Other closed-form modifications to Darcy’s law have been developed to relate volume fraction and geometric or empirical constants such as the maximum packing fraction to the permeability of a periodic medium comprised of parallel cylinders. Gebart (Gebart, B.R. 1992) derived an equivalent permeability based on the assumption of hexagonally-arranged fibers. Cai and Berdichevsky (Cai, Z. and A.L. Berdichevsky. 1993) extended a classic self-consistent approach, wherein a heterogeneous element was assumed to be embedded in an equivalent homogeneous

medium. The homogeneous medium was constructed such that the total flow and dissipation energy remained the same. Use of a no-slip boundary condition at the fiber surface and zero velocity gradient in the radial direction at the domain boundaries resulted in an equivalent permeability value. The improved self-consistent method took into account an additional parameter VA, the maximum packing capacity of fibers, to increase the accuracy of the model. Bruschke and Advani (Bruschke, M.V. and S.G. Advani. 1993) developed a closed-form solution for permeability by matching the lubrication solution for low porosities and an analytical cell model solution for high porosities. They found agreement between their hybrid, arrangement-specific closed-form solution and a numerical solution of the Navier-Stokes equations for flow around both hexagonal and square arrangements of cylinders (using a simulation package, POLYFLOW). Van der Westhuizen(Van der Westhuizen, J. and J.P. Du Plessis. 1996) used phase-averaged Navier-Stokes equations to calculate the permeability of representative unit cells, and reported agreement with experimental in-plane permeabilities. Their model did not assume any particular arrangement of fibers for longitudinal permeability, but used the maximum packing capacity for different arrangements of fibers to create an effective volume fraction for transverse permeability. Wang (Wang, C.Y. 1996) developed a similar relation for an array of rectangularly-packed fibers.

Computational fluid dynamics software can be used to solve the full Navier-Stokes equations to determine flow progression, although practically this can be done only for small domains. Several workers have developed intermediate special- purpose codes to model fluid flow in fabrics that account for effects such as capillarity, race tracking, saturation, etc. For example, Advani and co-workers developed "LIMS," (Pillai, K.M. and S.G. Advani. 1998) which is able to simulate edge effects by

implementation of a mass sink to the continuity equation to account for saturation. Chang and Hourng (Chang, C.-Y. and L.-W. Hourng. 1998) developed a two-dimensional model for tow impregnation, taking into account micro/macroscopic flow and void formation. Ambrosi and Preziosi (Ambrosi, D. and L. Preziosi. 1998) developed a model for flow dynamics in an elastically deforming environment.

Flow in tows versus gaps or voids has been specifically studied by a number of workers. Shih and Lee (Shih, C.H. and L.J. Lee. 1998), for example, used six different types of glass fiber reinforcements to determine the effect of fiber architecture on apparent permeability. The reinforcements included 4-harness woven, plain weave, random fiber and stitched fiber mats. They argued that the gap size between the tows and the connectivity of the gaps control permeability. Kolodziej (Kolodziej, J.A., etc., 1998) proposed a theoretical model which accounted specifically for gaps as caverns or fissures inside the bundle of fibers. Both diameter of fibers and also diameter of gaps inside the fiber bundles were incorporated in the model. They reported that tow heterogeneity can decrease or increase tow permeability, depending on the critical dimensionless radius of these gaps. Heterogeneity was identified as the probable cause of deviation of permeabilities from permeability models, which assume uniformity inside the fiber bundles.

The numerical simulation is usually made by the finite element analysis (Berdichevsky and Cai, 1993), finite difference (Gebart, 1992) and control volume methods (Lee, 1997) for idealized and/or simple preform structures. Regarding woven fabric, Rebenfeld and his students investigated the effective permeability in terms of the pore structure, weave type, fabric layering, fiber orientation and

compressibility (Rebenfeld, *et al*, 1992). When considering the heterogeneity, the combination of Navier-Stokes and Darcy equations with different permeability for flow in different portions of a preform extended to complicated fabrics (Lee, 1997).

The flow through multi-layer assemblies is complex. Rebenfel found that the permeability of multi-layer assemblies differed from those of their constituent layers (Rebenfel and Adams, 1991). In the homogeneous assemblies, the inter-layer pores can increase the effective in-plane permeability, while in heterogeneous assemblies; the permeability and anisotropy are governed by high-permeability layers or directions. They suggested a transverse flow mechanism to fill the low permeability layers and keep the fluid front macroscopically uniform. Mogavero and Advani investigated the effect of varying the order of lay-up of a fixed number of plies and the impact of varying the thickness of individual layers (Mogavero and Advani, 1997). Batch investigated the interface between layers in relation to compressibility and developed a model for calculating average volume fraction for multi-layer assemblies, where it was found that increasing the number of layers decreased the permeability. They attributed this to the blocking at the interface of adjacent layers, which created tortuous flow paths (Batch and Cumiskey, 1990). Loos studied the permeability of carbon multi-axial warp knit preforms (Loos et al, 1991). It was found that the introduction of through-thickness fibres significantly increased the permeability of the preforms, especially for the preforms with high volume fraction. The Kozeny-Carman equation was found to be adequate to provide a quantitative relationship between permeability and the preform porosity. But the through thickness fibres here are still different from those in 3D Multi-Layer Woven Fabrics.

Lekakou and co-workers investigated the relationship between the compressibility

and flow permeability of woven fabric assemblies (Lekakou et al, 1996b). Multi-layer assembly here means separate single-layer woven stacks. The interface is related to the sloughing or nesting (Mogavero and Advani, 1997), which is different from the stitching in integrally woven MWFs. Ko reported that stitching in multi-axial warp knitted fabrics can increase the fabric permeability, but the stitching here is still different from that in 3D MWFs (Ko and Du, 1997).

A large body of literature exists about the effects of fabric structures on the permeability. For the 3D MWFs, the key feature of stitched fabric is its interbundle stitches. But very limited information is available on the relationship between permeability and the effect of stitches. Shih and Lee proposed a parallel permeability model for flow through bi-directional stitched fabrics (Shih and Lee, 1998). The flow between the bundles is set by the Kozeny-Carman equation, and the effect of stitching was not specially mentioned. Cairns developed a model that incorporates Darcy's law in fibrous bundle regions and the channel flow equations between bundles (Cairns *et al*, 1999). This paper reported that two experimental systems, the stitched ±45 system and the stitched ±45/0 system cannot be predicted well by using the presented model. Cairns suggested that the permeability parameters needed to be re-evaluated with some account for the extensive stitching that was presented in these preforms. Loos studied the permeability of carbon multi-axial warp knit preforms (Loos *et al*, 1991). It was found that the introduction of through thickness fibres significantly increased the permeability of the preforms, especially for preforms with high volume fraction. The Kozeny-Carman equation was found to be adequate to provide a quantitative relationship between permeability and preform porosity. But the through thickness fibres here is still different from that in the 3D MWFs.

LundstrÖm also proposed a model for non-crimp stitched fabrics through theoretical analysis (LundstrÖm, 2000). It has been found that the flow in the interbundle channels was the most important and that the bundle flow could be neglected as to computations of the overall flow rate and consequently also as to the permeability. The results showed that the permeability of the fabrics varied considerably as a function of the direction of infiltration, although the geometrical variations were small. In the production direction of the fabrics the permeability was generally two to three times higher than it was in the perpendicular direction. On the other hand, the spread of the results between several samples was always measured to be higher in the high flow direction. The experiments also revealed that a choice of larger bundles in a fabric did not necessarily result in a higher permeability. The proposed simple model works well for certain cases, while it overrates the permeability in other cases. This suggests that if the real fabric should have the same geometry as the model, its permeability would be higher. Therefore, it is really significant and urgent to give a quantitatively study on the issue: how the inter-layer stitching affects the effective permeability? Such a study will be very helpful for the rational design of the stitched fabrics, the exact pre-simulation of molding process, and the global optimization of the processing parameters.

The structure of stitch in multi-layer woven fabrics is very complicated and variable. In this study, a model for description of the permeability of multi-layer woven fabrics is presented and compared with experimental data. Since composite materials are currently most often processed in thin shell-like structures, the discussion is restricted to the case of in-plane flow in the two dimensional textile fabrics.

In this study, there are types of woven fabrics. One is the multi-layer woven fabrics fabricated by the mono-filaments. This can eliminate the effects of other factors such as fiber bundle on the permeability and allow us to concentrate on the effect of fabric microstructure. Another one is the woven fabrics fabricated by the multi-filament yarn. Because these two types of multi-layer woven fabrics have different properties, so we develop two models to describe the permeability of these two different kinds of multi-layer woven fabrics.

In a RTM process, as the material is compressed due to the pressure. The cross-section of tows may no longer remain circular and change to elliptical shape. But in this study, our major objective is to study the effect of fabric structure on permeability. The fabric structure here is mainly referred to the micro-structure between the tows. Duo to the pressure, the tows and the micro-structure between them both will be compressed and deformed. Compared with the tow, the deformation of the structure between the tows may be significant and distinctly. So in this study, we ignore the transformation of the tows and focus on the micro-structure between the tows.

4.2 Mono-Filament Permeability Model

4.2.1 Characterization of Pore Microstructures

The permeability is a function of the preform architecture, pore structure and porosity, and different types of fiber preforms may have substantially different permeability at the same fiber volume fraction. The micrograph of fiber preform reveals considerably complicate microstructures of multi-layer woven fabrics. However, our experimental data showed that the variation in the alignment of the

fiber layers and the pore size distribution was regularly. Thus it is possible to find an analytical solution for permeability based on the concept of a unit cell.

Figure 4.l displays the top view of the three types of multi-layer woven fabrics fabricated by the mono-filaments. Each fabric has five layers in total and a layer being defined as containing both a warp and weft yarn. All weaves are designed as plain weaves and weft yarns are used as stitches to interconnect adjacent layers. The differences between these designs are the stitching density.

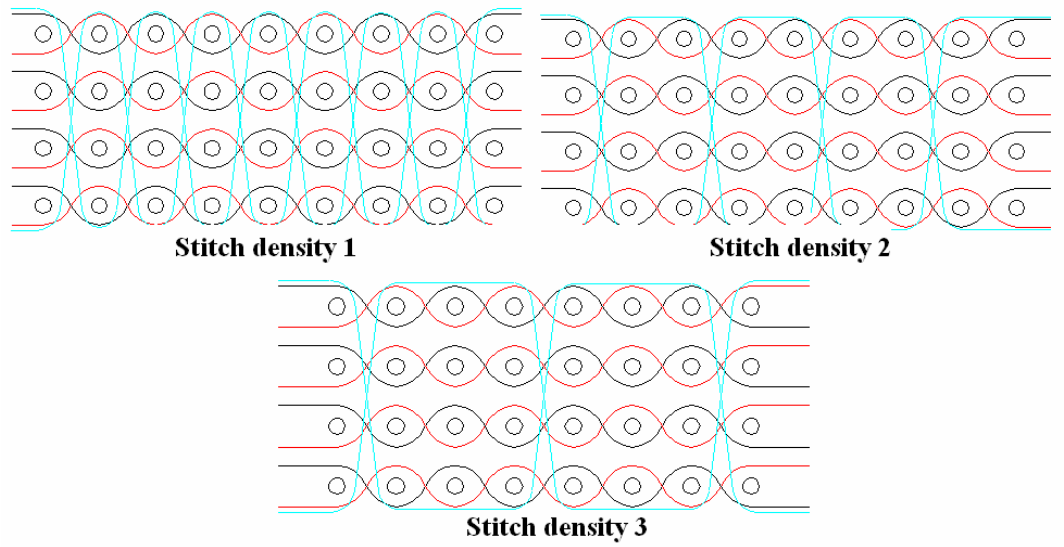

Figure 4.1 The Schematic for three different stitch models of multi-layer woven fabrics

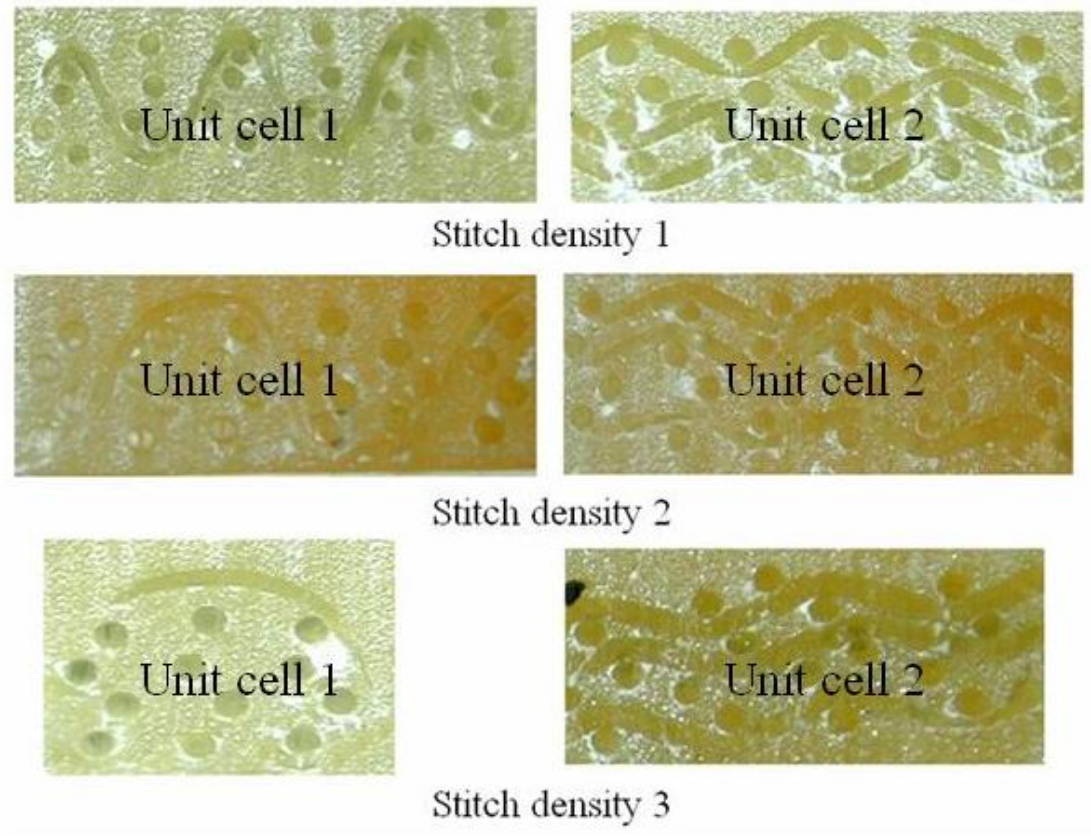

Figure 4.2 The cross-sectional view of three types of multi-layer woven fabrics with different stitch density

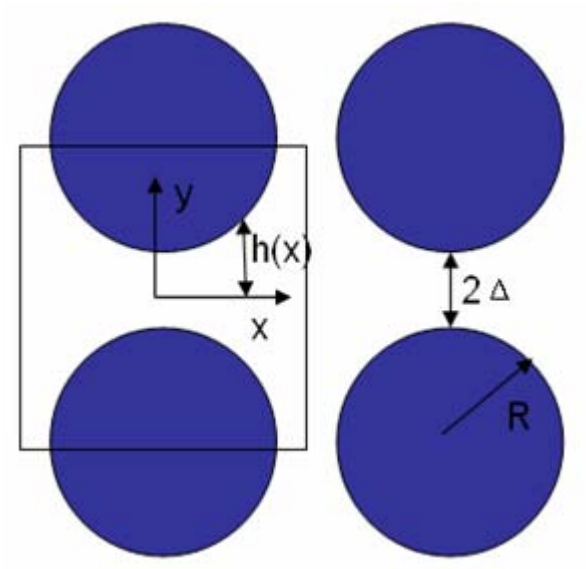

Figure 4.3 Definition sketch of the idealized mono-filament reinforcement arrangement and the representative unit cell of quadratic fiber packing.

4.2.2 Permeability Model of unit cell 1

From the cross-sectional view of three types of multi-layer woven fabrics, the structure of the preform can be idealized as a porous medium consisting of parallel fibers as shown in figure 4.3. Based on the assumption that the major contribution to the flow resistance comes from the narrow gap between the fibers, the permeability model therefore can be established as following:

The fibers are arranged in a periodic pattern so that we only need to consider the flow in one “representative unit cell”. The pattern that we are going to consider is the quadratic array. Let us assume that most of the resistance to flow which is perpendicular to the fibers comes from a small region close to the narrow gap formed between the fibers. If the fibers are very close to each other they form a channel with slowly varying area between them. Here we mean that the angle between the channel wall and the channel centre-line is small at all points along the channel.

For the flow in the slow-varying channels, the cross section area varying along the streamline direction is assumed to alter so slow that inertia effects can be neglected(in the present case this is true for all geometries, since generally in RTM the Reynolds number of the resin is very small. If a constant pressure difference is maintained between two stations, the pressure gradient will vary slowly in the streamline direction:

$$\frac{dp}{dx} = -\frac{3}{2}\frac{\mu q}{h^3(x)} \qquad (4\text{-}1)$$

Where h(x) is the half height of the channel, p is the pressure, u is the viscosity.

The total pressure drop between two stations: a and b, in the channel can be found from an integration of equation (1):

$$p_b - p_a = -\frac{3}{2}\mu q \int_a^b \frac{dx}{h^3(x)} \tag{4-2}$$

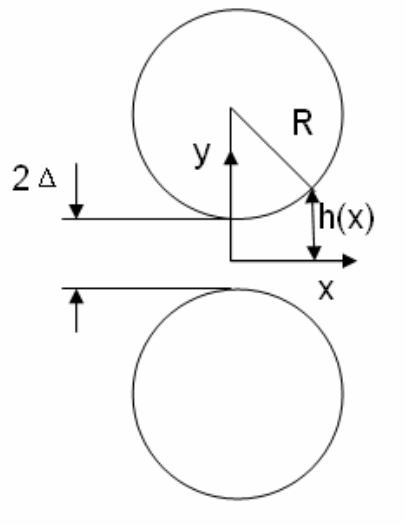

Figure 4.4 Definition sketch in the analysis of the flow between the fibers

From the Definition sketch over the coordinate system and the channel half height, the h(x) needed in the integral can be calculated by:

$$h(x) = \Delta + R\left(1 - \sqrt{1 - \frac{x^2}{R^2}}\right) \tag{4-3}$$

Which for x ≪ R, it can be written as

$$h(x) = \Delta + \frac{R}{2}\frac{x^2}{R^2} \tag{4-4}$$

Substitution of h(x) into equation (4-2) gives,

$$p_b - p_a = -\frac{3}{2}\mu q\int_a^b \frac{dx}{\left[\Delta + R(1--\sqrt{1-\frac{x^2}{R^2}})\right]^3} \tag{4-5}$$

By integrating the above integral equation and making some simplification based on the boundary conditions, we can get the following equation:

$$p_b - p_a = -\frac{9\pi}{16}\frac{\mu q}{\Delta^3}\sqrt{2R\Delta} \tag{4-6}$$

Which means that the pressure drop between two fibers in general can be written as:

$$\frac{\Delta p}{L} = -\frac{9\sqrt{2}\pi}{16L}\frac{\mu q}{R^2}(\frac{\Delta}{R})^{-5/2} \tag{4-7}$$

Comparing equation 4-7 with Darcy law, we can get the equation to calculate the permeability of porous medium.

$$K_1 = \frac{16}{9\pi\sqrt{2}}(\frac{\Delta}{R})^{5/2}R^2 \tag{4-8}$$

Equation 4-8 can be rewritten in terms of fiber volume fraction if we notice that the fiber volume fraction can be calculated by:

$$V_f = \frac{\pi/4}{(1+\Delta/R)^2} \tag{4-9}$$

From which we see that Δ/R is

$$\Delta/R = \sqrt{V_{f,\max}/V_f} - 1$$

where $V_{f,max}$ is the maximum fiber volume fraction which is achieved when the

adjacent fibers touch each other.

Substitution of Δ / R in equation (4-8) finally yields:

$$K_1 = \frac{16}{9\pi\sqrt{2}}(\sqrt{\frac{V_{f,\max}}{V_f}} - 1)^{5/2} R^2 \qquad (4\text{-}10)$$

4.2.3 Evaluation of $V_{f,max}$

The maximum fiber volume fraction in the permeability expression equation (4-10) corresponds to the maximum space occupied by the fibers in the preforms. The architecture the multi-layer woven fabrics considered in the study consists of a layer to layer interlacement. For this architecture, the maximum fiber volume fraction of these different stitch structures may be considered to vary from the quadratic array to the hexagonal array as shown in figure 4.5.

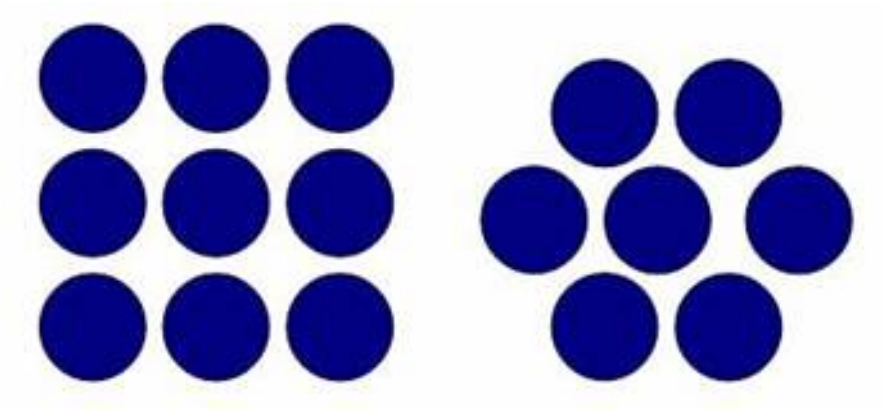

Figure 4.5 Definition sketch of quadratic and hexagonal array

For the quadratic array, the maximum fiber volume fraction is $\pi / 4$; for the

hexagonal array, the maximum fiber volume fraction is $\pi/2\sqrt{3}$. However, in this experiment, the maximum fiber volume fraction of the unit cell may be between these two values. A coefficient, C_f ($1 \le C_f \le 2/\sqrt{3}$), is thus introduced to define the maximum fiber volume fraction $V_{f,\max} = C_f \cdot \frac{\pi}{4}$.

If the coefficient C_f = 1, this means that the fiber in the unit cell is quadratic array, and $C_f = 2/\sqrt{3}$, fiber are arrayed in hexagonal model.

As shown in the experimental cross images, for the structure of stitch density 1, C_f = 1; for structure of stitch density 3, $C_f = 2/\sqrt{3}$; for structure of stitch density 2, $C_f = 1.1$.

4.2.4 Predicted Permeability of the Unit Cell 1

So from the Eq. (4-10), we can get the permeability of these three different structures of unit cell as show in figure 4.6.

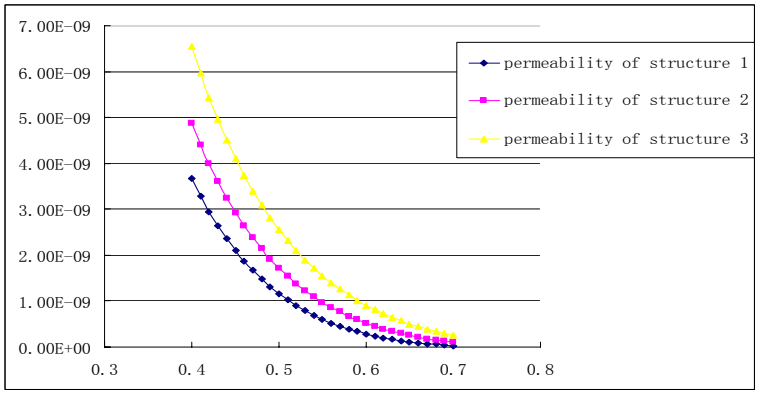

Figure 4.6 The permeability of three different structures of the unit cells

As shown in this figure, we can see that the permeability of stitch structure 3 is better than stitch structure 1. This is due to its easy going pathway arrangement, and

this is also testified by the subsequent experiment results as follows.

4.2.5 Permeability Model of unit cell 2

For the unit cell 2, the unit cell can be simplified as shown in figure 4.7. The permeability can be obtained from the expression for equivalent permeability of a rectangular channel. In this study, the width of channel is assumed to be L_a; the height of channel is L_b.

(a)

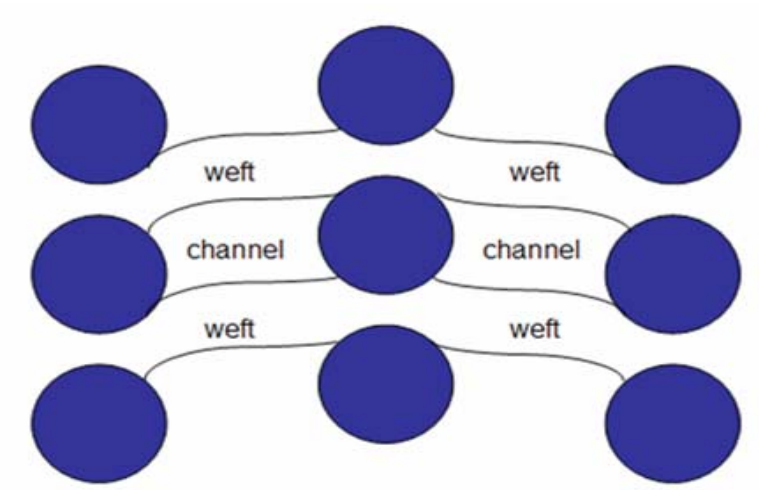

(b)

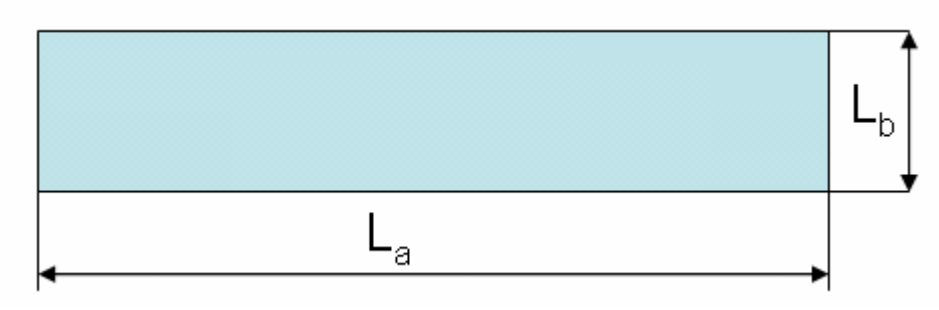

(c)

Figure 4.7 (a) architecture of the structure 2, (b) an idealized structure, (c) an idealized unit cell

The solution of the two-dimensional velocity field in an arbitrary duct geometry is governed by an equation of the Poisson form. Once the flow field is obtained, integration over the domain provides a relationship for the average flow rate with respect to the applied pressure gradient. For a rectangular duct with sides of length L_a and L_b,

$$u = -\frac{l_a^2}{12\mu}\left(\frac{dp}{dx}\right)\left[1 - \frac{192 l_a}{\pi^2 l_b}\sum_{n=1,3,5\ldots}^{\infty}\frac{\tanh(i\pi l_b / 2l_a)}{i^5}\right] \tag{4-11}$$

This result can be compared to the Darcy law in one dimension:

$$u = -\frac{k_{equ}}{\mu}\frac{dp}{dx} \tag{4-12}$$

Modeling the channel region as a porous medium of porosity 1.0, the average volume velocity may be equal to the average velocity provided by Equation (4-12). By comparison, we can obtain the permeability of this duct

$$K_2 = -\frac{l_a^2}{12}\left[1 - \frac{192 l_a}{\pi^2 l_b}\sum_{n=1,3,5...}^{\infty}\frac{\tanh(i\pi l_b / 2l_a)}{i^5}\right] \tag{4-13}$$

4.2.6 Permeability of Whole Structure

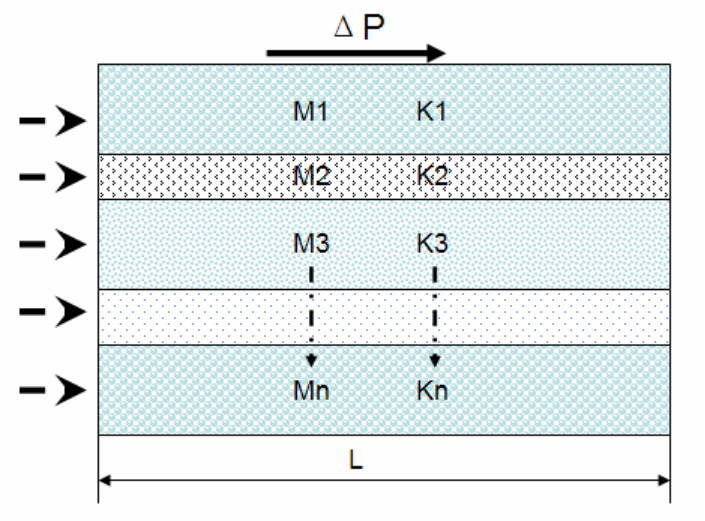

Figure 4.8 The Schematic of multi-layers laminar flow

As shown in figure 4.8, the permeability of each layer is represented by Kn, and the height is represented by Mn. The total flow rate through the multi-layer q and the total height can be expressed as following:

$$q = q_1 + q_2 + \ldots + q_n = \sum_{i=1}^{n} q_i \tag{4-14}$$

$$M = M_1 + M_2 + \ldots + M_n = \sum_{i=1}^{n} M_i \tag{4-15}$$

The pressure difference of each layer can be shown in following equation:

$$\Delta P = \Delta P_1 = \Delta P_2 = \ldots = \Delta P_n \tag{4-16}$$

From the Darcy law,

$$q_i = K_i M_i \cdot \frac{\Delta P_i}{L} \tag{4-17}$$

We can get the total flow rate

$$q = \sum_{i=1}^{n} q_i = \sum_{i=1}^{n} K_i M_i \cdot \frac{\Delta P_i}{L} = K_p \cdot M \cdot \cdot \frac{\Delta P}{L} \tag{4-18}$$

So the effective permeability of a multi-layer flow channel

$$K_p = \sum_{i=1}^{n} K_i \cdot M_i \Big/ \sum_{i=1}^{n} M_i \tag{4-19}$$

Where Kp is the effective permeability of a multi-layer flow channel.

Incorporating Eq. (4-10) and Eq. (4-13) into Eq. (4-19), we can get the final equation to calculate the effective permeability of multi-layer woven fabrics.

$$K_p = (K_1 M_1 + K_2 M_2)/(M_1 + M_2) \tag{4-20}$$

$$K_p = \frac{\frac{16}{9\pi\sqrt{2}}(\sqrt{\frac{V_{f,\max}}{V_f}} - 1)^{5/2} R^2 \cdot M_1 - \frac{l_a^2}{12}(1 - \frac{192 l_a}{\pi^2 l_b} \sum_{n=1,3,5...}^{\infty} \frac{\tanh(i\pi l_b / 2l_a)}{i^5}) M_2}{(M_1 + M_2)} \tag{4-21}$$

4.2.7 Experimental Results and Discussion

Table 4.1 reports the predicted principal effective permeability and steady state radial experimental results. It can be seen that the predicted results are in good agreement with those of the radial flow experiments.

Table 4.1(a). The permeability of the 3D woven fabrics for the stitch density 1

fiber volume farction	0.43	0.491	0.543	0.602
K1 from Equation (4-10)	2.64E-09	1.31E-09	6.94E-10	2.84E-10
K2 from Equation (4-13)	1.67E-09	9.87E-10	4.17E-10	2.04E-10
Kp from Equation (4-21)	2.15E-09	1.15E-09	5.55E-10	2.44E-10
Radial flow experiment	2.23E-09	1.20E-09	4.97E-10	2.33E-10

Table 4.1(b). The permeability of the 3D woven fabrics for the stitch density 2

fiber volume farction	0.44	0.503	0.551	0.609
K1 from Equation (4-10)	3.25E-09	1.72E-09	9.76E-10	4.53E-10
K2 from Equation (4-13)	1.67E-09	9.87E-10	4.17E-10	2.04E-10
Kp from Equation (4-21)	2.46E-09	1.35E-09	6.96E-10	3.29E-10
Radial flow experiment	2.35E-09	1.19E-09	6.70E-10	3.33E-10

Table 4.1(c). The permeability of the 3D woven fabrics for the stitch density 3

fiber volume farction	0.447	0.512	0.559	0.618
K1 from Equation (4-10)	4.11E-09	2.31E-09	1.40E-09	7.23E-10
K2 from Equation (4-13)	1.67E-09	9.87E-10	4.17E-10	2.04E-10
Kp from Equation (4-21)	2.89E-09	1.65E-09	9.07E-10	4.64E-10
Radial flow experiment	2.98E-09	1.54E-09	8.40E-10	4.27E-10

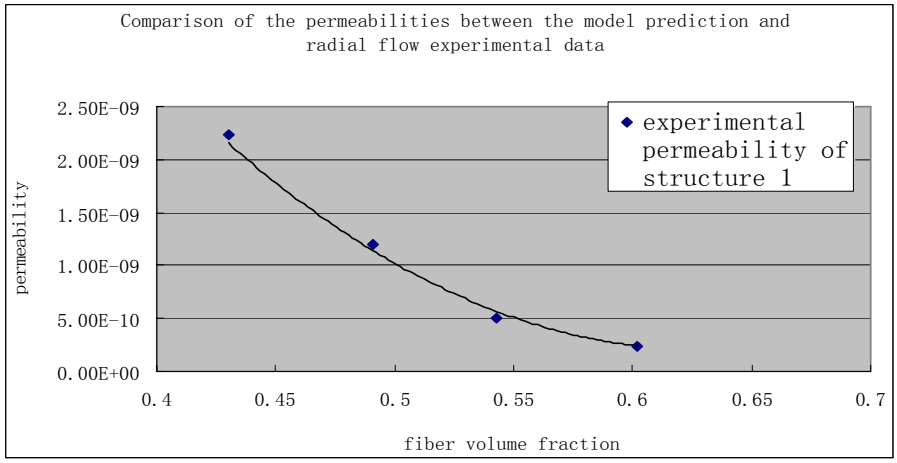

(a)

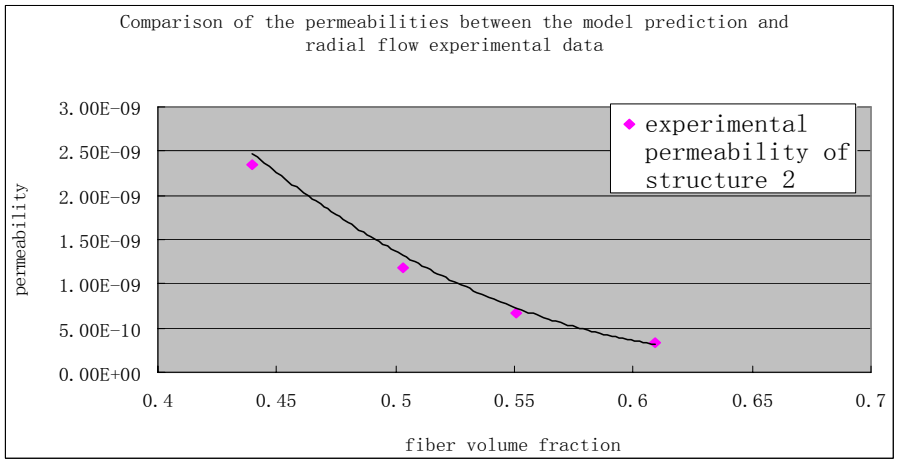

(b)

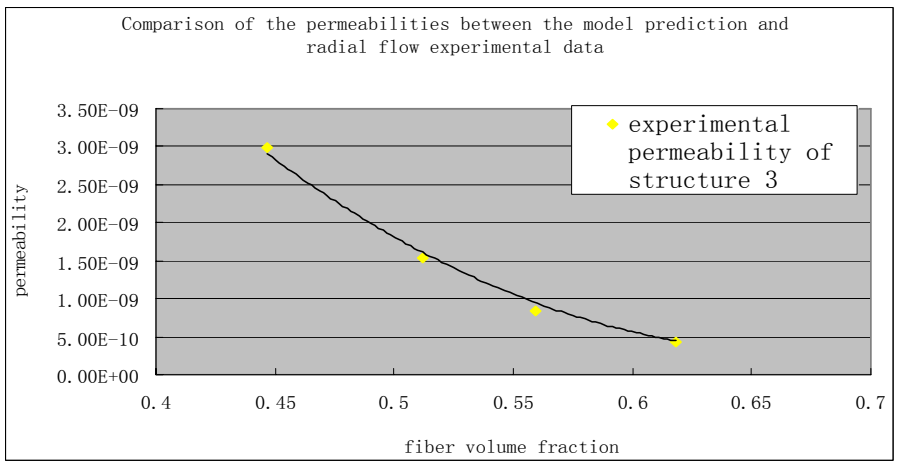

(c)

Figure 4.9 Comparisons in terms of the permeabilities between the model prediction and the experimental data

Figures 4.9(a), 4.9(b), 4.9(c) again compare the present model prediction and experimental results among the three different fiber preforms as a function of fiber volume fraction. As compared with the experimental results, the predictions given by the modeling generate less than 10% relative errors. Good agreement between the model prediction and experimental results is found in the fiber volume fraction ranges from $0.4<V_f<0.7$ for 3D multi-layer woven fabrics. This shows the validity of the present in-plane permeability model in the above range of fiber volume fraction.

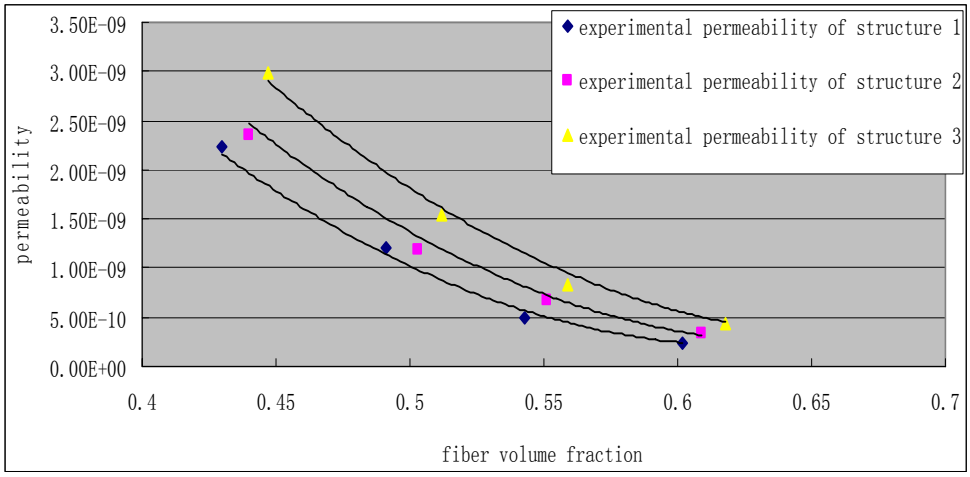

Figure 4.10 Comparison of the permeabilities among the 3D woven fabric performs with three different stitch density structures

The comparison shows that at the same fiber volume fraction, different stitching model fabrics have different permeability. For different stitching structure fabrics, the fabrics with the stitch structure 3 have better permeability than fabrics with the stitch structure 1. From the theory model analysis, this difference is due to the different stitch array and distribution in the fabric preforms. As testified by the experimental and numerical analysis, the fabrics with loose stitch array have better permeability than fabrics with compact stitch array. This is due to the different flow resistance introduced by different stitch array. For fabrics with stitch structure 3, the flow resistance from the stitch array is less than stitch 1, so the resin can flow more easily within it. Thus lead to the better permeability of stitch structure 3 than

other two structures. The experimental permeability testing results are also consistent with the theory model predictions.

4.2.8 Conclusion remarks

A simplified general permeability model for 3D multi-layer woven fabrics is developed in details based on the regular mono-filament arrangement in the unit cell geometry. The in-plan permeability model can be expressed in a simplified form related to the architectures of fiber preforms and the fiber volume fraction changes of fiber preforms under compression. The results show that the permeability of the mono-filament preforms is mainly determined by the arrangements of fibers and the channels between the fiber tows. The fabrics with loose stitch array have better permeability than fabrics with compact stitch array. This is due to the different flow resistance with regard to different stitch array. The looser of stitch structure, the more easy of the resin can flow through it. Thus lead to the better permeability of fabrics with loose stitch array. The results predicted by this model are compared with those from experiments and a good agreement is found in a broad range of fiber volume fraction.

4.3 Fractal permeability model

4.3.1 Fractal Characterization of Pore Microstructures in Fiber Preforms

Figure 4.11 displays a cross-sectional view of multi-layer woven preforms. There are two types of pores, a macro-pore (of the order of 10^{-3} m) between fibre tows and the micro-pores (10^{-6} ~10^{-5} m) inside the fibre tows. If several layers of fibre mats

were stacked together, the macro-pores of each layer would form macro-channels with the sizes of 10^{-3} m, see Figure 4.11, while micro-pores inside the fibre tows would form numerous tortuous micro-channels.

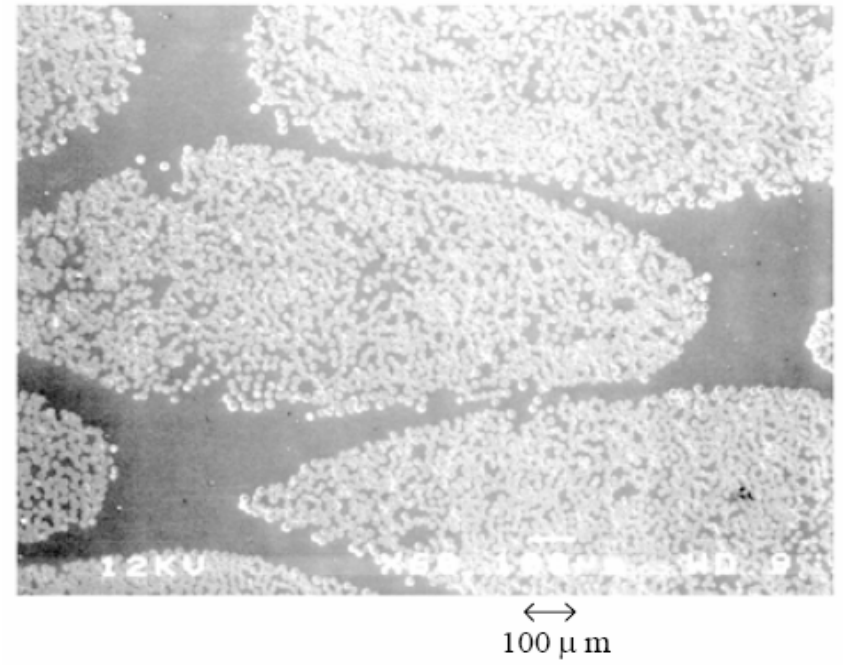

Figure 4.11 Micrograph of fibers and resin

Both the macro-channels and the micro-channels should follow the fractal scaling law given by (Mandelbrot, 1982).

$$L_t(\lambda) = \lambda^{1-D_T} L_0^{D_T} \qquad (4\text{-}22)$$

where D_T is the tortuosity fractal dimension, with $1 < D_T < 2$, representing the extent of convolutedness of capillary pathways for fluid flow through a medium, λ is the size of a pore channel in a fiber preform, and $L_t(\lambda)$ is its tortuous length along the flow direction.

For the macro-pores between fiber tows and the micro-pores inside fiber tows, its

cumulative size-distribution of pores in porous fiber preforms follow the fractal scaling law

$$N(L \geq \lambda) = \left(\frac{\lambda_{\max}}{\lambda}\right)^{D_f} \tag{4-23}$$

From Eq. (4-23), it can be found that

$$-dN = D_f \lambda_{\max}^{D_f} \lambda^{-(D_f+1)} d\lambda \tag{4-24}$$

Eq. (4-24) describes the scaling relationship of the cumulative pore number.

4.3.2 Fractal Model for Permeability

This model is related to the architectural parameters of preforms, the pore area fractal dimension D_f and the tortuosity fractal dimension D_T.

The total volumetric flow rate, Q, through the unit cell is a cumulative of the flows through all of the individual pore channels, including the macroscopic pore (gap or channel) between the fiber tows and the microscopic pores inside the fiber tows. The flow rate through a single pore channel is given by modifying the well known lubrication flow theory (Wheatcraft and Taylor, 1988).

$$q(\lambda) = \frac{-1}{6\mu} A\lambda^2 \frac{\Delta p}{L(\lambda)} \tag{4-25}$$

The total flow rate Q through the unit cell can be obtained by integrating the individual flow rate, $q(\lambda)$, over the entire range of pore sizes from the minimum pore size $\lambda = \lambda_{min}$ to the maximum pore size $\lambda = \lambda_{max}$ (Pitchumani and Ramakrishnan, 1999). According to Eqs. (4-22), (4-23) and (4-24), we have

$$Q = -\int_{\lambda_{\min}}^{\lambda_{\max}} q(\lambda) dN(\lambda) \qquad (4\text{-}26)$$

$$Q = -\int_{\lambda_{\min}}^{\lambda_{\max}} \frac{-1}{6\mu} A\lambda^2 \frac{\Delta p}{L(\lambda)} D_f \lambda_{\max}^{D_f} \lambda^{-(D_f+1)} d\lambda \qquad (4\text{-}27)$$

$$Q = \frac{A\Delta pD_f}{6\mu L_0^{D_T}(D_T - D_f + 1)} \lambda_{\max}^{1+D_T} \left(1 - \left(\frac{\lambda_{\min}}{\lambda_{\max}}\right)^{D_T - D_f + 1}\right) \qquad (4\text{-}27)$$

Since $1 < D_T < 2$ and $1 < D_f < 2$, there exist $D_T - D_f + 1 > 0$ and $0 < \left(\frac{\lambda_{\min}}{\lambda_{\max}}\right)^{D_T - D_f + 1} < 1$ in Eq. (4-27). Due to $\left(\frac{\lambda_{\min}}{\lambda_{\max}}\right) \sim 10^{-2}$, Eq. (4-27) can thus be reduced to,

$$Q = \frac{A\Delta pD_f}{6\mu L_0^{D_T}(D_T - D_f + 1)} \lambda_{\max}^{1+D_T} \qquad (4\text{-}28)$$

Using the Darcy law, we obtain the permeability equation as follows:

$$K = \frac{\mu L_0 Q}{\Delta PA} = \frac{\mu L_0^{1-D_T} D_f \lambda_{\max}^{1+D_T}}{6\mu(D_T - D_f + 1)} \qquad (4\text{-}29)$$

Obviously, the permeability of fiber preforms is mainly determined by the macro-pore (gap or channel) between the fiber tows. The previous study indicated that the permeability contribution from micropores inside the fiber tows is negligible (Yu and Li, 2001). Thus, only the tortuosity of macro-pore channel pathways is to be included in the present consideration. It can be found that the macro-pore channels are approximately straight, see figure 4.11. Therefore, $D_T = 1$ is applied in this investigation, and Eq (4-29) can be thus reduced to

$$K = \frac{D_f \lambda_{\max}^2}{2 - D_f} \qquad (4\text{-}30)$$

In which D_f can be expressed as $D_f = 2 - \frac{\ln \phi}{\ln(\lambda_{\min} / \lambda_{\max})}$ (4-31)

So from this final equation, it can be predicted that with the increase of λ_{max}, both D_f and K are increased with it also.

4.3.3 Experimental Studies

Experimental studies were carried out with the objectives of investigating the effects of stitch structure on the permeability. In this study, three different weave constructions were designed and tested. Figure 4.12 and 4.13 present structures and cross-sectional views of 3 different stitch structure fabrics and Figure 4.14 is the schematic of the resin channels and fabric subdomains. Figure 4.15 presents the comparisons of the experimental permeabilities.

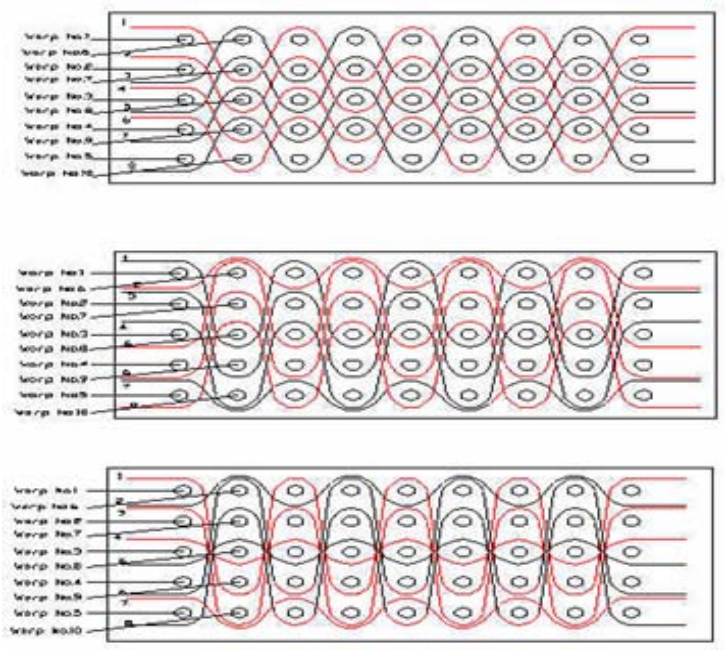

Figure 4.12 Structures of 3 different stitch structure fabrics

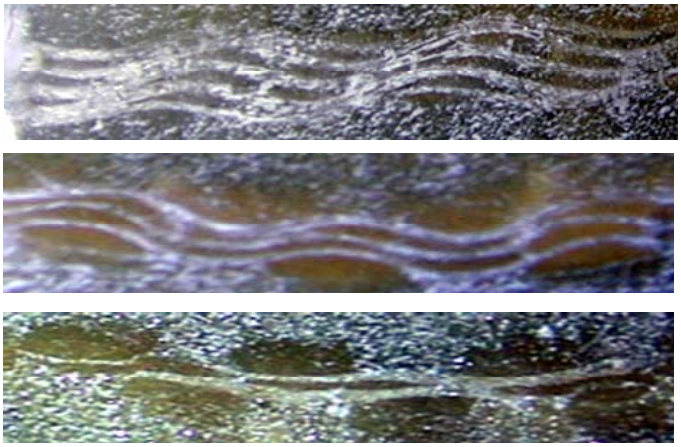

Figure 4.13 Experimental cross-sectional views of 3 different stitch structure fabrics

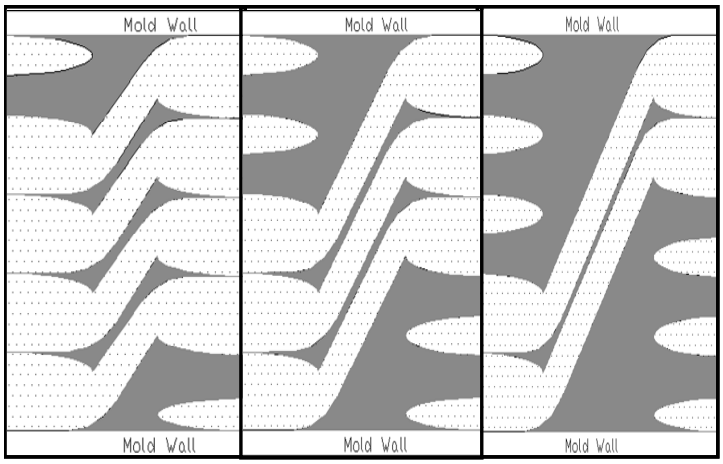

Figure 4.14 Schematic of the resin channels and fabric subdomains

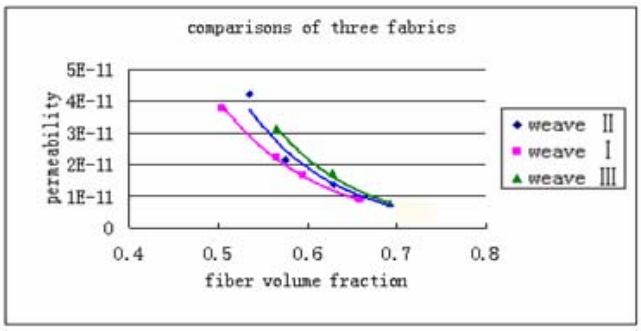

Figure 4.15 Comparisons of the experimental permeabilities

From these figures, it can be seen that from the weave Ⅰ to weave Ⅲ, the resin

channels increase, correspondingly is the increment of the maximum pore size λ_{max}. Therefore from final Eq. (4-30), it can be predicted that with the increase of λ_{max}, the permeability of fabric will increase too. And this is also testified by the experimental data as shown in figure 4.15.

When the fabrics is compressed, the $-\ln\phi$ is increased, $-\ln(\lambda_{min}/\lambda_{max})$ is decreased. According to the equation $D_f = 2 - \frac{\ln\phi}{\ln(\lambda_{min}/\lambda_{max})}$, then the D_f is decreased. As a result, the permeability in $K = \frac{D_f \lambda_{max}^2}{2 - D_f}$ also will be decreased. This is accord with the experimental results which the permeability is decreased with the decrease of porosity.

4.3.4 Concluding Remarks

A fractal permeability model for description of the disordered pore structures of preforms used in liquid composite molding processes was developed based on the fractal characteristics of pores in the fiber preforms. The permeability model was found to be a function of the pore area fractal dimension, the tortuosity fractal dimension, and the architectural parameters of fiber preforms. Experimental validation of the fractal model was conducted over a series of stitch structures and the trends predicted by the model are agreed with the experimental data.

4.4 Conclusion

In this chapter, the effects of fabric micro-structures and other properties of the multi-layer woven fabrics on the permeability have been discussed. A permeability model based on fractal theory has been established to predict the permeability of

preforms fabricated by porous yarns. Another permeability model based on unit cell of quadratic fiber packing has also been established to predict the permeability of the 3D multilayer woven fabrics fabricated with the mono-filaments.

For the 3D multi-layer woven fabrics fabricated with the mono-filament, the permeability model was related to the architectures of fiber preforms and the fiber volume fraction changes of fiber preforms. The experimental results show that the permeability of mono-filament preforms is mainly determined by the arrangement of the channels between the fiber tows. At the same fiber volume fraction, the fabrics with loose stitch array have better permeability than fabrics with compact stitch array. This is due to the different flow resistance with regard to different stitch array. For fabrics with loose stitch structure, the flow resistance from the stitch array is less than that of fabrics with tight stitch array. Thus lead to the better permeability of fabrics with loose stitch array. The results predicted by the numerical model are compared with those from experiments and a good agreement is found in a broad range of fiber volume fraction.

For the 3D multi-layer woven fabrics fabricated by porous yarns, a fractal permeability model was developed based on the fractal characteristics of pores in the fibre preforms to describe the disordered pore structures of preforms. The permeability model was found to be related to the pore area fractal dimension, the tortuosity fractal dimension, and the architectural parameters of fibre preforms. For fabrics with a rather large maximum pore size, λ_{max}, the flow resistance is relatively lower. Then the resin can impregnate more easily within it. Thus lead to better permeability and less void formation in fabrics. The experimental validation of the fractal model was conducted over a series of stitch structures and the tendency

predicted by the model agrees with the experimental data.

Chapter 5

Void formation

5.1 Introduction

Among the various manufacturing processes, RTM has been believed as a versatile and efficient process for the products of high-performance advanced textile composites due to their relatively short cycle time, low labor requirements and equipment costs. During the RTM processing, a liquid thermosetting resin is injected into a closed mold containing a prefabricated preform which is formed by fiber tows. Unfortunately, the fiber preforms always have complicated and non-uniform microstructure, and hence the local permeabilities between insider and outsider fiber tows may differ by several orders of magnitude. These non-uniform properties finally will lead to the formation of air voids on the micro scale (Parnas and Phelan, 1991; Patel and Lee, 1995; Chen, *et al*, 1995).

Previous researches (Yosida et al, 1986; Harper et al, 1987; Bowles and Frimpong, 1991; Feldgoise et al, 1991; Ghiorse and Jurta, 1991) revealed that the presence of voids is highly undesirable and has a deleterious effect on product mechanical properties including the inter-laminar shear strength, compressive strength, impact resistance and fatigue life. The research also revealed that the void formation and development is correlated to injection pressure, outlet pressure, resin properties (viscosity, surface tension), fabric characteristics (type and orientation of fibres, surface treatment), etc. Some studies (Chen *et al*, 1995; Hayward and Harris, 1990) reported that the quantities of voids would be reduced with the assistance of vacuum techniques, but cannot totally solve the problem. In recent years, the

problem of void formation has received much attention and has been studied extensively. However, the variety of the architectures of fibre preforms is too large to allow the prediction of void formation based on one general model only. Furthermore, the void formation in RTM seems to be inevitable and there is no proven way to eliminate voids completely (Chang and Hourng, 1998). Hence, the understanding of the void formation mechanism is an important task and is necessary for the mould and fibre preform design.

As well known, there are two scales of flow during RTM: one is the macro flow in the gaps between/ around the tows, and the other is the micro flow within tows. Based on this concept, several investigators have developed models to predict void formation in RTM. Parnas and Phelan developed a model to predict the air entrapment for flow through uni-directional fibre mats with the global flow transverse to the fibres (Parnas and Phelan, 1991). Chen also developed a model similar to that of Parnas and Phelan (Chen *et al*, 1995). The difference of these two models is that Chen *et al*. included the effects of capillary pressure on the impregnation of fibre tows. Also based on the concept of the two scales of flow, Chan and Morgan developed a model to analyse the resin flow and air entrapment during RTM of bi-directional non-woven fibre preforms (Chan and Morgan, 1992). Patel and co-workers carried out flow visualisation experiments of void formation in unidirectional stitched (Patel *et al*, 1995), bi-directional stitched and 4-harness woven fibreglass mat (Patel and Lee, 1995). They reported that fingering took place at the flow front because of permeabilities in the fibre tows and in the gaps between the fibre tows were different, and void formation was correlated to capillary number and the liquid-fibre-air contact angle. For axial flow, the microvoids were formed at

$Ca^* > 10^{-3}$, for transverse flow, the microvoids were formed at an even lower capillary number, $\sim 10^{-4}$. Once formed, the microvoids were difficult to purge and remained trapped even after bleeding the liquid at much higher flow rates than those at which they were formed (Rohatgi *et al*, 1996).

Several researchers have carried out theoretical analysis to describe the mechanism of void formation during RTM. Binetruy and Hilaire developed an analytical model to describe the tow impregnation where the global flow parallel to the fiber axis (Binetruy and Hilaire, 1998). Based on the study of the contribution of the axial and transverse flow mechanisms inside tows, this model shows that the main tow impregnation process is transverse to the fiber axis. A criterion has been established to indicate when the axial flow can be neglected to simplify the tow impregnation. Kang proposed a mathematical model to describe the mechanisms of void formation when global flow is transverse to fiber tow (Kang, *et al*, 2000). The model shows that for a given fiber preform, the effects of resin velocity and capillary pressure can be described by the capillary number. With proper calibration, it can predict the size and content of voids within fiber tows as well as between them.

The scope of current study is to carry out a theoretical analysis for in-plane impregnation in multi-layer woven fabrics (MWFs) to understand the mechanism of void formation. Unlike the previous work (Patel and Lee,1995), where the void is formed in the plane of one layer of woven fabric, in this thesis the void formation in the cross-section of MWFs was studied. Based on two simplified unit cells, which were identified from two typical multiple modes of MWFs, a mathematical model was developed to analyze the formation and size of voids. The flow front and void formation processes were also numerically simulated using control-volume method.

5.2 Numerical model of void formation

5.2.1 Unit cell of the plain woven fabric

First, let us consider one layer of plain weave fabric. The typical architecture is displayed in figure 5.1(a). As described by Simacek and Advani, there are two sub-domains within the preform (Simacek and Advani, 1996). One consists of the fiber tows (warp and weft) which are woven together to create interconnected network. Another one is a network of empty pores and channels around yarns. Due to the non-uniform permeability in these two sub-domains, during RTM processes, void are formed not only in the plane of fabric as described by Patel and Lee (Patel and Lee, 1995), but also in the cross-section of multi-layer woven fabric.

Three important geometry parameters of this fabric are tow thickness h, tow width l_b and width of channel between adjacent tows l_c. Usually, the ratio l_b / h is about 5 or more for most reinforcement used in composites processing, and the cross section of fiber tows are not circular but elliptical as shown in Figure5.1(b). The present study focuses on resin impregnation and void formation in the cross-section of MWFs. For the purpose of simplicity, the configuration of undulating yarns is approximated by linear segment and the cross-section of fiber tow is considered to be rectangular, then an idealized cross-section of one layer plain woven fabric for in-plane impregnation along x-direction can be obtained as shown in Figure 5.1(c).

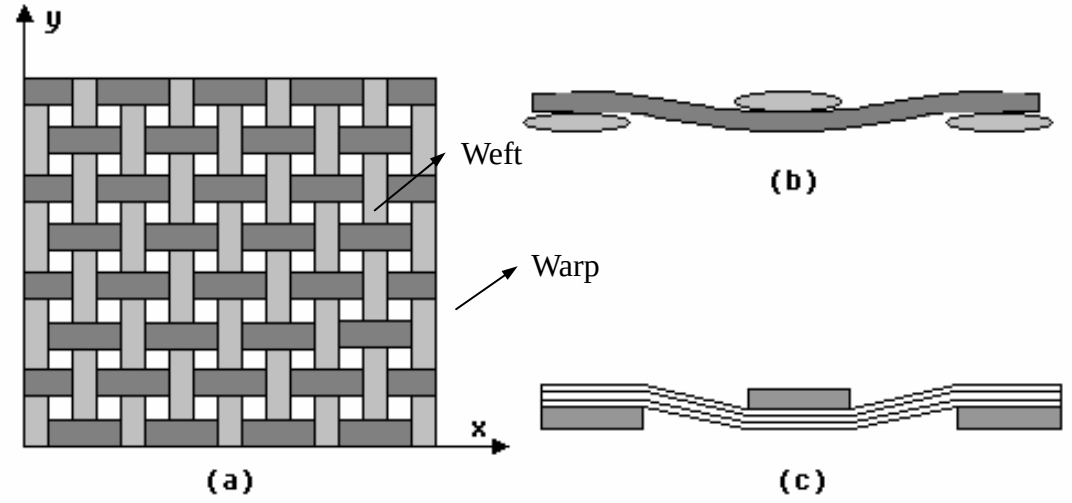

Figure 5.1 Architecture of the plain woven fabric

When multiple layers of woven fabric are stacked together, due to the in-plane displacement, two typical modes can be observed as shown in Figure 5.2 In mode I, there is no displacement between adjacent layers, while there is a displacement l_c in mode Π. The above analysis is strongly supported by image analysis as shown in Figure 5.3

Although the actual woven fabrics are 3D, in this simulation, we only consider the flow along the cross section of woven fabrics. So this 2D simulation model can simulate the flow along the cross section of 3D woven fabrics.

In both multiple modes, two unit cells for the void formation can be identified as shown in Figure 5.4 (a) and (b). It can be seen that the flow through the cross-section of the unit cell passes through not only the channel but also the weft and warp. Most resin would flow through the channels along the imposed pressure gradient, but it can also flow within warps and wefts. So we choose two paths as a representative cell, as shown in Figure 5.4 One way is along the weft tow while the other one is the flow in the channel and warp. As testified in the study of N. Patel, the formation of voids is mainly due to the velocity difference of resin in different paths (Patel and

Lee, 1995).

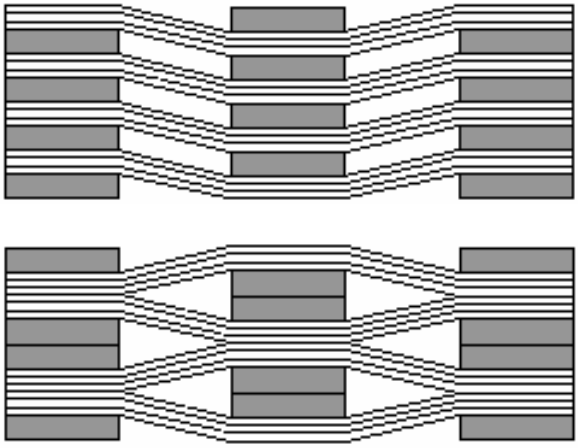

(a) mode I

(b) mode Π

Figure 5.2 Two typical multiple modes of MWFs

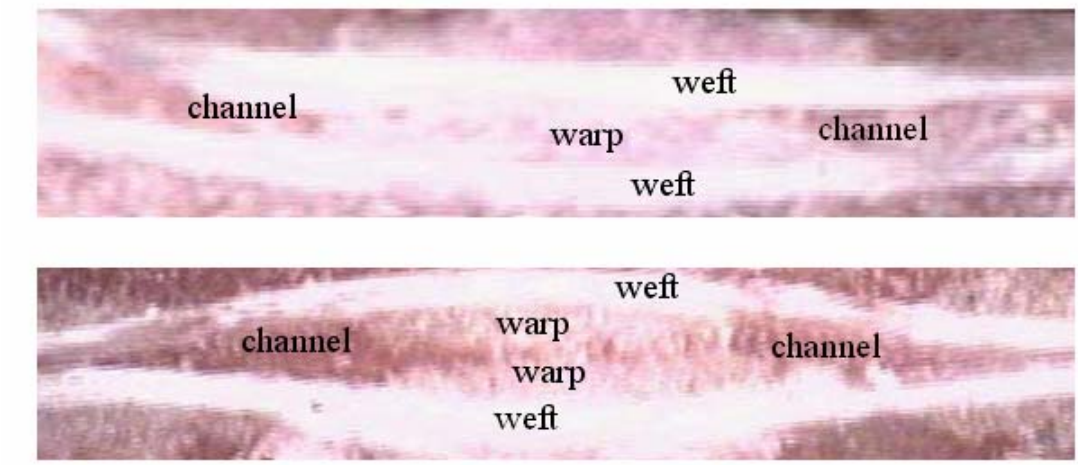

Figure 5.3 Typical cells of cross-section for MWFs

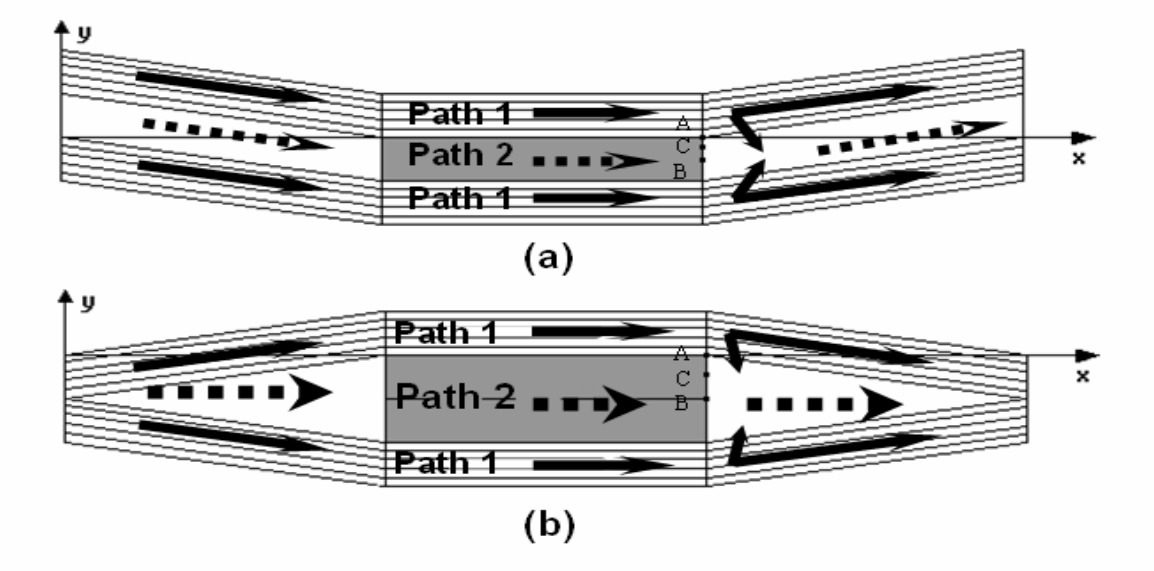

Figure 5.4 unit cells for mode I and mode Π

5.2.2 Void formation prediction based on newly developed model

In the case of high injection pressure, the effect of capillary is negligible; voids will form at the end of warp tow as shown in Figure 5.4. This will be discussed in more details as following. Since the thickness of fiber tows is far less than their width, the flow in path1 can be simplified to flow along a straight fiber tow. Then the time required for flow front to reach position A can be approximated by

$$t_1 = \frac{\mu (l_c + l_b)^2}{2 K_b^a (P_0 - P_f)} \tag{5-1}$$

where, μ is the viscosity of fluid, K_b^a is the axial permeability of fiber tow, P_0 and P_f are pressures at inlet and flow front, respectively. When flow front in path1 reaches position A, on one hand, resin will keep on to flow along weft, on the other hand, resin also will flow transversely to position B due the high permeability of channel between tows. The time T_1 for flow front to reach position B can be

obtained from the following analysis.

For the given coordinate system, see Figure 5.4, the transverse velocity at an arbitrary point C(y , x_c) between A and B takes the form

$$V^t = \frac{dy}{dt} = \frac{K_c (P_0 - P_f)}{\mu y}(1 - \frac{x_c}{x_f}) \qquad (5\text{-}2)$$

where, K_c is the permeability of channel, $x_c = l_c + l_b$, x_f is the $x-$coordinate of flow front along path1 when transverse flow reaches point C, which is given by

$$x_f = \sqrt{\frac{2K_b^a (P_0 - P_f)}{\mu} t} \qquad (5\text{-}3)$$

inserting Eq.(5-3) into Eq.(5-2) and integrating it with the boundary conditions:

$y = 0$ at $t = t_1$

$y = h_0$ at $t = T_1$ ($h_0 = h/2$ for model I, h for model Π)

We obtain

$$\frac{\mu h_0^2}{2K_c(P_0 - P_f)} = T_1 - \frac{2(l_c + l_b)\sqrt{T_1}}{\sqrt{\frac{2K_b^a (P_0 - P_f)}{\mu}}} + \frac{\mu (l_c + l_b)^2}{2K_b^a (P_0 - P_f)} \qquad (5\text{-}4)$$

Then

$$T_1 = (\frac{(l_c + l_b)}{\sqrt{\frac{2K_b^a (P_0 - P_f)}{\mu}}} + \frac{h_0}{\sqrt{\frac{2K_c (P_0 - P_f)}{\mu}}})^2 \qquad (5\text{-}5)$$

For flow in path 2, the fluid will alternatively flow within channel and the

fiber tows. We know that the transverse permeability in fiber tow is much lower than that of channel, at the same time the width l_c of channel is always less than or equal to the width l_b of tow. Then time T_2 required for flow front in path 2 to reach position B can be approximated by

$$T_2 = \frac{\mu l_b (l_c + l_b)}{2 K_b^t (P_0 - P_f)} \tag{5-6}$$

Dividing Eq.(5) by Eq.(6), this yields to the time ratio

$$\frac{T_1}{T_2} = \left(\frac{(l_c + l_b)}{\sqrt{\frac{2K_b^a (P_0 - P_f)}{\mu}}} + \frac{h_0}{\sqrt{\frac{2K_c (P_0 - P_f)}{\mu}}}\right)^2 \frac{2K_b^t (P_0 - P_f)}{\mu l_b (l_c + l_b)} \tag{5-7}$$

The above equation can be further simplified by the quantity analysis. Noticing that the ratio of $h_0/(l_c + l_b)$ is smaller- 10^{-1} to 10^{-2}, and ratio K_c / K_b^a is larger-10to 10^2 for most preforms used in composite processing. So the second term in Eq.(5) is much smaller than the first term. Then Eq.(7) can be simplified to

$$\frac{T_1}{T_2} = \frac{(l_c + l_b)^2 \mu}{2K_b^a (P_0 - P_f)} \cdot \frac{2K_b^t (P_0 - P_f)}{\mu l_b (l_c + l_b)} = \frac{(l_c + l_b)}{l_b} \cdot \frac{K_b^t}{K_b^a} \tag{5-8}$$

Usually, the ratio K_b^a / K_b^t is about 20 for the same fiber tow. At the same time, $l_c \le l_b$, so it seems that the void formation in the cross section of multi-layer woven fabric is inevitable. And the size of void mainly depends on the ratio K_b^a / K_b^t. In order to reduce the size and quantity of voids, it will be useful to use fiber tows with higher K_b^t for warp.

According to simplified model, the flow through the cross-section of MWFs

passes through five different basic sub-domains as shown in Figure 5.5 In this thesis, the permeability tensors of these sub-domains are defined respectively as follows.

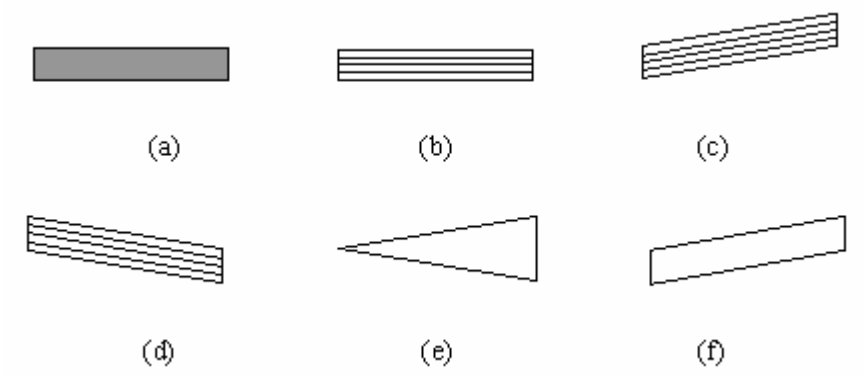

Figure 5.5 Sub-domains of MWFs

For sub-domain a, b, c and d, the permeability for flow along and transverse to fibers is often evaluated from Carman-Kozeny equation:

$$K = \frac{r_f^2}{4k} \cdot \frac{(1 - V_f)^3}{V_f^2} \qquad (5\text{-}9)$$

where r_f if the fiber radius, V_f is the fiber volume fraction, k is the kozeny constant which has been taken as $k_{//} = 0.5$ for flow along the fibers and $k_{\perp} = 10$ for flow transverse to the fibers (Gutowski, *et al*, 1987; Williams, *et al*, 1974). Since this equation cannot predict the phenomenon that the transverse flow will stop at the maximum fiber volume fraction, a number of further modeling studies of permeability have been preformed by Gutowski (Gutowski, *et al*, 1987), Gebart (Gebart, 1996), Cai and Berdichevsky (Cai and Berdichevsky, 1993). In this study, the fiber fractions employed were lower than $V_{f,\max}$, hence permeability was evaluated according to Eq.(5-9).

For sub-domain e and f, the permeability can be obtained from the expression for equivalent permeability of a rectangular shaped channel. In this study, the width of channel is assumed to be l_b, the height of channel is h for sub-domain f and 0-$h/2h$ for sub-domain e. The velocity at the boundary of these channels is set to Darcy velocity of fiber tows.

$$K_c = \frac{w_c^3}{h_c}\left[\frac{16}{\pi^5}\sum_{n=1,3,5...}^{\infty} -\frac{1}{n^5}\frac{\exp(n\pi\frac{h_c}{w_c})}{\exp(n\pi\frac{h_c}{w_c})+1}+\frac{1}{12}\frac{h_c}{w_c}\right]+\frac{K_b}{(1-V_f)} \qquad (5\text{-}10)$$

in which, $w_c = l_b$,

$$h_c = \begin{cases} h & for\ sub-domain\ f \\ 0-h\ or\ 2h & for\ sub-domain\ e \end{cases},$$

K_b and V_f are permeability and volume fraction of fiber tows, respectively.

5.3 Numerical Simulation of void formation

5.3.1 Governing equations

The preform in the mold is assumed to be rigid and is treated as porous medium, the flow in which is described by the following Darcy law:

$$\mathbf{U} = -\frac{1}{\mu}\mathbf{K}\cdot\nabla P \qquad (5\text{-}11)$$

in which, μ is the viscosity of resin. In a two-dimensional flow field,

$\mathbf{U} = (u_x, u_y)^T$ is the flow velocity vector,

$\nabla P = (\frac{\partial P}{\partial x}, \frac{\partial P}{\partial y})^T$ is the pressure gradient vector,

$\mathbf{K} = \begin{bmatrix} K_{xx} & K_{xy} \\ K_{yx} & K_{yy} \end{bmatrix}$ is the permeability tensor.

Inserting Eq.(5-11) into the continuity equation of incompressible fluid gives the governing equation for pressure distribution in flow field:

$$\nabla \cdot (\frac{1}{\mu} \begin{bmatrix} K_{xx} & K_{xy} \\ K_{yx} & K_{yy} \end{bmatrix} \begin{bmatrix} \frac{\partial p}{\partial x} \\ \frac{\partial p}{\partial y} \end{bmatrix}) = 0 \qquad (5\text{-}12)$$

The corresponding boundary conditions to be imposed can be stated as follows:

At injection gates:

$P = P_0$ (for constant pressure injection),

At mold wall

$\frac{\partial P}{\partial n_{wall}} = 0$,

At flow front

$P =$ atmospheric pressure P_f (high injection pressure),

After void is formed, the pressure in void is assumed to obey the ideal gas law: $P_v = \rho RT$, where ρ is the density of air, R the ideal gas constant.

The governing equation for the general 1-D isothermal flow in porous media is derived in Appendix B.

5.3.2 Control volume method

It is noticed that Eq.(5-12) is steady state . Although the mold filling process is time-depended, it can be treated as a series of steady-state problems by time increment. Within each time step, the pressure in flow field can be determined by Eq.(5-12). Generally, Eq.(5-12) need to be solved numerically. In the present simulation, control volume method is used.

The entire flow field is discretized into a finite element mesh firstly. In this simulation, three-node triangular element is used. One node corresponds to one control volume. A control volume is composed of several sub-areas. The number of sub-areas is the same with the number of node adjacent elements. The formation of control volume is illustrated in Figure 5.6. In Fig5.6, the region indicated by dashed lines is a control volume and the shaded region is a sub-area. Point i, j and k are nodes of a triangular element. Point a and b are midpoint of element sides, and point o is element centroid. Connecting point a, o and b, then a sub-area is formed as shaded region shown in Figure 5.6. The procedure for forming of other sub-area is analogous.

Integrating Eq.(5-12) over a control volume can lead to

$$\iiint_V \nabla \cdot \left(\frac{1}{\mu}\begin{bmatrix} K_{xx} & K_{xy} \\ K_{yx} & K_{yy} \end{bmatrix}\begin{bmatrix} \frac{\partial p}{\partial x} \\ \frac{\partial p}{\partial y} \end{bmatrix}\right) dV = 0 \qquad (5\text{-}13)$$

By using the Divergence theorem, the above equation can be written as

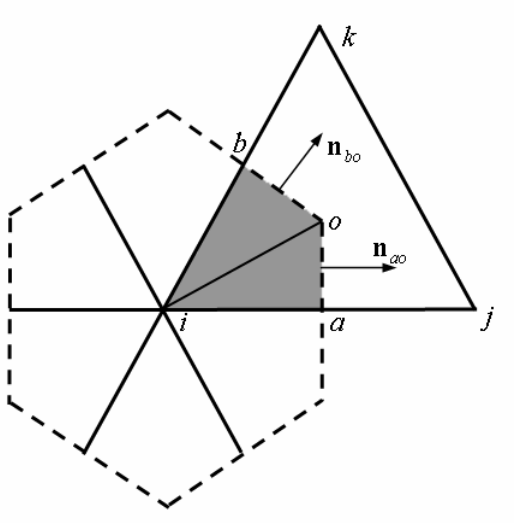

Figure 5.6 Control volume

$$\iint_S \left(\frac{1}{\mu}\begin{bmatrix} K_{xx} & K_{xy} \\ K_{yx} & K_{yy} \end{bmatrix}\begin{bmatrix} \frac{\partial p}{\partial x} \\ \frac{\partial p}{\partial y} \end{bmatrix}\right) \cdot \mathbf{n} ds = 0 \qquad (5\text{-}14)$$

Or $$\int_C \frac{h_z}{\mu}[n_x \; n_y]\begin{bmatrix} K_{xx} & K_{xy} \\ K_{yx} & K_{yy} \end{bmatrix}\begin{bmatrix} \frac{\partial p}{\partial x} \\ \frac{\partial p}{\partial y} \end{bmatrix} dL = 0 \qquad (5\text{-}15)$$

in which, h_z is the thickness of preform, the line C is along the boundary of control volume. If a control volume consists of m sub-areas, the integration along C can be divided into m parts. For each part, by the assumption of linear distribution of pressure in corresponding element, the pressure gradient can be written as (Yong, et al, 1991).

$$\begin{bmatrix} \frac{\partial p}{\partial x} \\ \frac{\partial p}{\partial y} \end{bmatrix} = \frac{1}{2A}\begin{bmatrix} \beta_1 & \beta_2 & \beta_3 \\ \gamma_1 & \gamma_2 & \gamma_3 \end{bmatrix}\begin{bmatrix} P_i \\ P_j \\ P_k \end{bmatrix} \qquad (5\text{-}16)$$

where, A is the area of the element, $\beta_i = y_j - y_k$, $\gamma_i = x_k - x_j$, i, j and k permute in natural order.

Then the total integration of Eq.(5-15) can be expressed as:

$$\sum_{i=1}^{m}\left\{\frac{h_z}{2A}\left\{l_{ao}[n_x\ n_y]_{ao} + l_{bo}[n_x\ n_y]_{bo}\right\}\cdot\begin{bmatrix}K_{xx} & K_{xy}\\ K_{yx} & K_{yy}\end{bmatrix}\begin{bmatrix}\beta_1 & \beta_2 & \beta_3\\ \gamma_1 & \gamma_2 & \gamma_3\end{bmatrix}\begin{bmatrix}P_i\\ P_j\\ P_k\end{bmatrix}\right\} = 0 \qquad (5\text{-}17)$$

where, l_{ao} and l_{bo} are length between points a and o, and b and o. Eq.(5-17) is linear algebraic equation, which can be written for all control volumes in the flow field. Together with the boundary condition, the pressure distribution in the flow field then can be solved.

Once the pressure field is determined, the velocity can be evaluated according to Eq.(5-11), the flow front is then advanced using FAN technique (Frederick and Phelan, 1997).

In this method, the whole domain is divided into a fixed grid system and a scalar parameter f is introduced for each cell to represent the ratio of occupied volume to the total volume. As the flow front advances, all of the control volumes can be classified into three categories as (see Figure 5.7):

f =1: filled region

0 < f < 1: flow front region

f =0: empty region

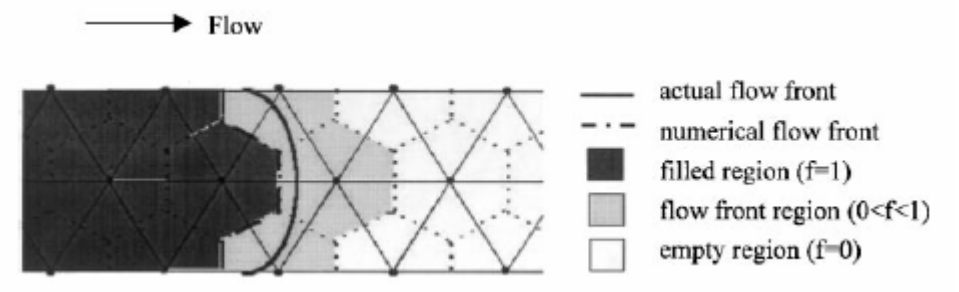

Figure 5.7 Illustration of the flow front advancing technique

For a selected volume (0 < f < 1) is calculated on the basis of the velocity field. The calculated volume of resin inflow is added to the original volume of resin in the flow front control volume. If the total resin volume in a control volume is equal to the volume of the control volume, that control volume is considered “full” (f = 1). The time increment is selected in such a way that one control volume can be filled simultaneously. This restriction of the time increment ensures the stability of the quasi-steady-state approximation. The new flow front in each time step can be estimated according to the velocity vector in the flow front and the time increment after the pressure field is determined. After the value *f* is updated, another pressure computation is performed for all the control volumes with *f* = 1. The procedure is repeated until the whole mold cavity is filled.

The time increment is determined in such a way that only one control volume is fully filled during the step, then

$$\Delta t = \min\left(\frac{V_i - V_i^f(t)}{Q_i(t)}\right) \tag{5-18}$$

where V_i is the volume of control volume i, $V_i^f(t)$ is the filled volume at time t, $Q_i(t)$ is the flow rate into the control volume. Once the time increment is determined, the volume of fluid that flows into each control volume at flow front can

be calculated. Then the flow front is advanced.

$$f_i(t+\Delta t) = \frac{V_i^f(t) + \Delta t \cdot Q_i(t)}{V_i} \tag{5-19}$$

A detailed flow chart of the numerical implementation is given in Figure 5.8.

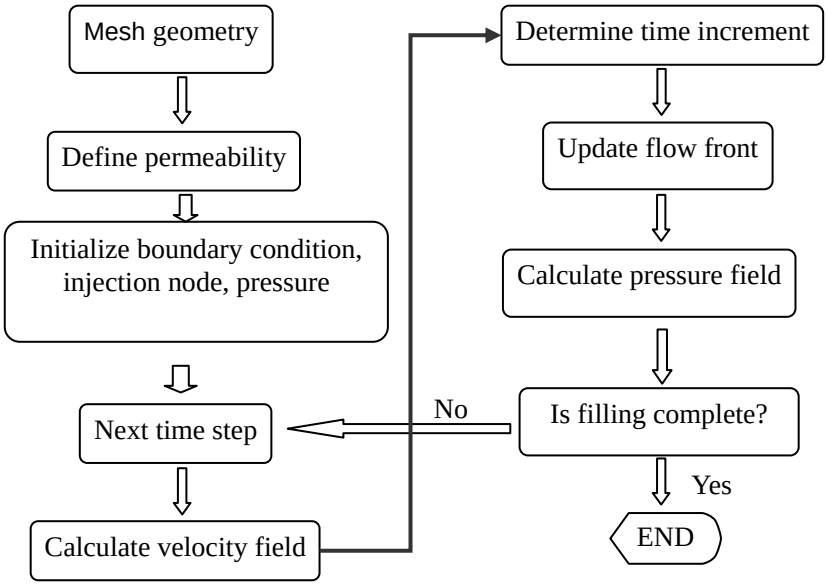

Figure 5.8 Flow chart of the numerical simulation using control-volume method

5.4 Results and discussion

5.4.1 Basic testing of numerical simulation

The numerical scheme outlined above has been implemented and tested by comparing with mold filling cases for which analytical solutions exist.

The first case tested was boundary injection from one side of a rectangular mold, see Figure 5.9. For constant injection pressure, the flow front position x_f at time t can be given by

$$x_f = \sqrt{\frac{2KP_0 t}{\mu}} \tag{5-20}$$

where, P_0 is the injection pressure, K the permeability of preform, μ the viscosity of fluid. Simulation was conducted for $P_0 = 200\,\text{kPa}$, $K = 1.0\times10^{-10}\,\text{m}^2$, $\mu = 0.01\,\text{Pa s}$. Predictions of flow front by simulation were in perfect agreement with the analytical as shown in Figure 5.10.

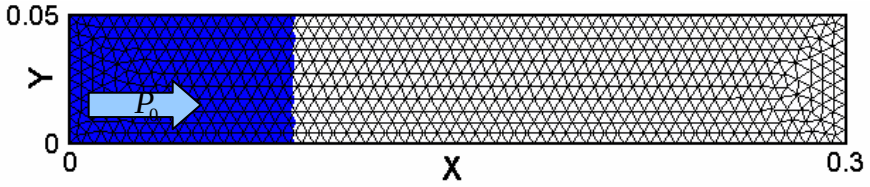

Figure 5.9 Boundary injection from one side of a rectangular mold

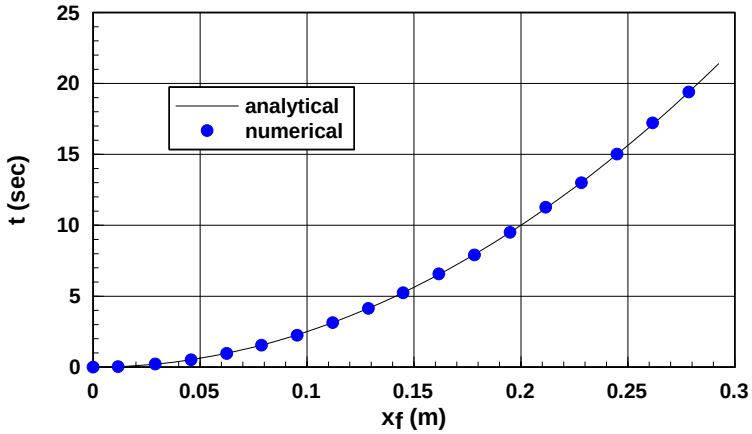

Figure 5.10 Comparison of analytical and numerical results of flow fronts

The second case tested was point injection from the center of a square preform. The resin will flow in radial directions from the center towards the preform edges. This results in a an ellipse shaped flow front, and the ratio a/b of its major axis to the minor axis is always equal to $\sqrt{K_1/K_2}$, where,

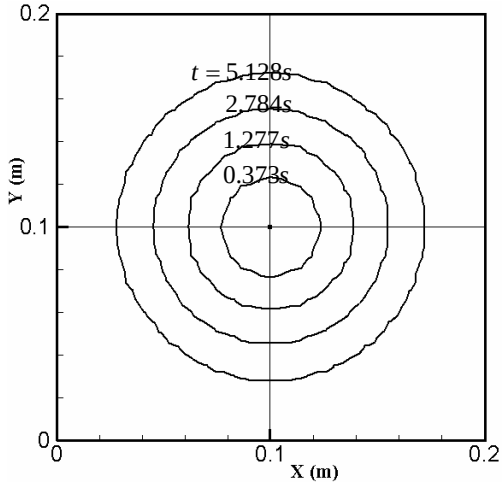

(a) Isotropic

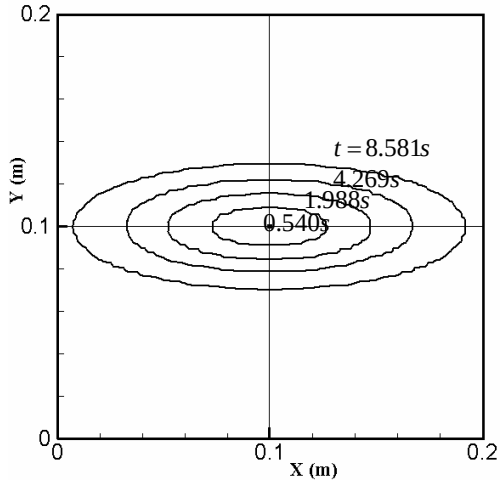

(b) Anisotropic

Figure 5.11: Flow fronts at different injection time of point injection in a square preform

K_1 and K_2 are the principal permeabilities of the preform in two directions. The numerically simulated shapes of the flow front are shown in Figure 5.11. For Figure 5.11(a), there is $K_1 = K_2 = 1.0 \times 10^{-10}$ m^2; for Figure 5.11(b), there is $K_1 = 1.0 \times 10^{-10}$ m^2, $K_2 = 1.0 \times 10^{-11}$ m^2. Excellent agreement can be observed between the numerical and analytical results of a/b.

It is noted that the flow fronts by simulation shown in Figure 5.11 are not very smooth. The reason is that the flow front is identified by the filling factors on a fixed mesh, and it can be tacked to the resolution by using more elements in flow domain.

5.4.2 Void formation in MWFs

In this section, the mold filling process and void formation in both unit cells of MWFs were silmulated using the above numerical scheme. The fluid employed in the simulations was silicone oil of a viscosity of 0.1934 Pa s, which were taken from experimental study of Patel (Patel, *et al*, 1995).

As described in section 2, since the thickness of fiber tow is far less than the width, hence, the unit cell of mode I (Figure 5.4(a)) can be further simplified to Figure 5.12, a cell with rectangular cross-section for both channel and warp/weft. This simplification was used by Yu and Lee to develop in-plane permeability model of MWFs (Yu and Lee, 2000). Then symmetry boundary condition can be imposed for the simulation of flow in both unit cells.

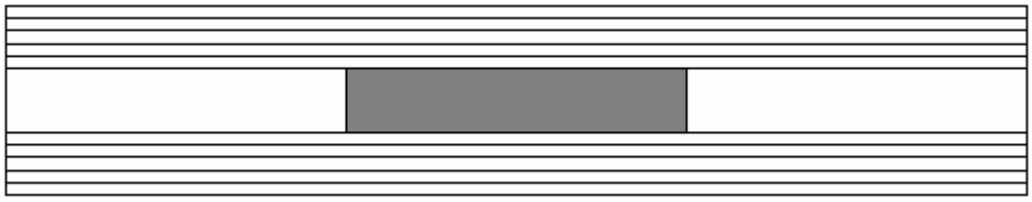

Figure 5.12 Simplified unit cells for mode I

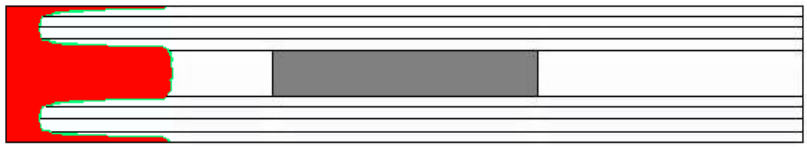

$t = 0.47 \times 10^{-4}$

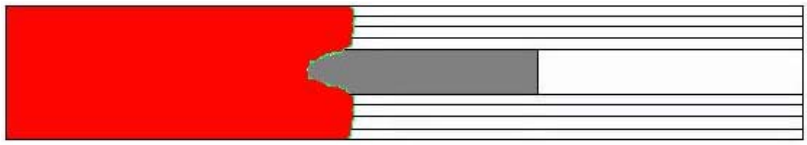

$t = 0.12 \times 10^{-2}$

$t = 0.85 \times 10^{-2}$

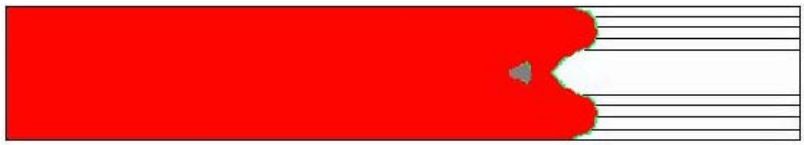

$t = 0.13 \times 10^{-1}$

(a) Flow fronts in unit cell of mode I

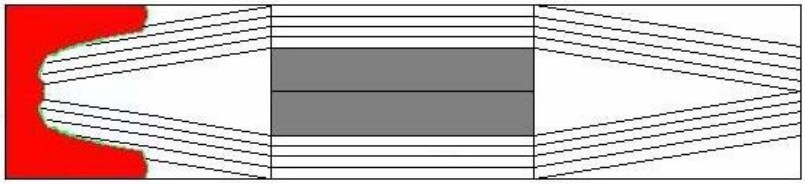

$t = 0.42 \times 10^{-4}$

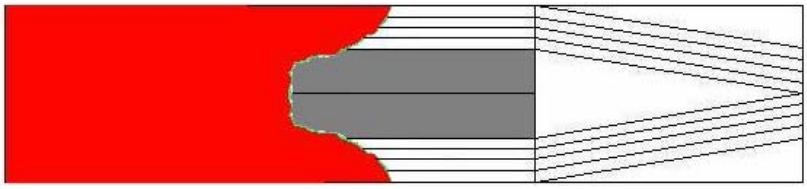

$t = 0.14 \times 10^{-2}$

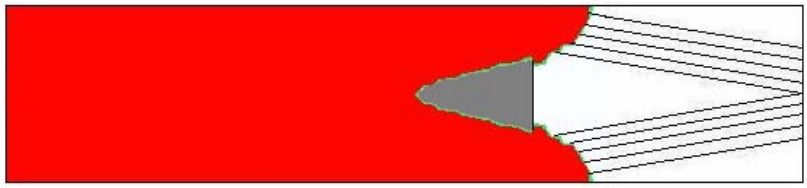

$t = 0.88 \times 10^{-2}$

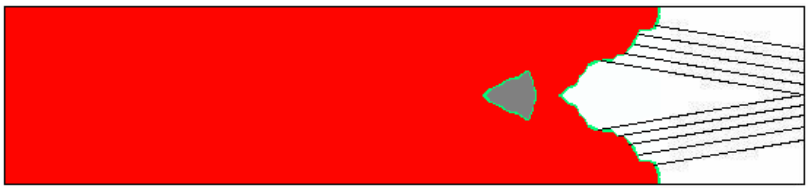

$t = 0.14 \times 10^{-1}$

(b) Flow fronts in unit cell of mode Π

Figure 5.13 Flow fronts at different stages of mold filling

In order to define different permeabilities for different sub-domains, the flow field was firstly meshed by sub-domain to sub-domain using software ANSYS 5.7, respectively. In the simulation of filling process, the boundary condition at the inlet can be either a constant volumetric flow rate or a constant injection pressure. Here, constant injection pressure was taken. And the pressures at inlet and flow front were set to be 5×10^5 Pa and 1×10^5 Pa, respectively. The fiber tows for weft and warp were the same with a fiber volume fraction of $V_{fb} = 0.45$ and fiber radius of

$r_f = 8\times10^{-6}$ m. Then the permeabilities of fiber tow evaluated according to the Carman-Kozeny relationship equation were:

$K_b^a = 2.63\times10^{-11}\,\mathrm{m}^2,\ \ K_b^t = 1.32\times10^{-12}\ \ \mathrm{m}^2.$

Figure 5.13 Shows the numerical simulation of flow fronts at various filling stages. The flow patterns in both unit cells are consistent to the analysis in section 2. In both unit cells, voids were formed at the end of warp. And the primary reason for void formation is the large difference in permeability between K_c, K_b^a and K_b^t. It can be observed that the void formed in the unit cell of mode I is smaller than that of mode Π for same parameters. This is understandable because there is only one warp between two adjacent wefts in mode I, but two for mode Π. Thus, the impregnation in the warp of mode I is much accelerated by the relatively high flow velocity in adjacent wefts. Furthermore, the channel before warp in mode Π triangle shaped, this also makes the flow in path 2 of mode Π slower than that of mode I.

It is also noted that the simulated time for voids to be formed at the end of warp, namely, the time for flow front in path 1 to reach position B, is less than that predicted according to Eq.(5-5). This is because that the impregnation in weft between two adjacent warps is accelerated due the high permeability in channel. In Eq.(5-5), this effect is not considered.

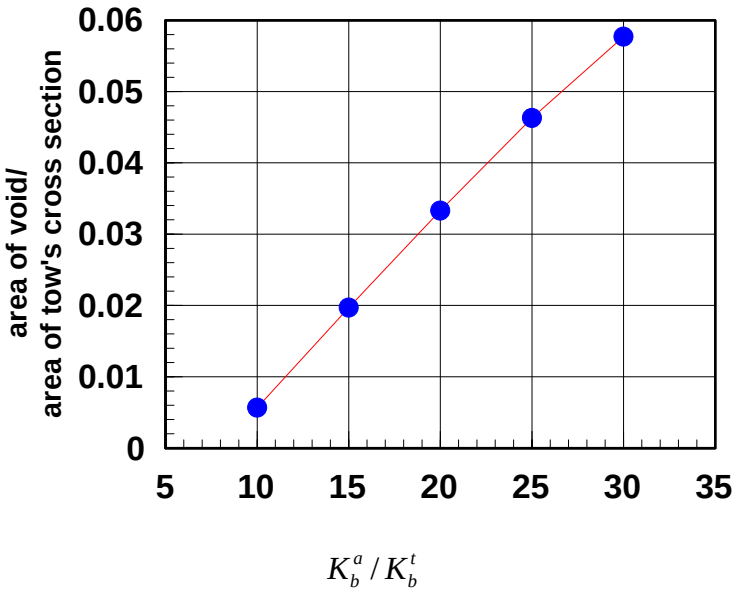

(a) mode I

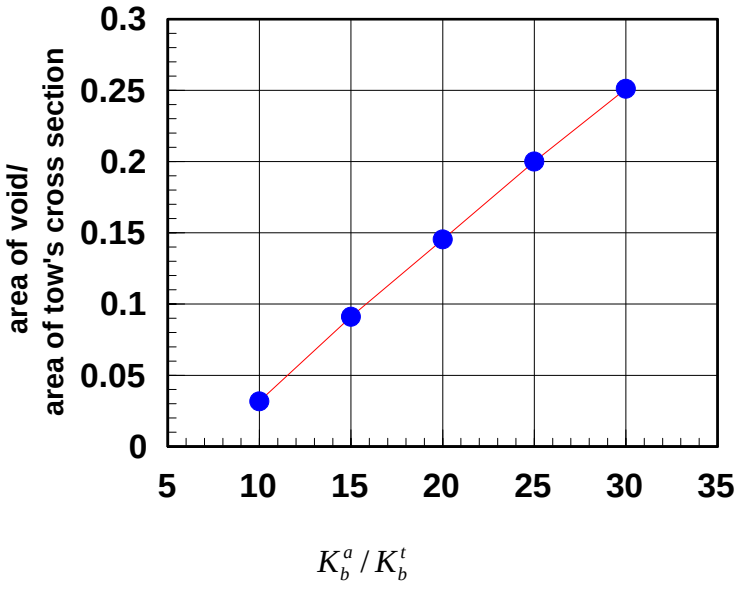

(b) mode Π

Figure 5.14 The size of void for different K_b^a / K_b^t

According to the analytical result of time ratio T_1 / T_2, it can be observed that K_b^a / K_b^t seems to be determinant on the size of void. In this study, void formation processes on different K_b^a / K_b^t were simulated. Figure5-14 presents the effect of changing K_b^a / K_b^t on the void size for both unit cells, which shows that larger

K_b^a / K_b^t corresponds to larger void size. And it seems that the size of void is proportional to the ratio of K_b^a / K_b^t as shown in Figure 5.14. This agrees with our analytical result in section 2.

5.4.3 Experimental results

Experiments were performed to measure the formation of voids and its location. The reinforcement used in this experiment is plain woven fabrics. Three plies of glass fiber mat were stacked with low fiber volume fraction. The resin used is a two-part epoxy/amine resin, LY564/HY2954, from Ciba–Geigy (Hawthorne,NY). LY564 is the base resin of a bisphenol. An epoxy containing a reactive diluent. HY2954 is a hardener of 3, 3′-dimethyl-4, 4′-diaminodicyclohexyl methane. The mix ratio of LY564 with HY2954 (parts by weight) is 100: 35. The resin had a Viscosity of 0. 617 Pa s at 25°C.

Resin was injected at the constant pressure (0.5MPa) into the mold. The longitudinal cross-section was examined using a microscope as shown in Figure 5.15. From these images, two typical modes of the plain woven fabric can be clearly recognized and the formation of voids is mainly located at the end of warp.

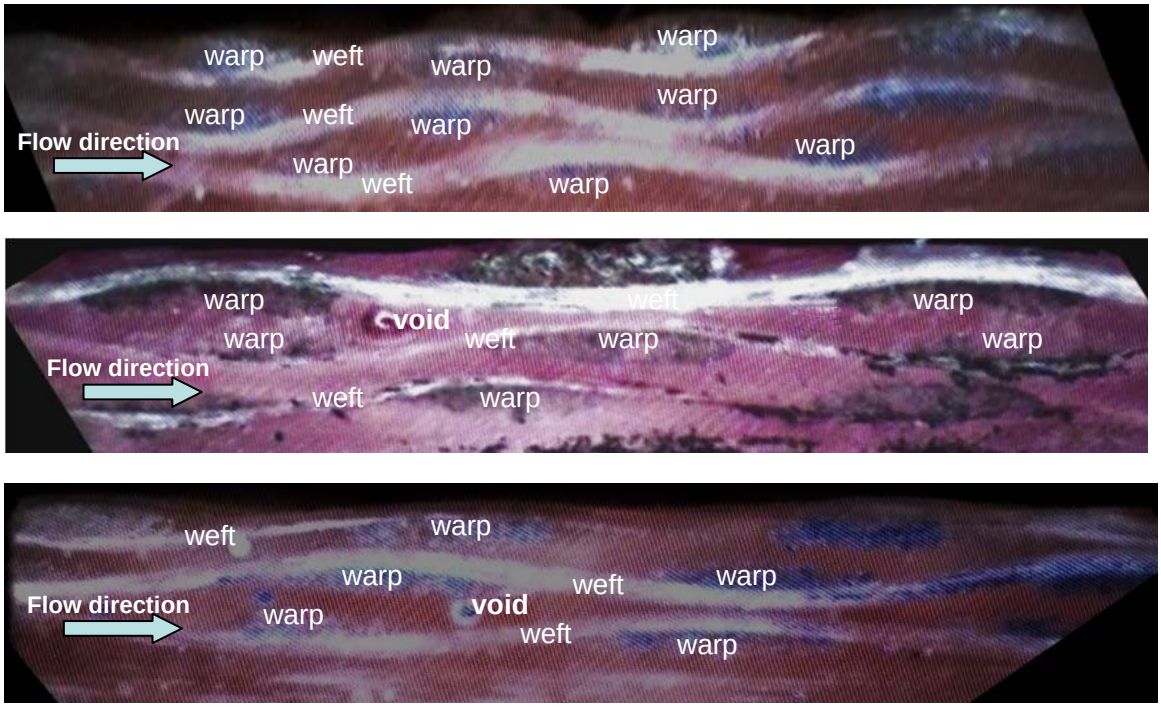

Figure 5.15. Experimental cross-sections of MWFs

5.5 Conclusion

Two simplified unit cells for in-plane impregnation in multi-layer woven fabric have been suggested. In addition a mathematical model has been developed to analyse the void formation in both unit cells during RTM processes. The model recognises non-uniform fibre permeability in different sub-domains of fibre preforms. Although a few simplifying assumptions have been introduced, the model still accounts for the key mechanisms of void formation in the cross-section of MWFs. And the location of the void predicted by this model agrees quite well with the experiments. The model also shows that the ratio of weft axial permeability K_b^a and warp transverse permeability K_b^t is determinant for the formation and size of void.

The flows in both unit cells also were numerically simulated using the control-volume method. The presented numerical scheme was firstly tested by

comparing with mould-filling cases for which analytical solutions exist. The simulated results, including flow fronts and effect of K_b^a / K_b^t, agree with the prediction according to analytical model. The size of void is proportional to the ratio of K_b^a / K_b^t (Hu, et al, 2003).

Chapter 6

Numerical simulation of effect of stitch

6.1 Introduction

In recent years, stitched fabrics have begun to attract increasing attention as reinforcing materials for high-performance composites. In addition to the features that other textile preforms commonly have, such as a unique combination of low weight, strength, toughness and flexibility, the advantages of stitched fabrics are their integrity and wide variety.

Among various manufacturing processes, Resin Transfer Moulding (RTM) is considered a versatile and more effective process for the production of high-performance advanced textile composites. RTM offers the promise of producing low-cost composite parts with complex structures and large near net shapes. Relatively fast cycle times with good surface definition and appearance are easily achievable. The ability to consolidate parts allows the saving of a considerable amount of time over conventional lay-up processes. Since RTM is not limited by the size of the autoclave or by pressure, new large complicated structures are achievable. However, the development of the RTM process has not fulfilled its full potential. For example, the RTM process is yet to be automated in operations such as preforming, reinforcement loading, demoulding, and trimming. Therefore, RTM can be considered an intermediate volume moulding process (Krolewski and Busch, 1990).

Several unresolved issues in RTM encountered by composite engineers are in the areas of process automation, preforming, tooling, mould flow analysis and resin

chemistry. During the last decade, rapid advances in RTM technology development have demonstrated the potential of the RTM process for producing advanced composite parts. The advantages and associated disadvantages of the RTM process are summarised. As this process is developing rapidly, some of its disadvantages may be overcome as the technology advances.

During the injection process of RTM, a liquid thermosetting resin is injected into a closed mould containing a prefabricated fabric which is formed by fibre bundles. This will result in two types of flow: a micro-scale flow within the fibre bundles and a macro-scale flow in the interbundle channels.

Due to complexity of the fabric structure, the flow of resin in a mould is very complicated, especially for 3D stitched fabrics. In order to ensure the high performance of composites, some problems, such as the formation of dry spots or voids, long injection times and incomplete filling, must be seriously considered and pre-simulated when designing fabrics and moulds. It is widely agreed that one of the key parameters that determines the flow characteristics of the mould-filling process, is the permeability (K) of the fabrics. The accuracy of pre-simulation depends crucially on the quality of available data for K and, most importantly, its variation throughout the fabric.

For flow within the porous medium of textile preform, a considerable amount of work has been done and a number of models for the estimation of permeability have been presented in the earlier studies (Berdichevsky and Cai, 1993; Bruschke and Advani, 1992; Carman, 1937; Gebart, 1992; Gutowski *et al*, 1987). A good review of the subject is given by Lee (Lee, 1997).

From the literature review, the permeability of complex-structured textile preform is mainly determined by the interbundle channel (pore). A great deal of research has focused on permeability of the interbundle channel within the preform. As for flow within the interbundle channel in the textile preform, it is always modelled using Navier-Stokes equations in most studies (Kolodziej *et al*, 1998; LundstrÖm, 2000; Shih and Lee, 1998). The boundary condition for these channels is set by the Darcy velocity of the bundles, directed along the flow. By using Darcy's law, the equivalent permeability of one rectangularly shaped interbundle channel can be expressed as (LundstrÖm, 2000):

$$K_{channel} = \frac{W_{channel}}{H_{channel}}\left[\frac{16}{\pi^5}\sum_{n=1,3,5...}^{\infty} -\frac{1}{n^5}\frac{\exp(n\pi\frac{H_{channel}}{W_{channel}})}{\exp(n\pi\frac{H_{channel}}{W_{channel}})+1}+\frac{1}{12}\frac{H_{channel}}{W_{channel}}\right]+\frac{K_b}{(1-V_{fb})} \qquad (6\text{-}1)$$

where $K_{channel}$ and K_b are the permeability of interfibre channel and intra-fibre bundle respectively, V_{fb} is the fibre volume fraction within the bundle, $H_{channel}$ and $W_{channel}$ are the height and width of channel, respectively. As shown in Figure 6.1, the entire fabric can then be modelled by Darcy's law with different permeabilities assigned to the fibre bundles and interbundle channel.

In addition to features that other textile preforms commonly have, such as a unique combination of light weight, strength, toughness and flexibility, the advantages of 3D Multi-Layer Woven Fabrics are their integrity, cheapness and their wide variety. A key feature of the structure is its through-the-thickness stitching. This type of fabric has begun to attract increasing attention for high-quality composites.

For 3D multi-layer woven fabrics, a key feature is their interbundle stitches. But very limited information is available on the relationship between permeability and

the effect of stitches. Shih and Lee (Shih and Lee, 1998) proposed a parallel permeability model for flow through bi-directional stitched fabrics. The flow between the bundles is set by the Kozeny-Carman equation (Carman, 1937), and the effect of stitch was not specially mentioned in the article. Cairns (Cairns *et al*,1999) developed a model that incorporates Darcy's law within fibrous bundles and channels that exist between bundles. The paper reported that incorporating channel flow is an important feature for properly modelling the RTM process. With this model, pressure profiles, resin velocities, and resin flow fronts are predicted accurately, and are available for manufacturing process development. The same materials were compared to fully stitched preforms. It was found that although the shapes for resin flow are similar between the experimental and analytical results, the stitch affects the permeability such that the uni-directional ply data do not accurately capture the times for resin flow. LundstrÖm (LundstrÖm, 2000) also proposed a model for non-crimp stitched fabrics through theoretical analysis. The interbundle channel was assumed to be rectangularly shaped and the equivalent permeability is modelled by Equation (6-1). A comparison between the model and experimental data shows that this model works well in certain cases, while it fails in other cases to predict the permeability perfectly. LundstrÖm suggested that one of the main reasons, which caused the discrepancy, was the assumption that the effect of stitch was negligible. LundstrÖm also mentioned that study of both the dry fabric and the impregnated samples yielded stitches that were actually located in some of the channels. It is really important to make a quantitative study of the issue as to how stitches affect the effectiveness of the permeability. Such a study will be very helpful for designing stitched fabrics, exact pre-simulation of moulding processes, and the optimisation of processing parameters.

The structure of 3D multi-layer woven fabrics is quite complicated and variable. In this work, we focused on its key feature, the interbundle stitch, and its effect on permeability. Several typical stitch structures were selected as the basic models, and the effect of stitches on permeability of the interbundle channel has been investigated through numerical simulation for various combinations of the stitch size, its off-centre position, slope, array, distribution density in the flow direction and the average Darcy velocity in the fibre bundle.

6.2 Numerical simulation

A numerical simulation process on equivalent permeability of interbundle channels is presented in this section.

6.2.1 Basic assumptions

For simplification, several assumptions are made as follows. (Patankar, 1980, Panton, 1984 and Morton, 1980)

1) The interbundle channel is rectangular shaped and has a uniform cross section in the flow direction,

2) Stitches is distributed periodically along the channel

3) The resin is a Newtonian fluid and flowing at low Reynolds number(much less than 1),

4) Stitches are treated as impermeable rigid cylinder and no deformation occurs during mould filling.

According to the assumption of periodical distribution of stitches, we only need to

consider the flow in one “representative cell” as shown in figure 6.1, in which, the domain indicated by real lines is the computational cell. L, W and H denote the length, width and height of the representative cell, respectively. Half of channel width is represented by $a = W/2$ and half of channel height is represented by $b = H/2$ and R is the radius of stitch. When stitches are located on the centerline of channel and perpendicular to the flow direction, the mirror symmetric boundary conditions can be set at each side, so the computational cell is the quarter of channel as shown in figure 6.1(a, e, f). Otherwise, computational cell is the half of channel as shown in figure 6.1(c, d).

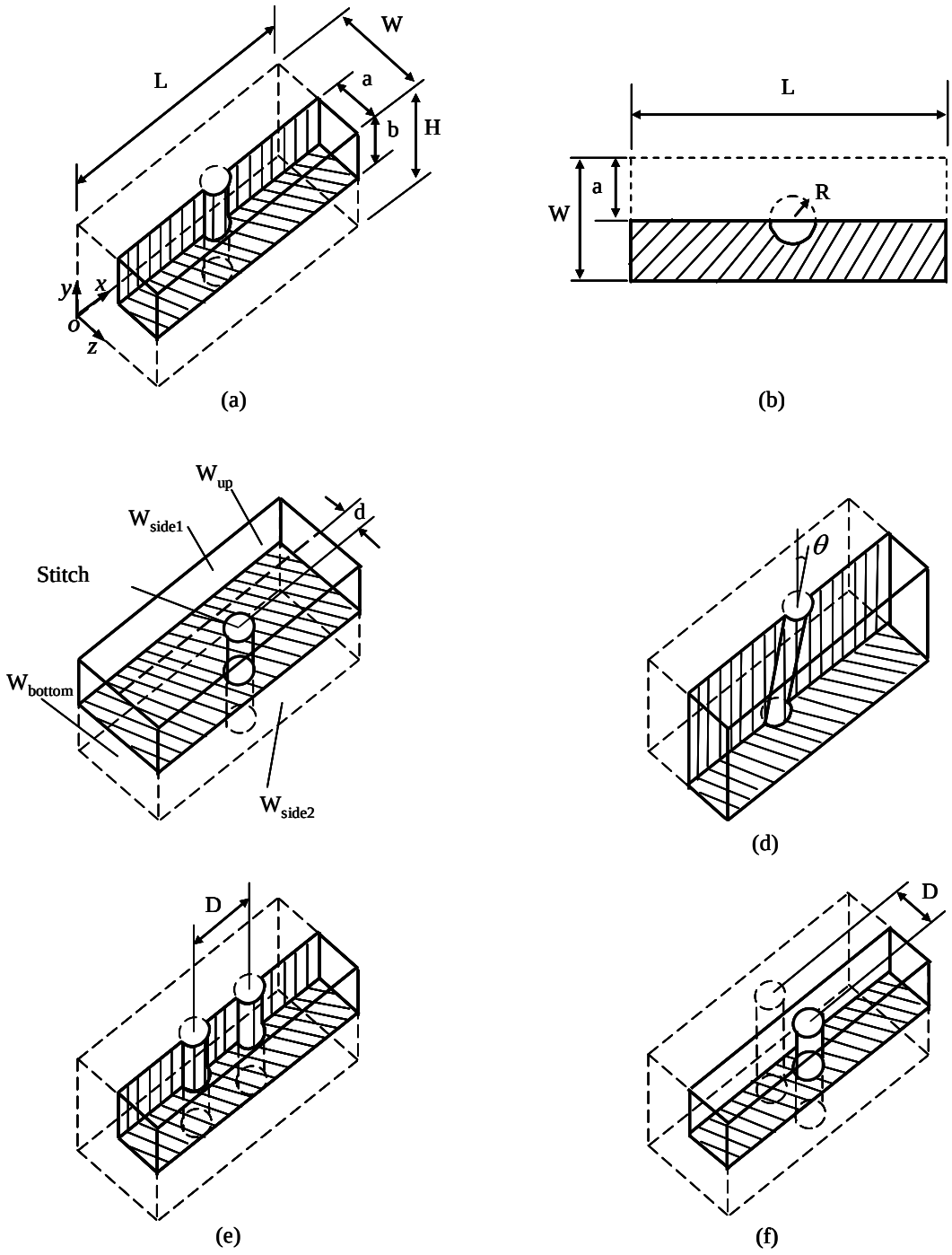

Figure 6.1 Computational cells for different situations

6.2.2 Governing equations

The problem to be solved is: how to determine the velocity fields and needed pressure gradient ($\Delta p / L$) along the computational cell for a given volumetric flow rate (Q), and to compute the equivalent permeability (K_e) from the Darcy law (Shih

and Lee,1998):

$$K_e = \frac{Q}{A}\frac{\mu}{\Delta p / L} \tag{6-2}$$

where A is the cross section area of channel, μ is the viscosity of fluid. And then, the effect of stitches on the equivalent permeability of interbundle channel can be obtained.

The governing equations for three-dimensional steady-state incompressible flow in the channel can be written as (Lee, 1997):

$$\rho\nabla\cdot(u\mathbf{u}) = -\frac{\partial p'}{\partial x} + \nabla\cdot(\mu\nabla u) + \frac{\Delta p}{L} + \rho F_x \tag{6-3}$$

$$\rho\nabla\cdot(v\mathbf{u}) = -\frac{\partial p'}{\partial x} + \nabla\cdot(\mu\nabla v) + \rho F_y \tag{6-4}$$

$$\rho\nabla\cdot(w\mathbf{u}) = -\frac{\partial p'}{\partial x} + \nabla\cdot(\mu\nabla w) + \rho F_z \tag{6-5}$$

$$\nabla\cdot\mathbf{u} = 0 \tag{6-6}$$

in which, $\mathbf{u} = (u, v, w)$ is the velocity vector, ρ is the density of fluid, $F_i (i = x, y, z)$ is the external body forces, the pressure p' is defined as

$$p' = p + \frac{\Delta p}{L}x \tag{6-7}$$

where p is the static pressure. The advantage of this transformation is that in the modified problem all variables have periodic boundary conditions at inflow and outflow boundaries.

In this study, three types of boundary condition (BC) are considered as follows:

BC1: $\mathbf{V} = \mathbf{0}$ on W_{up}, W_{bottom}, W_{side1}, W_{side2},

BC2: $\mathbf{V} = \mathbf{0}$ on W_{up}, W_{bottom},

$\mathbf{V} = \mathbf{V}_b$ on W_{side1}, W_{side2},

BC3: $\mathbf{V} = \mathbf{V}_b$ on W_{up}, W_{bottom}, W_{side1}, W_{side2}.

where V_b is the Darcy velocity in the fibre bundles that form the channel. The boundary conditions used on other boundaries are fixed flow rate on inflow and outflow boundaries, and no-slip conditions on the surface of the stitches (Happel and Brenner, 1986).

For governing equations, if we generalize the variables with functions ϕ and S_ϕ, then equations (6-3), (6-4) and (6-5) can be written in a generalized form as follows:

$$\rho\nabla\cdot(\phi\mathbf{u}) = \nabla\cdot(\mu\nabla\phi) + S_\phi \tag{6-8}$$

The present problem is solved with FLUENT software based on the control volume technique. The entire computation domain is first divided into discrete control volume using two types of grid: hexahedron and tetrahedron. Then the integration of governing equations on the individual control volumes will construct equations for discrete dependent variables as follows:

$$\int_{CV}\rho\nabla\cdot(\phi\mathbf{u})dV = \int_{CV}\nabla\cdot(\mu\nabla\phi)dV + \int_{CV}S_\phi dV \tag{6-9}$$

$$\int_{CV}\nabla\cdot\mathbf{u}dV = 0 \tag{6-10}$$

6.2.3 Computation of Governing Equations

The FLUENT software provides three different solver formations out of which "segregated solver" is chosen for the present problem. The steps are illustrated in Figure 6.2. The pressure-velocity coupling is conducted based on SIMPLE algorithm (LundstrÖm, 2000; Nakayama, 1995).

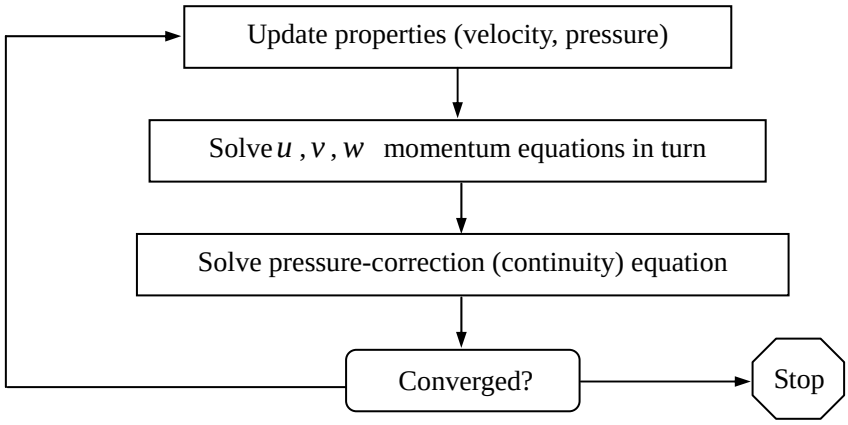

Figure 6.2 Steps of segregated solution method

Computation is done at a very low Reynolds number ($\mathrm{Re} << 1$) so as to make the flow effectively a creeping flow. The computational error is checked by comparing the results by varying mesh size and increasing node numbers. Figure 6.3 shows the convergence of the calculation vs. node number for computational cell shown in figure 6.1(a). When determining the mesh size, a compromise is reached by considering both the accuracy and the computational time. The estimated error in the worst case is less than 1%, and in most cases the error is around 0.1-0.5%.

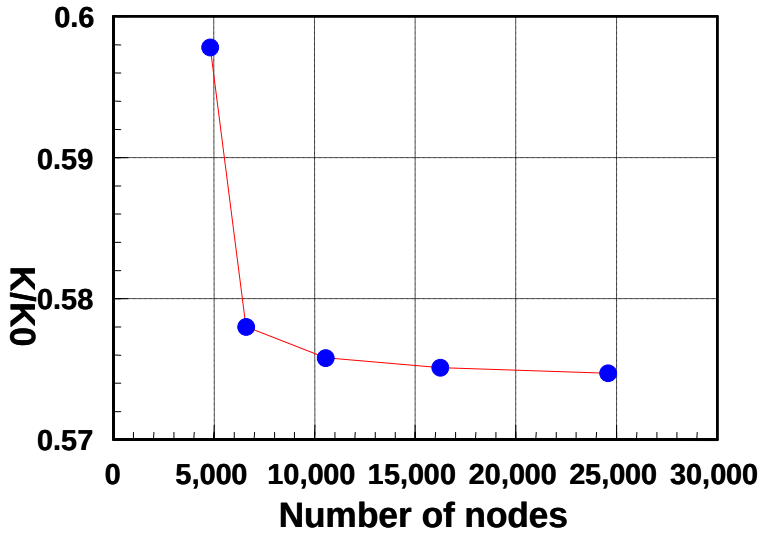

Figure 6.3 Convergence of numerical simulation

In all computations, the convergence criterion is that the permeability must approach a stationary value. It was fairly easy to judge from the figure 6.3 that when the number of the nodes is above 10,000, the value of K/K0 is converged to a certain value and the convergence graph is monotonous.

6.3 Results and Discussion

We now present the results of numerical simulation. The effect of stitches on the equivalent permeability of the interbundle channel is presented by the value of $K/K0$ where K and $K0$ are the permeabilities of the channels with and without stitches, respectively. It should be particularly noted that $K0$ is different for different boundary conditions and geometrical structures (Hu, etc., 2003).

6.3.1 The Effect of Stitch Size, Distribution Density

In this section, we consider that there is only one stitch in one representative cell, and the stitch is located on the centerline of channel and perpendicular to the flow

direction. The corresponding computational cell is shown in figure 6. 1(a). Based on this computational cell, the effect of stitch on the permeability of the interbundle channel has been investigated for various combinations of stitch size (R/a), distribution density in the flow direction (L/W), and the ratio of V_b with V_a, in which $V_a = Q/A$ is the average velocity in channel corresponding to the given flow rate.

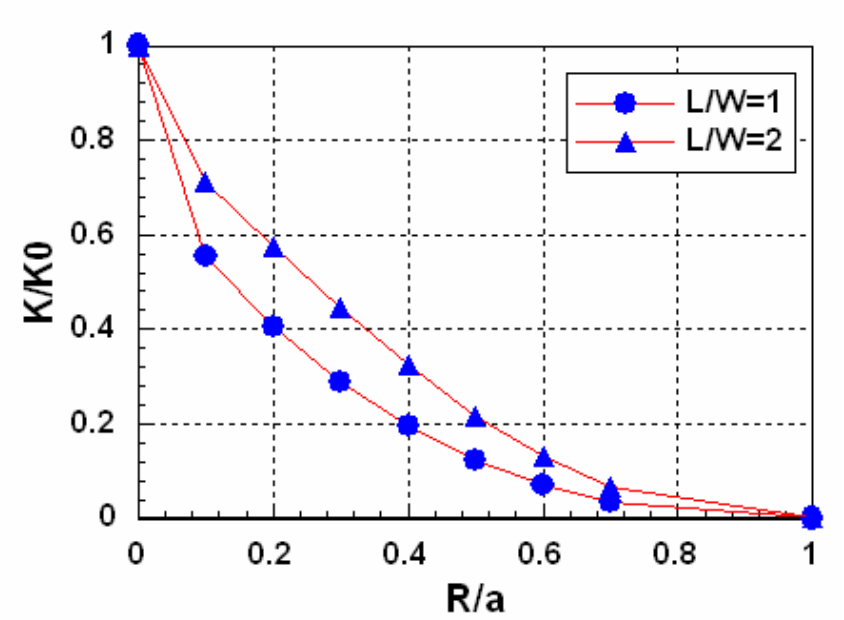

(a) BC1 (V_b/V_a=0.4)

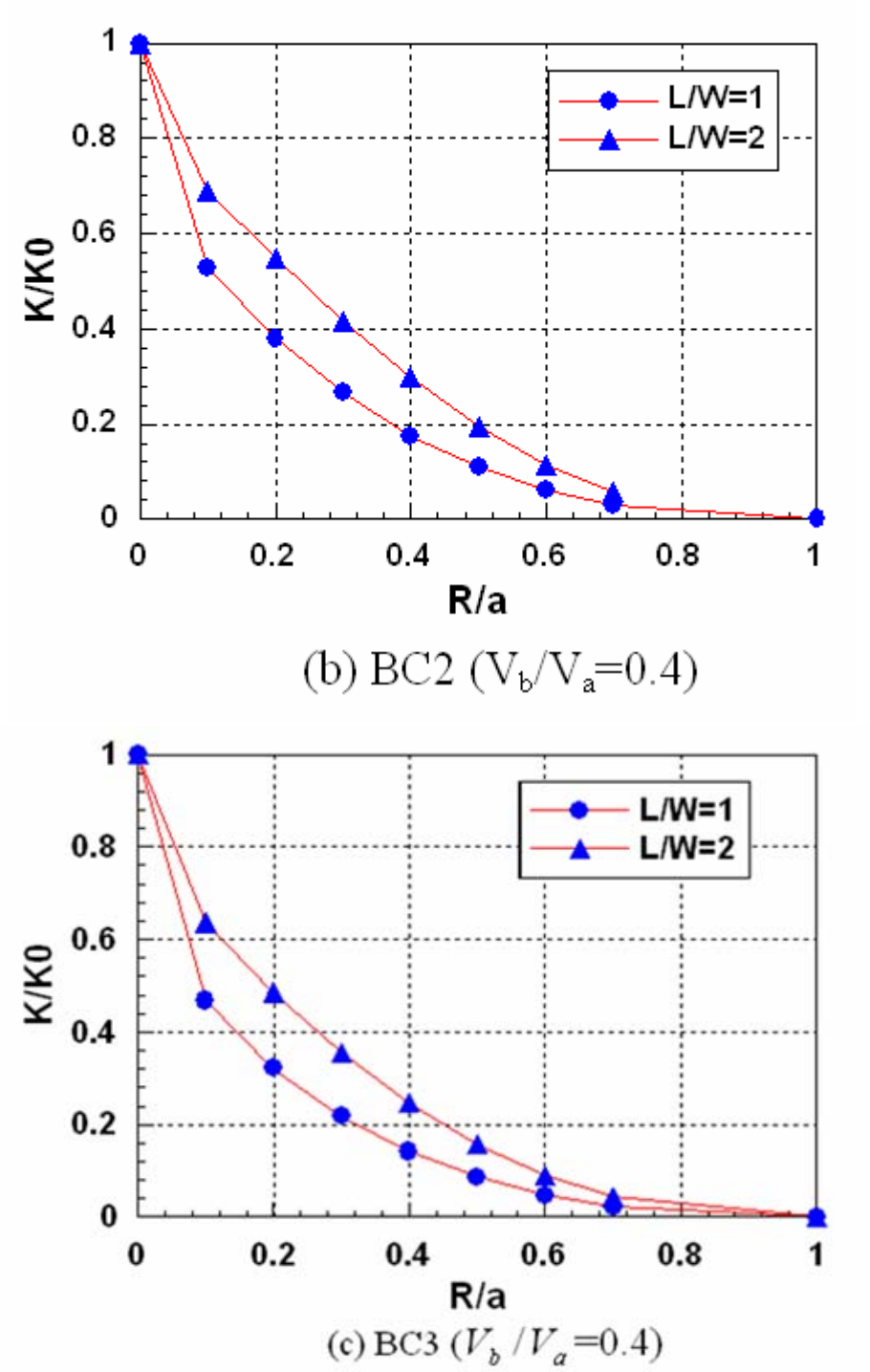

Figure 6.4 Change of *K/ K0* with *R/a* on different boundaries conditions

Figure 6.4 shows the variation of $K/K0$ with R/a for different boundary conditions and distribution densities. As shown in these figures, it is evident that stitches may severely influence the permeability of the interbundle channel. For all simulated cases, the value of $K/K0$ is less than 0.80 at R/a=0.1, and is around

0.10 at R/a =0.6. Obviously, the effect of stitches can't be neglected when establishing effective permeability model. We also note that there is similar variation of $K/K0$ with R/a for different conditions, but the extent of influence is different for different boundary conditions or different distribution densities. It can be seen more clearly in figure 6.5 and figure 6.6.

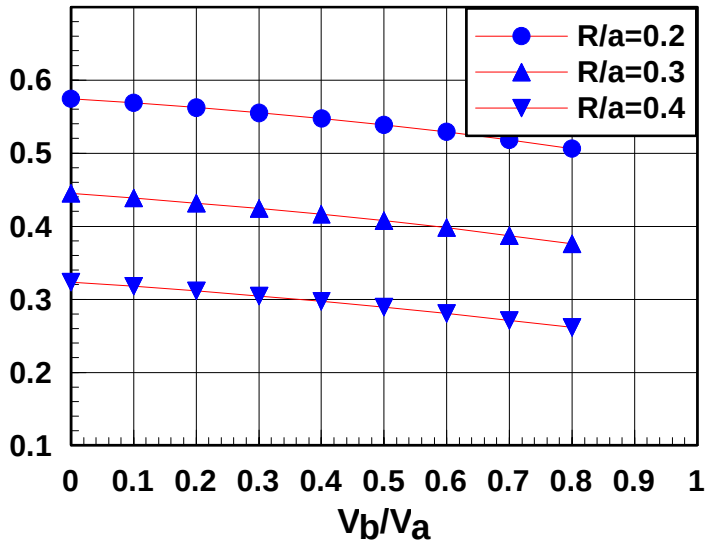

(a) BC2 (L/W =2.0)

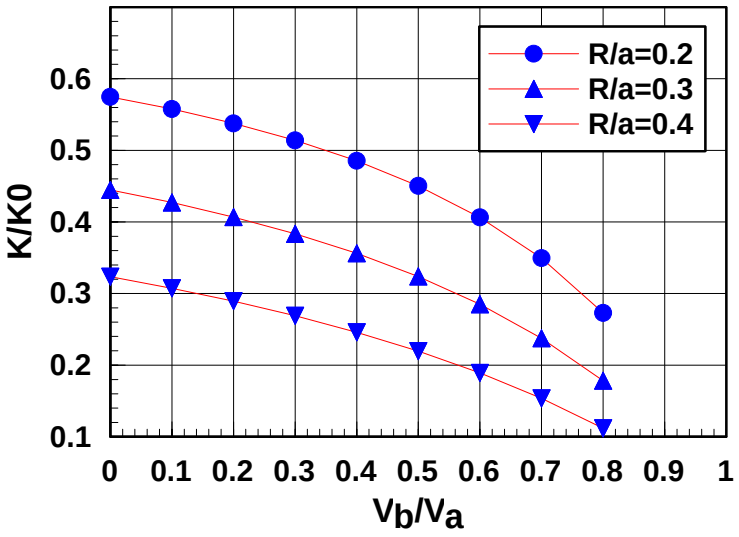

(b) BC3 (L/W =2.0)

Figure 6.5 Changes of $K/K0$ with V_b/V_a for boundary condition BC2 and BC3

In figure 6.5, the variation of $K/K0$ with V_b/V_a for different R/a and the

same L/W is presented. For all simulated cases, $K/K0$ decrease with the increasing of V_b/V_a, especially for boundary condition BC3, where the effect of V_b/V_a on the value of $K/K0$ is much higher than that for BC2. The value of $K/K0$ is reduced about 50 percent when V_b/V_a is increased from 0.1 to 0.8 for BC3. Thus, the effect of stitches on the permeability of the interbundle channel is different with different boundary conditions. .It is known that, for a given pressure drop Δp, the larger the average flow velocity V_b in the fibre bundle, the higher the permeability.

The stitch distribution density in the flow direction is expressed by the value of L/W. If W is kept constant, then larger L/W means the sparser distribution. The effect of L/W on the value of $K/K0$ is shown in figure 6.6. There is a fairly linear relationship between $K/K0$ and R/a, but the slope of change is different for different cases. For the same boundary condition, the slope decreases with the increasing R/a. This means that the effect of stitch distribution density decreases with the increase of R/a.

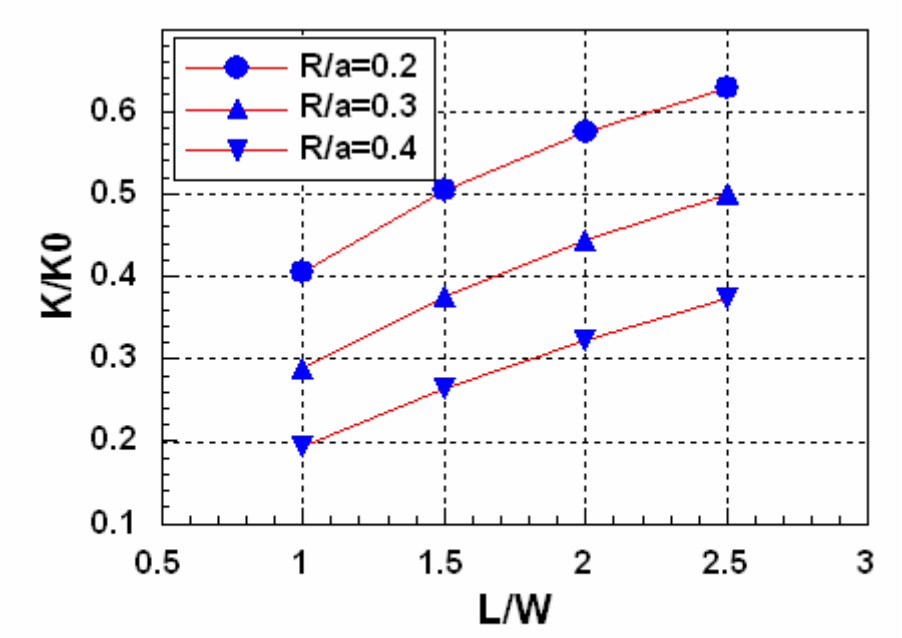

(a) BC1 (V_b/V_a=0.4)

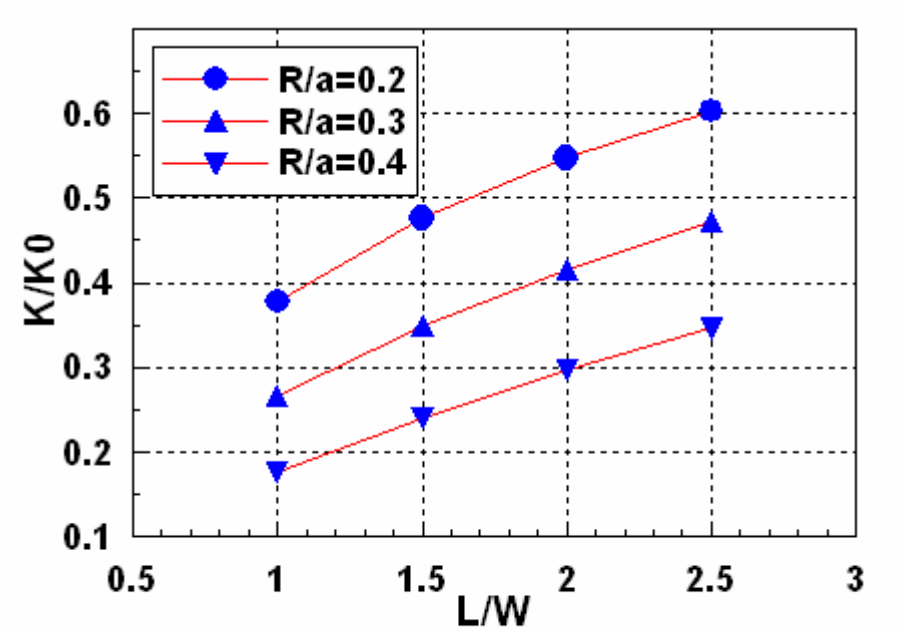

(b) BC2 (V_b/V_a=0.4)

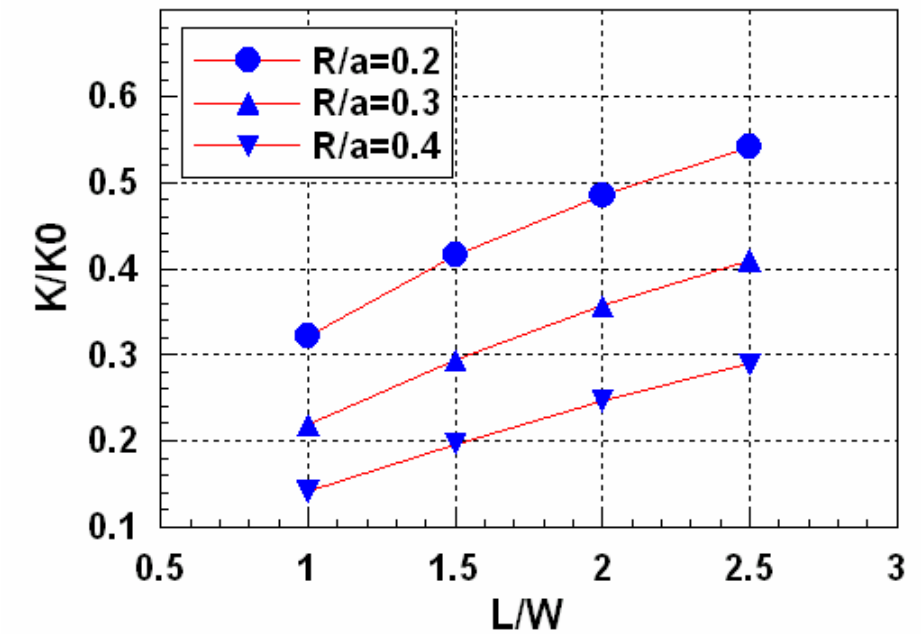

(c) BC3 (V_b / V_a=0.4)

Figure 6.6 Changes of $K/K0$ with L/W on different boundaries conditions

All the simulations are performed with the condition that channel height H is equal to width W. Certainly, the variation of H may affect the value of $K/K0$.

When H tends to infinity, the flow in channel can be simplified into a two-dimensional model as shown in figure 6.1(b). In this study, some cases based on 2D model also are simulated and the results are shown in figure 6.7 Comparing it with the corresponding results in figure 6.4, we can find that the trend of $K/K0$ varies with the R/a is same, i.e. the $K/K0$ decreases with the increasing of R/a when other parameters are the same.

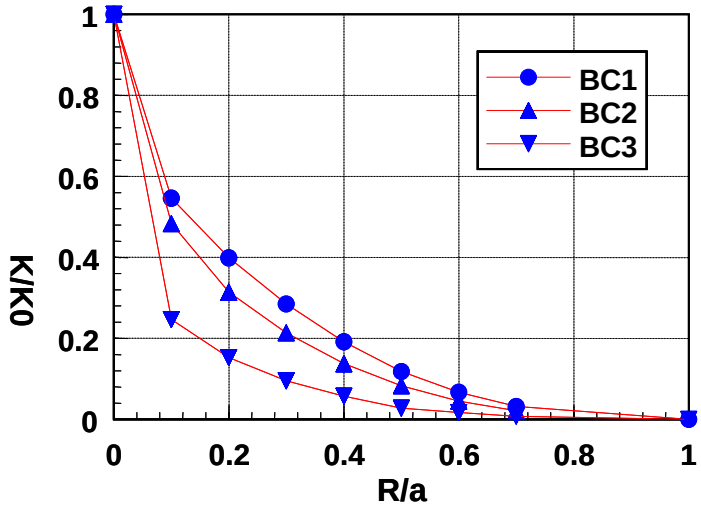

Figure 6.7 Results of 2D simulation: change of $K/K0$ with R/a

(L/W =2.0, V_b/V_a =0.4)

The impregnation process for different stitch radius was also simulated by the finite element simulation. The schematic of the simulation unit cell is show in figure 6.8. Where the effect of stitch size is represented by the ration between the stitch radius and channel length(R/a).

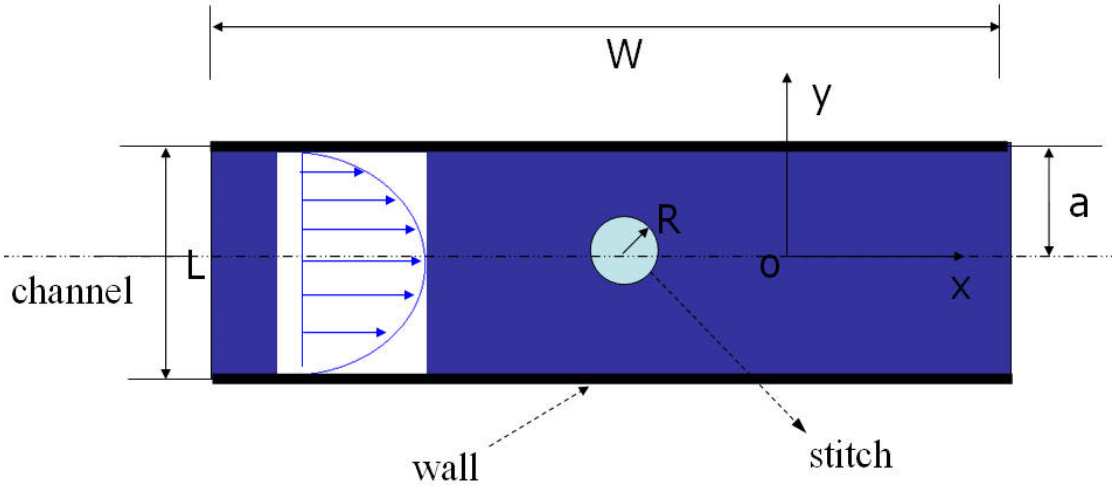

Figure 6.8 Unit cell of channel flow with different stitch size

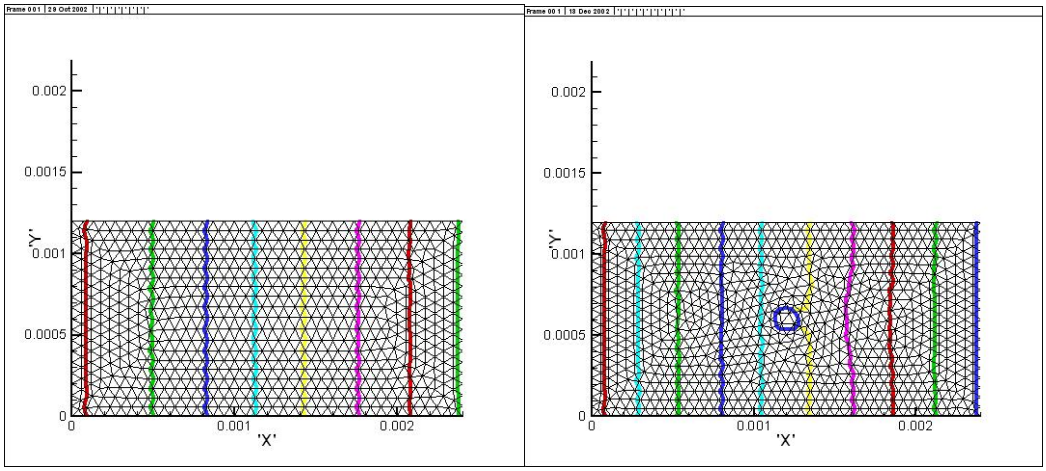

(a)R/a=0 (b) R/a=0.167

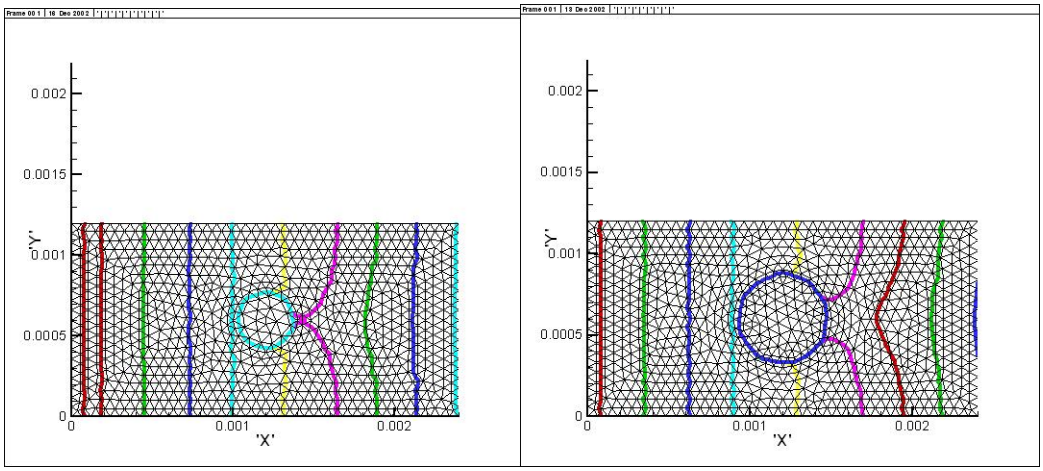

(c) R/a=0.33 (d) R/a=0.5

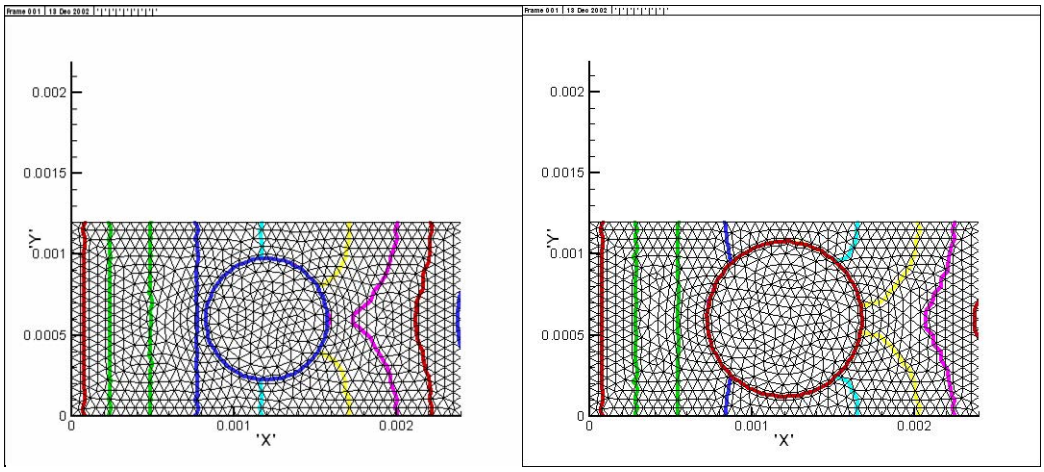

(e) R/a=0.667 (f) R/a=0.833

Figure 6.9 The simulation impregnation process of resin flow through the unit cell of channel with different stitch size

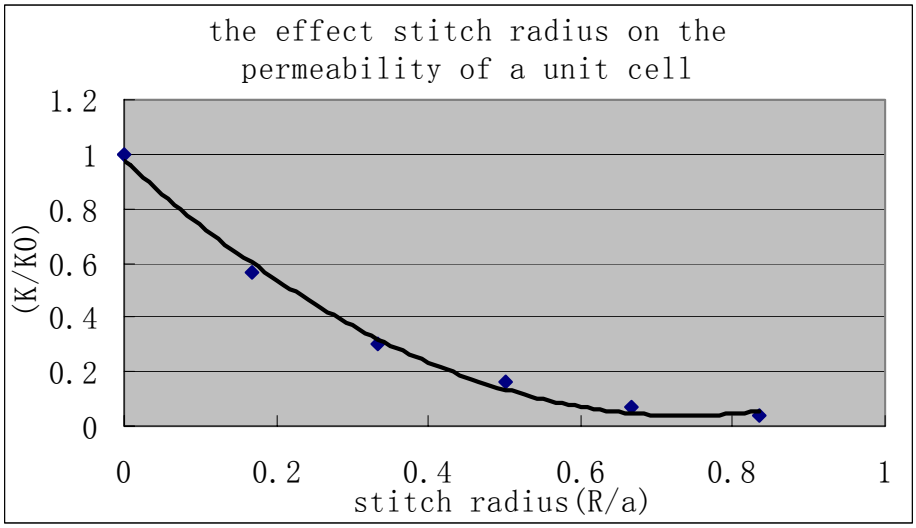

Figure 6.10 the effect of stitch size on permeability

Based on the finite element method, the impregnation process of resin flow through the unit cell of channel with stitch off-center position is show in following simulation figure 6.9.

The effect of stitches on the equivalent permeability of the interbundle channel is presented by the value of K/K0. The effect of stitch size on permeability is shown in Figure 6.10, in which the x-coordinate is R/a, where R is the stitch radius and a is

the channel width.

As shown in Figure 6.10, it is evident that stitches size may severely influence the permeability of the interbundle channel. The permeability is decreased quickly with the increase of stitch radius. These simulation results also correspond with the results analysis by FLUENT as shown in Figure 6.4.

6.3.2 The Effect of Stitch Off-Center Position in Channel

Stitches in the interbundle channel do not always lie on the centreline. They are often off-centre as shown in Figure 6.1(c). In this case, the upper half of channel is selected as the computational cell. The simulation results are shown in Figure 6.11, in which, the x-coordinate is d/a where d is the distance between the stitch centre and channel centreline. Other parameters, R/a is 0.2, L/W is 2.0, and V_b/V_a is 0.4. Apparently, the effect of stitch on the permeability of channel is very different for different off-centre positions. When d/a increased from 0 to 0.8, i.e. the stitch location is moved from the centreline to close to the wall, the value of K/K0 is increased about 50 percent. In other words, the effect is decreased 50 percent. So if we want to weaken the effect of stitch on the permeability of the interbundle channels, and then to make the flow of resin in the channel smooth, it is better to keep the stitch off-centre in the interbundle channel.

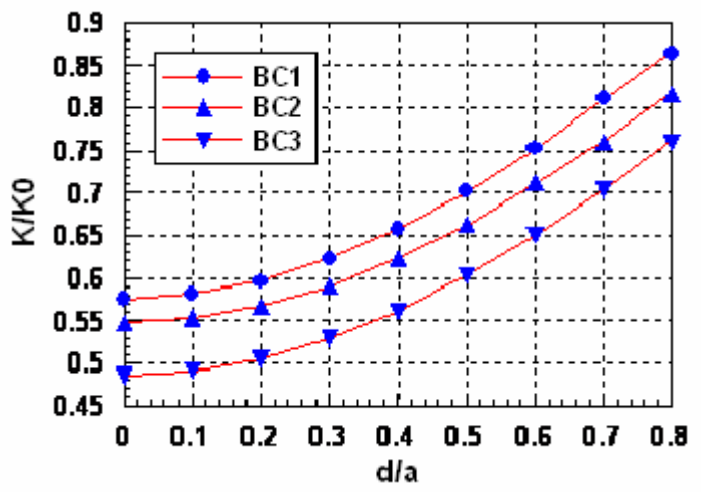

Figure 6.11 Change of $K/K0$ with d/a

The effect of stitch off-centre position in the channel is also further testified by the simulated impregnation process analysed by the finite element method as follows.

A schematic of the simulation unit is show in Figure 6.12, where the stitch off-centre position in the channel is represented by the distance between the stitch centre and channel centreline (d/a). For the simulated case in this section, L/W is 0.5.

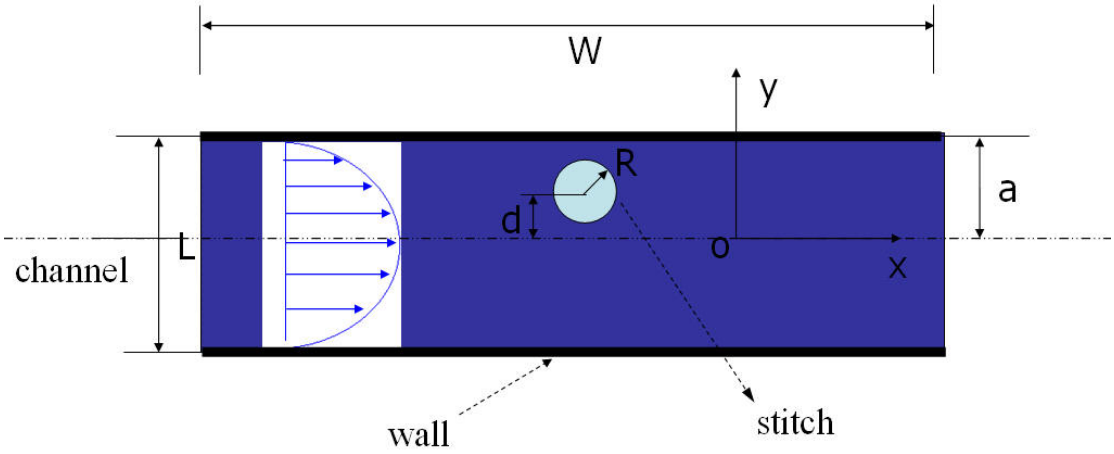

Figure 6.12 Unit cell of channel flow with stitch off-center position

Based on the finite element method, the impregnation process of resin flow through the unit cell of channel with stitch off-center position is show in the following simulation figures.

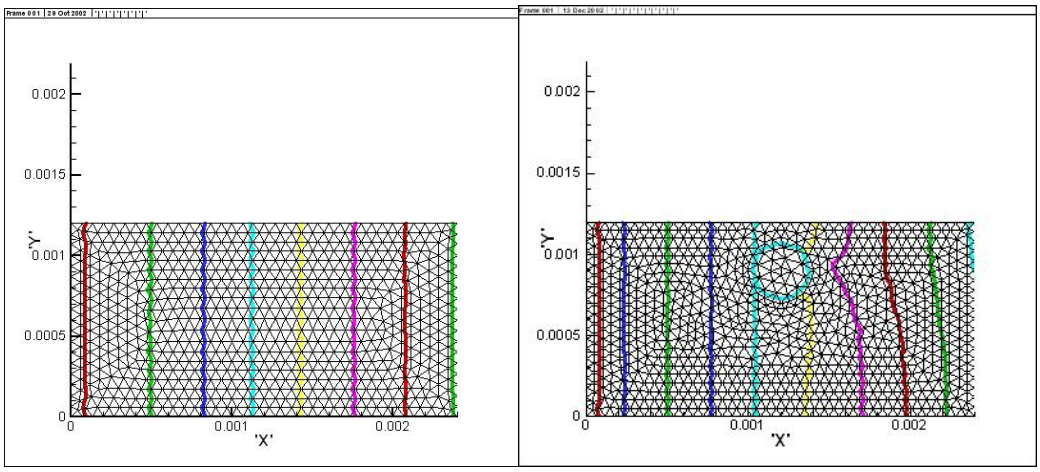

(a) unit cell without stitch (b) d/a=0.667

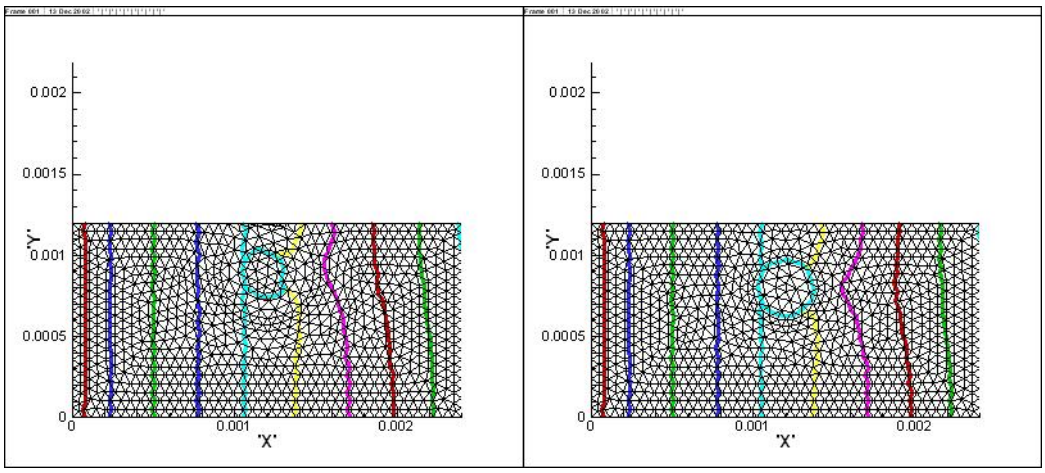

(c) d/a=0.5 (d) d/a=0.333

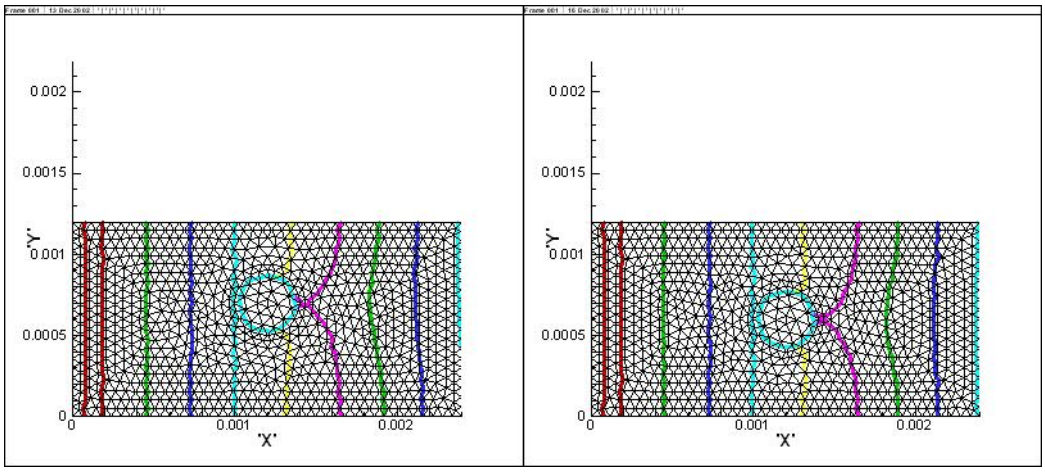

(c) d/a=0.167 (d) d/a=0

Figure 6.13 The simulation impregnation process of resin flow through the unit cell of channel with stitch off-center position

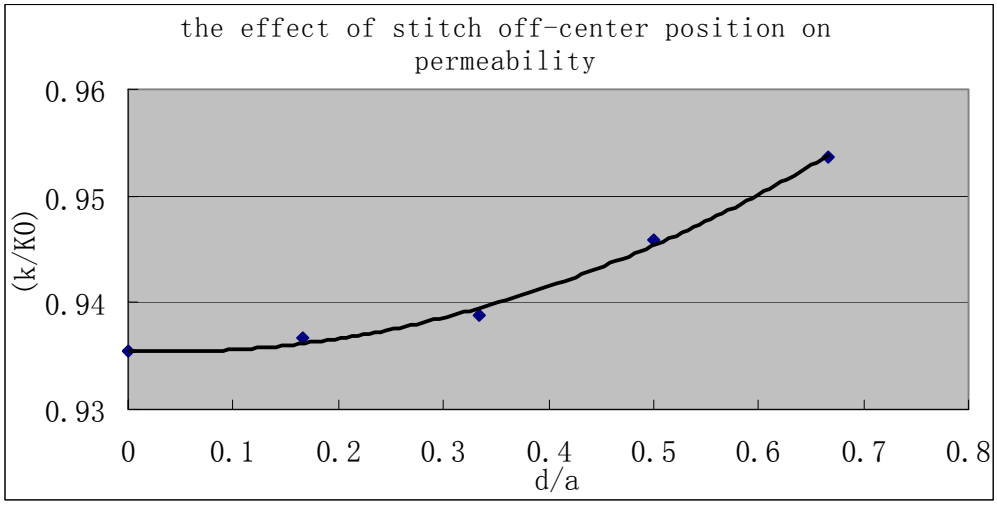

Figure 6.14 the effect of stitch off-center position on permeability

Based on Darcy's law, the effective permeability of the unit cell can be calculated from the simulation impregnation process. The effect of stitches on the equivalent permeability of the interbundle channel is presented by the value of K/K0, where K and K0 are the permeability of the channel with and without stitches respectively. The effect of stitch off-centre position on permeability is shown in Figure 6.14, in which, the x-coordinate is d/a, where d is the distance between the stitch centre and the channel centreline. Apparently, the effect of stitch on the permeability of channel is very different for different off-centre positions. When d/a increased from 0 to 0.7, i.e. the stitch location is moved from the centreline to close to the wall, the value of K/K0 is increased accordingly. These simulation results are consistent with the results analysis by FLUENT.

In other cases, the stitch is always inclined towards the interbundle channel as shown in Figure 6.1(d). So it is very necessary to make clear how the stitch slope will affect the equivalent permeability of the channel. The angle between stitch orientation and y-axis is defined as θ. In this section, the variation of $K/K0$

with θ is investigated by keeping other parameters constant, such as R/a at 0.2, L/W at 2.0, and V_b/V_a at 0.4. As shown in Figure 6.15, the permeability of channel at θ=0o, 10o, 20o, 30o is simulated for different boundary conditions. The results show that $K/K0$ decreases with increasing θ, but the difference for a unit increment of θ is very small when $\theta \leq$ 10o. This corresponds to the increment of surface area of stitch in the channel with increasing θ. Therefore, it can be predicted that $K/K0$ will decrease more quickly for larger θ. Comparing with other parameters, such as off-centre position and size, the effect of slope on the value $K/K0$ is relatively weaker.

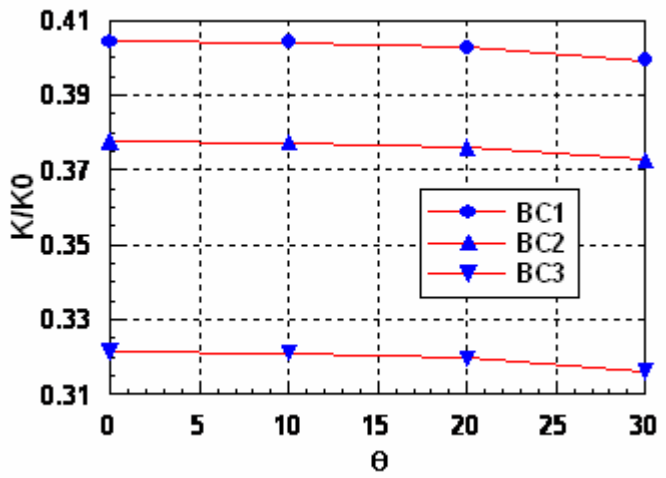

Figure 6.15 Change of $K/K0$ with stitch slope θ

6.3.4 The Effect of Stitch Array

When there are two or more than two stitches in one representative cell, the effect of stitches on permeability of the channel must be different with different arrays. In this thesis, two situations are considered. Firstly, we consider that two stitches are located on the centreline, and arrayed up and down along the flow direction as shown in Figure 6.1(e). We define this situation as array-1. Then two stitches are arrayed to be eudipleural to the centreline of the channel, as shown in Figure 6.1(f).

We define this situation as array-2. In both situations, the distance between two stitches is marked as D. For all simulated cases in this section, R/a is 0.2, L/W is 2.0, and V_b/V_a is 0.4.

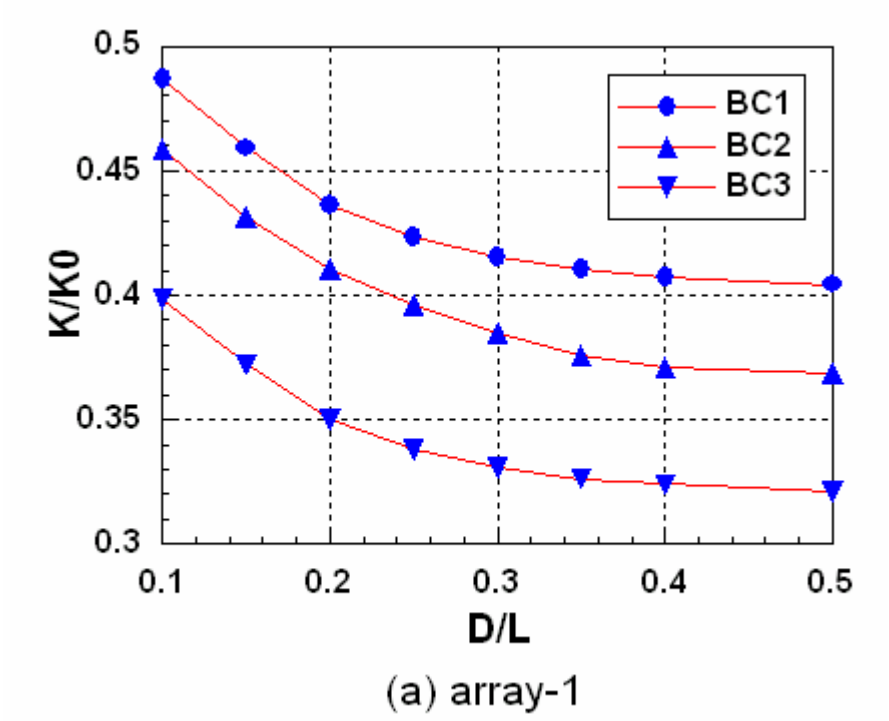

(a) array-1

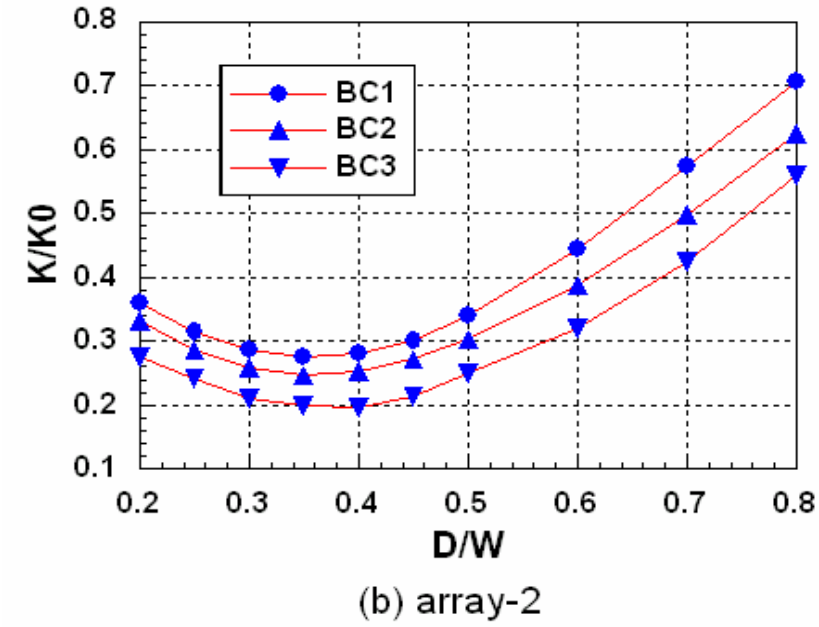

(b) array-2

Figure 6.16. Change of $K/K0$ with L / W in case of array-1 and array-2

In case of array-1, the variation of $K/K0$ with D/L is shown in Figure 6.16(a).

In this case, when D/L is equal to 0.1, two stitches should remain in contact with each other. The simulation results show that $K/K0$ at D/L =0.1 is relatively higher, and decreases quickly at first and then slowly with the increasing of D/L. When D/L is equal to 0.5, the value of $K/K0$ should be the same as the case where there is only one stitch in the representative cell for L/W =1.0.

In case of array-2, when D/W is equal to 0.2, two stitches also should remain in contact with each other, and when D/W is equal to 0.8, the stitch should touch the sidewall of the channel. The simulation results are shown in Figure 6.16, which shows that the variation of $K/K0$ with D/W is not monotonous. When two stitches move simultaneously from the centre to the sidewall of the channel, $K/K0$ decreases firstly, when D/W is equal to 0.35-0.40, $K/K0$ reaches its minimum, and then increases linearly. The difference between the minimum and maximum of $K/K0$ is about 3 times. Therefore, a slight change in stitch array will induce a distinct variation of the permeability of the channel.

The impregnation process for the case of array-2 was also simulated by the finite element simulation. The schematic of the simulation unit is shown in Figure 6.17, where the stitch off-centre position in the channel is represented by the ratio between the stitch centre distance and the channel length (d/b).

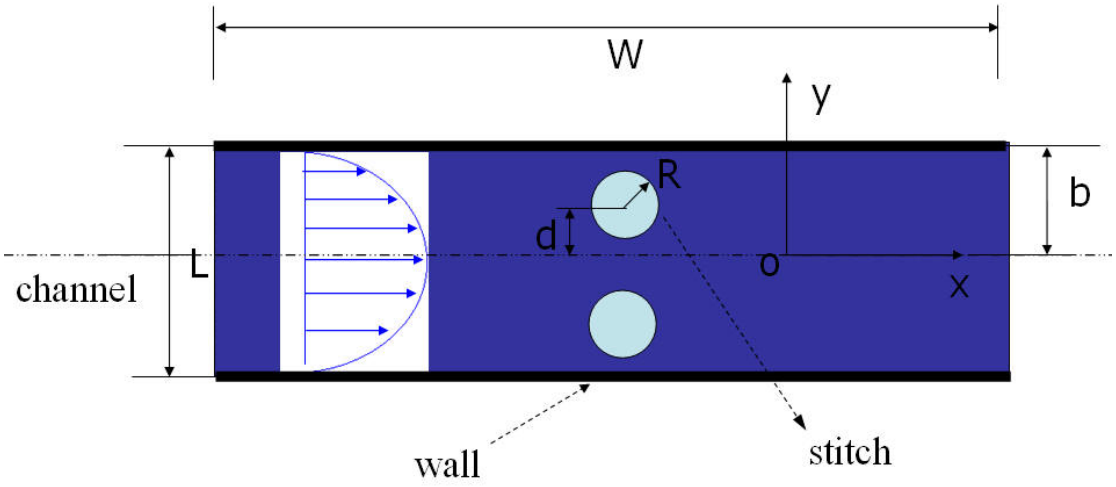

Figure 6.17 Unit cell of channel flow with stitch off-center position(2 stitches)

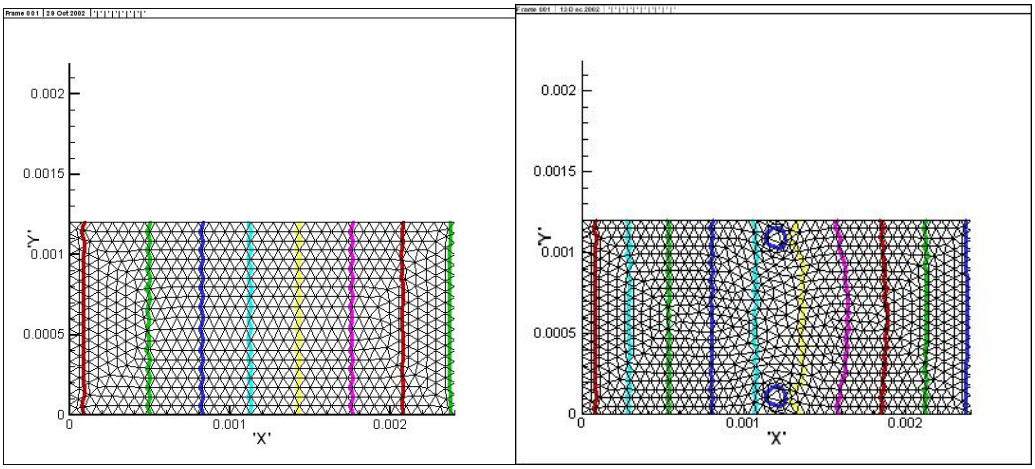

(a) unit cell without stitch (b) d/b=0.75

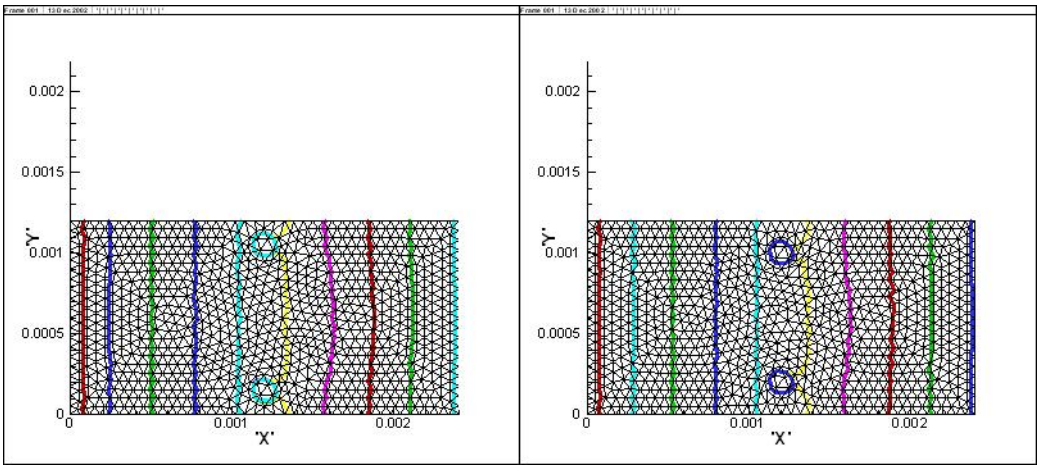

(c) d/b=0.67 (d) d/b=0.5

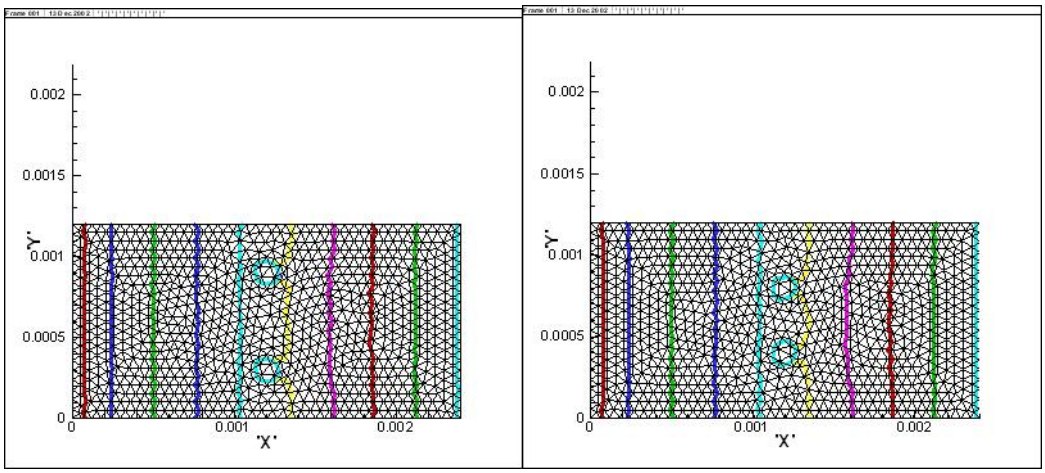

(e) d/b=0.33 (f) d/b=0.25

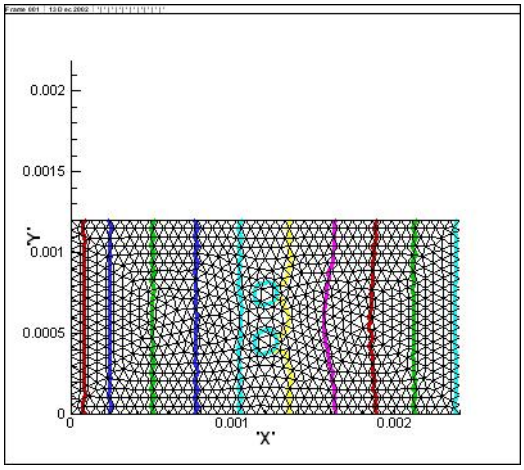

(g) d/b=0.1667

Figure 6.18 The simulation impregnation process of resin flow through the unit cell of channel with stitch off-center position

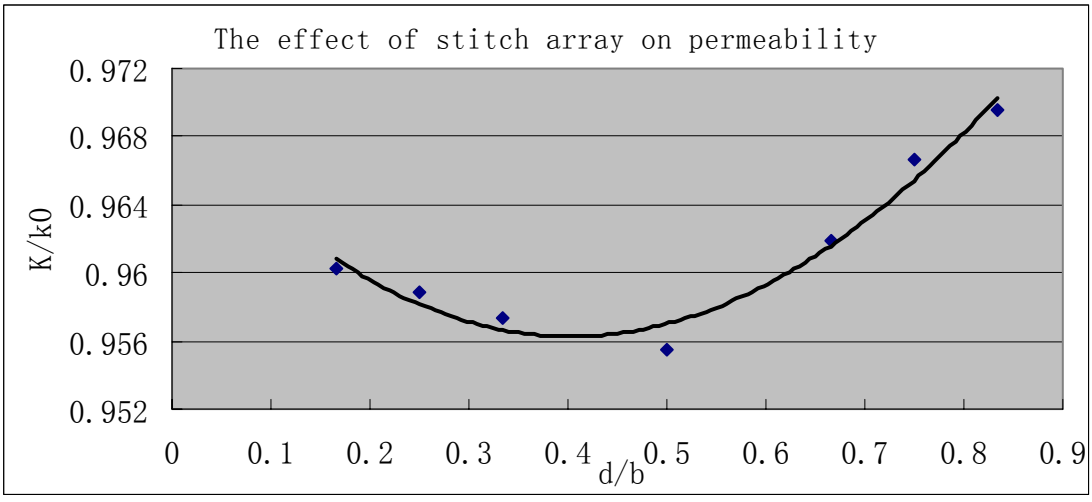

Figure 6.19 the effect of stitch off-center position (2 stitches) on permeability

The effect of stitches on the equivalent permeability of the interbundle channel is presented by the value of K/K0. The effect of stitch off-centre position on permeability is shown in Figure 6.19, in which the x-coordinate is d/b, where d is the half-length of the channel and b is the distance between the stitch centres respectively. The stitch off-centre position can be expressed by d/b.

In this figure, when d/b is equal to 0.1667, two stitches also should keep touch each other, and when d/b is equal to 0.8333, the stitch should touch the side-wall of the channel. The simulation results are shown in figure 6.19, which shows that the change of K/K0 with d/b is not monotonous. When two stitches approach closer, K/K0 decreases firstly, when d/b is equal to 0.4-0.5, K/K0 reaches its minimum value. Then with the increase of d/b, K/K0 also increase linearly. These simulation results also correspond with the with the results analysis by FLUENT.

6.4 Conclusion

Numerical simulations of flow in the interbundle channel with stitch have been carried out, and the effect of stitch on the equivalent permeability of the interbundle channel has been revealed. The results show that stitches may severely affect the permeability of channels, even if their size is relatively smaller. So this effect has to be considered when establishing an effective permeability model for multi-layer fabrics with stitches.

The numerical simulation results also suggest that the effect of stitch is quite different for different stitch size, off-centre position, slope, array, distribution density in the flow direction, and average Darcy velocity in fibre bundles. Therefore, with only one variable, usually the radius of stitch, R, the permeability status of the

interbundle channel is still very uncertain.

The effect of stitches on the equivalent permeability of the interbundle channel is presented by the value of $K/K0$. The numerical simulation results suggest that the effect of stitches is quite different for different stitch size, off-centre position, slope, array, distribution density in the flow direction, and average Darcy velocity in fibre bundles. The value of $K/K0$ will decreased with the increase of stitch size, slope and average Darcy velocity in fibre bundles, and will also decreased with the increase of off-centre distance. When there are two stitches in a representative cell, for up and down array (array-1), the value of $K/K0$ will decrease with the increasing of space between two stitches. For left and right array (array-2), when two stitches move simultaneously from the centre to the side-wall of channel, $K/K0$ decreases firstly, and then increases linearly.

Chapter 7

Conclusion and Future Work

7.1 Summary and conclusion

The geometrical properties, the permeability and the infiltration properties of 3D multi-layer woven fabrics were explored in this study. This thesis first focused on analysing the structures of 3D multi-layer woven fabrics, then established the permeability models of the 3D multi-layer woven fabrics and for the void formation mechanism in the fabrics. The experimental studies and numerical simulation used to confirm and check theoretical results were also carried out. The major techniques used for this study included computer numerical simulation, mathematical modelling and experimental analysis.

The summary and conclusion of this thesis contains four parts: namely permeability tests, permeability models, numerical simulation, and finally void formation.

7.1.1 Permeability Test

The permeability is a key aspect in fibre reinforced composite fabrication. It determines key processing parameters, such as filling time and injection pressure. Therefore, the strength of the composites and mould filling during the injection step would be influenced. The permeability is a property that is dependent on the size of the fibres and the fibre architecture. It can be treated as a tensor and it generally has different values in different directions. Knowledge of the permeability values is also essential for the development of highly permeable fibre reinforcements. Hence,

methods to measure the permeability were developed. This work focuses on the in-plane permeability, which was of interest for liquid composites moulding techniques such as the Resin Transfer Moulding (RTM) process.

The in-plane permeability of the fibre reinforcement was determined through two principal methods, the parallel flow technique and the radial flow technique. By considering the advantages of radial flow method, we designed a set of experimental apparatuses based on the two-dimensional radial flow method. In this project, the final equation to calculate the permeability of the preform was deduced. The relationship between the permeability and the experimental parameters, such as injection pressure, fluid viscosity and flow velocity was therefore investigated.

In order to study the permeability of 3D multi-layer woven fabrics, the multi-layer woven fabrics with different stitch parameters were also investigated. The fabric properties such as fabric structure, microstructure of stitch, and permeability were then determined. The influences of the stitch parameters on permeability were evaluated and compared with the numerical simulation analysis. It was found that both weave designs and stitching methods would affect the permeability of 3D multi-layer woven fabrics. The experimental results were consistent with the prediction from the numerical model.

7.1.2 Permeability Model

Although permeability is the most important property for the 3D multi-layer woven preforms, it has only been investigated by several researchers in limited studies. Moreover, many of the measured data did not seem to agree with each other. Hence, the development of a permeability model for fiber reinforcements is an

important task. Although some researchers have contributed tremendous efforts to measure fabric permeability, the vast variety of the architectures makes it impossible to evaluate the permeable performance of the performs through only experiments. Thus, a predictive permeability model is desirable. The key issues for the permeability predictions are the architectures of fabrics and permeability changes with the porosity of fibrous reinforcements under compression. Few researchers studied the permeability models for fiber preforms, especially the permeability model of 3D multi-layer woven fabrics.

Realizing the limitations of most existing models which do not offer realistic representation of the woven fabric architecture, the present developments introduce the notion of a micro/macro unit cell from a different perspective and is based on a more realistic representation of the three-dimensional fabric architecture which includes stitch, spacing and other fabric parameters. This work focused on the development of a permeability model based on the concept of the resin flow in a unit cell, which can reflect the key features of the actual architecture of the fiber preforms.

In the section of permeability model, the effect of fabric micro-structure and other properties of the multi-layer woven fabrics on permeability were discussed. A permeability model based on fractal theory was established to predict the permeability of the preforms fabricated by the porous yarns. Another permeability model based on unit cell of quadratic fiber packing was also established to predict the permeability of the 3D multi-layer woven fabrics fabricated by mono-filaments.

For the 3D multi-layer woven fabrics fabricated by mono-filament, the in-plan permeability model could be expressed in a simplified form which was related to the

architectures of fiber preforms and the fiber volume fraction changes of fiber preforms under compression. The experimental results showed that the permeabilities of the mono-filament preforms are mainly determined by the arrangements of fibers and the channels between the fiber tows. The fabrics with loose stitch array have better permeability than fabrics with compact stitch array. This is due to the different flow resistance with regard to different stitch array. The looser of stitch structure, the more easy of the resin can flow through it. Thus lead to the better permeability of fabrics with loose stitch array. The results predicted by this model are compared with those from experiments and a good agreement is found in a broad range of fiber volume fraction.

For the 3D multi-layer woven fabrics fabricated with porous yarns, a fractal permeability model for elucidating the disordered pore structures of preforms used in liquid composite molding processes was developed based on the fractal characteristics of pores in the fiber preforms. The permeability model was found to be related to the pore area fractal dimension, the tortuosity fractal dimension, and the architectural parameters of fiber preforms. For fabrics with a rather large maximum pore size λ_{max}, the flow resistance is relative lower. Then the resin can impregnate more easily within it. Thus lead to he better permeability and less void formation in fabrics. The experimental validation of the fractal model was conducted over a series of stitch structures and the tendency predicted by the model is agreed with the experimental data.

7.1.3 Numerical Simulation

The micro-structure of the 3D woven fabrics is quite complicated and variable. In the study of the effect of stitch model on the permeability of 3D multi-layer woven

fabrics, it is time consuming and onerous to test and analyze many kinds of samples experimentally. So it is not only desirable but also necessary to analyze the permeability of complicated structure fabrics through the numerical simulation.

In this work, several typical structures were selected as the basic models, and the effect of stitches on the permeability of the interbundle channel has been investigated through numerical simulation for various combinations of the stitch size, its off-centre position, slope, array, distribution density in the flow direction and the average Darcy velocity in fibre bundles. Based on Darcy's law and the governing equations for three-dimensional steady-state incompressible flow in the channel, the numerical simulation was established to predict the effect of various stitch parameters on the permeability of whole unit cell.

Numerical simulations of flow in the interbundle channel with stitch were carried out, and the effect of stitch on the equivalent permeability of the interbundle channel was revealed. The results showed that stitches could severely affect the permeability of channels, even if its size was relatively smaller. So this effect has to be considered when establishing the effective permeability model of multi-layer fabrics with stitches.

The numerical simulation results also suggested that the effect of stitch was quite different for different stitch size, off-centre position, slope, array, distribution density in the flow direction, and the average Darcy velocity in fibre bundles.

The effect of stitches on the equivalent permeability of the interbundle channel was presented by the value of $K / K0$. The numerical simulation results suggested that the effect of stitches was quite different for different stitch size, off-centre position, slope,

array, distribution density in the flow direction, and average Darcy velocity in fibre bundles. The value of $K/K0$ will decreased with the increase of stitch size, slope and average Darcy velocity in fibre bundles, and will also decreased with the increase of off-centre distance. When there were two stitches in a representative cell, for up and down array (array-1), the value of $K/K0$ would decrease with the increasing of space between two stitches. For left and right array (array-2), when two stitches moved simultaneously from the centre to the sidewall of channel, $K/K0$ decreased firstly, and then increased linearly.

7.1.4 Void Formation

During the RTM processing, a liquid resin is injected into a closed mold containing a prefabricated preform which is formed by fiber tows. Due to the complicated and non-uniform microstructure of the fiber preform, the permeability of the preforms may differ by several orders of magnitude between insider and outsider fiber tow. These non-uniform properties finally will lead to the formation of air voids on the micro scale. The presence of voids is much undesired and has a deleterious effect on product mechanical properties, such as inter-laminar shear strength, compressive strength, impact resistance and fatigue life. It is significant to establish a model to reveal the mechanism of void formation in fabrics and eliminate it.

In order to establish the model of void formation in multi-layer woven fabrics, two simplified unit cells for in-plane impregnation in multi-layer woven fabric were suggested. And a mathematical model was developed to analyze the void formation in both unit cells during the RTM processes. The model recognizes non-uniform fiber permeability in different sub-domains of fiber preforms. Although a few simplifying assumptions were introduced, the model still accounted for the key

mechanisms of void formation in the cross section of MWFs. And the location of the void predicted by this model agreed quite well with the experiments. The model also showed that the ratio of weft axial permeability K_b^a and warp transverse permeability K_b^t was determinant for the formation and size of void.

The flow in both unit cells also was numerically simulated using the control-volume method. The presented numerical scheme was firstly tested by comparing with mold filling cases for which analytical solution existed. The simulated result, including flow fronts and effect of K_b^a / K_b^t, agreed with those predicted by analytical model.

7.2 Future Research

In order to continue the researches in this field, some studies are recommended for future investigation and development as follows.

7.2.1 Experimental Verification

Effects of other stitch parameters, especially the stitch off-center position, the array and the distribution density, need to be verified by fabricating and testing the 3D multi-layer woven fabrics. The results obtained from the numerical simulation of stitch effect should be compared with and verified by the experimental results.

7.2.2 Numerical Simulation

Although the control volume technique was proposed to simulate the flow process and the pressure distribution in the 3D multi-layer woven fabrics in this thesis, it is still necessary to improve the numerical simulation analysis anyhow. In particular,

the present 2D simulation model may be improved to a 3D model. In addition, in order to increase the stabilization of the simulation model, we can use a quadratic element instead of the present triangle element.

The simulation model used in this thesis may also be extended by taking into account the effect of injection pressure on the preshaped preforms. So the future simulation model can also simulate the changes of the preforms under the injected fluid pressure.

7.2.3 Void Formation

The basic model of void formation in multi-layer woven fabrics was established. To further investigate the mechanism of the formation of void in the 3D multi-layer woven fabrics, this model may be extended to simulate the effect of other fabric parameters such as stitch structure on the void formation.

Appendix A

Analytical solution for 1-D isothermal flow

Let us observe the flow of fluid into a 1-D cavity as shown in Fig. A1. For this problem, Darcy's law and continuity equation are expressed as:

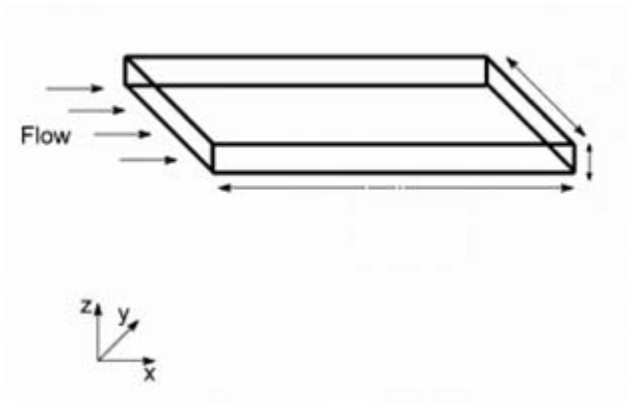

Figure A1. Geometric details of one-dimensional test problem: injection at horizontal position

$$u = -\frac{k}{\mu}\left(\frac{dp}{dx} + \rho g\right) \tag{A1}$$

$$\frac{du}{dx} = 0 \tag{A2}$$

Substituting Darcy's law into Eq. (A2) yields:

$$\frac{d}{dx}\left(-\frac{k}{\mu}\left(\frac{dp}{dx} + \rho g\right)\right) = 0 \tag{A3}$$

This is the governing equation for 1-D flow, and the boundary conditions are

$$\left.\begin{array}{l} p = p_{inj} \text{ for constant injection pressure} \\ q = q_{inj} \text{ for constant injection flow rate} \end{array}\right\} \text{ at x=0} \tag{A4a}$$

$$p = p_{vac} \; at \;\; x = x(t_{ff}) \tag{A4b}$$

in which moving front, $x(t_{ff})$ is expressed as:

$$u = \phi \frac{dx}{dt} \tag{A5}$$

We assume a linear function of fluid velocity for permeability as:

$$k = a + bu \tag{A6}$$

Analytical expressions for 1-D flow under constant injection pressure

The solution of Eq. (A3) is

$$p\,(x, t_{ff}) = p_{inj} + \frac{p_{vac} - p_{inj}}{x\,(t_{ff})}\, x \tag{A7}$$

Substitution of this equation into Eq. (A1) without gravity contribution, using Eqs. (A5) and (A6), and further simplification leads to the following expression:

$$\phi(x(t) - \frac{b}{\mu}(p_{inj} - p_{vac})\frac{dx(t)}{dt} = \frac{a}{\mu}(p_{inj} - p_{vac}) \tag{A8}$$

The boundary conditions for this differential equation are

$$\left.\begin{array}{l} x(\mathrm{t}) = 0 \;\; \text{at t} = 0 \\ x(\mathrm{t}) = \mathrm{x}(\mathrm{t}_{\mathrm{ff}}) \;\; \text{at t} = \mathrm{t}_{\mathrm{ff}} \end{array}\right\} \tag{A9}$$

The solution of Eq. (A8) leads to the following relation for the flow front location at time t_{ff}:

$$\left[\frac{1}{2}x^2(t_{ff}) - \frac{b}{\mu}(p_{inj} - p_{vac})x(t_{ff})\right] = \frac{a}{\mu}(p_{inj} - p_{vac})t_{ff} \quad \text{(A10)}$$

For the case of velocity dependent permeability with no vacuum at the flow front, p_{vac}=0, Eq. (A10) becomes:

$$\left[\frac{1}{2}x^2(t_{ff}) - \frac{b}{\mu}p_{inj}x(t_{ff})\right] = \frac{a}{\mu}p_{inj}t_{ff} \quad \text{(A11)}$$

If one assumes a constant permeability with a vacuum at the flow front, Eq. (A10) is simplified into:

$$\frac{1}{2}x^2(t_{ff}) = \frac{k}{\phi\mu}(p_{inj} - p_{vac})t_{ff} \quad \text{(A12)}$$

Analytical expressions for 1-D flow under constant injection flow rate.

The solution of Eq. (A3) leads to following expression for pressure distribution:

$$p(x,t_{ff}) = p_{inj}(t_{ff}) + \frac{p_{vac} - p_{inj}(t_{ff})}{x(t_{ff})}x \quad \text{(A13)}$$

By substituting Eq. (A13) into Eq. (A1), we get the following relation for inlet pressure with no vaccum at the flow front

$$p_{inj}(t_{ff}) = (\frac{q_{inj}\mu}{kS} + \rho g)Z(t_{ff}) \quad \text{(A14)}$$

in which $Z(t_{ff})$ denotes the position of the flow front according to notations in Fig. 6. For horizontal mold filling with a vaccum at the flow front, inlet pressure is obtained by:

$$p_{inj}(t_{ff}) = \frac{\mu q_{inj} x(t_{ff})}{kS} + p_{vac} \qquad \text{(A15)}$$

When the permeability is a function of fluid velocity, the following equation is obtained by substituiting Eq.(A13) into Darcy's law and considering Eq. (A6):

$$p_{inj}(t_{ff}) = \frac{\mu q_{inj} x(t_{ff})}{aS + bq_{inj}} \qquad \text{(A16)}$$

in which p_{vac} has been set to zero.

Appendix B

The governing equation for two dimensional flow

For the general anisotropic case the governing equation for two dimensional flow in porous media reads as follows:

$$K_{xx}\frac{\partial^2 p}{\partial x^2}+K_{yy}\frac{\partial^2 p}{\partial y^2}+K_{zz}\frac{\partial^2 p}{\partial z^2}=0 \qquad \text{(B1)}$$

As permeability is assumed to be a symmetric tensor there is an angle w for which the mixed permeability term in the above equation becomes zero (Borg, 1963). The angle w has to be limited as $\tan 2\phi$ which is defined uniquely only in an interval of $\pm 45^{\circ}$. There are now three unknowns which need to be determined in the flow experiments (K1, K2 and ϕ) hence flow front measurements need to be taken in three directions. Using the same transformation law as before (Adams, etc., 1988; Chan and Hwang, 1991) but with the additional rotation as defined in

$$X' = r\cos\phi$$
$$Y' = -r\sin\phi$$

The quasi-isotropic permeability can be written as:

$$K' = r'^2_f\,[2\ln(\frac{r'_f}{r'_0})+(\frac{r'_0}{r'_f})^2-1]\cdot\frac{\varepsilon\mu}{4\Delta pt} \qquad \text{(B2)}$$

The radius r' is related to the *x* and *y* coordinates by

$$r' = \sqrt{x'^2+y'^2}$$

or

$$r' = \sqrt{(\frac{k_2}{k_1})^{\frac{1}{2}} x'^2 + (\frac{k1}{k2})^{\frac{1}{2}} y'^2}$$

and fully expanded :

$$r' = r\sqrt{(\frac{k_2}{k_1})^{\frac{1}{2}} \cos^2\varphi + (\frac{k1}{k2})^{\frac{1}{2}} \sin^2\varphi} \qquad \text{(B3)}$$

where $r = \sqrt{x^2 + y^2}$

Eq. (B3) is applicable to both the inlet and the flow front radius and is evaluated for the three measurement directions I, II and III (see Fig. B1 and Fig. B2).

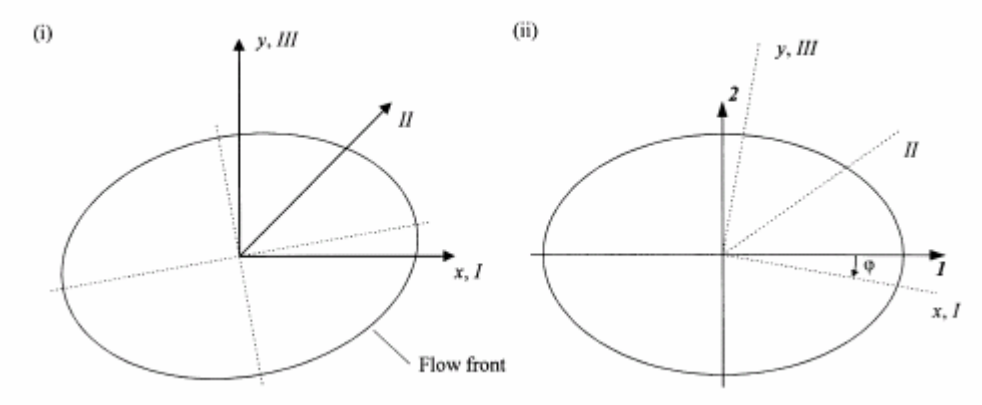

Figure B1. Rotation of coordinate system for permeability measurement in an arbitrary direction.

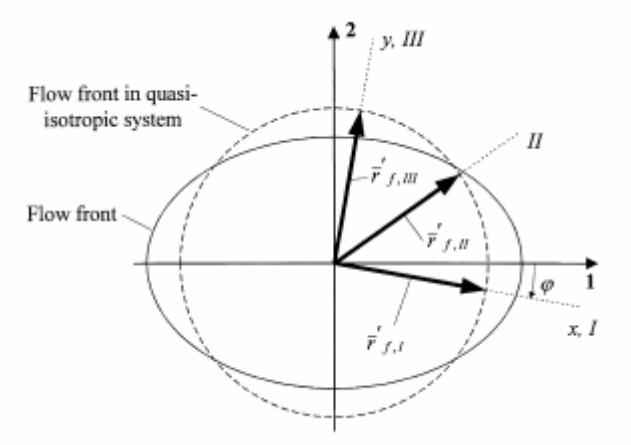

Figure B2. Transformation to quasi-isotropic system

The quasi-isotropic radii obtained from Eq. (B3) for the flow front position measured in the three directions, $r'_{f,\mathrm{I}}$, $r'_{f,\mathrm{II}}$ and $r'_{f,\mathrm{III}}$, are shown in Fig. 4. The inlet radii (not shown in Fig. 4) are transformed in exactly the same way. Direction *I* means that *y* equals zero, for direction *II* *x* equals *y* and for direction *III* *x* equals zero(Weitzenbo, etc., 1999).

Thus for direction *I* the flow front radius is equal to:

$$r'_{f,\mathrm{I}} = r_{f,\mathrm{I}}\sqrt{(\frac{k_2}{k_1})^{\frac{1}{2}}\cos^2\varphi + (\frac{k1}{k2})^{\frac{1}{2}}\sin^2\varphi} \qquad \text{(B4)}$$

and the inlet radius is:

$$r'_{o,\mathrm{I}} = r_{o,\mathrm{I}}\sqrt{(\frac{k_2}{k_1})^{\frac{1}{2}}\cos^2\varphi + (\frac{k1}{k2})^{\frac{1}{2}}\sin^2\varphi} \qquad \text{(B5)}$$

Similar expressions can be derived for directions II and III (Weitzenbo, J.R., 1996). The angle of rotation for direction *II* and *III* are $\phi - 45^\circ$ and $\phi - 90^\circ$ respectively.

By evaluating Eq. (B2) for orientations *I*, *II* and *III* and extracting the constant terms the three basic equations to determine the permeability can be set up:

$$K' = F_{\mathrm{I}}\left((\frac{k_2}{k_1})^{\frac{1}{2}} \cos^2\varphi + (\frac{k1}{k2})^{\frac{1}{2}} \sin^2\varphi \right) C \qquad \text{(B6)}$$

$$K' = F_{\mathrm{II}}\left((\frac{k_2}{k_1})^{\frac{1}{2}} (1+\sin 2\varphi) + (\frac{k1}{k2})^{\frac{1}{2}} (1-\sin 2\varphi) \right) C \qquad \text{(B7)}$$

$$K' = F_{\mathrm{III}}\left((\frac{k_2}{k_1})^{\frac{1}{2}} \sin^2\varphi) + (\frac{k1}{k2})^{\frac{1}{2}} \cos^2\varphi) \right) C \qquad \text{(B8)}$$

where C is

$$C = \frac{\mu\varepsilon}{4\Delta p} \qquad \text{(B9)}$$

and Fi equals (for $i = I, II, III$)

$$F_i = \frac{N_i}{t_i} \qquad \text{(B10)}$$

With

$$N_i = r_{f,i}^2 [2\ln(\frac{r_{f,i}}{r_{0,i}}) + (\frac{r_{0,i}}{r_{f,i}})^2 - 1]$$

The flow front and inlet radii are defined as follows:

$$r_{f,i} = \sqrt{x_{f,i}^{\ 2} + y_{f,i}^{\ 2}}$$

$$r_{o,i} = \sqrt{x_{o,i}^{\ 2} + y_{o,i}^{\ 2}}$$

where $x_{f,i}$, $y_{f,i}$ and $x_{o,i}$ and $y_{o,i}$ are the coordinates of the flow front (f) and inlet (o) in the physical system.

By rearranging Eqs. (B6) and (B8) an expression for the principal permeability $K1$

is obtained

$$K_1 = F_{\mathrm{I}} \frac{(A-D)}{(A-\frac{D}{\cos 2\phi})} C \qquad \text{(B11)}$$

As well as K_2 ,

$$K_1 = F_{\mathrm{II}} \frac{(A-D)}{(A+\frac{D}{\cos 2\phi})} C \qquad \text{(B12)}$$

where the average *A* and the difference *D* are defined as:

$$A = \frac{F_{\mathrm{I}} + F_{\mathrm{III}}}{2}, \quad D = \frac{F_{\mathrm{I}} - F_{\mathrm{III}}}{2} \qquad \text{(B13)}$$

To find the angle of rotation Eq. (B7) is divided by *K*'

$$1 = \frac{F_{\mathrm{II}}}{2} \left\{ \frac{(1+\sin 2\phi)}{K_1} + \frac{(1-\sin 2\phi)}{K_2} \right\} \mathrm{C} \qquad \text{(B14)}$$

Substituting Eqs. (B11) and (B12) for *K*1 and *K*2 in Eq. (B14) and rearranging yields:

$$\varphi = \frac{1}{2} \tan^{-1} (\frac{A}{D} - \frac{A^2 - D^2}{F_{\mathrm{II}} D}) \qquad \text{(B15)}$$

Eqs. (B11), (B12) and (B15) define the permeability in two dimensions.

Appendix C

Computer program for simulation

```
!!!!!!!!!!!!!!
!  This program is for the simulation of mold filling with triangle
element
!!!!!!!!!!!!!!
      parameter(Nnode=,Nele=)
      real*8 p(Nnode)
      real*8 x(Nnode),y(Nnode),Cx(Nele),Cy(Nele)
      real*8 f(Nnode),Area(Nele),volume(Nnode)
      real*8 A(Nnode,Nnode)
      real*8 KXX(Nele),KYY(Nele),KXY(Nele),KYX(Nele)
      real*8 Vx(Nele),Vy(Nele)
      real*8 Inlet(Nnode)
      integer ID(Nnode),DI(Nnode)
      integer ele(Nele,3),adjele(Nnode,10)
      real*8 visco
      real*8 Hz,Ttotal
      integer ai
```

```
      integer i,j,kk
      character*1 ch
      data Hz/1.0/
      data ch/'s'/
      visco=
      Ttotal=0.0
!     read information of node and element
      open(2,file='element.txt')
      do i=1,Nele
         read(2,*)ai,ai,ai,ai,ai,ai,ele(i,1),ele(i,2),ele(i,3),ai
      enddo
      close(2)
      open(2,file='node.txt')
      do i=1,Nnode
         read(2,*)ai,x(i),y(i),ai
      enddo
      close(2)
      do i=1,Nele
         KXX(i)=
```

```
        KYY(i)=

        KXY(i)=0.0

        KYX(i)=0.0

    enddo

    do i=1,Nnode

        f(i)=0.0

        Inlet(i)=0.0

    enddo

    do i=1,Nnode

        p(i)=0.0

    enddo

    do i=1,Nnode

        if(  (  (x(i)-0.00)*(x(i)-0.00)+(y(i)-0.00)*(y(i)-0.00)  ).LT.


(0.004*0.004)    ) then

            f(i)=1.0

            Inlet(i)=1.0

            p(i)=

            endif
```

```
      enddo
      call nodeele(Nnode,Nele,ele,x,y,Hz,adjele,Cx,Cy,Area,volume)
            do II=1,2000
            write(*,*) II
            call
goforward(Nnode,Nele,f,p,KXX,KYY,KXY,KYX,Area,volume,ele,adjele,vis
co,&
                                    Hz,Ttotal,x,y,Cx,Cy)
            do i=1,Nnode
                  if(Inlet(i).EQ.1.0) then
                        f(i)=0.0
                  endif
            enddo
            do i=1,Nnode
                  ID(i)=0
                  DI(i)=0
            enddo
            ip=0
            do i=1,Nnode
```

```
                if(abs(f(i)-1.0).LT.1.0d-15) then
!                   write(*,*) i,f(i)
                    ip=ip+1
                    ID(i)=ip
                    DI(ip)=i
                endif
            enddo
!           write(*,*)ip
            call
solvepressure(Nnode,Nele,f,p,KXX,KYY,KXY,KYX,Area,ele,adjele,visco
,A,&
                                Hz,Ttotal,x,y,Cx,Cy,Inlet,ip,ID,DI)
                    call writedat(Nnode,Nele,II,Ttotal,ele,f,p,x,y,ch)
    enddo
    end
    include "sprintf.f90"
    include "GGJ.f90"
!*************************************************************
!*************************************************************
```

```
subroutine
goforward(Nnode,Nele,f,p,KXX,KYY,KXY,KYX,Area,volume,ele,adjele,
visco,&
                                    Hz,Ttotal,x,y,Cx,Cy)
    real*8 p(Nnode),Q(Nnode),Area(Nele),volume(Nnode)
    real*8 x(Nnode),y(Nnode),Cx(Nele),Cy(Nele)
    real*8 f(Nnode), TT(Nnode)
    integer IR(Nnode),QI(Nnode)
    integer ele(Nele,3),adjele(Nnode,10)
    real*8 KXX(Nele),KYY(Nele),KXY(Nele),KYX(Nele)
    real*8 Dt,Hz,visco,Var1,Var2
    real*8 gama1,gama2,gama3,bata1,bata2,bata3
    real*8 lacx,lacy,lbcx,lbcy,xb,yb,xc,yc,px,py
    real*8 Ttotal
          integer kq
    integer it,ik,jk,ie,n1,n2,n3
!     To identify the node on flow front
    do i=1,Nnode
       IR(i)=0
```

```
enddo
    do ik=1,Nnode
    if(f(ik).NE.1.0) then
        do jk=1,10
        if(adjele(ik,jk).NE.0) then
            ie=adjele(ik,jk)
            n1=ele(ie,1)
            n2=ele(ie,2)
            n3=ele(ie,3)
            IR(ik)=IR(ik)+AINT(f(n1))+AINT(f(n2))+AINT(f(n3))
        endif
        enddo
    endif
enddo
    do i=1,Nnode
    QI(i)=0
enddo
kq=0
do ik=1,Nnode
```

```
            if(IR(ik).NE.0) then
!           write(*,*)ik,IR(ik)
                kq=kq+1
                QI(kq)=ik
            endif
        enddo
!       write(*,*)kq
!       To calculate the inflow rate of front control volume
        do i=1,kq
            ik=QI(i)
!           write(*,*)'ik=',ik,x(ik),y(ik)
            Q(i)=0.0
            do jk=1,10
            if(adjele(ik,jk).NE.0) then
                ie=adjele(ik,jk)
                n1=ele(ie,1)
                n2=ele(ie,2)
                n3=ele(ie,3)
!               write(*,*)jk,n1,n2,n3
```

```
                if(n2.EQ.ik) then
                    n2=n3
                    n3=n1
                    n1=ik
                    else if(n3.EQ.ik) then
                    n3=n2
                    n2=n1
                    n1=ik
                    else
                    n1=n1
                    n2=n2
                    n3=n3
                endif
!               write(*,*)jk,n1,n2,n3
                var1=Hz/(2.0*Area(ie)*visco)
                xa=(x(n1)+x(n2))/2.0
                ya=(y(n1)+y(n2))/2.0
                xb=(x(n1)+x(n3))/2.0
                yb=(y(n1)+y(n3))/2.0
```

```
                lacx=Cy(ie)-ya

                lacy=-(Cx(ie)-xa)

                lbcx=-(Cy(ie)-yb)

                lbcy=Cx(ie)-xb

                gama1=x(n3)-x(n2)

                gama2=x(n1)-x(n3)

                gama3=x(n2)-x(n1)

                bata1=y(n2)-y(n3)

                bata2=y(n3)-y(n1)

                bata3=y(n1)-y(n2)

                px=bata1*p(n1)+bata2*p(n2)+bata3*p(n3)

                py=gama1*p(n1)+gama2*p(n2)+gama3*p(n3)

                if(abs(f(n2)-1.0).LT.1.0d-10) then
!               write(*,*)'n2=',n2,y(n2)


    Q(i)=Q(i)+var1*(lacx*(KXX(ie)*px+KXY(ie)*py)+lacy*(KYX(ie)*px+
KYY
(ie)*py))

                endif

                if(abs(f(n3)-1.0).LT.1.0d-10) then
```

```
!                 write(*,*)'n3=',n3,y(n3)


      Q(i)=Q(i)+var1*(lbcx*(KXX(ie)*px+KXY(ie)*py)+lbcy*(KYX(ie)*px+
KYY
(ie)*py))
                  endif
            endif
            enddo
!           write(*,*)Q(i)
            TT(i)=volume(ik)*(1-f(ik))/Q(i)
!           write(*,*)TT(i)
      enddo
      Dt=TT(1)
      do i=1,kq
            if(TT(i).LT.Dt) then
            Dt=TT(i)
            endif
      enddo
      Ttotal=Ttotal+Dt
!     write(*,*)Dt
```

```
            do i=1,kq
            ik=QI(i)
            f(ik)=f(ik)+Dt*Q(i)/volume(ik)
!           write(*,*)ik,f(ik)
      enddo
                  end
      subroutine
solvepressure(Nnode,Nele,f,p,KXX,KYY,KXY,KYX,Area,ele,adjele,visco
,A,&
                                    Hz,Ttotal,x,y,Cx,Cy,Inlet,ip,ID,DI)
      real*8 p(Nnode),Area(Nele),volume(Nnode)
      real*8 x(Nnode),y(Nnode),Cx(Nele),Cy(Nele)
      real*8 f(Nnode),Inlet(Nnode)
      real*8 A(Nnode,Nnode),B(ip),C(ip)
      integer ID(Nnode),DI(Nnode)
      integer ele(Nele,3),adjele(Nnode,10)
      real*8 KXX(Nele),KYY(Nele),KXY(Nele),KYX(Nele)
      real*8 Hz,visco,Var1,Var2
      real*8 gama1,gama2,gama3,bata1,bata2,bata3
```

```
      real*8 lac,lbc,nacx,nacy,nbcx,nbcy,xb,yb,xc,yc,px,py
      real*8 Ttotal
            integer kq,ip
      integer it,ik,jk,ie,n1,n2,n3
            do i=1,ip
        B(i)=0.0
        do j=1,ip
        A(i,j)=0.0
        enddo
      enddo
!     calculate coefficient matrix
      do i=1,ip
        ik=DI(i)
        do jk=1,10
        if(adjele(ik,jk).NE.0) then
            ie=adjele(ik,jk)
            n1=ele(ie,1)
            n2=ele(ie,2)
            n3=ele(ie,3)
```

```
!       write(*,*)jk,n1,n2,n3
        if(n2.EQ.ik) then
            n2=n3
            n3=n1
            n1=ik
            else if(n3.EQ.ik) then
            n3=n2
            n2=n1
            n1=ik
            else
            n1=n1
            n2=n2
            n3=n3
        endif
!       write(*,*)jk,n1,n2,n3
        xa=(x(n1)+x(n2))/2.0
        ya=(y(n1)+y(n2))/2.0
        xb=(x(n1)+x(n3))/2.0
        yb=(y(n1)+y(n3))/2.0
```

```
lac=sqrt((Cy(ie)-ya)**2+(Cx(ie)-xa)**2)

lbc=sqrt((Cy(ie)-yb)**2+(Cx(ie)-xb)**2)

        var1=Hz*lac/(2.0*Area(ie)*visco)

var2=Hz*lbc/(2.0*Area(ie)*visco)

nacx=(Cy(ie)-ya)/lac

nacy=(xa-Cx(ie))/lac

nbcx=(yb-Cy(ie))/lbc

nbcy=(Cx(ie)-xb)/lbc

gama1=x(n3)-x(n2)

gama2=x(n1)-x(n3)

gama3=x(n2)-x(n1)

bata1=y(n2)-y(n3)

bata2=y(n3)-y(n1)

bata3=y(n1)-y(n2)

        it1=ID(n1)

it2=ID(n2)

it3=ID(n3)

        A(it1,it1)=A(it1,it1)+&
```

```
     var1*(nacx*(KXX(ie)*bata1+KXY(ie)*gama1)+nacy*(KYX(ie)
*bata1+KYY(ie)*gama1))+&
     var2*(nbcx*(KXX(ie)*bata1+KXY(ie)*gama1)+nbcy*(KYX(ie)
*bata1+KYY(ie)*gama1))

                    if(it2.NE.0) then

                    A(it1,it2)=A(it1,it2)+&
     var1*(nacx*(KXX(ie)*bata2+KXY(ie)*gama2)+nacy*(KYX
(ie)*bata2+KYY(ie)*gama2))+&
     var2*(nbcx*(KXX(ie)*bata2+KXY(ie)*gama2)+nbcy*(KYX
(ie)*bata2+KYY(ie)*gama2))

                    else

                    B(it1)=B(it1)-&

                         var1*p(n2)*(nacx*(KXX(ie)*bata2+KXY(ie)*gama2)
+nacy*(KYX(ie)*bata2+KYY(ie)*gama2))-&

                         var2*p(n2)*(nbcx*(KXX(ie)*bata2+KXY(ie)*gama2)
+nbcy*(KYX(ie)*bata2+KYY(ie)*gama2))

               endif

               if(it3.NE.0) then

                    A(it1,it3)=A(it1,it3)+&
     var1*(nacx*(KXX(ie)*bata3+KXY(ie)*gama3)+nacy*(KYX
(ie)*bata3+KYY(ie)*gama3))+&
```

```
      var2*(nbcx*(KXX(ie)*bata3+KXY(ie)*gama3)+nbcy*(KYX
(ie)*bata3+KYY(ie)*gama3))
                  else
                  B(it1)=B(it1)-&
                        var1*p(n3)*(nacx*(KXX(ie)*bata3+KXY(ie)*gama3)
+nacy*(KYX(ie)*bata3+KYY(ie)*gama3))-&
                        var2*p(n3)*(nbcx*(KXX(ie)*bata3+KXY(ie)*gama3)
+nbcy*(KYX(ie)*bata3+KYY(ie)*gama3))
               endif
         endif
         enddo
   enddo
   !     calculate pressure field
   call GGJ(Nnode,A,ip,B,L,JS)
   do i=1,ip
         it=DI(i)
         p(it)=B(i)
   enddo
         do i=1,Nnode
         if(Inlet(i).EQ.1.0) then
```

```
            f(i)=1.0
        endif
    enddo
    end
    subroutine nodeele(Nnode,Nele,ele,x,y,Hz,adjele,Cx,Cy,Area,volume)
    real*8
x(Nnode),y(Nnode),Cx(Nele),Cy(Nele),Area(Nele),volume(Nnode)
    integer ele(Nele,3),adjele(Nnode,10)
    real*8 a,b,c,s,xa,xb,ya,yb,Hz,totalarea,totalvolume
    integer i,j,ie,kk,n1,n2,n3
!   find the element which is adjacent to the node
     do i=1,Nnode
    do j=1,10
        adjele(i,j)=0
    enddo
    enddo
    do i=1,Nnode
        kk=0
        do j=1,Nele
```

```
            if(ele(j,1).EQ.i) then
                kk=kk+1
                adjele(i,kk)=j
                else if(ele(j,2).EQ.i) then
                kk=kk+1
                adjele(i,kk)=j
                else if(ele(j,3).EQ.i) then
                kk=kk+1
                adjele(i,kk)=j
            endif
        enddo
    enddo
```

! calculate the coordinate of element's centroid and the area of element

```
    do i=1,Nele
        n1=ele(i,1)
        n2=ele(i,2)
        n3=ele(i,3)
        Cx(i)=(x(n1)+x(n2)+x(n3))/3.0
```

```
        Cy(i)=(y(n1)+y(n2)+y(n3))/3.0

        a=sqrt((x(n1)-x(n2))**2+(y(n1)-y(n2))**2)

        b=sqrt((x(n1)-x(n3))**2+(y(n1)-y(n3))**2)

        c=sqrt((x(n3)-x(n2))**2+(y(n3)-y(n2))**2)

        s=(a+b+c)/2.0

        Area(i)=sqrt(s*(s-a)*(s-b)*(s-c))

    enddo

!   calculate the volume of control volume

    do i=1,Nnode

        volume(i)=0.0

        do j=1,10

        if(adjele(i,j).NE.0) then

            ie=adjele(i,j)

            n1=ele(ie,1)

            n2=ele(ie,2)

            n3=ele(ie,3)

!           write(*,*)i,n1,n2,n3

            if(n2.EQ.i) then

                n2=n3
```

```
                n3=n1
                n1=i
                else if(n3.EQ.i) then
                n3=n2
                n2=n1
                n1=i
                else
                n1=n1
                n2=n2
                n3=n3
            endif
!           write(*,*)i,n1,n2,n3
            xa=(x(n1)+x(n2))/2.0
            ya=(y(n1)+y(n2))/2.0
            xb=(x(n1)+x(n3))/2.0
            yb=(y(n1)+y(n3))/2.0
            a=sqrt((x(n1)-xa)**2+(y(n1)-ya)**2)
            b=sqrt((x(n1)-Cx(ie))**2+(y(n1)-Cy(ie))**2)
            c=sqrt((Cx(ie)-xa)**2+(Cy(ie)-ya)**2)
```

```
                s=(a+b+c)/2.0
                volume(i)=volume(i)+Hz*sqrt(s*(s-a)*(s-b)*(s-c))
!               write(*,*)a,b,c,s,volume(i)
                a=sqrt((x(n1)-xb)**2+(y(n1)-yb)**2)
                b=sqrt((x(n1)-Cx(ie))**2+(y(n1)-Cy(ie))**2)
                c=sqrt((Cx(ie)-xb)**2+(Cy(ie)-yb)**2)
                s=(a+b+c)/2.0
                volume(i)=volume(i)+Hz*sqrt(s*(s-a)*(s-b)*(s-c))
!               write(*,*)a,b,c,s,volume(i)
                continue
            endif
            enddo
        enddo
        totalarea=0.0
        totalvolume=0.0
        do i=1,Nele
            totalarea=totalarea+area(i)
        enddo
        do i=1,Nnode
```

```
            totalvolume=totalvolume+volume(i)
        enddo
!       write(*,*)Hz, totalarea,totalvolume
        continue
        end
```

subroutine writedat(Nnode,Nele,II,Ttotal,ele,f,p,x,y,ch)

```
        real*8 f(Nnode),p(Nnode)
!       real*8 Vx(Nele),Vy(Nele)
        real*8 x(Nnode),y(Nnode)
        integer ele(Nele,3)
        real*8 Ttotal
         integer Nnode,Nele,i,j,kk
         character*20 filename,ch*1
        if(mod(II,10).EQ.0) then
            call sprintf(filename,ch,II,'.dat',1)
            open(2,file=filename)
            write(2,'(a)')'TITLE=" spectralelement"'
            write(2,'(a)')'VARIABLES= "X","Y","p","f"'
            write(2,100)Nnode,Nele
```

```
            do i=1,Nnode
                write(2,200)x(i),y(i),p(i),f(i)
!           if(x(i).EQ.0.5.and.y(i).EQ.0.0) then
!               write(*,*)i
!           endif
            enddo
            do i=1,Nele
                write(2,*)ele(i,1),ele(i,2),ele(i,3)
            enddo
            close(2)
        endif
!       if(mod(II,1).EQ.0) then
!       open(2,file='fillstatus.dat', position='APPEND')
!       write(2,300) Ttotal
!       do i=1,Nnode
!           write(2,300)f(i)
!       enddo
!       close(2)
!       endif
```

```
      open(2,file='time.dat', position='APPEND')
            write(2,400)II,Ttotal
      close(2)
      100 format('zone N=',2x,I4,2x,'E=',I4,2x,'F=FEPOINT,ET=TRIANGLE')
  200 format(4E12.3)
  !300      format(E12.6)
  400       format(I6,2x,E12.6)
      end
```

subroutine GGJ(Nnode,A,N,B,L,JS)

```
      real*8 A(Nnode,Nnode),B(N),JS(N)
      real*8 T
      L=1
      do k=1,N
            D=0.0
            do i=k,N
            do j=k,N
                  if(abs(A(i,j)).GT.D) then
                        D=abs(A(i,j))
```

```
                JS(k)=j
                IS=i
            endif
        enddo
        enddo
        if(D+1.0.EQ.1.0) then
            write(*,120)
            L=0
            return
        endif
120         format(1x,'fail')
        do j=k,N
            T=A(k,j)
            A(k,j)=A(IS,j)
            A(IS,j)=T
        enddo
        T=B(k)
        B(k)=B(IS)
        B(IS)=T
```

```
do i=1,N
    T=A(i,k)
    A(i,k)=A(i,JS(k))
    A(i,JS(k))=T
enddo
T=A(k,k)
do j=k+1,N
    if(A(k,j).NE.0.0) A(k,j)=A(k,j)/T
enddo
B(k)=B(k)/T
do j=k+1,N
    if(A(k,j).NE.0.0) then
        do i=1,N
            if((i.NE.k).and.(A(i,k).NE.0.0)) then
                A(i,j)=A(i,j)-A(i,k)*A(k,j)
            endif
        enddo
    endif
enddo
```

```
            do i=1,N
                if((i.NE.k).and.(A(i,k).NE.0.0)) then
                    B(i)=B(i)-A(i,k)*B(k)
                endif
            enddo
        enddo
        do k=N,1,-1
            if(k.NE.JS(k)) then
                T=B(k)
                B(k)=B(JS(k))
                B(JS(k))=T
            endif
        enddo
        return
        end
```

subroutine sprintf(a,addr,i,suf,n)

```
!subroutine parameters
    character a*20,addr*n,suf*4
    integer i
```

```
!local variables
    integer i1,i2,i3
    character c5,c4,c3,c2,c1
    if(i.lt.10) then
        c1=char(i+48)
        a=addr//c1//suf
    elseif(i.lt.100) then
        i2=i/10
        i1=i-10*i2
        c2=char(i2+48)
        c1=char(i1+48)
        a=addr//c2//c1//suf
    elseif(i.lt.1000) then
        i3=i/100
        i2=(i-100*i3)/10
       i1=i-(i3*10+i2)*10
        c3=char(i3+48)
        c2=char(i2+48)
        c1=char(i1+48)
```

```
      a=addr//c3//c2//c1//suf
   elseif(i.lt.10000) then
      i4=i/1000
      i3=(i-1000*i4)/100
     i2=(i-(i4*1000+i3*100))/10
     i1=i-i4*1000-i3*100-i2*10
     c4=char(i4+48)
      c3=char(i3+48)
      c2=char(i2+48)
      c1=char(i1+48)
      a=addr//c4//c3//c2//c1//suf
   elseif(i.lt.100000) then
      i5=i/10000
      i4=(i-10000*i5)/1000
     i3=(i-(i5*10000+i4*1000))/100
     i2=(i-i5*10000-i4*1000-i3*100)/10
     i1=i-i5*10000-i4*1000-i3*100-i2*10
     c5=char(i5+48)
     c4=char(i4+48)
```

```
        c3=char(i3+48)

        c2=char(i2+48)

        c1=char(i1+48)

        a=addr//c5//c4//c3//c2//c1//suf

      else

        print*,'unexpected file number'

        stop

    endif

end
```

References

Adams K. L., Miller B., Rebenfeld L. Forced in-plane flow of an epoxy resin in fibrous networks. Polymer Engineering and Science 1986;26(20):1434–1441.

Adams K. L., Russel, W. B., Rebenfeld L. Radial penetration of a viscous liquid into a planar anisotropic porous medium. International Journal of Multiphase Flow 1988;14(2):203–215.

Adams K.L. & L. Rebenfeld(1991), permeability characteristics of Multilayer Fiber Reinforcements, Part 2: Theoretical Model, Polym. Compos., p186.

Advani, V. M., Effective Average Permeability of Multi-layer Preforms in Resin Transfer Molding, Composites Science and Technology 56, 1995.

Agarwal, B. D., Broutman, J., Analysis and Performance of Fiber Composites, Wiley, New York, 1980.

Ambrosi, D. and L. Preziosi. 1998. “Modeling Matrix Injection through Elastic Porous Preforms,”Composites Part A, Vol. 29, Nos. 1–2, pp. 5–18.

Askeland, D.R., The Science and Engineering of Materials, PWS Publishing Co., Boston, 1994

Batch, G.L. & Cumiskey, S. (1990), Miltilayer compaction and flow in composites processing, 45th Annual conference, SPI, pp1-11/session 9-A

Berdichevsky, A. L., and Z. Cai, 1993. “Preform Permeability Predictions by Self-Consistent Method and Finite Element Simulation,” Polym. Compos., 14(2):132-143.

References

Binetruy C, Hilaire. Tow impregnation model and void formation mechanisms during RTM. Journal of Composite Materials 1998; 32(3):223-45.

Blake, F.C. 1922. “The Resistance of Packing to Fluid Flow,” Transactions of the American Institute of Chemical Engineers, Vol. 14, pp. 415–421.

Borg S.F. Matrix-tensor methods in continuum mechanics. Princeton, New Jersey: D. Van Nostrand Company Inc, 1963.

Bowles K.J., Frimpong S. ,Void effects on the interlaminar shear strength of unidirectional graphite-fiber-reinforced composites. Journal of Composite Materials 1991; 26:1487-1509.

Brandt, J., Drechsler, K. and Meistring, R., The application of threedimensional fibre preforms for aerospace composite structures. In Proceedings of an international symposium organised by the European Space Agency and held at ESTEC. Noordwijk, The Netherlands, 21-23 March, 1990, pp. 7 l-77.

Brandt, J., Drechsler, K., Mohamed, M., and Gu, P., “ Manufacture and Performance of Carbon/Epoxy 3-D Woven Composites”, Proc. 37th Int. SAMPE Symposium, Anaheim, CA,(1992).

Brown, R. T., and Ashton, C. H., Automation of 3D braiding machines, paper presented at 4th textile Structural Composites Symposium, 24-26 July, 1989

Bruno, P. S., Keith, D. O. and Vicario, A. A. Jr, Automatically woven three dimensional composite structures, SAMPE Quarterly, 17(4), 10-16, 1986.

References

Bruschke, M. V & Advani, S. G. 1992. Flow of Generalized Newtonian Fluids Across a Periodic Array of Cylinders. J. Rheol., 37: 479-498.

Bruschke, M.V. and S.G. Advani. 1993. “Flowof Generalized Newtonian Fluids across a Periodic Array of Cylinders,” Journal of Rheology, Vol. 37, No. 3, pp. 479–498.

Byun, J. H. and Chou, T. W., Process-microstructure relationships of 2-Step and 4-Step braided composites. Composites Science and Technology, 1996,56,235-251.

Cai Z., Berdichevsky AL. An improved self-consistent method for estimating the permeability of a fiber assembly. Polymer composites 1993; 14(4):314-23.

Carirns, D. S., Humbert, D. R. & Mandell, J. F. 1999. Modeling of Resin Transfer Molding of Composite Materials with Oriented Unidirectional Plies. Composites part A: applied science and manufacturing, 30: 375-382

Carman, P. C. 1937. “Fluid flow through Granular Beds,” Trans. Int. Chem. Eng., 15:150-166.

Carter E. J., Fell A. W., Summerscales J. A simplified model to calculate the permeability tensor of an anisotropic fibre bed. Composites Manufacturing 1995;6(3/4):228–235.

Chan A. W., Hwang S-T. Anisotropic in-plane permeability of fabric media. Polymer Engineering and Science 1991;31(16):1233–1239.

Chan AW, Morgan RJ. Sequential multiple port injection for resin transfer

moulding of polymer composites. SAMPE Quarterly 1992; 23:45-9.

Chan, A.W., Larive, D.E. and Morgan, R.J., Anisotropic Permeability of Fiber Preforms: Constant Flow Rate Measurement , Journal of Composite Materials, 27(10): 996–1008, 1993.

Chang C.Y., Hourng L.W., Study on void formation in resin transfer molding. Polymer Engineering and Science 1998; 38(5):809-18.

Chen Y.T., Davis H.T., Macosko C.W., Wetting of fiber mats for composites manufacturing: 1. Visualization experiments. AICHE Journal 1995; 41(10):2261-81.

Chou, S. and Wu. C. J., A study of the physical properties of epoxy resin composites reinforced with knitted glass fibre fabrics. Journul of Reinforced Plastics and Composites, 1992, ll(11, November). 1239-1250.

Chou, T. W. and Ko, F. K., Textile structural composites. In Composite Materials Series, Vol. 3, Elsevier, Amsterdam,1989

Chui, W. K., Glimm, J. , Tangerman, F.M. , Jardine, A. P. , Madsen, J. S. ,

Coulter, J.P. and S.I. Guceri. 1988. “Resin Transfer Molding: Process Review, Modeling and Research Opportunities,” Proceedings of Manufacturing International ’88, Atlanta, GA, pp. 79–86.

Cox, B. N., Dadkhah, M. S. and Morris, W. L., On the tensile failure of 3D woven composites. Composiles, Part A, 1996,27A, 447-458.

Curiskis, J. I., Weft knitting technology and advanced composite material, CRC-AS Seminar, Sydney, Australia, 1996

Donnellan, T. M. and Leek, R., Process modeling in resin transfer molding as a method to enhance product quality, SIAM Rev., 39: 714-727, 1997.

Daniel, I. M. (1993) “Composites Materials”, in Handbook on Experimental Mechanics, Kobayashi, A.S.eds., Chapter 19, VCH Publishers, Inc. New York, N. Y. :(2nd Rev. Ed.), pp. 829-904

Darcy HPG. Les fontaines bibliques de la ville de Dijon. Paris: Victor Dalmont, 1856.

Dickinson, L.C., M. H. Mohamed, A. Bogdanovich, “3D Weaving: What, How, and Where”, Proceedings of 44th International SAMPE Symposium, pp. 303-312, (May 1999).

Dickinson, L. C., Farley, G. L., and Hinders, M. K. “Trans-Laminar Reinforced Composites: A Review,” Journal of Composites Science and Technology, Vol. 21, pp. 241-248, Jan., 1999.

Dickinson, L.C. and M. H. Mohamed, “Recent Advances in 3D Weaving for Textile Preforming”, Proceeding of the ASME Aerospace Division, Book No. H01214, pp. 3-8, (2000).

Dow, N.F. and Ramnath, V. 1987. Analysis of Woven Fabrics for Reinforced Composite Materials. NASA Contract Report 178275.

Dow, R.M. 1989. New Concept for Multiple Directional Fabric Formation. Proc. 21st Intern. SAMPE Tech. Conf., September 2.528.

Du, G. W. and Chou, T. W., Analysis of three-dimensional textile preforms for multidirectional reinforcement of composites. Journal of Materials

Science. 1991.26. 3438-3448.

Du, G. W. and Ko, F. K., Unit cell geometry of 3-D braided structures. Journal of Reinforced Plastics and Composites, 1993, 12(7, July), 752-768.

Edwards, D. and Hamson, M., Mathematical Modeling Skills, Macmillan Press Ltd. London, 1996

Feldgoise S., Foley M.F., Martin D., Bohan J., The effect of microvoid content on composite shear strength. Proceedings of the 23rd International SAMPE Symposium.1991, p259-273.

Fowler, A. C., Mathematical models in Applied Sciences, Cambridge University Press, 1997.

Frank, K. Ko and Guang- Wu Du, Processing of Textile Preforms. Advance Composites Manufacturing. T. G. Gutowski. Canada, John Wiley & Sons, Inc.: 157-206, 1997.

Frederick R., Phelan J.R. Simulation of the injection process in resin transfer molding. polymer composites 1997; 18(4):460-76.

Fujita., Yokoyama, A. and Hamada, H., Simulation of mechanical behaviors of knitted fabric composites by numerical analysis method. In Proceedings of the American Society for Composites, Tenth Technical Conference. 18-20 October, 1995, pp. 581-590.

Fukuta, K. and Aoki, E., 3D fabrics for composites, paper presented at 15th Textile Research Symposium, Philadephia, PA, Sep. 1986

Fukuta, K., Aoki, E., Onooka, R. and Magatsuka, Y., Application of latticed

structural composite materials with three dimensional fabrics to airtificial bones, Bull. Res. Inst. Polymers Textiles, 131, 159, 1982.

Fukuta, K., Onooka, R., Aoki, E. and Nagatsuka, Y. in Kawabata, S. (Ed.), 15th Text. Res. Symp., The Textile Machinery Society of Japan, Osaka, 1984, pp. 36-38.

Griffen, D.A., Ashwill, T.D., "Alternative Comoposite Materials for Megawatt-Scale Wind Turbine Blades: Design Considerations and Recommended Testing," 2003 ASME Wind Energy Symposium, AIAA-2003-0696, 191-201.

Gebart B.R., Permeability of unidirectional reinforcements for RTM. Journal of Composite Materials 1992; 26(8):1100-33.

Geoghegan, P. J., Dupont ceramics for structural applications- the SEP Noveltex technology, 3rd textile Structural Composites Symposium, Philadelphia, PA, 1-2 June, 1988

Ghiorse S.R., Jurta R.M., Effects of low frequency vibration processing on carbon/epoxy laminates. Composites 1991; 22(1):3-8.

Gutowski T.G., Cai Z., Bauer S., Boucher D., Kingery J., and Wineman S. Consolidation experiments for laminate composites. Journal of Composite Materials 1987; 21:650-69.

Gutowski, T. G., T. Morigaki & Z. Cai. 1987. "The Consolidation of Laminate Composites," J.of Compos.Mater., 21:172-188.

Hahn, H. T. and Tsai, S. W., Nonlinear elastic behavior of unidirectional

composite laminae. Journal of Composite Materials. 1973, 7(January), 102-118.

Happel, J., Brenner, H., Low Reynolds Number Hydro-dynamics, Mechanics of Fluids and Transport Process,Martinus Nejhoff, Boston, 1986

Harper B.D., Staab G.H., Chen RS. A note on the effects of voids upon the hygral and mechanical properties of AS4/3502. Journal of Composite Materials 1987; 21:280-89.

Hasselbrack, S.A. , Pederson, C.L. and Seferis, J.C., Evaluation of Carbon-Fiber Reinforced Thermoplastic Matrices in a Flat Braid Process, Polymer Composites 13[1], 38-46 (1992).

Hayward J.S., Harris B., Effect of process variables on the quality of RTM moulding. SAMPE Journal 1990; 26(3):39-46.

Hirt D. E., Adams K. L., Prud'Homme R. K., Rebenfeld L. In-plane radial fluid flow characterization of fibrous materials. Journal of Thermal Insulation 1987;10:153–172.

Hu, J. L., Liu, Yi, Shao, X. M., Effects of fabric stitch model on preform permeability, submitted to Composites: part A.

Hu, J. L., Liu, Yi, Shao, X. M., Study on void formation in multi-layer woven fabrics, Composites: part A, 2003

Hu, J. L., Liu, Yi, Shao, X. M., The Effect of Stitch on the Permeability of interbundle Channels in Stitched Fabrics, Textile Research Journal, 2003.

Iihikawa, T. and Chou, T. W., Stiffness and strength behavior of woven

fabric composites. Journal of Materials Science, 1982, 17, 321 l-3220.

Ishikawa, T. and Chou, T. W., In-plane thermal expansion and thermal bending coefficients of fabric composites. Journal of Composite Materials, 1983, 17(2), 92-104.

Ishikawa, T. and Chou, T. W., Nonlinear behavior of woven fabric composites. Journal of Composite Materials, 1983,17(5), 399-413.

Ishikawa, T. and Chou, T. W., One-dimensional micromechanical analysis of woven fabric composites. AZAA Journal, 1983, 21(12), 1714-1721.

Kang M.K., Lee W.I., Hahn H.T., Formation of microvoids during resin-transfer molding process. Composites Science and Technology 2000; 60:2427-2434

Kheir, N. A., On a mathematical model for inhomogeneous deformation of composites, International Applied Mechanics, Vol. 32, No. 5, pp. 41-48, 1996.

Kittel, C. Introduction to Solid State Physics, John Wiley and Sons, New York, 1967.

Ko, F. K. & G. W. Du (1997), Processing of textile preforms, Advanced Composites Manufacturing, edited by T.G. Gutowski, P157

Ko, F.K. and Du, G.W., preform fiber architecture for composites, Ceramic Bull., 68(2), 1989.

Ko, F.K. and Du, G.W. 1992. Processing and Structures of Textile Preforms for Composites. Proc. Science and Innovation in Polymer Composites

Processing, MIT, Cambridge, MA, July 16-17.

Kolodziej, J.A., Dziecilak, R. & Konczak, Z. 1998. “Permeability Tensor for Heterogeneous Porous Medium of Fibre Type,” Transport in Porous Media, 32: 1-99.

Kozeny, J. 1927. “Ueber Kapillare Leitung des Wassers im Boden,” Sitzungsberichte, Akademie der Wissenschaften in Wien, Vol. 136, pp. 271–301.

Krolewski, S. and Busch, J., 1990, The competitive position of selected composites fabrication technologies for automotive applications, Proc. 35th Intern. SAMPE Symp., pp. 1761-1771.

Kuo, W. S., Elastic behaviour and damage of three-dimensional woven fabric composites. In The Tenth Inlemarional Conference on Composite Materials. Whistler, British Columbia, Canada, 14-18 August, 1995, pp. 301-308.

Lai, C.-L. andW.-B. Young. 1997. “Model Resin Permeation of Fiber Reinforcements after Shear Deformation,” Polymer Composites, Vol. 18, No. 5, pp. 642–648.

Laroche, D., Khanh, V. T. and Julien, H., Forming of woven fabric composites. Journal of Composite Materials, 1994, 28(18), 1825-1839.

Larson, E.,“Pressure Bag Molding: Manufacturing, Mechanical Testing, Nondestructive Evaluation, and Analysis,” Master’s Thesis in Mechanical Engineering, Montana State University-Bozeman, January 2004. K. Han, S. Jiang, C. Zhang, B.Wang, “Flow Modeling and Simulation of SCRIMP™ for Composites Manufacturing,” Composites Part A, Jan 2000, Vol. 31, 79-86

Lee, L. J., 1997. “Liquid Composite Molding,” Advanced Composites Manufacturing, Edited by Timothy G.Gutowsiki, P393.

Lekakou, C. , Johari, M. A. K., Norman D. and Bader, M. G., Measurement techniques and effects on in-plane permeability of woven cloths in resin transfer moulding, Composites Part A: Applied Science and Manufacturing, Volume 27, Issue 5, 1996a, Pages 401-408

Lekakou C. , Johari M. A. K. , Bader M. G ., Compressibility and Flow Permeability of Two-Dimensional Woven Reinforcements in the Processing of Composites. Polymer Composites, 17, pp666-672,1996b.

Loos, A. C., M. H. Weidermann, and D.E.Kranbuchi,”processing of advanced textile structural composites by RTM”, Proc. 5th Textile Structural Composites Symp., Drexel University, Philadephia, Dec.4-6, 1991.

LundstrÖm, T. S., 2000. “The Permeability of non-crimp Stitched Fabrics,” Composites part A: applied science and manufacturing, 31:1345-1353.

Mahale, A.D., Prud’Homme, R.K. and Rebenfeld, L., Quantitative Measurement of Voids Formed During Liquid Impregnation of Nonwoven Multifilament Glass Networks Using an Optical Visualization Technique , Polymer Engineering and Science, 32(5): 319–326, 1992

Maistre, M. ,Three-Dimensional Multi-Directional Structure, U. S. Patent No. 4,219,597, August, 1980.

Mallick, P.K., Fiber Reinforced Composites: Materials, Manufacturing, and Design, Marcel Dekker Inc., New York, 1988.

References

Mallick, P. K. (1993), Fiber-Reinforced Composites-materials, manufacturing, and design, Marcel Dekker, Inc., New York.

Mandelbrot, B.B., The Fractal Geometry of Nature,W.H. Freeman, New York, 1982, pp. 23–57.

Mandell, J.F., Samborsky, D.D., Cairns, D.S.,“Fatigue of Composite Materials and Substructures for Wind Turbine Blades,” SAND 2002-0771, March 2002 Schey, J. A.,Introduction to Manufacturing Processes, McGraw-Hill, New York, 2000.

Mandell, J.F., Samborsky, D.D., Wahl, N.K., Sutherland, H.J.,"Testing and Analysis of Low Cost Composite Materials Under Spectrum Loading and High Cycle Fatigue Conditions," Proceedings of The 14th International Conference on Composite Materials (ICCM-14), Society of Manufacturing Engineers, San Diego, California, July 14 - 18, 2003. Paper 1811. (2003)

Martin, G.Q. and J.S. Son. 1986. “Fluid Mechanics of Mold Filling for Fiber Reinforced Plastics,” Proceedings of the Second Conference on Advanced Composites, 18–20 November 1986, Dearborn, MI, pp. 149–157.

Miller, E., Textiles: Properties and Behaviour. Batsford, London, 1973.

Mogavero J. & S.G. Advani(1997), Experimental investigation of Flow Through mulyi-layer preforms, Polym. Compos., Oct., Vol. 18(5), p649

Mohamed, M. H., Bogdanovich, A. E., Dickinson, L.C., Singletary, J. N., and Lienhart, R. B., “A New Generation of 3D Woven Fabric Preforms and Composites,” SAMPE Journal, 2001, Vol. 37, No. 3, May/June, pp. 8-17.

References

Mohamed, M. H., Schartow, R. W., Knouff, B. J., “Light Weight Composites for Automotive Applications,” Proceedings of SAMPE 2003 Conference, Long Beach, CA, May 11 – 15, 2003.

Morton M. Denn, Process Fluid Mechanics, pp.35, Prentice Hall, NJ, 1980.

Murthy, D. N. P., Page, N. W. and Rodin, E. Y., Mathematical Modeling- A tool for problem solving in engineering, physical, biological and social sciences, PERGAMONPRESS. Oxford, 1990

Naik, N. K. and Ganesh, V. K., Prediction of on-axes elastic properties of plain weave fabric composites. Composites Science and Technology, 1992,45(2), 135-152.

Naik, N. K., Shembekar, P. S. and Hosur, M. V., Failure behavior of woven fabric composites. Journal of Composites Technology and Research, 1991, 13(l), 107-l 16.

Naik, R. A., Failure analysis of woven and braided fabric reinforced composites. Journal of Composite Materials, 1995, 29(17), 2334-2363.

Naik, R. A., Ifju, P. G. and Masters, J. E., Effect of fibre architecture parameters on deformation fields and elastic moduli of 2-D braided composites. Journal of Composite Materials, 1994,28(7), 656-68 1.

Naik, R.N., Analysis of Woven and Braided Fabric Reinforced Composites,” NASA CR-194930, June 1994.

Nakayama, A., PC-Aided Numerical Heat Transfer and Convective Flow, CRC Press, Boca Raton, 1995.

Panton, R. L., Incompressible Flow (JohnWiley & Sons, New York, 1984).

Parnas R. S., Salem A. J., A comparison of the unidirectional and radial in-plane flow of fluids through woven composite reinforcements. Polymer Composites 1993;14(5):383–394.

Parnas R. S, Phelan Jr F. R. The effect of heterogenous porous media on mold filling in resin transfer molding. SAMPE Quarterly 1991; 22:53-60.

Parnas, R.S., quid Composite Molding, Carl Hanser, Munich, 2000.

Pastenbaugh, J., Aerospatiale technology, paper presented at 3rd textile Structural Composites Symposium, Philadelphia, PA, 1-2 June, 1988

Pastore, C.M. and Cai, Y.J. 1990a. Applications of Computer Aided Geometric Modeling for Textile Structural Composites. Proc. 2nd Intern. Conf. Computer Aided Design in Composite Material Technology, Brussels, Belgium, April,25-27

Patankar, S.V., Numerical Heat Transfer and Fluid Flow, Hemisphere, London, 1980.

Patel N, Lee LJ. Effects of fiber mat architecture on void formation and removal in liquid composite molding. Polymer Composites 1995;16(5):386-99.

Patel N, Rohatgi N, Lee LJ. Micro scale flow behavior and void formation mechanism. Polymer Engineering and Science 1995; 35(10): 837-51.

Phelan, F. R., 1991. “Advanced Composite Materials: New Developments and Application Conf. Proc.”, Detroit, MI, Sept., P.175.

Pierre Freland, D. G., Francois Trochu, Concurrent Methods for Permeability Measurement in Resin Transfer Molding, Polymer Composites 17, 1996

Pillai, K.M. and S.G. Advani. 1998. “Numerical Simulation of Unsaturated Flow in Woven Fiber Preforms during the Resin Transfer Molding Process,” Polymer Composites, Vol. 19, No. 1, pp. 71–80.

Pitchumani R., and Ramakrishnan B., A fractal geometry model for evaluating permeabilities of porous preforms used in liquid composite molding, Int. J. Heat Mass Transfer 42 (1999) 2219–2232.

Popper, P., and McConnell, R., Anew 3D braid for integrated parts manufacturing and improved delamination resistance- the 2-step method, 32nd International SMAPE Symposium and exhibition, 1987, pp. 92-102.

Raz, S. 1987. Warp Knitting Production. Heidelberg, Germany: Melliand.

Rohatgi V., Patel N. and Lee L.J., Experimental investigation of flow-induced microvoids during impregnation of unidirectional stitched fiberglass mat. Polymer Composites 1996; 17:161-70.

Ruan, X. P. and Chou, T. W., Experimental and theoretical studies of the elastic behavior of knitted-fabric composites. Composifes Science and Technology, 1996.56, 1391- 1403.

Rudd C. D., Morris D. J, Chick J. P, Warrior N. A., Material characterization for SRIM, 4th International Conference on Automated Composites (ICAC ’95), Nottingham, UK, Vol. 1, 1995, p. 211–218.

Rudd, C. D. Long, A. C., Kendall K. N. and G. E. Mangin, (1997), Liquid

Molding Technologies, Woodhead Publishing Ltd.

Rudd, C.D., A.C. Long, P. McGeehin, and P. Smith. 1996. “In-Plane Permeability Determination for Simulation of Liquid Composite Molding of Complex Shapes,” Polymer Composites, Vol. 17, No. 1, pp. 52–59.

Scardino, F. L., Introduction to textile structures, in textile structural composites, Chou, T. W., and Ko, F. K. eds, Elsevier, Covina, CA, 1989.

Schwartz, M. M., Composite Materials: Processing, Fabrication and Applications, Prentice Hall, 1997.

Shih, C. H. & Lee, L. J. 1998. “Effect of Fibre Architecture on Permeability in Liquid Composite Molding,” Polym. Compos., 19(5):629-639.

Shojaeia, A., Ghaffariana, S.R., Karimianb, S.M.H., “Numerical simulation of three-dimensional mold filling process in resin transfer molding using quasi-steady state and partial saturation formulations”, Composites Science and Technology 62 (2002) 861 – 879

Simacek, P., Advani, S.G., Permeability model for a woven fabric. Polymer Composites 1996; 17:887-99.

Singletary, J.N. and A.E. Bogdanovich, “Processing and Characterization of Novel 3-D Woven Composites,” Proceedings of SAMPE 2001 Conference, Long Beach, CA, May 6 – 10, 2001

Skartsis, L., Kardos, J.L. and Khomami, B., Resin Flow Through Fiber Beds During Composite Manufacturing Processes, part 1 and part2, Polym. Eng. Sci., 32(4), p221 and p231, 1992.

Skramstad, J.D.,“Evaluation of Hand Lay-Up and Resin Transfer Molding in Composite Wind Turbine Blade Manufacturing,” Master’s Thesis in Mechanical Engineering, Montana State University-Bozeman, August 1999.

Smith, P., C.D. Rudd, and A.C. Long. 1997. “The Effect of Shear Deformation on the Processing and Mechanical Properties of Aligned Reinforcements,” Composites Science and Technology,Vol. 57, pp. 327–344.

Spencer, D.J. 1983. Knitting Technology. New York: Pergamon Press.

Van der Westhuizen, J. and J.P. Du Plessis. 1996. “An Attempt to Quantify Fibre Bed Permeability Utilizing the PhaseAverage Navier-Stokes Equation,” Composites Part A,Vol. 27A, pp. 263–269.

Um, M. K. and Lee, W. I. , A study on the mold filling process in resin transfer molding, Polymer Engineering and Science, 31: 765-771, 1991.

Wang, T. J., C. H. Wu, & L. J. Lee(1994), In-plane permeability measurement and analysis in liquid composite molding, Polym. Compos. Vol.15(4), P278

Wang, C.Y. 1996. “Stokes Flow through an Array of Rectangular Fibers,” International Journal of Multiphase Flow, Vol. 22, No. 1, pp. 185–194.

Weitzenböck, J. R. , Shenoi R. A. and Wilson, P. A., Measurement of three-dimensional permeability, Composites Part A: Applied Science and Manufacturing, Volume 29, Issues 1-2, 1998, Pages 159-169.

Weitzenböck, J. R. , Shenoi R. A. and Wilson, P. A., Radial flow permeability measurement. Part A: Theory, Composites Part A: Applied

Science and Manufacturing, Volume 30, Issue 6, June 1999, Pages 781-796

Weitzenböck, J. R. , Shenoi R. A. and Wilson, P. A., Radial flow permeability measurement. Part B: application, Composites, Part A: Composites Part A: Applied Science and Manufacturing, Volume 30, Issue 6, June 1999, Pages 797-813.

Weitzenbock, J. R. and Wilson, P. A., Measurement of Principal Permeability with the Channel Flow Experiment, Polymer Composites 20, 1998.

Weitzenbo¨ck J.R. Flow characterization in resin transfer moulding, PhD thesis, University of Southampton, November 1996, 212 p.

Wheatcraft, S. W., Tylor, S. W., An explanation of scale dependent dispersivity in heterogeneous aquifers using concepts of fractal geometry. - Water Resour. Res. 24, 566-578, 1988.

Williams, D. J., new knitting methods offer continuous structures, Adv. Composites Eng., Summer, 12-13, 1978.

Williams JG, Morris CEM, and Ennis BC. Liquid flow through aligned fiber beds. Polymer Engineering and Science 1974; 14(6):413-19.

Wu, W. L., Kotaki, M., Fujita., Hamada, H., Inoda, M. and Maekawa, Z. I., Mechanical properties of warp-knitted, fabric-reinforced composites. Journal of Reinforced Plastics and Composites, 1993, 12(10, October), 1096-l 110.

Yang, J.M. and Chou, T.W., Thermo-Elastic Analysis of Triaxially Woven Fabric Composites, in Textile Structural Composites, edited by Tsu-Wei Chou and Frank K. Ko, Elsevier, New York, 1989, pp. 265-277.

References

Yong W. B., Han K, Fong L. H., Lee L. J., Flow simulation in molds with preplaced fiber mats. Polymer Composites 1991; 12(6):391-403

Yosida H. T., Ogasa T., Hayashi R., Statistical approach to the relationship between ILSS and void content of CFRP. Composites Science and Technology 1986; 25, 3-18.

Yu B., Lee L.J. A simplified in-plane permeability model for textile fabrics. Polymer Composites 2000; 21(5):660-85.

Yu, B. M. and Li, J. H., Some fractal characters of porous media, Fractals, Vol. 9, No. 3 (2001) 365-372.